

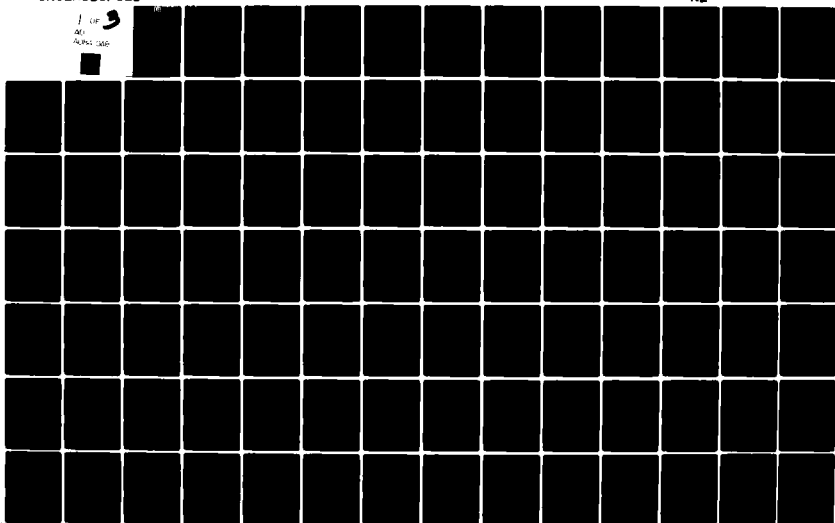
AD-A084 048

CAMBRIDGE UNIV (ENGLAND) DEPT OF CIVIL ENGINEERING F/G 8/13  
CENTRIFUGAL MODELLING OF SOIL STRUCTURES. PART I. CENTRIFUGAL M--ETC(U)  
MAR 79 D J GOODINGS, A N SCHOFIELD DA-ERO-76-6-040

UNCLASSIFIED

NL

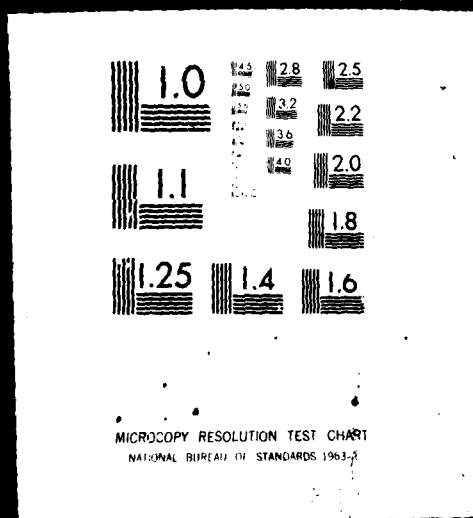
1 of 2  
AD  
A084 048



1 OF 3

AD

A084 048



ADA 084048

LEVEL

P-4083972

CENTRIFUGAL MODELLING OF SOIL STRUCTURES  
PART I

CENTRIFUGAL MODELLING OF SLOPE FAILURES

Final Technical Report

by

Deborah Janet Goodings

March 1979

EUROPEAN RESEARCH OFFICE

United States Army

London England

GRANT NUMBER DA-ERO - 76-G-040

A. N. Schofield

Approved for Public Release; distribution unlimited

FILE COPY

80

5

8

085

REPORT DOCUMENTATION PAGE		READ INSTRUCTIONS BEFORE COMPLETING FORM
1. REPORT NUMBER (6)	2. GOVT ACCESSION NO. DDA084048	3. RECIPIENT'S CATALOG NUMBER (2)
4. TITLE (and Subtitle) Centrifugal Modelling of Soil Structures Part I Centrifugal Modelling of Slope Failures		5. TYPE OF REPORT & PERIOD COVERED Final Technical <i>rept.</i> 6 May 76-5 May 79
7. AUTHOR(s) Deborah Janet Goodings Andrew N. Schofield		6. PERFORMING ORG. REPORT NUMBER
9. PERFORMING ORGANIZATION NAME AND ADDRESS Department of Civil Engineering University of Cambridge Cambridge, U.K.		8. CONTRACT OR GRANT NUMBER(s) DAERO-76-G-040 <i>me</i>
11. CONTROLLING OFFICE NAME AND ADDRESS U. S. Army Research & Standardization Group (Eur) Box 65 FPO NY 09510		10. PROGRAM ELEMENT, PROJECT, TASK AREA & WORK UNIT NUMBERS ITI61102BH57/01 <i>17</i>
14. MONITORING AGENCY NAME & ADDRESS (if different from Controlling Office) U. S. Army Engineers Waterways Experiment Station P. O. Box 631 Vicksburg, MS 39180		12. REPORT DATE March 1979
		13. NUMBER OF PAGES 196 <i>(12/28)</i>
		15. SECURITY CLASS. (of this report) Unclassified
		15a. DECLASSIFICATION/DOWNGRADING SCHEDULE
16. DISTRIBUTION STATEMENT (of this Report)  Distribution Unlimited		
17. DISTRIBUTION STATEMENT (of the abstract entered in Block 20, if different from Report)		
18. SUPPLEMENTARY NOTES  <div style="text-align: right; font-size: 2em;">411 742</div>		
19. KEY WORDS (Continue on reverse side if necessary and identify by block number) Soil mechanics, embankment stability, slope stability, centrifuge modelling, clay slopes, mine waste slopes, sea clay, landslides, flow slides, scale modelling, scaling laws.		
20. ABSTRACT (Continue on reverse side if necessary and identify by block number)  This research investigated slope failure in two prototype soil materials using the technique of reduced scale centrifugal modelling. Champlain Sea clay, a sensitive, fissured, cemented clay from Canada, was sampled intact and shipped to Cambridge. It was shaped into nineteen different soil models, and in these, three classes of failure were observed: intact slope failure, slope degradation and flowsliding. The importance of time dependent horizontal stress release and of the fissure network, seemed important in model response, and the effect		



of uplift forces was also observed. In nineteen coal mine waste embankment dam models, throughout which the soil particle size distribution was altered for modelling of difference prototype soil conditions, three classes of failure were observed: intact slope failure in response to throughflow conditions, failure by erosion, and retrogressive rate of construction failure. The importance of particle size distribution, of embankment preparation by compaction in lifts, of a clay foundation layer, and of the inclusion of highly permeable sections in the embankment, both drained and undrained, were all studied in the course of the experiments. Conventional methods of prediction of slope stability and erosion were applied to the models. The scaling laws for centrifugal modelling of water movement were examined, and the requirement for reduced scale modelling of seepage and erosion were found to be mutually incompatible.

Accession For	
NTIS GRA&I	<input checked="checked" type="checkbox"/>
DDC TAB	<input type="checkbox"/>
Unannounced	<input type="checkbox"/>
Justification	
By	
Distribution	
Availability Codes	
Dist	Available/or Special
A	

Centrifugal Modelling of Slope Failures

by

Deborah Janet Goodings

A dissertation submitted for the degree  
of Doctor of Philosophy  
at  
Cambridge University

Clare College

March, 1979.

ABSTRACT

This research investigated slope failure in two prototype soil materials using the technique of reduced scale centrifugal modelling.

Champlain Sea clay, a sensitive, fissured, cemented clay from Canada, was sampled intact and shipped to Cambridge. It was shaped into nineteen different soil models, and in these, three classes of failure were observed: intact slope failure, slope degradation, and flowsliding. The importance of time dependent horizontal stress release and of the fissure network, seemed important in model response, and the effect of uplift forces was also observed.

In nineteen coal mine waste embankment dam models, throughout which the soil particle size distribution was altered for modelling of different prototype soil conditions, three classes of failure were observed: intact slope failure in response to throughflow conditions, failure by erosion, and retrogressive rate of construction failure. The importance of particle size distribution, of embankment preparation by compaction in lifts, of a clay foundation layer, and of the inclusion of highly permeable sections in the embankment, both drained and undrained, were all studied in the course of the experiments. Conventional methods of prediction of slope stability and erosion were applied to the models. The scaling laws for centrifugal modelling of water movement were examined, and the requirements for reduced scale modelling of seepage and erosion were found to be mutually incompatible.

PREFACE

My development as an engineer and a researcher over the past three and a half years has been largely a product of the Cambridge Soil Mechanics group as a whole, but I am in particular grateful for the continuous encouragement and generosity of supervision which Professor A.N. Schofield has given to me during that time.

The Cambridge geotechnical centrifuge is an unusually large and novel machine, and in development of all new operations, the Director and Assistant Director of Research, Professor Schofield and Dr R.G. James, give much thought to the safe and effective development of new test techniques, and participated in several of the tests reported in this thesis. Dr J.F.A. Sleath from the Hydraulics group also was generous in supplying guidance to me in the area of erosion and sediment transport.

The actual experimental work in this thesis was accomplished with the assistance of the technical support staff at the Engineering Laboratories. Help was available from the workshops, and the concrete and structural research laboratories whenever required, but the efforts put forward for this work were largely the product of the technicians of the Soil Mechanics group. Mr R.E. Ward, responsible for organising the group effort, with assistance from Mrs V. Johnson, Mr W. Balodis, and Mr P. Finlay were important in the work. The main efforts, however, came from two fronts: Mr J. Doherty, and Mr W. Gwizdala, who tackled difficult new problems with expertise during the process of model construction at the main laboratory, were of great importance to this research; Mr C. Collison, with the assistance of Mr S. Boniface, and Mr C. Hodgson, at the centrifuge, saw through the long centrifuge test programme with endurance and skill. To these people the research is indebted, and the fine working atmosphere in the soil mechanics laboratories is of their making.

The production of this thesis was possible through the capable efforts of Mrs S. Venn, who typed the manuscript, and Mrs F. Summerfield, who drew many of the figures.

The work was carried out under research grants from the U.S. Army Corps of Engineers, with their assistance in the provision and laboratory testing of mine waste samples; the National Research Council of Canada supported collaboration with Dr R.J. Mitchell in the work of sampling and shipping intact specimens of Champlain Sea clay.

It is also appropriate to acknowledge here, my parents, my most constant, albeit biased benefactors throughout the course of my research.

I certify that, except where specific reference is made in the text to the work of others, the contents of this dissertation are original, and have not been submitted to any other university.

CONTENTS

	<u>Page No.</u>
Abstract .. .. .	(i)
Preface .. .. .	(ii)
Contents .. .. .	(iv)
List of symbols .. .. .	(vi)
 CHAPTER 1 - GEOTECHNICAL CENTRIFUGAL MODELLING .. .. .	 1
1.1 Centrifugal Modelling Background .. .. .	1
1.2 Numerical Slope Stability Analysis .. .. .	4
1.3 Centrifuge Slope Stability Analysis .. .. .	7
1.4 Principles and Validity of Centrifugal Modelling .. .. .	9
 CHAPTER 2 - THE CAMBRIDGE GEOTECHNICAL CENTRIFUGE FACILITY .. .. .	 14
2.1 Cambridge Geotechnical Centrifuge .. .. .	14
2.2 Centrifugal Model Containers .. .. .	16
2.3 Water Supply .. .. .	18
2.4 Pore Pressure Measurement .. .. .	20
2.5 Photography and Video Test Records .. .. .	21
 CHAPTER 3 - CHAMPLAIN SEA CLAY - INTRODUCTION .. .. .	 23
3.1 Landslides in Champlain Sea Clay .. .. .	23
3.2 Geological History of the Ottawa Area Champlain Sea Clay .. .. .	 27
3.3 Landslide Mechanisms in Ottawa Area Champlain Sea Clay .. .. .	 28
3.4 Yielding and Mechanical Strength of Ottawa Area Champlain Sea Clay .. .. .	 32
3.5 Object of the Model Tests .. .. .	37
3.6 Selection of the Rockcliffe Site .. .. .	37
3.7 The Rockcliffe Landslide and Clay .. .. .	38
3.8 Retrieval of the Rockcliffe Samples .. .. .	41
3.9 Rockcliffe Soil Properties Measured in Cambridge .. .. .	45
 CHAPTER 4 - CHAMPLAIN SEA CLAY - EXPERIMENTS .. .. .	 50
4.1 Model Preparation .. .. .	50
4.2 Logic of the Test Programme .. .. .	54
4.3 Definition of Failure .. .. .	57
4.4 Experimental Procedure and Results .. .. .	59
4.5 Discussion .. .. .	70
4.5.1 Measurements of in-test soil response .. .. .	70
4.5.2 Drainage conditions at failure .. .. .	75
4.5.3 Discussion of the individual tests .. .. .	77
4.5.4 General trends in model behaviour .. .. .	81
4.6 Conclusion .. .. .	90

CHAPTER 5 - COAL MINE WASTE - INTRODUCTION	.. .. .	92
5.1 Mine Waste	.. .. .	92
5.2 Coal Mine Waste Disposal Practice	.. .. .	93
5.3 Engineering Properties of Coal Mine Waste	.. .. .	95
5.4 Slope Stability in Embankment Dams	.. .. .	98
5.5 Object of the Model Tests	.. .. .	102
5.6 The Coal Mine Waste Test Material	.. .. .	103
CHAPTER 6 - MINE WASTE - EXPERIMENTS	.. .. .	105
6.1 Logic of the Test Programme	.. .. .	105
6.2 Model Preparation	.. .. .	107
6.3 The Rationale Behind Changes in Particle Size Distribution	.. .. .	110
6.4 Changes in Particle Size Distribution	.. .. .	113
6.5 Definition of Failure	.. .. .	116
6.6 Experimental Procedure and Results	.. .. .	116
6.7 Effects of Water Flow in Centrifugal Models	.. .. .	127
6.7.1 Darcy's law	.. .. .	128
6.7.2 Scaling of flow nets and adjacent regions of moisture	.. .. .	131
6.7.3 Seepage forces	.. .. .	133
6.7.4 The Chezy and Manning formulae	.. .. .	135
6.7.5 Erosion and sediment transport	.. .. .	138
6.8 Discussion	.. .. .	145
6.8.1 Individual tests and prototype relevance	.. .. .	145
6.8.2 Regular slope stability analysis	.. .. .	153
6.8.3 Surface erosion and sediment transport	.. .. .	157
6.8.4 Comments on particle size distribution	.. .. .	166
6.9 Conclusions	.. .. .	170
CHAPTER 7 - GENERAL CONCLUSIONS	.. .. .	172
7.1 Slope Failures	.. .. .	172
7.2 Centrifugal Modelling	.. .. .	173
References	.. .. .	175
Table 4.2	.. .. .	182
Table 6.2	.. .. .	185
Table 6.3	.. .. .	188
Photographic Plates	.. .. .	189

LIST OF SYMBOLS

$a$	dimensionless numerical constant
$c$	dimensionless numerical constant
$c'$	effective cohesion
$c_u$	undrained cohesion
$c_v$	coefficient of consolidation
$d$	(depth of flow (diameter of pipe or soil pore
$D$	multiple of $H$ signifying depth from crest of slope to point below
$D_{10}$ $D_{30}$ $D_{50}$ $D_{85}$	diameter of particles at which 10%, 30%, 50%, or 85% of soil is finer
$e$	void ratio
$E'$	effective Young's modulus
$F_s$	seepage force $\perp$ bed/unit area
$g$	earth's gravitational acceleration
$h$	difference in height between two columns of water
$h_c$	height of continuous capillary rise
$H$	(slope height (length of longest drainage path
$i$	hydraulic gradient
$i'$	pressure gradient
$j$	seepage force/unit volume
$k$	engineering coefficient of permeability
$k'$	Olivier's constant
$kg$	kilograms
$kN$	kilonewtons
$K$	empirical constant characterising porosity of soil structure



$l$	straight line distance between two points
$m$	slope stability coefficient
$m$ (subscript)	model
$m$	metres
$mm$	millimetres
$min$	minutes
$n$	(slope stability coefficient (Manning's roughness coefficient (dimensionless numerical constant
$N$	(scale of model, compared to prototype (centrifugal loading in multiples of earth's gravitational acceleration
$N_d$	number of equipotential drops in a flow net
$N_f$	number of flow channels in a flow net
$N_s$	stability number
$p'$	effective spherical pressure (CSSM)
$p$ (subscript)	prototype
$q$	(axial deviator stress (flow/unit width
$q_c$	collapse flow/unit width
$q_s$	bed load rate in $m^3$ /unit time/unit width
$q_t$	threshold flow
$r_u$	pore pressure ratio
$R$	(hydraulic mean radius (pore radius
$Re$	Reynolds number
$Re_x$	shear Reynolds number
$s$	seconds
$S$	$\sin$ (longitudinal slope angle)
$t$	time
$T_s$	surface tension
$u_*$	shear velocity
$v$	discharge velocity

$V$	fluid velocity
$x$	space axis
$z$	space axis
$\beta$	slope angle
$\gamma$	unit weight of soil
$\gamma_p$	unit weight of pore fluid
$\gamma_s$	unit weight of solids
$\gamma_w$	unit weight of water
$\eta$	$\frac{q}{p}$ stress ratio
$\lambda$	dimensionless numerical coefficient
$\mu$	static viscosity
$M$	critical state frictional constant
$\nu$	kinematic viscosity
$\nu'$	effective Poisson's ratio
$\rho$	(density ( $\phi'$ triaxial
$\sigma_3$	minor principal stress
$\tau$	shear stress
$\tau_c$	critical shear stress
$\tau_o$	boundary shear stress
$\phi'$	effective angle of friction
$\psi$	Shields number
$\psi_s$	Shields number under seepage conditions.

## CHAPTER 1

### GEOTECHNICAL CENTRIFUGE MODELLING

#### 1.1 Centrifugal Modelling Background

Reduced scale centrifugal modelling in soil mechanics is a recently developed technique in Britain. When the first such research was begun fourteen years ago, previous published literature was limited to the work of Pokrovsky and Fyodorov (1936), who with their colleagues in the USSR were the first to investigate basic principles of geotechnical centrifuge modelling; more peripherally, Rydweski (1958), at Cambridge, had examined stresses in concrete buttress dams, and Hoek (1965), in South Africa, applied the technique to rock behaviour in mines. Within this framework, Avgherinos and Schofield (1969) began experimenting.

The technique has since been applied to a variety of geotechnical problems, which have included slope stability (Terstepanian and Goldstein (1969), Lyndon (1972)), reinforced earth (Bolton (1972)), foundations design (Polshin et al (1973)), embankments on soft foundations (Endicott (1970), Beasley (1973), Bassett (1973)), behaviour of off shore gravity platforms (Rowe (1978)), rockfill dams (Mikasa et al (1969)), flexible culverts (English (1973)), drawdown in sandstone aquifers (Howsam (1974)), stability of slurry trenches and buried cylinders (Bolton et al (1973)), retaining walls in sand (Wind (1976)), and riverbank stability (Hird (1974), Padfield (1978)). In addition, certain USSR publications have become available: stress distribution and foundation settlement (Pokrovsky and Fyodorov (1935)), and some general texts on theory and use of centrifuge modelling in the construction and mining industry (Pokrovsky and Fyodorov (1968, 1969), and Malushitsky (1975)). A full account of completed centrifuge research is attempted by Scott and Morgan (1977). The research at Cambridge further expands into the ongoing examination of dynamic loading (Morris (1979)), buried pipes (Britto (1979)), and tunnels under

pressure (Mair (1979)).

Geotechnical centrifuge modelling facilities were first fully developed in the USSR, but were not widely publicised by them, and while the technique has recently begun to receive attention also in Japan, Denmark, France and the United States, all developments of this research outside the USSR rely heavily upon recent British experience.

The object of modelling techniques developed in engineering is to provide better understanding of macroscopic prototype events, such as geotechnical failures with unknown mechanisms. It is typical that a modelling technique will require initial theoretical validation, and the problems of the technique and its limitations determined. Further along the path of development, the technique must be tested against full scale phenomena to establish its usefulness in prediction. Such a logical path was followed at Cambridge, initiated by Avgherinos (1969), who demonstrated the feasibility and usefulness of the centrifuge modelling technique in an idealised drawdown problem of soil mechanics, followed by Endicott (1970) and Beasley (1973), who reached a point at which they could work on simple prototype-model comparison. In parallel at the University of Manchester Institute of Science and Technology (UMIST), Lyndon (1972) undertook a complete centrifuge modelling exercise for the Lodalen clay cutting prototype failure, from intact sampling at the prototype site near Oslo, to the final comparison of model and prototype, and he was satisfied that correct modelling had been achieved. Hird (1974), at UMIST, and Padfield (1978), at Cambridge, took on the more difficult task of investigating a soil mechanics problem, not entirely understood: the instability of flood embankments under uplift conditions. Their success is inevitably limited to the field of mechanics because the prototype failures which would be required for detailed comparison are (fortunately) rare, and dangerous exceptions rather than the rule.

Throughout this work, the typical problem selected for investigation has been slope instability, chosen both for its usually clear-cut evidence of failure, and for its importance in soil mechanics. The research in this thesis, founded upon the advancements of its predecessors, selected for examination slope failure in two different prototype soils. The simultaneous introduction of prototype material and slope instability problems which are not entirely understood was a significant complication to the investigation, due to the variable and somewhat unpredictable nature of natural soils, but it also involved an advancement in the application of the technique to real prototypes.

The first problem selected for study was slope stability in sensitive Canadian Champlain Sea clay. Large upland areas in southern Quebec and eastern Ontario have been lost in the development of large retrogressive landslides which on occasion evolve into flowslides. Extensive laboratory and field study, reviewed by Crawford (1968) and Penner and Burn (1978), has been successful in illuminating many characteristics of the clay, and centrifugal modelling was a logical new direction for research.

The second problem investigated was slope failure in coal mine waste embankment dams. Such waste heaps have not always been designed with adequate care, as disasters such as those at Aberfan, Wales in 1966 (Davis, Harding and Lawrence (1967)) and at Buffalo Creek, West Virginia in 1972 (Corp, Schuster and McDonald (1975)) have emphasised. Incomplete appreciation of the relevant factors have been to blame in general. Centrifugal model testing provided a new avenue for studying these factors.

Both materials have been observed to develop conventional slope instability characteristics, but the debris from the prototype landslides has been known sometimes to develop into an uncontrolled, fast moving flow of viscous, but liquefied material. While conventional instability was the primary point of interest in the present model test series, insight

into this unusual phenomenon of liquefaction was also an objective of the research.

The research was undertaken in part with support from the U.S. Army Corps of Engineers, under a grant with a wide scope entitled "Studies in Liquefaction", and with support from Canadian and U.S. collaborators who provided clay specimens and mine waste material for tests.

## 1.2 Numerical Slope Stability Analysis

The correct calculation of slope stability is an important component of civil engineering design. The usual approach to the problem is by numerical methods which endeavour to characterise the response of soil by simple equations, which are empirically fitted to observed soil data obtained under what are assumed conditions of effective stress. The ambition to predict with more exact equations the behaviour of a history dependent material such as soil, is a very proper academic quest, but in normal engineering practice, only an engineering approximation is hoped for. Even this is not an easy accomplishment.

It is an important characteristic of any method of engineering analysis that a balance be struck between the completeness of the theory and the correctness of predictions, and the ease of application. When Taylor (1937) proposed his version of total stress slope stability analysis, he compared it to other methods in current use. It was not so much the superiority of results which distinguished Taylor's method, but rather the ease of application permitted by the formulation of slope stability charts. This simplicity was sufficient to ensure the continued use of his method for many years.

When the concept of effective stress parameters and their application to slope stability problems became appreciated (the importance of this work was recently emphasised by Janbu (1977)), Bishop realised that the major impediment to its application was the absence of slope stability

charts which would simplify design in a way comparable to Taylor's charts Bishop and Morgenstern (1960) produced charts of stability coefficients based upon the effective stress limit equilibrium analysis proposed by Bishop (1955), which are still in common use today.

Bishop was not the only one to develop new slope stability analysis since Taylor (1937). Recently Fredlund and Krahn (1977) prepared a comparison of slope stability analysis methods developed over the past thirty years and still in current use. The methods differed not so much in their approach to the failure mechanisms, but rather in the simplifying assumptions made, and the type of equilibrium assessed, force or moment equilibrium. The six methods considered included the Fellenius method, the simplified Bishop method, Spencer's method, the Janbu simplified and Janbu rigorous methods, and the Morgenstern-Price method, and they were applied to six sample stress conditions on a given slope. Remarkably similar evaluations of stability were obtained and of these, Fredlund and Krahn considered that Spencer's and Morgenstern and Price's methods gave the truest indication of slope stability: both methods satisfied moment and force equilibrium. They remarked, however, on the substantially greater computation time required for these two methods, and in examining the other four, they concluded that the simplified Bishop method gave the consistently best approximation of safety factor when compared to the Spencer and Morgenstern-Price methods, but with much less computation time. Of course a large number of standard problems can be solved without computation, by reference to charts, and in that connection the charts prepared by Bishop and Morgenstern, and by Spencer are correctly based and easy to use.

Bishop and Morgenstern (1960) pointed out one interesting difference between the alternative methods which resulted from their simplifying assumptions. Although the resulting safety factors may be similar, the location of the critical failure plane by the alternative methods is not

unique: it is typical of collapse load calculations that a true full scale prototype failure mechanism need not always be determined, even though a reasonable assessment of stability may be achieved.

It is important to bear in mind that the engineering value of a method of analysis is not judged by its similarity of prediction to other numerical methods, but rather its ability to predict the behavior of a full scale prototype soil slope. A few comparisons have been made of different methods of analysis for a given failure, for example a study on the Buffalo Creek mine waste dam failure by Corp et al (1975). They back-analysed the slope stability failure by elastic-plastic, finite-element method and compared it to analysis using the Bishop method. The mode of failure predicted by the two methods was similar, as was the safety factor calculated in both cases in the vicinity of unity. Both were capable of predicting failure in retrospect when the correct soil parameters were used.

Back-analysis is useful in cases where one known failure may be used to predict the stability of other similar slopes, but the engineer's objective is that prediction before failure should eventually be achieved. A variety of factors may diminish the usefulness of any numerical stability approach, quite independent of the equilibrium conditions assumed. These include proper assessment, through sound engineering judgement, of the important site features, the most adverse likely conditions, and most importantly, appreciating the soil response under these conditions which will govern the behaviour of the slope. Bjerrum (1973) devoted considerable attention to this latter aspect, emphasising the influence of time effects, and anisotropy on soil behaviour, and the importance of testing high quality, representative, soil samples on the stress path most likely to occur in the field.

Despite these stipulations, current methods of numerical analysis may offer good engineering assessment of slope stability, and their val-



idity is depended upon in engineering practice with usually satisfactory results. Failures which do occur, however, testify to some inadequate phase in the analysis, and previous to centrifugal modelling, the only other approach to soil mechanics problems in which behaviour was influenced by the self-weight of the soil, was by the costly, difficult, and sometimes dangerous process of full scale trials. Safe, reduced scale centrifuge models, within which boundary conditions can be manipulated, and important events continually monitored, are an excellent alternative to, or at the very least, a logical preliminary step before, full scale trials. Two critical disadvantages of numerical analysis are eliminated by centrifugal modelling: the assumption of the correct failure mechanism, and the analysis of soil strength characteristics. The next section will discuss the still limited evidence of the value of centrifugal modelling in natural soils.

### 1.3 Centrifuge Slope Stability Analysis

The object of engineering slope stability analysis is to successfully predict the safety of a prototype soil slope under a variety of possible adverse conditions. By obtaining both the safety factor and an approximation to the probable failure surface, proper design of embankments and cuttings may be achieved. If a reasonable estimate of soil behaviour, as compared to the prototype, is achieved, then the analysis is 'successful' in engineering terms. Although academic benefits may be derived from comparison between numerical and centrifugal slope stability predictions, either method, if proven to give good results, would be sufficient alone for engineering design application.

Centrifugal modelling in soil mechanics using natural soil from real prototype situations, has demonstrated not only reasonable agreement with numerical methods but has been compared favourably with prototype behaviour; in some cases centrifugal prediction has even given better estimates than numerical analysis.

Research done as early as Pokrovsky and Fyodorov (1936) produced a closer correlation between stress measured in situ and that measured in a centrifuge model, than that calculated theoretically, and in addition gave good prediction of prototype foundation settlement. Later work at Cambridge in natural soil further confirmed good correlation between centrifuge models and prototype behaviour, by Endicott (1970), Beasley (1973) and Lyndon (1972).

Endicott (1970) endeavoured to predict embankment settlement on a layered substrata by centrifugal modelling using natural soils from the prototype site. Settlement 265 days after prototype construction was remarkably close to that predicted.

Lyndon (1972) undertook a full modelling investigation of a well documented rotational landslide in clay, which occurred in a railway cutting in Lodalen, Norway, in 1954. In that research he defined the cause of failure to be swelling subsequent to stress relief, and observed a model landslide in which the slip surface coincided almost precisely with that located in the prototype.

Beasley (1973), on the other hand, had a different class of success. He endeavoured to model a prototype failure in a fly ash lagoon embankment. Failure per se was not observed in his model, but the strains detected, defined a state of limiting equilibrium, according to a complementary triaxial test programme. He concluded that prototype behaviour had been modelled, additionally confirmed by correct identification of the failure surface, contrary to that predicted by numerical analysis.

This experimental evidence suggested that centrifugal modelling of prototypes using natural soil gives good prediction of behaviour and that it may be directly applied to prototype design. Lyndon's work implied that no additional analysis was necessary in the event that slope failure was observed, whereas Beasley's work indicated that familiarity with the stress-strain properties of the soil was necessary for correct inter-

pretation of model behaviour in terms of the prototype. In the case of settlement of embankment foundations, direct correlation with the prototype was achieved without further interpretation.

This experimental work helped to establish the correctness and value of centrifugal model testing by investigating simple prototype problems. Application to new slope instability problems using prototype soil was the subject of this thesis.

#### 1.4 Principles and Validity of Centrifugal Modelling

In physical scale modelling of soil mechanics problems, the two governing principles were formulated by Pokrovsky and were restated by Lyndon and Schofield (1978) as follows:

1. If soil with identical friction, cohesion, and density is formed into two geometrically similar bodies, one a prototype of full scale, and one a model of  $\frac{1}{N}$  scale, then if the  $\frac{1}{N}$  scale model is accelerated so that its weight increases  $N$  times, the stresses at corresponding points are similar if they are similar on the boundaries.
2. If excess pore pressure distributions have once been made to correspond in model and prototype, all subsequent processes of primary flow of water are correctly modelled after time,  $t_m$ , in the model that is less than time,  $t_p$ , in the prototype in the ratio  $\frac{t_m}{t_p} = \frac{1}{N^2}$ .

While the second principle, regarding pore pressure dissipation, is an inherent property of any reduced scale soil model, achievement of the first principle, requiring an increase in self weight, may be attempted by one of three methods. One may be by the substitution of heavy minerals for the original soil, so that although cohesion and friction of both are identical, the density of the substitute is  $N$  times heavier than the original. Since heavy metals like lead or mercury are only four or five times as dense as quartz, it is clear that this method of substitution cannot offer much scope; an additional difficulty would be to obtain

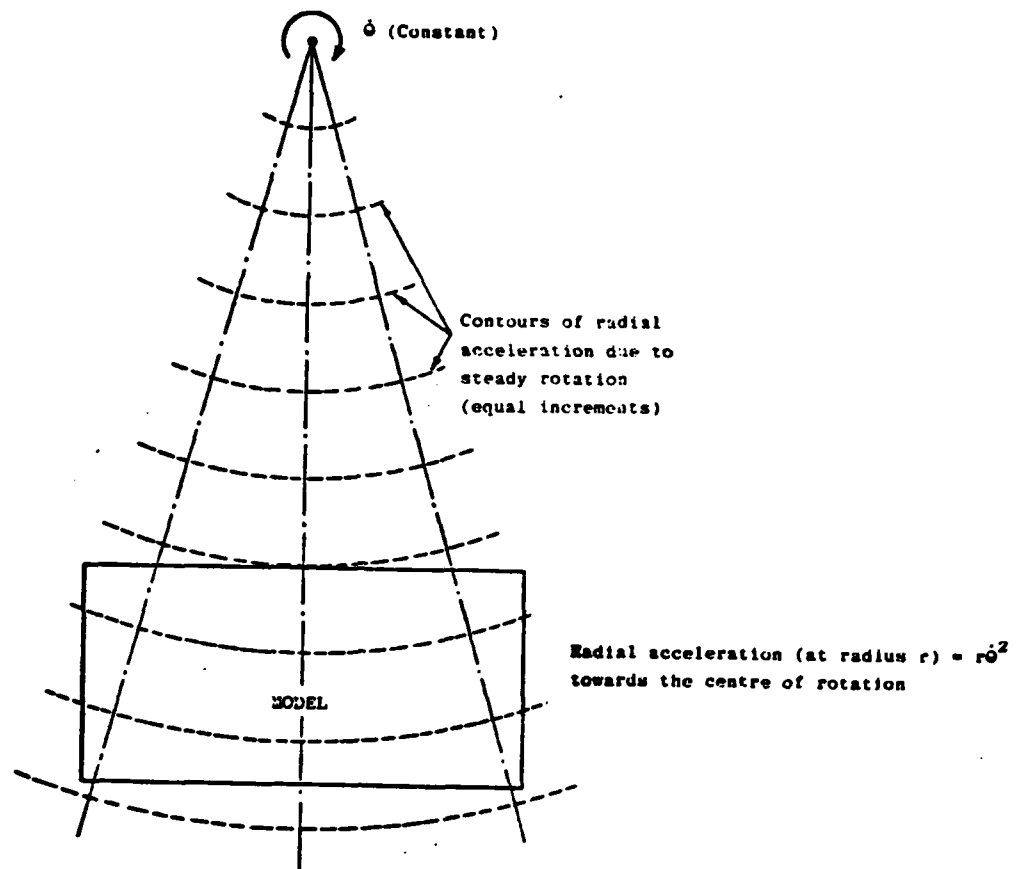


Figure 1.1 - Radial Acceleration Field ( Hird, 1974 )

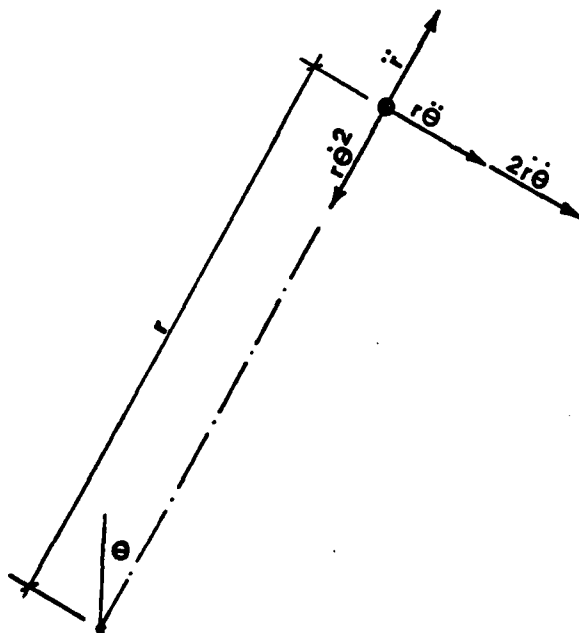


Figure 1.2 - Components of Acceleration ( Horizontal Rotation )  
( Hird, 1974 )

the same behaviour at contact points between particles of substitute material, as occurs at contact points between soil particles.

Alternatively, seepage pressure gradients may apply body forces equivalent to an increased self weight within the model soil, however when the prototype is a saturated soil body, it is seldom possible for the direction of flow to simulate prototype conditions. Also, in practice when this method has been tried there have been serious problems of variation of permeability within the soil, either in surface cracks which allow pressures to penetrate too deeply into a soil body, or in surface cakes within which pressure gradients become concentrated. In general, unless the model soil has uniform permeability, soil behaviour may be incorrect.

The third option, the one selected for this research, is centrifugal acceleration of a natural soil model, such that the self weight of every element in a model  $N$  times smaller in every dimension is increased  $N$  times, to duplicate the prototype stress distribution.

The field of gravity on the surface of the earth is regarded as constant and parallel through any engineering structure. In a centrifuge, which rotates in a horizontal plane, as defined by earth's gravity, the artificial field of acceleration exerted on a model at the end of the centrifuge arm is curved and varies with depth through the model, (figure 1.1). In addition to the principle radial component of acceleration,  $r\dot{\theta}^2$ , there are transient radial and tangential accelerations,  $\ddot{r}$ ,  $r\ddot{\theta}$ , and the Coriolis acceleration,  $2\dot{r}\dot{\theta}$ , and the constant one gravity force of the earth, acting perpendicular to the artificially exerted acceleration (figure 1.2). Hird (1974) provided an in depth examination of these secondary accelerations (of which the Coriolis acceleration has no counterpart in earth's gravitational field) and explained how they may affect dynamic phenomena.

The effects of the curvature of the centrifugal acceleration field

may be diminished by limiting the width of the model in its dimensions perpendicular to the axis of rotation. Pokrovsky and Fyodorov (1968) suggested that the ratio of the width of the model to the radius of rotation should be not larger than 0.2, resulting in a change in the angle of acceleration of  $6^{\circ}$  at the extremities. Significant complication arises in building curved models (see Endicott (1970)), and a plane model within this width restriction is suggested, positioning where possible, the important features near the centre of the model. Variation in acceleration with depth may also be limited. Pokrovsky and Fyodorov (1968) considered that if the complete model height is restricted to 15% of the radius of rotation of the model, then the variation in acceleration will be tolerable.

Ideally the material in this reduced scale centrifugal model will have the same fabric, structure, sensitivity, and stress history as the prototype, and during the test period will be subjected to the same loading path, boundary stresses and pore pressure distribution, as experienced in the prototype. Only then will friction, cohesion, and density be identical. In the case of a clay, the way to ensure the closest possible similarity is by intact sampling at the prototype site, selecting soil at the point of lowest strength in the prototype profile and then, by centrifugal modelling, bring<sup>ing</sup> the model into equilibrium under prototype stress conditions. This is not an insignificant feat in itself: the sampling process, by causing unrealistic unloading and reloading, introduces new, unrepresentative aspects to the soil stress history, and in addition, application of stresses to replicate the prototype stress history may be either unfeasible or impossible.

The structure of the soil itself may give rise to concern if there are any inherent structural features in the prototype soil, such as fibrous organic intrusions, varves, fissures, or in the case of larger grained soils, the large size of the grains themselves, which may play

a role much out of proportion in the model, as compared to their role in the prototype. Attention must then be paid to their unscaled influence on model behaviour. Beasley (1973) examined some centrifuge footing tests on a uniform sand between the scales of  $N = 31$  and  $N = 79$ ; no systematic variation was identified. The problem of fissures may be more serious, although according to Craig (1973), Rowe's centrifuge tests in heavily overconsolidated, fissured London clay, correctly modelled an excavation failure. Lo (1970) has also considered the relationship of the size of sample to the frequency of fissuring, in conventional laboratory tests and concluded that in sufficiently large samples, prototype behaviour may be observed.

Certain other considerations are also important. The soil should ideally be free from unscaled second order events, such as creep, and if a particular mode of soil behaviour cannot be duplicated at a reduced scale, for example strain softening, where the loss of strength is a function of displacement, then events such as progressive failure, and post failure displacements may not be easily modelled. Beasley (1973) encountered such a problem, and suggested that the stress-displacement relationship in soil, and the unscaled thickness of a failure zone may depend upon particle size.

The increase in strain rate which may be experienced in the model as a result of the faster rate of consolidation predicted by the second principle of modelling, may cause an increase in soil strength. For a model of scale  $\frac{1}{100}$ , Padfield (1978) calculated that an increase in strength as much as 12% may occur.

Various model boundary effects, such as side friction, may also artificially alter soil response. Pokrovsky and Fyodorov (1968) suggested that the supporting effects of side friction may be counter-balanced by the increase in acceleration through the depth of the model. Beasley (1973) considered Rowe's experience which indicated that the

height:width ratio of slope models, the steepness of the slope, and the particle size adjacent to the lubricating boundary layer were all important in determining the effects of side friction. Effects less than 10% were suggested by Beasley, decreasing as the strength of the clay exceeded that of the lubricant.

This considerable list of limitations on centrifugal modelling is not unimportant, but it may obscure the advantages of the technique: provided the loading and boundary conditions imposed on the natural prototype soil are representative of field conditions, then the mechanisms observed in the model are not hypotheses. The critical failure conditions observed may be measured, and each soil element has been automatically subjected to precisely the correct stress path. The large size of the centrifuge model is capable of representing more realistically than other laboratory tests, its inherent weaknesses, strengths and peculiarities, each playing its correct role in that stress situation.

As Lyndon (1972) pointed out, the approaches of the model maker and the numerical analyst differ widely. Each acquires an understanding of the problem in a very different fashion, and if both are able to predict reasonably, the prototype events, then both are equally valid approaches. There is no doubt that both have their place: the numerical method is a usually less costly and convenient design tool, in cases of well understood soil response, while centrifugal modelling is an empirical, explorative technique, useful for problems which are not, as yet, fully defined qualitatively. It is inevitable that problems explored on the centrifuge will be reduced to equations and symbols for numerical analysis, and thus the methods progress hand in hand, not precluding the value of each other.



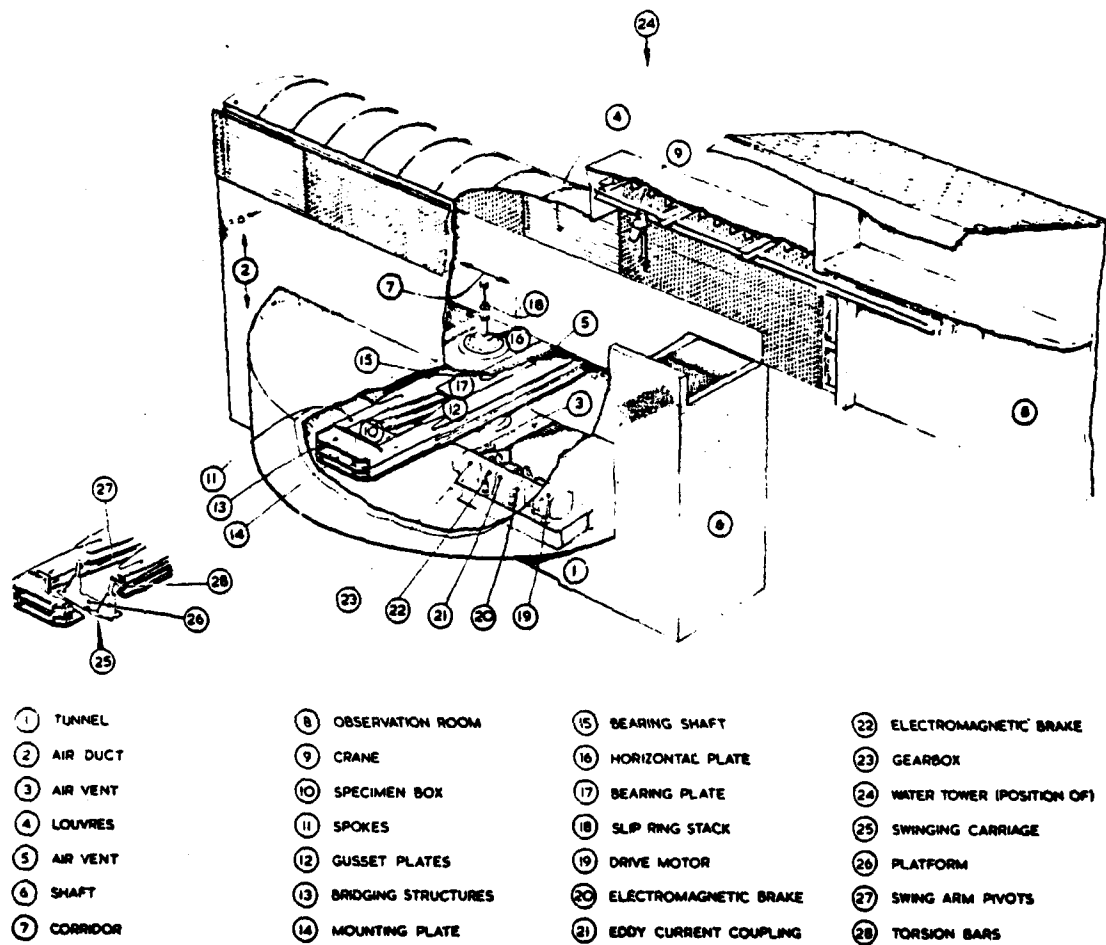


Figure 2.1 - Cambridge Geotechnical Centrifuge

## CHAPTER 2

### THE CAMBRIDGE GEOTECHNICAL CENTRIFUGE FACILITY

#### 2.1 Cambridge Geotechnical Centrifuge

The Cambridge geotechnical centrifuge was designed by Mr P.W. Turner to the specifications of the late Professor K.H. Roscoe and his colleagues. It was constructed by the staff of the University Engineering Department workshops. It was assembled at its site on Madingley Road on the West University site, and the first machine proof test was executed on September 30, 1974. A complete description of the facility is given by Turner (1976); a summary description of the centrifuge will be given here with reference to the numbering scheme in figure 2.1.

The general arrangement of the centrifuge is in four levels. At the lowest level, below the ground surface, in a rectangular concrete chamber, 1, is the drive unit of the centrifuge, to which access is gained by a vertical shaft, 6, direct from the upper levels and not through the centrifuge chamber.

The centrifuge chamber, directly above the drive unit tunnel but still lying entirely below ground surface, is a squat, cylindrical, reinforced concrete shell with one metre thick walls. The interior dimensions of the chamber measure 2 m deep and 10.65 m in diameter. Reinforcing of the axis of rotation is sufficient to sustain a short term out of balance period.

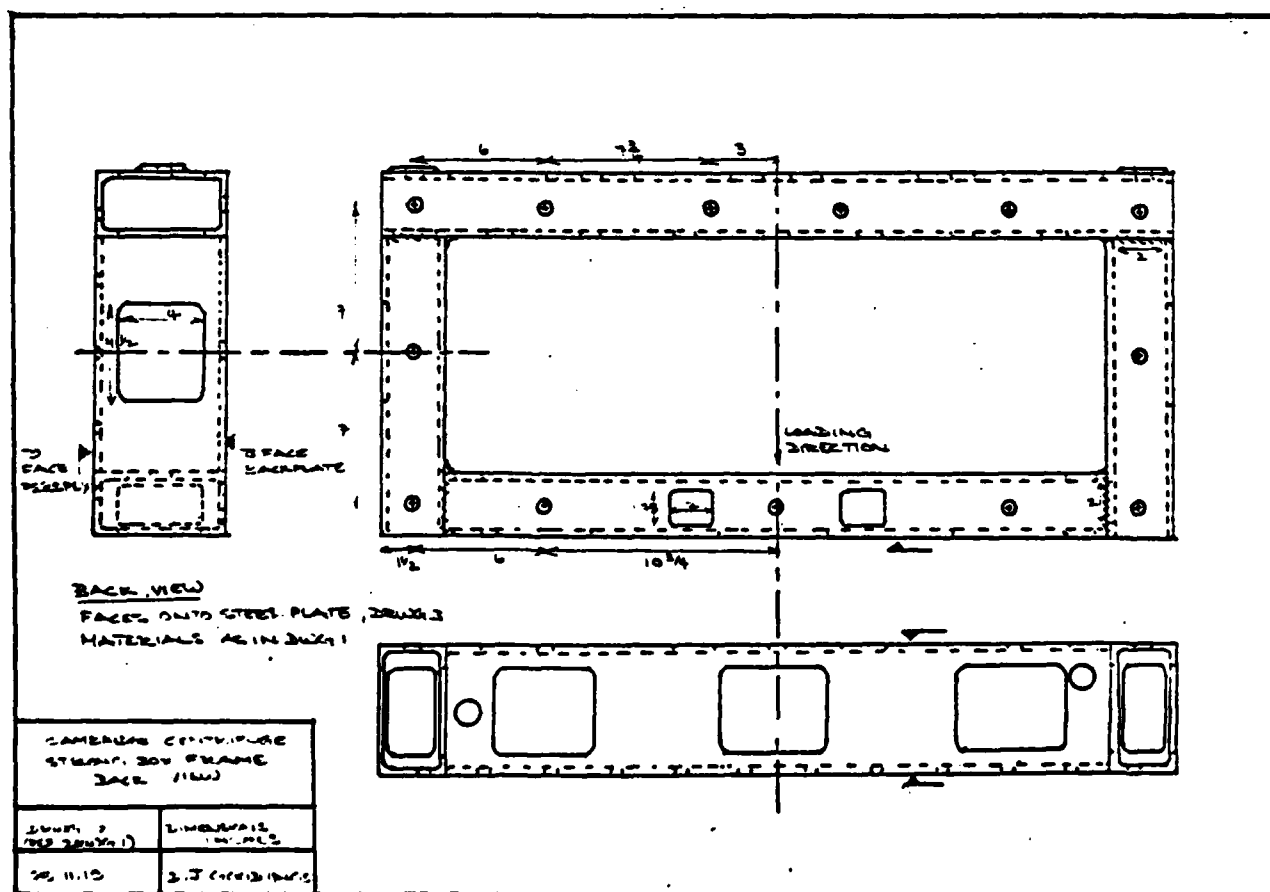
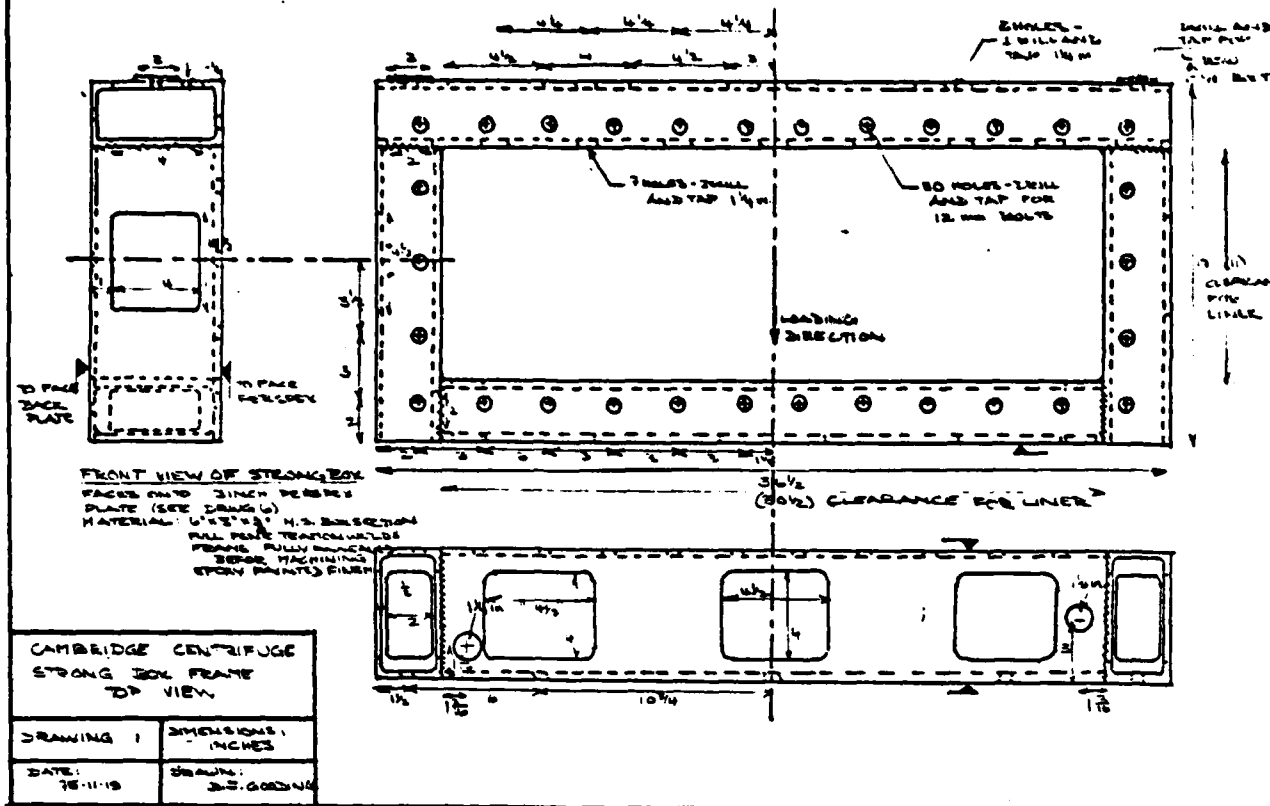
Above this chamber is a two metre wide corridor, also below ground level, with a 10 mm thick steel plate deck. On this level is mounted the apparatus for ~~still~~<sup>flash</sup> photography, seen in the background of figure 2.2, which views and illuminates the model by stroboscope through perspex windows. Marking the centre of rotation is the slip ring stack, 18, comprised of eighty low noise slip rings, four power rings, and ~~four~~<sup>eight</sup> hydraulic or compressed air rings.

Figure 2.2 was photographed from the ground level observation and control area, from which all monitoring and test operation is undertaken. Separating the observation area from the centrifuge area are two 12 mm thick steel doors, not shown in figure 2.1, which are closed during centrifuge tests in excess of 50g, and when explosive charges are used in the model tests.

The drive unit of the facility is a constant <sup>speed</sup> electric motor driving the rotating structure of the centrifuge through a water cooled <sup>Eddy</sup> current coupling, and worm and wheel gear box. The 225 kw A.C. motor, 19, is coupled to the eddy current coupling, 21, through an electromagnetic brake, 22, with a second brake situated between the coupling and the gear box. Increase in the speed of rotation of the centrifuge is achieved by the application of constant torque until the desired speed is achieved, after which time that speed is maintained within  $\pm 1\%$ . Reduction in the speed of rotation is achieved by the reverse process until the coupling becomes ineffective, at which point the electromagnetic brake takes over. The drive unit was designed to achieve a model acceleration at a working radius of 4 m, equal to 165g, although actual full speed will attain 155g on a warm day, and 150g in winter, due to the change in viscosity with temperature, of the centrifuge lubricating oil.

The rotating structure of the centrifuge, figure 2.3, is composed of four hollow rectangular spokes, 10 m long, 406 mm by 203 mm in cross section, bolted together at the ends by bridging structures, 13, and attached to the central bearing shaft by welded gusset plates, 12.

The original stationary model mounting arrangement, 14, which caused the model to lie always on the horizontal, was replaced by a superior swinging carriage system, 25, involving a platform, 26, held by two arms attached to the spokes by two pivots, 27. This permits the soil surface of the models to remain perpendicular to the direction of acceleration.



Figures 2.4 and 2.5 - Strongbox Design - Top View and Back View

As the centrifuge speed increases, the platform gradually swings up until it is perpendicular to the direction of radial acceleration. When the force in the pivots reaches a given value, the swinging platform seats into a fixed mounting; further load is shed from the pivots into the massive rotating structure. The size of this platform limits the model size: the largest model container now used has an inside diameter of 850 mm.

The hollow bearing shaft, 15, which is 600 mm in diameter and 2 m long, carries at either end a self-aligning spherical roller bearing. All gravity loads are carried by the lower bearing. The total weight of the rotating structure is fifteen tonnes.

## 2.2 Centrifuge Model Containers

Two identical centrifuge strong boxes to contain the soil models were designed by the author and built in the University Engineering Department workshops, for these model tests. The containers were required to provide rigid boundaries to the models at <sup>maximum</sup>~~top~~ centrifugal loadings, to permit a variety of loading conditions and perturbations to be applied aside from the increase in self weight of the soil during the centrifuge test, to permit monitoring of various model responses, both visually and electrically, and lastly, to provide a useful, practical and versatile size space, for a variety of models not always visualised at the design stage. The maximum model dimensions selected must also take into consideration the balance between limitations on the maximum feasible size of intact sampling, and the importance of samples large enough to be representative of soil properties, and to be able to model large scale models.

The maximum model dimensions selected were 775 mm long, by 260 mm high. The width 152 mm, was the same as that selected by Avgherinos (1969), as being narrow enough to observe plane strain response, while wide enough to reduce side friction effects. In a model of maximum height, 260 mm,



the variation in centrifugal acceleration force exerted on the model is  $\pm 3.4\%$  relative to the mid-height of the model; the maximum length, 775 mm, means that for features at the extremities, the radial acceleration will act at a maximum deviation from the perpendicular by  $5.8^\circ$ . The largest prototype which may be modelled within these dimensions at 150g would be a 22.5 m slice of a feature 42 m high and 116 m long.

The design adapted by the author for the tests in this research was that of the original "liner" and box system by Avgherinos (1969). The new boxes housed the model in a frame of four 152 mm by 76 mm by 10 mm mild steel hollow box sections, with a 13 mm thick mild steel back plate reinforced against deflection by a grid of 13 mm mild steel ribs, 152 mm, and 140 mm deep. The frame was enclosed in the front by a removable 80 mm thick perspex sheet of good visibility, and clamped to the box by a mild steel frame held by thirty high tensile UNBRAKO bolts. Such a design was calculated to be able to safely contain at 165g the worst loading of a full box of heavy viscous liquid, with specific gravity equal to 2.05. The minimum safety factor at 165g of any single component was equal to five. The design drawings are shown in figures 2.4 to 2.9.

The back plate reinforcing ribs were convenient for fastening on such accessories as water supply vessels, electrical connector boxes, and compressed air valves and their moisture traps, which prevented unwanted water from accumulating in the valves. Displacement transducers were mounted through the top box section, and a manometer was affixed directly to the steel clamping frame.

The "liner", an innovation of Avgherinos (1969), was also designed. It was a U-shaped structure made of aluminium alloy, 20 mm thick, which fit snugly into the centrifuge strong box. It served the multiple purposes of permitting minimal strain during handling of an intact clay specimen at the model preparation stage, of creating great versatility in regulating water into and out of the model cavity by liner modification,





and of sealing the cavity on three sides by means of an embedded GACO seal. The thickness of the liner reduced the maximum model dimensions by 40 mm in length and 20 mm in height.

In the case of cohesionless material, where it may not be important to manipulate the natural soil as an intact specimen, the liner may be eliminated, provided suitable alterations can be made to the box itself to permit the control of ground water during the test. In the event that the liner is not used, the water tightness of the model cavity may be achieved, in the absence of the GACO seal, by the continuous welds along the interface of the back plate section of the box and the basic box section frame, and along the perspex face of the model by a gasket eliminator compound.

### 2.3 Water Supply

For the models tested in this research, a variety of different water supply configurations were required, evolving with the changing modelling techniques. In the clay models, the liner played an integral part in the control of ground water, aided by an arrangement of pneumatic valves and the water reservoir, all on the exterior of the strong box, which controlled variation in water levels during the test runs; two hydraulic systems resulted. The coal mine waste embankment tests had one basic system of plumbing which did not include the liner, but involved an overhead 12 l water cylinder, and use of the bottom hollow box section. These systems will be explained here.

The two basic hydraulic systems of the clay model tests are shown schematically in figures 2.10a and 2.10b. In figure 2.10a initial submerged consolidation was achieved by shutting valve a and feeding water by water supply 1, to the water reservoir, which fed directly to the model cavity through a sand filter at the rear of the embankment. The water level was maintained at level Y, by the height of the overflow

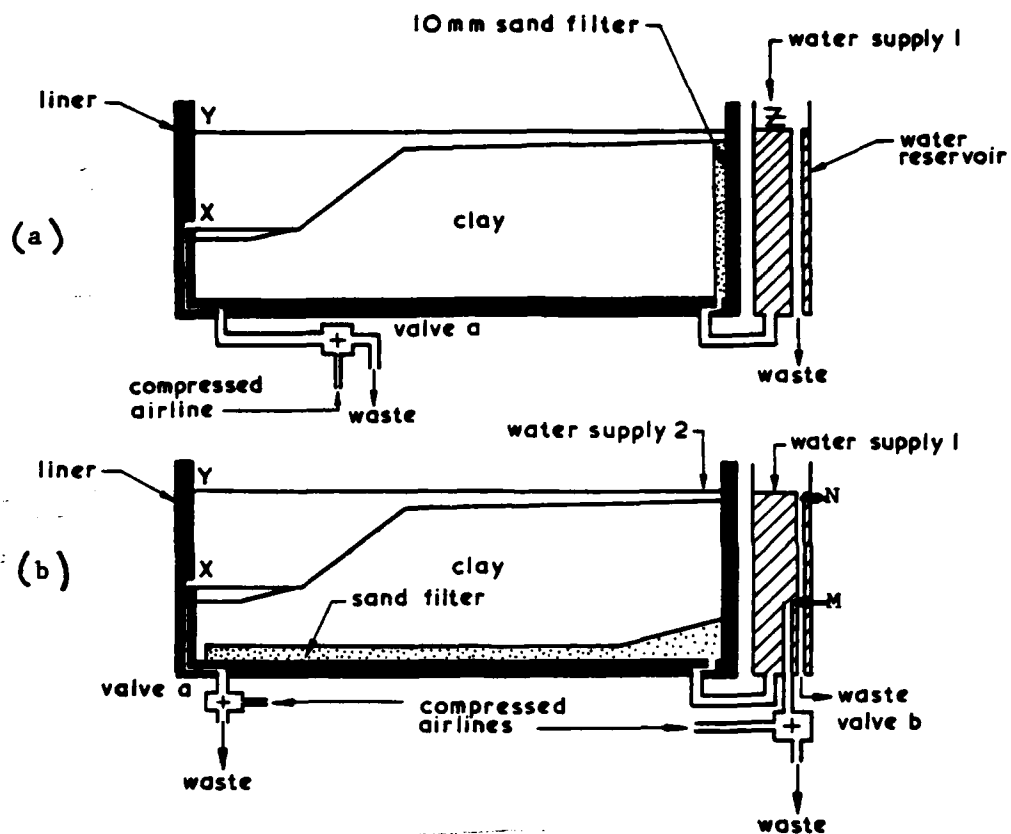


Figure 2.10 - Hydraulic Systems - Clay Models

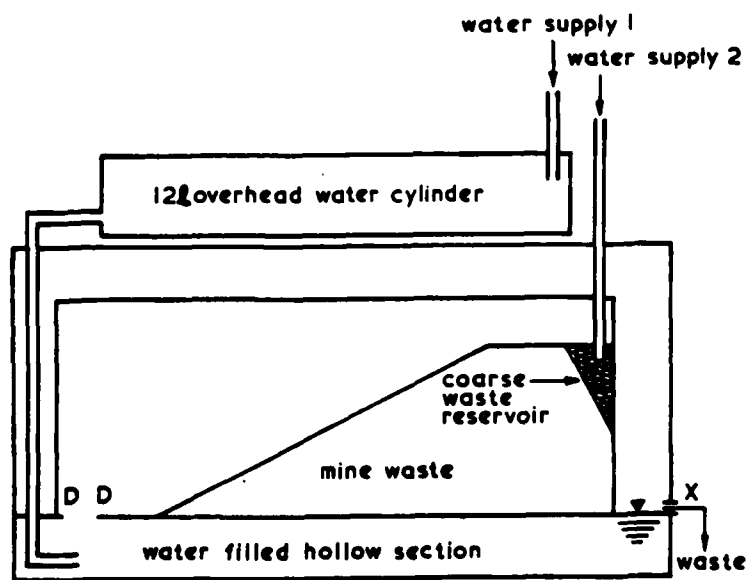


Figure 2.11 - Hydraulic System - Coal Mine Waste Models

standpipe Z\*. When this period of consolidation was completed, the valve a was opened, draining the water to the exit level X. By maintaining the water level in the water reservoir at point Z, a horizontal ground water table through the soil was to be achieved, accompanied by a constant surface runoff, overflowing from the supply to the sand filter, both draining continuously to level X.

In figure 2.10b, the system was modified to accommodate a more complex hydraulic system. The initial consolidation of the model submerged to depth Y, was achieved by filling the box to that level before the test, and shutting valve a. When the level was to be lowered, valve a was opened to permit drainage to exit level X. Uplift to some degree was constantly applied to the underside of the model, communicated along its length by a 15 mm medium sand filter (Leighton Buzzard 14/25). The minimum uplift imposed was controlled by overflow standpipe M, draining to waste through valve b; higher uplift was applied by shutting off valve b, and therefore standpipe M, until the reservoir rose to the level of overflow standpipe N. Continuous surface runoff was maintained by a second water supply line 2. All excess water drained out through exit X.

Water supply to the coal mine waste models was achieved without the liner but included the strong box bottom hollow section and an overhead 12 l water cylinder, as shown schematically in figure 2.11. An opening D-D was cut to permit landslide debris to fall into the water filled cavity of the bottom box section, draining level with D-D through exit X. A 12 l overhead cylinder was used to flush along debris which may have accumulated, blocking the hole D-D. The water supply line 2 fed water directly to the triangular coarse mine waste reservoir; this coarse material, 2.36 mm to 12.7 mm, dissipated the force of rapid water inflow,

---

\*Note that there exists a difference in actual heights between Y and Z, due to the curvature of the water surface caused by the curved centrifugal acceleration field.

preventing severe erosion of the finer embankment soil.

The rate at which water was supplied directly to the models through water supply line 2 was not easily controlled, restricted in maximum rate not only by the diameter of the feed lines, but also by the amount of water which the hydraulic slip rings would carry. This latter aspect was to some extent variable from test to test.

#### 2.4 Pore Pressure Measurement

Pore pressure changes in soil may result from "internal" or "external" change in state. The externally caused changes in a model are the direct results of changes in ground water table imposed by the researcher; monitoring these changes guarantees to the model maker that the changes he wished to implement, have been achieved. Internally induced changes in pore pressure are due to the soil response in shear to various perturbations. Monitoring internal changes gives an indication of soil behaviour, which the numerical analyst may study. This latter measurement, however, is more difficult to achieve: the measuring device must be precisely in the correct region, without altering soil response. Pore pressure measurement in these experiments was more successful from the point of view of the model maker, rather than the numerical analyst.

Effectiveness of pore pressure measurement depends on the permeability of the soil. Lyndon (1972) pointed out that for soils with a permeability of  $10^{-6}$  m/s or more, simple visual measurements using a manometer, was most suitable. Accordingly, manometers were used in the coal mine waste embankment tests for almost instantaneous visual recording, in most models.

In the clay models, where permeability may be very low, Druck Ltd miniature pore pressure transducers were used, with good response, in some of the later models. These transducers consisted of a 6 mm diameter porous tip over a strain-gauged diaphragm with linear voltage output over a

300 kN/m<sup>2</sup><sup>pressure</sup>/range. Values were recorded manually during the tests from a digital volt meter.

## 2.5 Photography and Video Test Records

Still photography was used to permanently record selected moments of the centrifuge model tests. The camera was mounted on a frame above the centrifuge chamber, on the level of the 2 m wide steel surfaced corridor, and viewed the model from above, through a perspex viewing window. Illumination of the model was achieved by a stroboscope, coordinated with the pass of the centrifuge under the viewing window.

Two cameras were used in the process of the tests, both capable of taking self developing polaroid pictures, useful during the test, and high quality negatives, suitable for later displacement analysis. The first camera, however, required manual changing of each photographic plate, limiting the speed of consecutive photographs, and the centrifuge safety regulations further restricted access to the camera during speed changes, and at speeds exerting greater than 50g. The second camera, a Haselblad, was equipped with a self advancing 70 mm film cartridge adapted for remote control triggering.

A second and very significant viewing facility was acquired during the progress of this research, which far excelled polaroid pictures for monitoring the model state during the test: the installation of a Sony television camera, fastened to the rotating structure of the centrifuge. This camera gave a continuous instantaneous, and permanent, replayable record of many of the centrifuge tests, cast up on a closed circuit television screen and recorded on videotape, figure 2.12. The accompanying audio track was used to record simultaneous observations and experimental steps. In order not to subject the video camera to higher accelerations than necessary, it was mounted as close as possible to the axis of the centrifuge, on a ~~steel~~<sup>duraluminium</sup> bracket. The quartz hallogen lights, installed

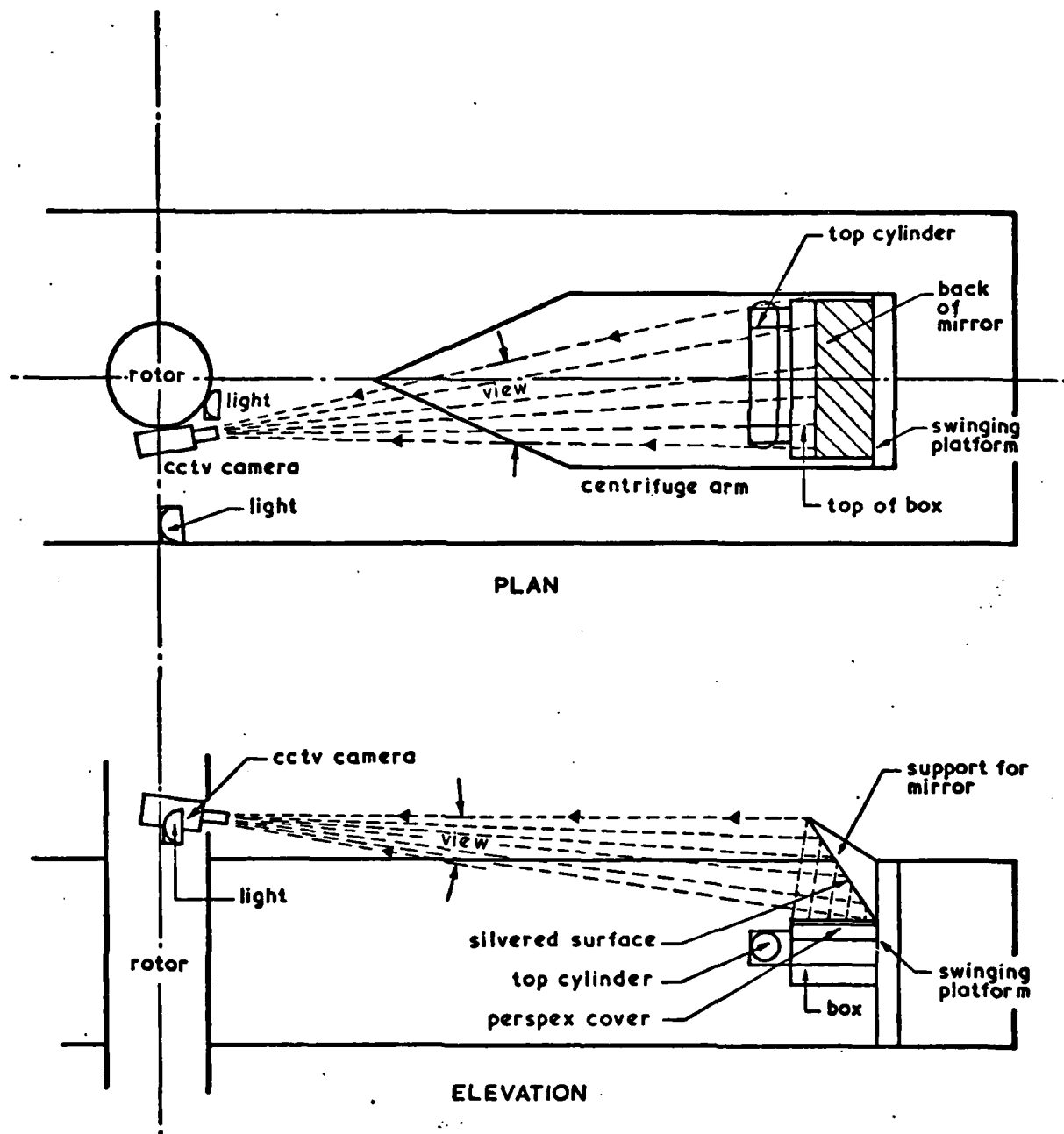


Figure 2.13 - Viewing Set-up for Video Recording

to illuminate the model, were mounted slightly cantilevered, in order to deflect the glare of their reflection off the perspex to the camera.

Since the video camera viewed along the arm of the centrifuge nearly parallel to the perspex face of the model, a mirror was needed to reflect the image of the model to the line of view of the camera. The installation of a braced perspex mirror at an angle sufficient to reflect an undistorted image, resulted in blocking the overhead view of the still photography camera, figure 2.13. For several experiments this compromise was a tolerable concession in order to determine the qualitative response of the model to various stimuli, while sacrificing the high quality still photography test record. When the mechanisms were more clearly understood, a different compromise was made: the mirror was remounted on a brace at a shallower angle which reflected a ~~distorted~~<sup>foreshortened</sup> image to the video camera, but which permitted a clear view from above for still photography. This arrangement proved to be the best for obtaining high quality photography at the right instant in the test, while still permitting interaction of the researcher with the observed model response.

### CHAPTER 3

#### CHAMPLAIN SEA CLAY - INTRODUCTION

##### 3.1 Landslides in Champlain Sea Clay

The sensitive Champlain Sea clays which overlies large areas of eastern Ontario and southern Quebec in Canada, pose a troublesome problem in planning and construction, in particular in areas under demand for urban expansion. Amongst other problems encountered by engineering projects founded in this clay, the frequency and size of landslides is formidable. Known landslides in this clay, larger than one acre in area, have been tabulated, numbering greater than seven hundred and fifty and of these, fifty of the largest ones which have been documented have been responsible for the loss of twenty thousand acres of uplands and the deaths of over one hundred people (Mitchell and Markell (1974)).

The unusual nature of Champlain Sea clay was recognised long ago by Dawson (1899), when he surveyed the mammoth flowslide which occurred in 1894 in St Albans, Quebec, involving sixteen hundred acres in area, and an estimated six hundred million cubic yards of soil. Two of the largest recent slides occurred in the spring of 1971: one on the South Nation River in eastern Ontario involving seventy acres and eight million cubic yards of soil, but claiming no victims (Eden et al (1971)), and a second slide in St Jean Vianney in central southern Quebec, only slightly larger in size, but tragically responsible for the deaths of thirty-one people (Tavenas et al (1971)).

The boundary of the area afflicted with this material is defined by the limits of the ancient Champlain Sea, from which the clay is named. The unifying feature of all these Champlain Sea clays, in addition to their similarity of origin and susceptibility to landslide activity, is



their high degree of sensitivity\*. A great deal of attention has been paid to the reasons explaining this, and contrary to early suppositions, the reasons currently accepted in Canada are not the same as for the sensitive Norwegian clays. The unusual behaviour of Canadian Champlain Sea clay is most often attributed to cementation bonding which developed early in its deposition history (Sangrey, (1972)).

The nature of the landsides which occur in the Champlain Sea clays is often not restricted to that of a simple, single, deep seated slip, but may progress into a large, catastrophic earthflow. Mitchell and Markell (1974) studied the problem of predicting the type of landslide to which a given slope is susceptible, by undertaking a programme of field survey and literature review of slides which had occurred throughout the entire area of the ancient Champlain Sea, in both Ontario and Quebec. They defined a distinct order to the progression of landsliding, which involved three classes of soil movement. Each slide, they said, begins with an initial shallow, slip which may be predicted using normal, drained, long term slope stability analysis. This may, in turn, be followed by retrogressive flow sliding during which the landslide boundaries are expanding step by step into the upper terrace of the slope. Within this phase the conditions of failure become transformed from the original problem of drained instability, now gradually involving deeper layers of material, until at a distance of approximately  $4H \cot \beta^{\dagger}$  from the toe of the slope,

---

\* Bjerrum (1973) defines sensitivity as the ratio of the undrained shear strengths in an undisturbed and a completely remoulded condition. It is usually measured by laboratory vane tests or fall-cone tests.

Most normal clays exhibit a sensitivity between 1 and 4, and "sensitive" clays are those which have a sensitivity greater than 4. In the extreme condition of a "quick" clay, the sensitivity is greater than 16 (Terzaghi and Peck, 1948).

<sup>†</sup> Where H = slope height, and  $\beta$  = angle of slope inclination.

an earthflow may develop. Such earthflow involves undrained, plastic, work-softening flow, causing the already large landslide to spread in size until it is stopped either by topographic or stratigraphic features, or when the energy dissipated equals the energy released at the backscarp as the crater widens.

Within each class of failure, the identifying characteristic at each slope was found to be the stability number,  $N_s = \frac{\gamma H}{C_u}$  \*: sites where landslides did not progress past the stage of a single deep seated slip had a stability number throughout the depth of slope consistently less than six in value; sites where retrogressive flowsliding was observed had stability numbers approximately equal to six; and in the instance of areas of earthflows, the value of the stability number exceeded six, at or above the depth of failure. Surprisingly, the correlation of type and distance of retrogression with degree of sensitivity, was much more obscure, although sensitivity is a necessary condition.

The similarity of origin, and property of marked loss of strength upon remoulding, belies the regionality of the clay properties. Along the lower St Lawrence River, and the Saguenay River, which drains Lake St John, the clay demonstrates a characteristic of a heavily over-consolidated clay (high  $p'_c$  values, as defined by Bjerrum (1973)), whereas the clay of the poorly drained, upper St Lawrence River valley is softer and only slightly over-consolidated. Both of these clays are characterised by banding, which reflects changing conditions during the period of deposition.

The clays of the Ottawa River valley are again different as a result of its higher, better drained topography, and its subtly different geological history (see section 3.2 below). These two factors have given rise to

---

\* where  $N_s$  = stability number,  $\gamma$  = unit weight of the soil,  $H$  = height of slope,  $C_u$  = peak undrained cohesive strength measured by in situ vane tests; this is the inverse of Taylor's (1937) stability number

a two tiered soil profile: the lower and softer clay is the product of the original Champlain Sea deposition under marine conditions, and the upper one the product of fresh water erosion and deposition of that original marine clay. Both are homogeneous in nature, although they are marked by a network of fissures which is very dense in the fresh water clay, and less so in the marine clay, and extends far below the depths of weathering. This latter feature distinguishes the Ottawa area clays in particular, and is the basis for a completely different mode of slope failure (Eden and Mitchell (1973)).

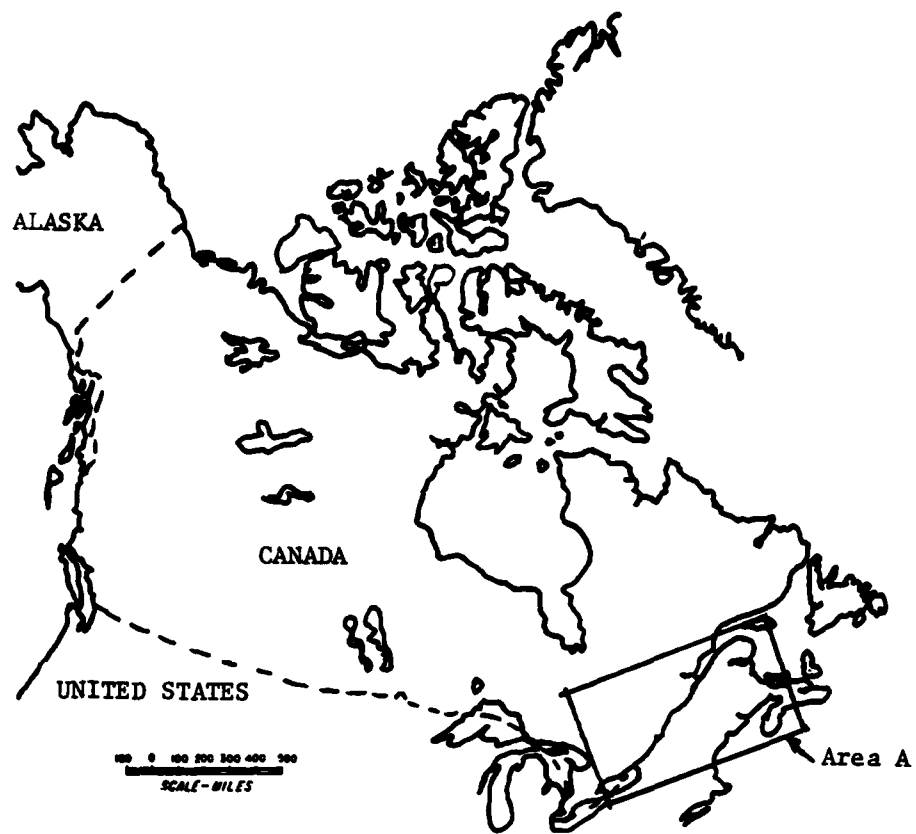
Regional studies intended to predict landslide susceptibility have been made: one by La Rochelle et al (1970) in the upper St Lawrence River valley, and one by Sangrey and Paul (1971) in the Ottawa area.

La Rochelle et al (1970) attached importance to the configuration of the underlying bedrock which governs the ground water pressure gradient; this hypothesis has not been tested beyond that region.

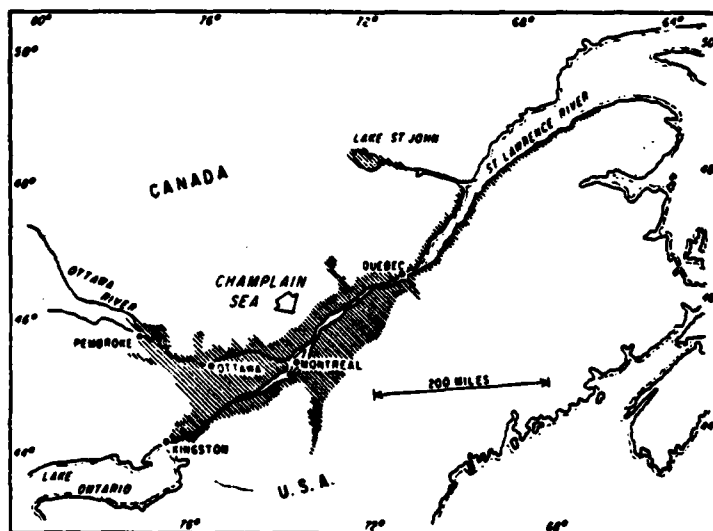
Sangrey and Paul (1971) investigated the influence of the fissures. Landsliding in the Ottawa area, they noted, is confined almost exclusively to the upper densely fissured, fresh water clay, and rarely extends into the less fissured, but softer and more sensitive underlying marine clay. The fissured nature of the clay permits a dilative failure mode to occur at stresses much less than the strength of the cementation bonds. Although the boundary between the two clays may be defined by the abrupt change in pore water chemistry, they lent no significance to this difference.

Eden and Mitchell (1970) also noted that slope failures in the Ottawa area occur only where inclinations are greater than  $22^{\circ}$ , although the slope height at failure may vary from 10 m to 30 m.

The mechanisms of slope failure were obscured for a long time by the unusual nature of the clay and its consequent failure modes. Bjerrum (1973) gave emphasis to the geological history and post depositional changes



(a) Canada



(b) The Champlain Sea ( Area A above)

Figure 3.1 - The Champlain Sea ( Crawford, 1968 )

of the soil. It is therefore wise to next consider this.

### 3.2 Geological History of the Ottawa Area Champlain Sea Clay

The last glaciers which covered the St Lawrence and Ottawa River valleys of Canada during the late Wisconsin continental glaciation, withdrew some 11,000 to 12,000 years ago. As the ice mass retreated, the isostatically depressed Ottawa River valley was flooded by the sea to a level 210 m above the present sea level at Ottawa and 190 m at Montreal. This inland sea, named the Champlain Sea, figure 3.1, changed in size as the glacier which formed its northern shore, retreated. When the isostatic rebound of the continent exceeded the eustatic rise of the sea level, after the final retreat of the glaciers, 8,000 to 9,000 years before present, the Champlain Sea was largely drained, although isolated lakes remained for sometime after.

During the retreat of the glacier, an abundance of finely ground rock was released in the meltwater, and sedimented in thicknesses 33 m to 66 m deep in the Ottawa area, and as deep as 80 m in the Montreal area. The pattern of particle size distribution and sequence depended on the distance from, and the nature of the source; apparent distortions in the bedding suggest that slumping occurred in its early history.

In addition to providing a source of sediment, the melting glacier supplied an influx of fresh water which gradually changed the water quality from salt, to a brackish condition. After the Champlain Sea had drained, further large fresh water discharges from the Great Lakes basin poured down the then much larger ancient Ottawa River, eroding and redepositing the marine clays in the Ottawa area. As a consequence of this particular geological history, at levels less than 100 m above present sea level in this Ottawa area, a layer of stiff clay, often more than 6 m thick and non-marine in character, overlies the soft, and more sensitive original marine clay (Karrow (1961), Gadd (1963), Sangrey and

Paul (1971)).

Two subtle post-depositional changes were especially important to the behaviour of the present Ottawa area Champlain Sea clay. These changes caused the development of a fissured, cemented clay.

Early in the history of the clay, cementation bonding occurred which imparted a strength greater than the stress of the final overburden, while preserving an open, high voids ratio structure. A range of compounds which may be responsible for the cementation is discussed by Sangrey (1972), but the process still remains something of a mystery.

The cause of the fissured nature of the Ottawa area Champlain Sea clay far below the possible depths of weathering is another mystery. Eden and Mitchell (1970) suggest this may have been the result either of stress relief as the overburden was removed, with the conflicting influence of the cementation bonds and the swelling pressures, or fatigue felt in the cemented clay as seasonal temperature and groundwater changes caused long periods of repeated loading and unloading.

La Rochelle et al (1970), explained that all such sensitive clays deposited in the whole area of the ancient Champlain Sea were originally referred to as "Leda clay", after the Leda fossils reported to have been found by an early geologist. Gadd (1963) recommended that the name be changed to Champlain Sea clay, since none of the Leda fossils have been found in more recent investigations.

### 3.3 Landslide Mechanisms in Ottawa Area Champlain Sea Clay

In spite of Mitchell and Markell's (1974) attempt to make some broad generalisations on types of landslides in Champlain Sea clay, the marked regional variation in details of strength characteristics, caused by the different geological backgrounds, severely restricts the applicability of detailed slope stability analysis beyond the limits of any given area; in that sense the research described here is limited, being

concerned only with the nature of slope instability in the Ottawa area.

In the vicinity of the city of Ottawa, massive earthflows seldom occur, however retrogressive landslides initiated by a simple deep seated slip, are not infrequent, and cause concern for both potential and existing structures. Understanding these slides so that proper design or remedial work may be undertaken has obvious importance, and was the subject of much attention.

The two principle sets of studies take conflicting positions. K.Y. Lo, at the University of Western Ontario, proposed that the mechanism of failure responsible for the landslides was a progressive failure of the type discussed by Bishop (1967). R.J. Mitchell and W.J. Eden, from Queen's University at Kingston, and the National Research Council of Canada, respectively, supported a conventional limit equilibrium approach to the instability problem, with a dilative-frictional failure mode.

Bishop (1967) defined progressive failure as a phenomenon whereby a locally overstressed region of soil is strained until its peak strength is exceeded, whereupon some adjacent soil is forced to take up the excess load. This material also responds in the same manner and a zone of failure propagates to the soil boundaries, at which point failure occurs. Bishop recommended that structures built with or on soil susceptible to progressive failure be designed according to a post peak failure envelope.

Lo (1972) defined two necessary characteristics for soils in which progressive failure may occur: they must possess both a strain-softening, post-peak stress-strain relationship, and stress strain discontinuities. Lo and Morin's (1972) investigation, using Champlain Sea clay from the upper St. Lawrence River valley in a programme of conventional, strain controlled, constant  $\sigma_3$  triaxial tests, demonstrated that the soil exhibited marked initial anisotropy, brittle strain-softening behaviour, rate of testing effects upon the peak strength value, and non-uniformity of stress and strain distribution in the soil, any combination of which is sufficient for progressive failure. Tavenas et al (1978) also noted time dependent

effects in a lower St Lawrence River valley clay.

Although this implied that Lo's slope stability analysis should be executed by a finite element approach with progress of failure during a succession of time intervals, a satisfactory but conservative initial stability analysis may be achieved using the residual strength value in regular limit equilibrium analysis. In Lo's triaxial test programme, a large decrease in strength was noted until large strain had occurred in the order of 50%, but the relevant post peak strength referred to by Lo and Morin (1972) occurred after much smaller strain, in the order of 15%.

Lo and Lee (1974) reinforced the validity of their position by back analysing eleven known failures, not only in the region of origin of the clay test specimens, but also in the Ottawa area. Their success, they suggested, indicated that their results have geographically extensive significance. They considered that this wide applicability confirmed the correctness of their use of residual strength, which is insensitive to site specific characteristics such as anisotropy, in situ pore fluid, and test type. They also referred to work done by Mitchell and Eden (1972) which involved the monitoring of slope movement over three years, one slope of which later failed, and took these movements to be the indication of imminent, time dependent, progressive failure.

Mitchell (1975) maintained that strength characteristics are not only strictly limited to a given region, especially in the Ottawa area where the unusual fissure characteristic dominates low stress soil behaviour, but that the stress path and stress region are even more important. Mitchell's examination of field conditions indicated that the average effective normal stress on observed failure surfaces was in the order of  $20 \text{ kN/m}^2$ , and consistently less than  $100 \text{ kN/m}^2$ . Slope failures were observed to be preceded by the opening of tension cracks with much greater horizontal than vertical displacement, accompanied by very wet conditions, and ending with debris which had broken along pre-existing



fissures into a mass of nodules, all suggesting a dilative failure mode. When an in situ stress path at the correct stress level was followed in his drained, stress controlled, constant  $p'$  triaxial programme, these characteristics were also noted in the test specimens, and he noted a distinct absence of any time effects, anisotropic peculiarities, or appreciable strain softening. Although the yield point was identified at strains in the vicinity of 1%, the clay was capable of sustaining loads greater than yield load, at much greater values of strain, (Mitchell and Wong (1973), and he therefore rejected the progressive failure concept. He demonstrated also, that if the same Ottawa area clay as he subjected to constant  $p'$  tests, is alternatively subjected to a conventional triaxial stress path, then a different failure mode, similar to the strain softening results of Lo and Morin (1972), may be observed. Eden and Mitchell (1970) tested the validity of these strength parameters by back calculating the failures of three Ottawa area landslides using the simplified Bishop (1955) limit equilibrium approach.

Mitchell and Eden (1972), monitoring field slope movements, noted that pore pressure is a critical feature in slope stability analysis. When a clay specimen is loaded to within 85% of its failure load, stable strain can be induced and arrested by the fluctuation of pore pressure. Time effects are felt because of the restriction which permeability places upon the rate of water supply to the dilating area. As dilation occurs, however, the permeability is increased, so that provided the water is available, the negative pore pressures associated with dilation are almost immediately quenched. It has been observed that in the absence of tension cracks, a slope may settle to a lower angle, the upper terrace moving down, the toe moving out and some bulging occurring, without the slope demonstrating abrupt landslide characteristics.

Mitchell's hypothesis seems to be the more logical position, and appears to be verified by field observation and successful back calculation.

Against this background it is clear that the centrifuge tests may be able to provide a further insight into failure mechanisms by being able to observe and monitor actual, albeit miniature, landslides at the instant in which they occur, but a correct understanding of the yielding and mechanical strength of soil in the Champlain Sea clay slopes, may illuminate the results of these centrifuge tests, as will be seen in the next section.

### 3.4 Yielding and Mechanical Strength of Ottawa Area Champlain Sea Clay

The apparent similarity between the Champlain Sea clays and the Norwegian quick clays, both demonstrating a dramatic loss of strength upon remoulding at the in situ water content was recognised early in the study of soil mechanics, and an attempt was made to draw upon Norwegian experience for an understanding of the Canadian problem. A great deal of attention was focussed upon determining the causes for sensitivity (see for example, Penner (1965), Cabrera and Smalley (1973), and Torrance (1975a)), the component of cohesion (Crawford (1963), La Rochelle et al (1973)), and upon documenting both settlements (Crawford (1953), Burn and Hamilton (1968), Bozozuk and Labrecque (1969)), and of course landslides, (see Mitchell and Markell (1974) for references to 41 large documented landslides). When at last it became clear that the behaviour and reasons for sensitivity of Canadian Champlain Sea clays were not the same as for the Norwegian quick clays (Sangrey (1970), Sangrey and Paul (1971)), and that the unusual nature of their behaviour could be largely attributed to cementation (Townsend et al (1969)), which had previously been obscured by both the disturbing effects of the sampling methods (Raymond et al (1971)), and the regionality of the clay properties (Eden and Mitchell (1970)), work which began to yield reasonable and useful predictions of soil behaviour began to appear. Many authors have contributed to the assembling of information on this clay. However, the best in depth analysis

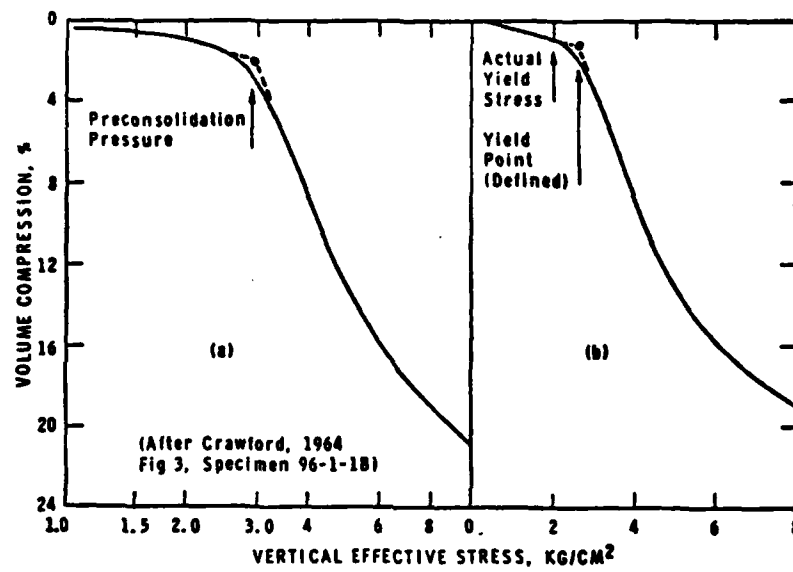


Figure 3.2 - Typical Consolidation Curves for Champlain Sea Clay  
( Mitchell, 1970b)

of the mechanical strength and yielding of Ottawa area Champlain Sea clay is contained in two papers: Mitchell (1970b) and Wong and Mitchell (1975). The earlier paper interprets the results of tests performed on samples from the Rockcliffe 1967 landslide site in the Ottawa area and the later paper examines the behaviour of clay taken from an excavation within the city of Ottawa, which is considered to have very similar properties. The general characteristics of yielding and mechanical strength are presented, as they will be here also, within the framework of the critical state theory, first presented by Roscoe et al (1958).

A naturally cemented clay can be identified in a test as simple as the one-dimensional consolidation test, by two salient features which distinguish it from non-cemented clay. The shape of the curve when volume compression is plotted against vertical effective stress, for example in figure 3.2, shows an abrupt increase in compressibility, and this is followed by an inflection in the curve, in the vicinity of the apparent preconsolidation pressure. These features are associated with the rupture of cementation bonds, rather than the normal yielding observed in non-cemented soils as the stress exceeds the original preconsolidation stress. Sangrey (1972) suggested that the extrapolation of the lower, steeper part of the curve back to the initial shallow segment would define the true original overburden, which is otherwise obscured by the strength of the cementation bonds. The abrupt change in soil behaviour which occurs at the yield point is the first and most obvious division demarcating different modes of behaviour.

The soil behaviour before yielding is quasi-elastic in nature: compression is small and mainly recoverable. Perfectly elastic behaviour may be defined in terms of two effective parameters: Young's modulus,  $E'$ , and Poisson's ratio,  $\nu'$ . The quasi-elastic behaviour of the Ottawa area clay may also be described in terms of these parameters, although as the stress level approaches yield, an increase in both is noted: at low

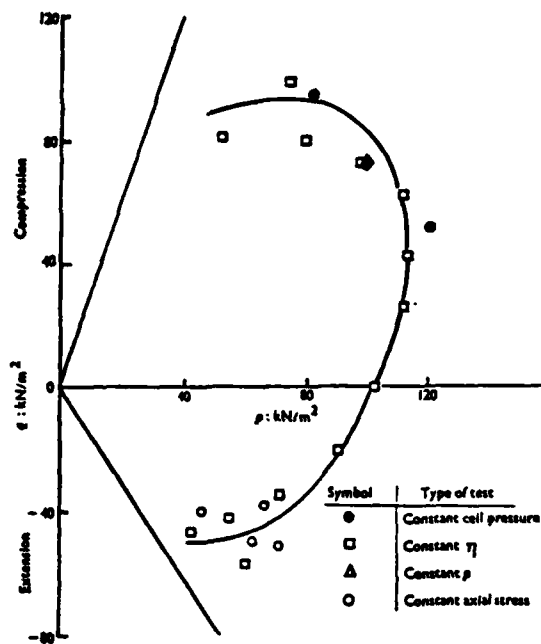


Figure 3.3 - Yield in p-q Plane for Vertical Samples  
(Wong and Mitchell, 1975)

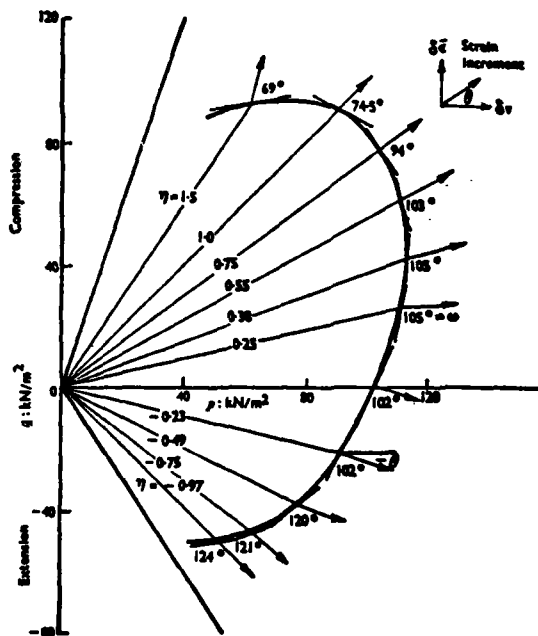


Figure 3.4 - Experimental Evaluation of the Normality Condition  
(Wong and Mitchell, 1975)

pressures,  $E'$  and  $\nu'$  range from  $10 \text{ MN/m}^2$  and  $0.20$ , respectively, to values of  $25 \text{ MN/m}^2$  and  $0.30$  as yield is approached. This variation is attributed to the influence of the network of microfissures.

At very small distortional strain, equal to approximately  $1\%$ , the soil yields. Deformation thereafter is large and generally irrecoverable, in the nature of plastic behaviour. The establishment of a unique yield envelope which defines the combinations of stresses beyond which behaviour is plastic, and thus may constitute engineering failure, is a valuable design tool. This curve was determined from drained triaxial tests following a constant  $\eta$  ( $= \frac{q}{p}$ ) stress path, and confirmed to be independent of the stress path by similar results from constant  $p$  and conventional constant cell pressure tests, figure 3.3. The asymmetry of the yield curve, however, indicates anisotropy which is attributed to the directionality of the cementation bonds which were formed under a  $K_0$ , anisotropic stress system. At high stresses, when the cementation bonds have been destroyed, these effects are eliminated.

Once the soil has passed its yield point, its response to further stress is plastic. Wong and Mitchell (1975) set out to test their experimental data against the plasticity model discussed by Roscoe et al (1958). The first difference noted was a disagreement with normality, that is the rule which predicts that the vectors of plastic strain increments, following initial yield, will be perpendicular to the tangent of the yield curve plotted in  $p$ - $q$  space, according to the current  $\eta$  ratio. The Ottawa Champlain Sea clay did not adhere to this theory, figure 3.4. Thus, abandoning assumptions regarding normality and work dissipation, they proposed a plasticity model specifically designed to describe their experimentally derived flow rule. In comparing their equation for the empirically defined flow rule to the Cam-clay model, they found that the energy dissipated due to irrecoverable volumetric strain was significant under all stress ratios, unlike the assumptions of Cam-clay, and that

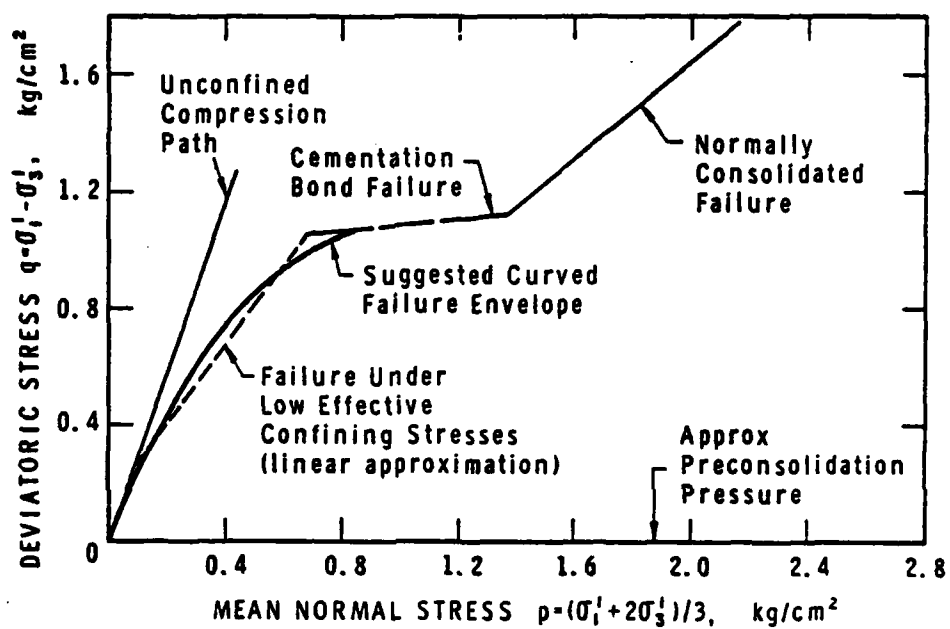


Figure 3.5 - Mechanical Strength of Champlain Sea Clay in Triaxial Compression ( Mitchell, 1970a )

there was a closer resemblance to Roscoe and Burland's (1968) "modified Cam-clay" flow rule. Further analysis and calibration of the experimental data led to the formulation of equations describing plastic potential and the yield locus, and these equations were successful in nearly replicating the experimentally established yield surface. Stress-strain, and volumetric-distortional strain curves were also predicted satisfactorily.

These equations were derived with extensive examination of experimental data, however they noted, by making the reasonable assumption that all Ottawa area cemented sensitive clays are governed by initial yield curves which are similar in shape to that derived by Wong and Mitchell (1975), the trends established may be directly applied to predictions of behaviour of this class of clays by merely establishing the apparent preconsolidation pressure in an isotropic consolidation test.

The mechanical strength of Champlain Sea clay also seems to be at variance with the simple critical state theory of soil failure, which predicts failure to occur at a constant critical ratio of  $\frac{q}{p} = M$ . This disagreement arises from the cemented and fissured structural peculiarities of the clay. The failure characteristics are very much dependent upon the current average stress region, figure 3.5.

In the lowest stress range, failure occurs in a dilatant fashion. The dense network of fissures opens up, drawing in water to satisfy the resulting negative pore pressures, and finally failing by breaking into a blocky rubble of irregular, prismatically shaped pieces, 1 mm to 10 mm on a dimension. These nodules are quite sensitive themselves when remoulded, however in this stress range this remoulding does not naturally occur. This low average stress range and failure mode is consistent with natural slope stability problems. The relation of  $q$  to  $p$  at failure is defined by a curved line, which emphasises the importance of testing at the field stress levels.



The next intermediate stress region is associated with a different mode of failure. Instead of dilation, failure occurs by shearing through the fissure blocks, breaking down the cementation bonds until a continuous rupture surface forms. For a given specimen orientation the deviatoric stress at failure is approximately constant, but anisotropy is noticed at this stress level, attributed to the directionality of the cementation bonds. This stress region is applicable to the design of structures adding additional weight to the soil in cases such as embankments or foundations.

In the highest stress region, the structural peculiarities of the soil, the fissures and cementation bonding, have been destroyed, and the soil behaviour reverts to that predicted by the critical state theory, failing at a constant  $\eta$  ratio. This stress range however is of little practical significance.

Mitchell and King (1977) have investigated the effect of cyclic loading on Ottawa area Champlain Sea clays, which may be significant in designs where vibrations may occur in the form of either earthquakes, winds or waves or blasting and foundations for vibrating machinery. They found that an effective stress failure may occur in an undrained specimen due to the buildup of excess pore pressures, accompanied by distortional strains much larger than the customary static case where yield occurs at 1%. The initial confining pressure and the magnitude of the cycling deviatoric stress are both important factors, although it is unlikely that a short duration of loading cycles (less than one hundred) will cause failure unless the static strength of the soil is exceeded. In designs where cyclic loading is anticipated to be a problem, a minimum safety factor of two is recommended.

### 3.5 Object of the Model Tests

The object of these tests was to observe and define the mechanisms of failure occurring in slopes cut in cemented, sensitive, Ottawa area Champlain Sea clay. Soil samples from one site were to be formed into a variety of slope models and tested on the geotechnical centrifuge. One check on the significance of the phenomena observed could be their relation to a full scale failure in the same material. This would be possible if the site from which the samples were to come had had a particular failure which occurred and was well documented.

Regardless of whether the correctness of the centrifugal modelling could be partly confirmed in this way, by taking a variety of models with different shapes, the factors relevant to this method of modelling could be defined. In any case, the fundamental groundwork would be established and the researcher would be free to examine the various factors affecting soil response and causing failure.

### 3.6 The Selection of the Rockcliffe Site

The selection of a site for sampling and centrifuge modelling of slope stability in Champlain Sea clay was done with the guidance of R.J. Mitchell at Queen's University at Kingston, Canada, and reflected many practical considerations.

In April 1967, a landslide occurred at the Canadian Forces Base Rockcliffe, located in the vicinity of the city of Ottawa on the south bank of the Ottawa River. The failure involved one major slip followed by one or two retrogressions, encompassing one acre in area and thirty thousand cubic yards of soil. Although not a massive and major earthflow, the landslide was large enough, and attracted sufficient attention from engineers in the Ottawa area to be well documented with respect to both its overall external characteristics, and its soil properties, while at the same time, it was typical of slides in the Ottawa River banks in

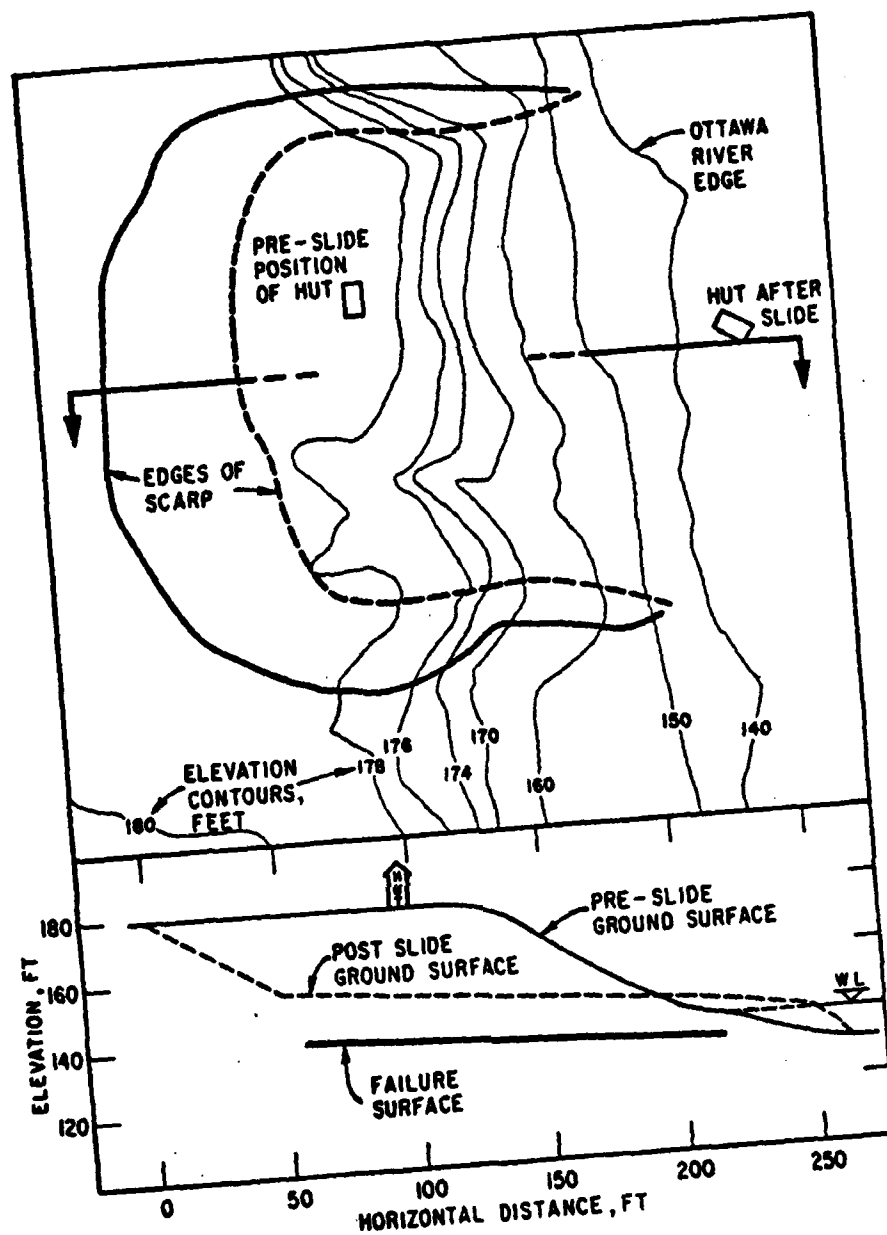


Figure 3.6 - Plan and Profile of the Rockcliffe Landslide ( Mitchell, 1970a )

the Ottawa area. It was suitable for centrifugal modelling because it was of dimensions which could be modelled within the speed, and model size limitations of the Cambridge geotechnical centrifuge.

The soil involved was macroscopically uniform, in contrast to the usual banding observed in the Champlain Sea clay in other areas, although there was a dense network of fine fissures which would remain unscaled in reduced scale modelling. The clay was cemented, which meant that provided no strain was permitted, the soil structure and in situ pore pressures would remain constant even when removed from the in situ conditions, giving an excellent chance of retrieving and transporting high quality samples to Cambridge (Crawford (1963), Bjerrum (1973)).

Equally important practical reasons for the site selection included Mitchell's interest in the area and its accessibility, from which samples could be retrieved. Future field work was also planned by Mitchell, and so he agreed to obtain and forward the necessary soil samples to Cambridge.

### 3.7 The Rockcliffe Landslide and Clay

The landslide which occurred at Rockcliffe during the unusually wet spring of 1967 is shown in plan and profile in figure 3.6. The slide was described as having occurred with one major slip followed by one or two observed retrogressions. The slope before the slide was a uniform natural slope varying from  $24^{\circ}$  to  $27^{\circ}$  in inclination, with a top terrace draining toward the river at an angle of  $0.5^{\circ}$ . The crest of the slope stood at elevation 55 m above sea level, with a height of 12 m; the depth of failure was 14 m and the final backscarp, 8 m in height. The total distance of retrogression was 67 m, and the width of the crater was also 67 m (Mitchell and Markell (1974)).

The soil profile at the site is illustrated in figure 3.7. The soil is described as stiff, grey, fairly uniform, moderately sensitive clay, with a dense network of fine fissures throughout and below the depth

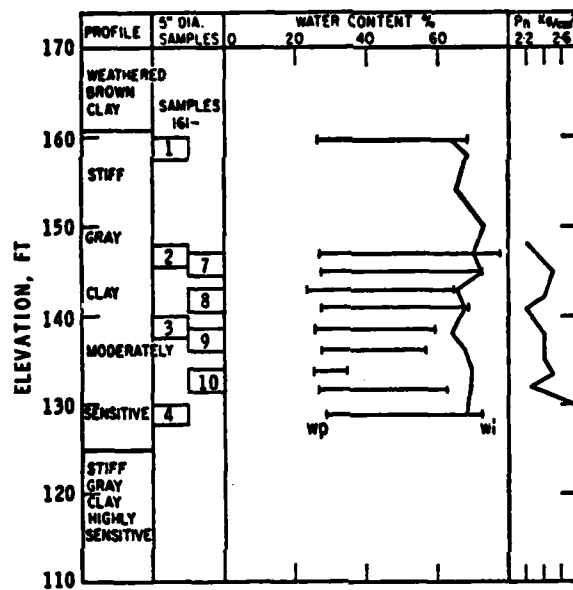


Figure 3.7 - Rockcliffe Landslide Soil Profile ( Mitchell, 1970b )

of failure. Mitchell and Markell (1974) characterised the soil as:

water content	68%
liquid limit	80%
plastic limit	30%
sensitivity	35
unit weight	16 kN/m <sup>3</sup>
specific gravity	2.8 (Crawford (1963)).

The soil contains 54% clay size, which in a general mineralogy analysis of the Ottawa area clays, recorded in two papers by Soderman and Quigley (1965), and Sangrey (1972) has the approximate proportions of:

illite (hydrous mica)	50-60%
iron chlorite	10-15%
vermiculite	5-10%
montmorillonite	5%
quartz and feldspar	10-20%
pseudo chlorite	5-10%*.

Mitchell and Markell (1974) record the <sup>chemical</sup>~~cation~~ pore water <sup>composition</sup>~~concentration~~ of Rockliffe as:

calcium	4.6 ppm
sodium	375 ppm
potassium	22 ppm
Magnesium	4.7 ppm
Iron	0.1 ppm <sup>†</sup>

\* Both Penner (1965) and Cabrera and Smalley (1973) drew attention to the mineral composition of this clay, emphasising the non-swelling nature of illite, and the presence of quartz and feldspar, primary minerals which both have small surface areas and thus low interparticle attraction, as compared to typical clay minerals.

<sup>†</sup> Penner (1965) established that, contrary to the conclusions of Norwegian research into sensitive clays, sensitivity in Canadian Champlain Sea clay was not a function of salt content, but he found that it may be related more effectively to electrokinetic potential. Sangrey and Paul (1971) however, have suggested that the ratio of sodium to calcium ions may be useful to determine the conditions of deposition: high values being indicative of marine conditions, and low values of fresh water conditions, however they do not define typical ranges.

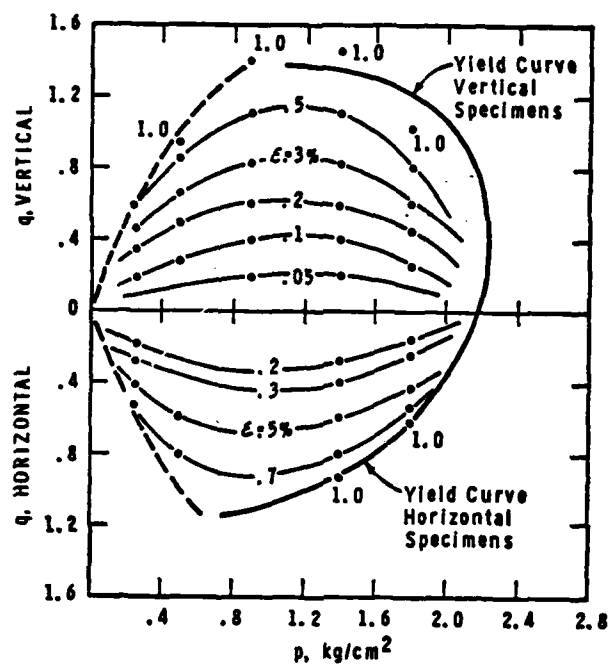


Figure 3.8 - Contours of Equal Strain from Constant  $p'$  Tests  
( Mitchell, 1970b )

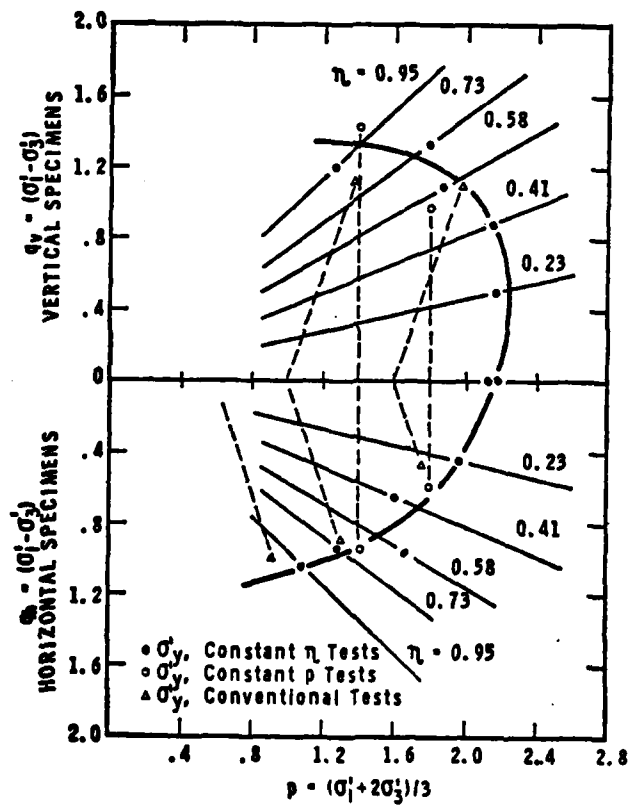


Figure 3.9 - Yield Curves in Triaxial Compression ( Mitchell, 1970b )

The cementing agents may be one of a number suggested by Sangrey (1972), including calcium carbonate, aluminium and iron hydroxide, or organic compounds and amorphous manganese oxides.

Field work done by Williams\* to investigate permeability showed notable variation according to the measuring method used, and most markedly when compared to laboratory test results. He concluded that the best field test, using piezometers, gave a value of  $k = 1.5 \times 10^{-5}$  mm/s. It should be remembered however, that permeability increases as dilation occurs. (Eden and Mitchell (1970)).

The strength characteristics of the clay were derived by Eden and Mitchell (1970), and Mitchell (1970b), using predominantly constant  $p'$ , stress controlled triaxial tests, which are similar to the stress path of the field slope stability problem (Mitchell (1975)), and which have the additional advantage of permitting the observation of volumetric strain due to shear, rather than to volume changes, which would occur under a changing mean normal stress. Eden and Mitchell (1970) found that the resulting strength parameters were insensitive to sample depth, once below the weathered crust, so that all data of specimens retrieved from all levels were equally significant in analysis.

Mitchell (1970b) established unique strain contours, figure 3.8, preceding yield, and concluded from their orientation that the original consolidation stress ratio,  $\eta$ , was in the order of 0.41. The preconsolidation pressure, he also found, varied from 200 kN/m<sup>2</sup> at 3 m deep, to 250 kN/m<sup>2</sup> at 12 m (Mitchell (1970a)). He defined a unique yield curve for the Rockcliffe clay, for yielding which occurs at strains in the order of 1%, figure 3.9. He noted that this curve is independent of time and stress path effects, but is influenced markedly by anisotropy.

---

\* D. Williams, Queen's University, Canada, personal communication (1978).



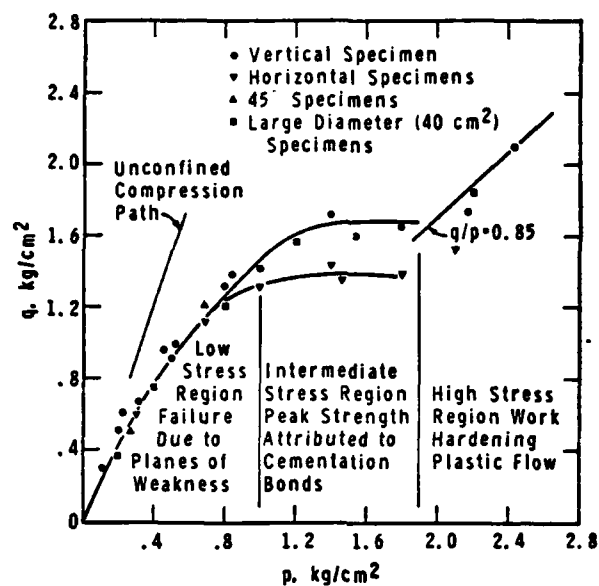


Figure 3.10 - Mechanical Strength ( Mitchell, 1970b )

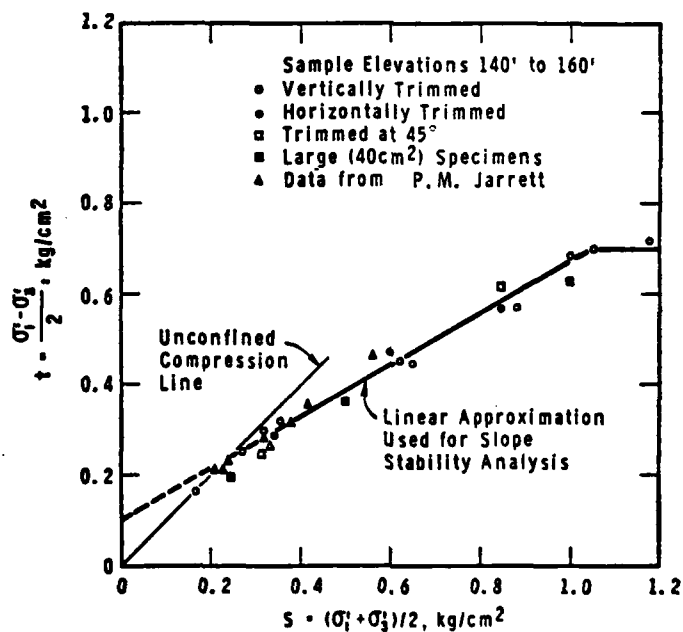


Figure 3.11 - Strength of Rockcliffe Clay ( Eden and Mitchell, 1973 )

Failure may occur after prolonged straining, and some work hardening in a constant  $p'$  stress path test; the failure envelope is defined by figure 3.10. The stress region relevant to slope stability analysis is that where  $p' \leq 100 \text{ kN/m}^2$ . Failure occurs by dilation, the soil breaking into nodules along microfissures found throughout the depth of the soil. Failure is insensitive to specimen orientation, rate of testing, and stress path. The curving nature of the critical stress ratio in this low stress region indicates that if the soil strength is described using the conventional effective cohesion and friction parameters, then their values must vary according to the mean effective stress at failure.

For the Rockcliffe landslide the relevant values of cohesion and friction are  $c' = 12 \text{ kN/m}^2$ , and  $\phi' = 33^\circ$  (see figures 3.11 and 3.12), and using the Bishop (1955) slope stability limit equilibrium analysis, assuming total saturation so that  $r_u = 0.62$ , the safety factor is in the vicinity of one. Trial slip circles in the analysis correctly predict at least one retrogression, when the circles are forced to be tangent to the failure surface established by vane testing (Eden and Mitchell (1970)).

The values of undrained cohesion from the vane tests range from  $35 \text{ kN/m}^2$  to  $100 \text{ kN/m}^2$ , with a sharp differentiation at the failure surface. (Mitchell (1970a)). Using Mitchell and Markell's (1974) method for predicting the type of failure based on the stability number,  $N_s = \frac{\gamma H}{c_u}$ , only the lowest values of strength reported at the Rockcliffe site would indicate it to be a possible site for an earthflow, and the indication of average strength is that the site is more likely to exhibit retrogressive sliding, which was in fact the case.

### 3.8 Retrieval of the Rockcliffe Samples

Eight separate soil samples were retrieved from the Canadian Forces Rockcliffe Base in Ottawa, and shipped to Cambridge over the course of ten months for use in centrifuge modelling. The cost was borne by the

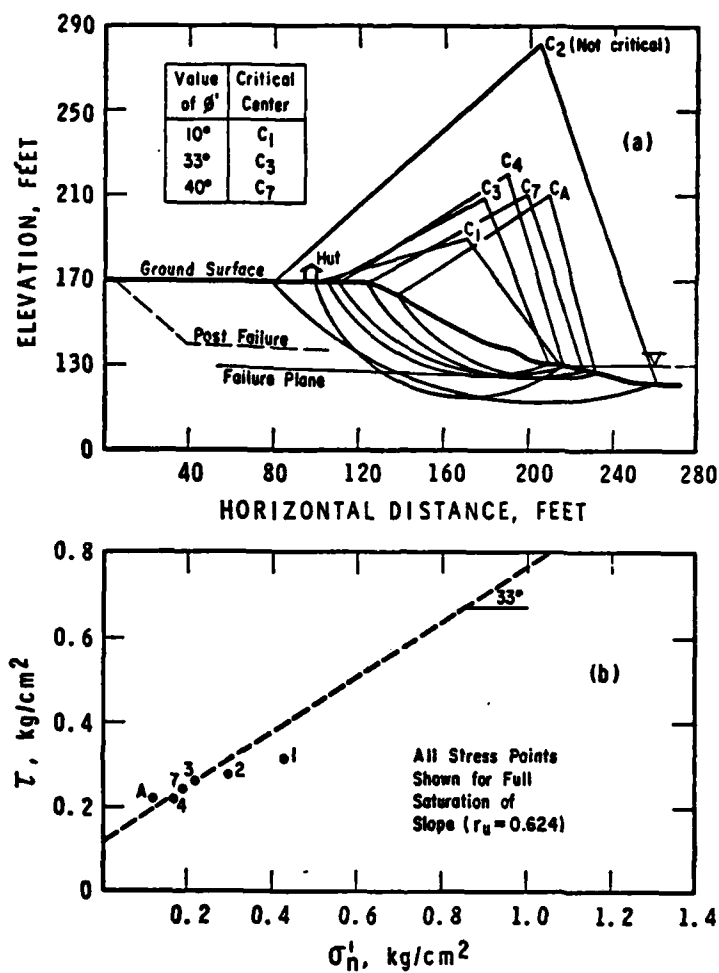


Figure 3.12 - Analysis of the Rockcliffe Landslide

(a) Critical Circles

(b) Critical Stress Points ( Eden and Mitchell, 1973 )

National Research Council of Canada through a research grant to Dr R.J. Mitchell of Queen's University at Kingston, Canada. Dr Mitchell very generously undertook to personally retrieve, pack and send off to England, the requested samples. The author was present during the first sampling exercise in October 1976, but not for the second exercise in June 1977.

The prototype Rockcliffe landslide which had been selected for this research, had occurred dangerously close to an airfield and its hangar, and was regraded soon after the slide occurred. It was therefore not possible to retrieve samples at the original site. Some five hundred metres downstream, however, was a scarp from a small single slip landslide which had occurred in the spring of that year, 1976. This site, on which further research work was projected by Queen's University, was selected for sample retrieval. The elevation was approximately the same as the site of the large landslide upstream, and the fresh scarp, marked by further tension cracks in the weathered crust, seemed to present an ideal site for sampling.

The depth of sample retrieval for all eight specimens was in the region of sample '1' in figure 3.7, a depth of approximately 4 to 4.5 m below the elevation of the terrace. This was below the weathered crust and the effects of surface grass vegetation, and within the depths of constant groundwater. The soil appeared as a moist, grey, uniform, cohesive mass, with its typical fine network of fissures.

The first sampling exercise in October 1976 involved two specimens: one retrieved in a painted steel vertical cylinder of 3 mm in thickness, 953 mm in diameter, and 508 mm deep, with sharpened bottom steel cutting edge, and the other one in a steel horizontal cylinder, 3 mm in thickness, 508 mm in diameter, 608 mm long, also sharpened at one end. The sampling containers, obviously retrieving very differently sized specimens, required two methods of application.

The larger container was designed to be used by pushing it vertically into a bench of soil. To this end a bench was cut into the scarp of the recent slide; this bench was large enough for sampling and was below the shallow layer of recent surface weathering. The sample ring was placed level on the bench and a heavy wooden skid positioned on top. The ring was pressed into the soil, first jacked until it was securely level, and then pushed completely in, in one stroke by the arm and bucket of an excavator. The surrounding soil was dug away and the final cut beneath the sample was accomplished using a wire pulled beneath the sample ring. The sample was slid onto the wooden skid and removed to the top of the terrace by the excavator. In the side of the now deepened bench the other 508 mm diameter tube was pushed horizontally with one continuous motion of the excavator bucket and was dug out. Both specimens were transported back to Kingston by van, where the uncovered soil surfaces were sealed with wax.

The second group of samples to be received involved six horizontal tubes, 3 mm thick, 356 mm diameter, 760 mm long. These were retrieved in June 1977, at the same site and depth, in a fashion similar to the previous horizontal tube sample. The author was not present for this retrieval exercise.

The samples were packed for shipping in three different manners. The large diameter sample was first capped with concrete. It was then removed to a special shipping pallet which had been prepared by driving four lag screws through it such that the soil sample could sit amongst them; in addition, this pallet had been resurfaced with a rigid concrete slab 25 mm in thickness. The sampling ring was withdrawn, restraining the sample by its concrete cap. The remaining bare cylinder of soil was immediately wrapped in cheesecloth, sprayed with polyurethane foam and a concrete shell poured around it, and including the lag screws, so that the concrete surrounded sample and the pallet were one single, one ton

package.

This packing of the large vertical sample was undertaken in December 1976 for a January 1977 shipping across the ocean. It was transported by train to Quebec city, where, despite efforts to impress upon the shipping company the temperature sensitive nature of the soil, it was exposed to unheated conditions for seven days during an unusually cold January before it was loaded into the hold of the ship.

When this first sample was received in England the concrete shell had a major crack across its diameter and down one side. Clear water leaked from the crack and a bore hole indicated that the soil had settled some 75 mm over its original 440 mm depth. The soil was disturbed and somewhat drier than in situ moisture content, but it was not remoulded. The fissured blocks were quite intact themselves. It appeared that the sample had undergone freezing, and this seemed to be confirmed by Mitchell\*, according to the soil description.

This unfortunate occurrence resulted in shipping the other of the first samples by air, courtesy of the Canadian Armed Forces. The 508 mm diameter horizontal tube sample was packed in a wooden crate protected by polystyrene pellets and resting on end on a thick foam rubber mat. This sample was received in April 1977 in a satisfactory condition.

The last six samples, retrieved in June 1977 were packaged in a combination wooden crate and pallet. The cylinders were prepared by capping the waxed soil surface with concrete, and then casting light weight, shock absorbent vermiculite concrete around the six samples, as a single block within the crate. This final shipment arrived in July 1977 by ship, in a satisfactory condition.

Details of the soil properties measured in Cambridge are given in the next section.

---

\*R.J. Mitchell, 1977, Queen's University, Canada, personal communication.

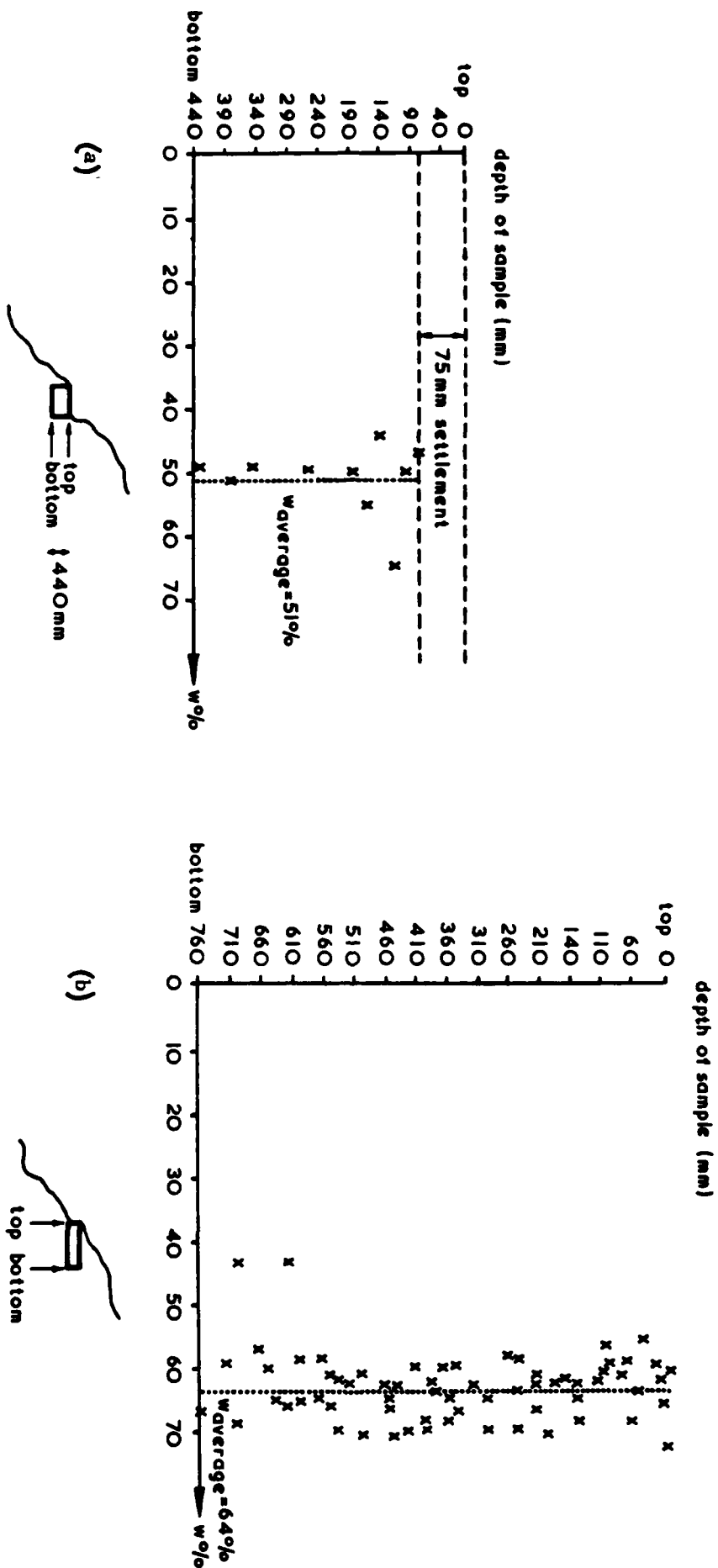


Figure 3.13 - Moisture Contents of Soil Samples upon Arrival  
 (a) CSC1 through CSC4 (frost damaged soil)  
 (b) CSC10, CSC20 through CSC25

### 3.9 Rockcliffe Soil Properties Measured in Cambridge

The Champlain Sea clay samples which arrived in Cambridge from Canada had been subjected to the multiple rigors of sampling, and transport over a long and multi-staged journey. There is no doubt that the vibrations and jolting imposed an unnatural stressing condition on the soil, in spite of the beneficial effects of the cementation bonds and the exact fitting containers. Even if strain was not permitted, certain changes may have occurred which may manifest themselves in the form of lower strength, depending upon the effects of sampling (Raymond et al (1971)), or in the chemical changes in pore water chemistry over the period of storage (Torrance (1975b)). Ideally the process should have ensured that the clay properties several months later, and after this journey, were identical to those in the ground. It is more rational however to accept the inevitability of differences.

All soil samples received in Cambridge were tested as each was opened to be used, to evaluate their similarity to the Canadian laboratory results published from tests on Rockcliffe site soil specimens (see section 3.7). The description of the soil properties as measured in Cambridge is divided into two groups, according to the sample condition on arrival: the properties of the soil taken from the first, large, frost damaged specimen, are considered separately from the properties of the clay taken from the seven horizontally retrieved tube samples.

The moisture content of the first, damaged sample was significantly less than field values. The upper 115 mm varied a great deal in water content, perhaps because the upper surface had lost moisture through evaporation into the 75 mm void which had formed from the sample settlement. The bottom 250 mm of the sample, conversely, was quite uniform. The reduced moisture content averaged 51% overall, figure 3.13a, and was reflected in the consistency of the material: the upper, drier soil resembled a rubble of stiff blocks, while the lower, apparently more intact



material appeared severely fissured but moist to the touch. When remoulded, the easily detached blocks, about 10 mm by 10 mm in dimension, were easily broken down into smaller, stiff nodules, and these nodules in turn, were sensitive and could be remoulded into a creamy paste.

Although this vertical sample had somewhat questionable properties, it was large, weighing in the order of 500 kg. The seven horizontal tube samples were smaller, and weighed only 1000 kg all together. It was clearly necessary to make the best use possible of all of this unusual soil, and there could be no question of discarding the largest single sample.

All the horizontal tube samples were of higher quality, and in contrast to the vertical sample, the soil gave the impression of being a moist, homogeneous, cohesive mass, much more like the in situ material. The moisture content of these samples was well within the in situ values between 58% and 71% with few exceptions, and averaging at about 64%, figure 3.13b. The soil consistency displayed the in situ behaviour of breaking easily into small nodules, which were themselves sensitive.

Although the soil for one model made from a horizontal tube specimen seemed somewhat stiffer than for the other models during preparation, the measured moisture content was not out of the ordinary. Moisture loss may well be initiated along the microfissures causing them to open, but the loss may not appreciably involve the moisture content of the nodules, the latter of which dominates moisture content values. This moisture loss may thus be hidden.

Index tests on the clay indicated that the soil had a liquid limit of 76%, and a plastic limit of 31%. Using the Swedish Fall Cone, on the undisturbed horizontal tube samples, calibrated for cemented Champlain Sea clays by Garneau and Le Bihan (1977), the undrained cohesion measured between 62 kN/m<sup>2</sup> and 109 kN/m<sup>2</sup>, and the remoulded strengths between 11 kN/m<sup>2</sup> and 3 kN/m<sup>2</sup>, respectively; this defined sensitivity values of between 6

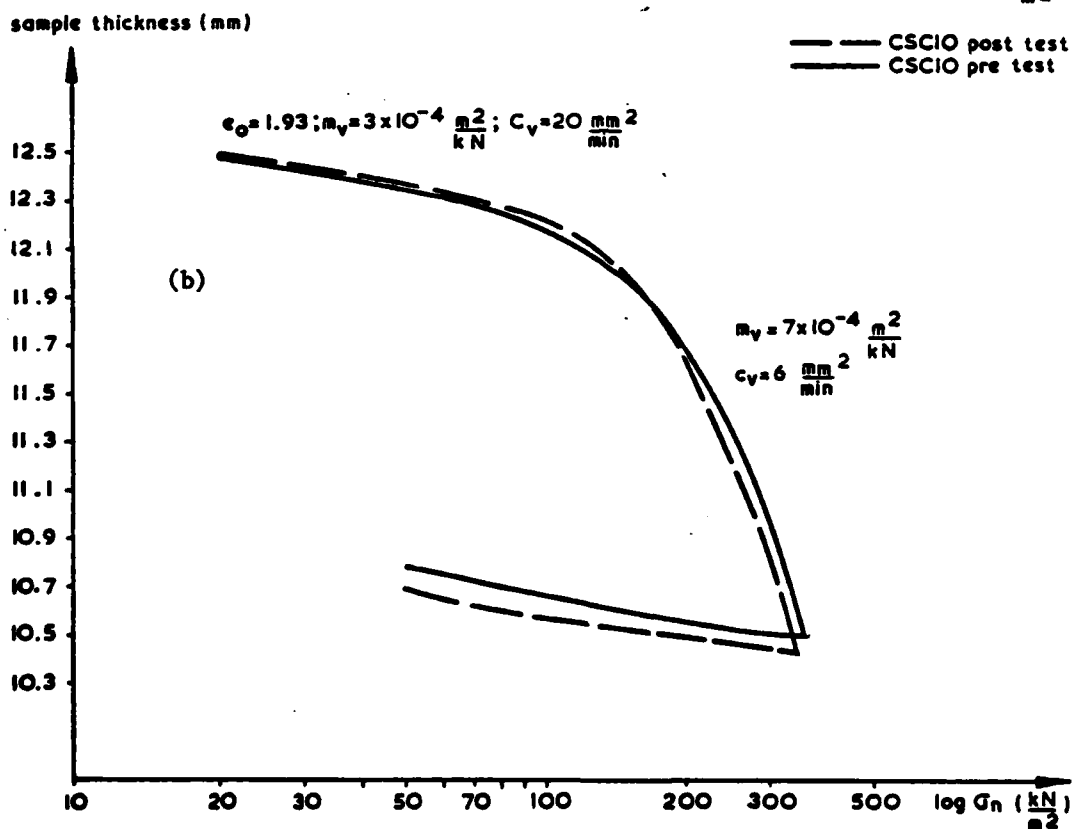
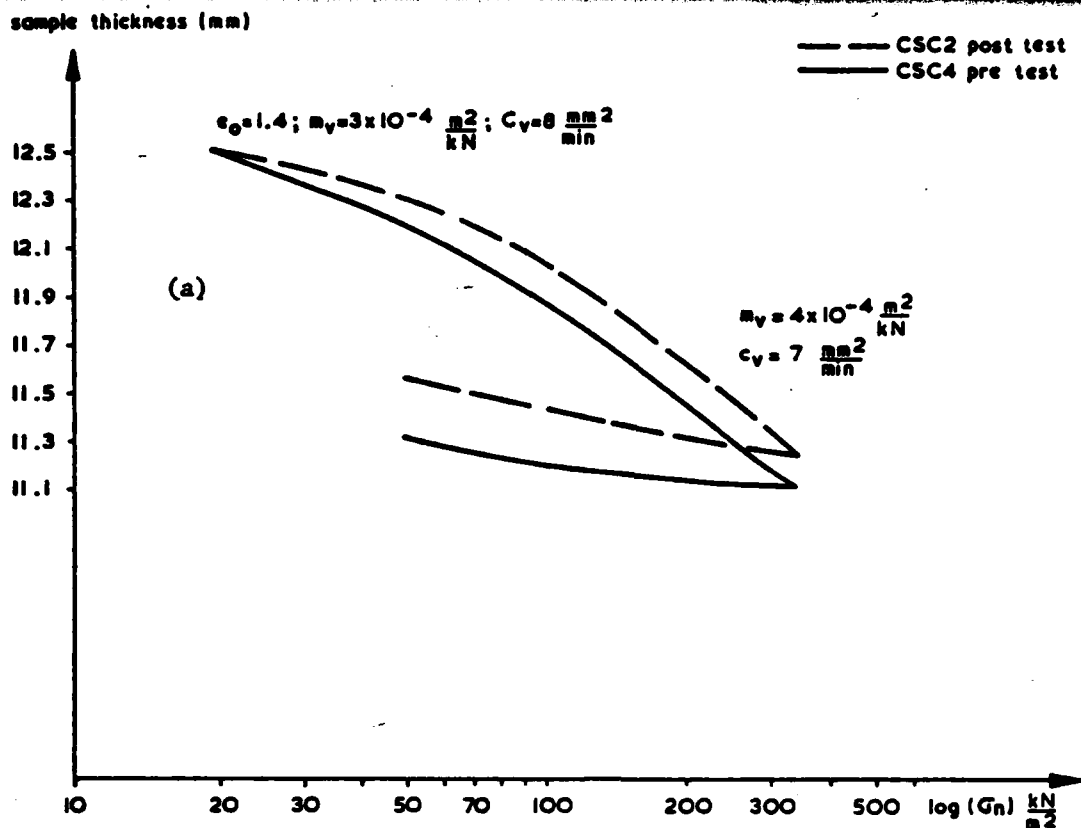


Figure 3.14 - Oedometer Curves Before and After Centrifugal Loading  
 (a) curves typical of frost damaged soil  
 (b) curves typical of undamaged soil

and 36. These indices agree well with those recorded in section 3.7.

It is worth noting here that when the proposal to retrieve and ship large undisturbed Champlain Sea clay samples to Cambridge was first made, most experienced Canadian research workers were pessimistic about the success of the project. The techniques developed in collaboration with Mitchell therefore represent a useful advance. The samples thus obtained were used to produce eleven separate soil models, with the following designations:

first vertical sample (damaged)	CSC 1, 2, 3, 4
first horizontal sample	CSC 10
second group of horizontal samples	CSC 20, 21, 22, 23, 24, 25.

Mitchell (1970b) remarked that naturally cemented clays display two distinct characteristics in an oedometer test: an abrupt increase in compressibility, followed by an inflection in the curve of the volumetric compression vs vertical effective stress, in the vicinity of the pre-consolidation pressure. This behaviour represents the breaking of bonds which are usually indicative of the strength of the cementation rather than the effects of the original overburden. Consolidation tests on the soil specimens received, indicated the following trends. The first damaged sample seemed to have suffered a marked loss of its strength which arises from the cementation bonds, exhibiting ill-defined preconsolidation pressures both before and after centrifugal loading, figure 3.14a. If any values of  $p'_c$  are indicated, they are in the vicinity of 80 kN/m<sup>2</sup> for the soil before centrifugal testing, and 110 kN/m<sup>2</sup> for the soil after testing. The second group of undisturbed tube samples displayed much more clearly the characteristics of the naturally cemented soils, although the limited available load on the small spring loaded oedometers used, may have obscured any noticeable development on the curve of the inflection after  $p'_c$  was exceeded. The curves before and after centrifugal loading

are almost identical, and reveal an apparent preconsolidation pressure in the order of  $190 \text{ kN/m}^2$ . Preconsolidation pressures for the Rockcliffe site compare well for that depth at  $200 \text{ kN/m}^2$ , (Mitchell (1970a)).

The value determined from these consolidation tests for permeability,  $3 \times 10^{-7} \text{ mm/s}$ , is of limited value. The water during consolidation must flow out of a soil nodule, and then along a fissure, the second path having a much greater permeability than the former. It is the latter path, however, which is significant in slope failures, and the permeability of the fissure system increases with dilation.

Triaxial tests were also attempted on all the specimens received, although as Raymond et al (1971) experienced, the considerable number of failures during the preparation of specimens was a problem, especially with the limited material available, and in particular with samples taken from material before centrifugal loading.

Tests were performed at constant  $p'$ , as drained, stress controlled, compression tests, all within the lower stress range of  $p' \leq 100 \text{ kN/m}^2$ . All specimens were prepared vertically in one size of 38 mm diameter and 76 mm in length, from block samples. Drainage from one end only was made available, and the time between stress increments adjusted accordingly to permit dissipation of excess pore pressure. Unlike the tests executed on specimens in Canada, rotating bushings with reduced piston friction were not used, although the effect was felt to be small in most cases. No back pressure was used, and this omission was felt to affect the measured soil behaviour: the lack of saturation in some cases was emphasised by air appearing in the burette during the later test stages. The values derived from these tests must thus be viewed only as a qualitative indication of the state of the soil.

The mode of failure observed in the triaxial samples consistently demonstrated dilation at or before failure, and the nodular blocky structure characteristic of failure in fissured clay was noted when the

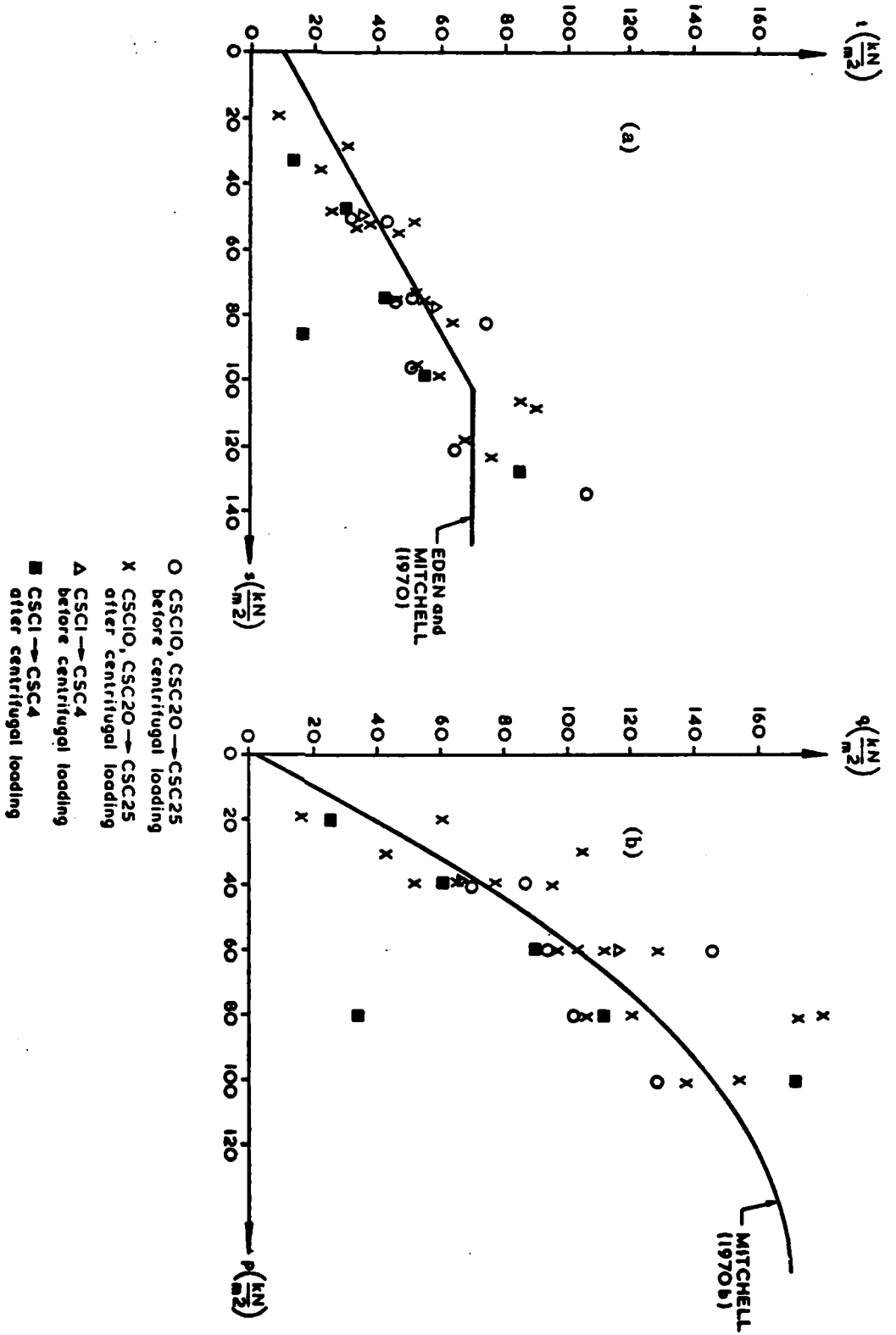


Figure 3.15 - Triaxial Compression Failure Envelope from Constant  $p'$  Tests

(a)  $s$  vs  $t$   
(b)  $p$  vs  $q$

apparatus was dissembled. Figures 3.15a and b display the test results compared to the results obtained by Mitchell (1970b) and Eden and Mitchell (1970). They show a definite scatter, although the curve from the published data still marks the approximate average of these tests. This stress region, which is sensitive to the interlocking of the nodules defined by the network of fissures, demonstrates higher strengths in the samples taken from soil which has undergone centrifugal loading, than from soil which has been taken from the specimens just transported across the ocean. It is almost as if the centrifuge loading had returned them to their original, closely packed state. Note also that the samples taken from the first, damaged soil specimen, lie below the curves in both figures 3.15a and 3.15b, but still suggest the same shape of failure envelope.

The tests discussed in this section suggest that the Champlain Sea clay used in the centrifuge tests of this research, resembles the soil properties as measured in the Canadian laboratories by Mitchell (1970b), and Eden and Mitchell (1970). Even after the adverse conditions of transport to Cambridge, and formation of the samples into centrifuge models, a good representation of the in situ soil behaviour may be anticipated. In the first, damaged sample, the greatest difference when compared to in situ soil properties, appeared to be the destruction of cementation bonds, and reduction in moisture content. Even this sample may be expected to give some indication, although perhaps less exact, of in situ soil behaviour.

Table 4.1

## Model Dimensions

	Model	Dimensions - mm								$\angle \beta$	Comments
		a	b	c	d	e	f	g	h		
	CSC1,2	82	217	438	80	96	200	210	-	25.6	unenclosed vertical filter
	CSC3	82	38	617	80	96	200	210	-	70	unenclosed vertical filter
	CSC3	82	180	475	80	96	200	210	-	30	unenclosed vertical filter failed 70° slope cut to 30°
	CSC3	370	87	280	80	96	200	210	-	50	unenclosed vertical filter failed 30° slope cut to 50°
	CSC4	82	104	551	80	100	200	210	-	45	enclosed vertical filter dimension f varied from 100 mm + 125 mm + 150 mm
	CSC10	82	217	310	80	96	200	210	128	25.6	short sample: unenclosed vertical filter - h
	CSC20	82	217	373	80	96	201	210	65	25.6	enclosed vertical filter extra toe room
	CSC21	82	146	338	80	96	198	210	70	35	enclosed vertical filter extra toe room overflow box
	CSC22	82	217	268	80	96	200	210	70	25.6	enclosed under filter extra toe room overflow box
	CSC22	282	123	232	80	81	185	195	-	40	as above with slope steepened to 40°
	CSC23	82	123	362	80	96	200	210	70	40	enclosed under filter extra toe room overflow box; 2 pwp transducers remove hatched wedge
	CSC24	-	216	320	-	-	216	238	-	45	enclosed under filter lead surcharge 0.45 kN/m <sup>2</sup> 2 pwp transducers
	CSC25	-	170	365	-	-	170	188	-	45	enclosed under filter lead surcharge 0.36 kN/m <sup>2</sup> 2 pwp transducers

• pore pressure transducer

## CHAPTER 4

### CHAMPLAIN SEA CLAY - EXPERIMENTS

#### 4.1 Model Preparation

The introduction of natural soil, especially a material as difficult to handle as Ottawa area Champlain Sea clay, to the technique of centrifugal modelling, required the development of new approaches to, and methods of model preparation, which matured over the period of research. This section will outline the resulting techniques adopted to produce the models, the dimensions of which are detailed in Table 4.1.

The first soil sample which arrived in Cambridge was disturbed due to frost damage which occurred en route. This specimen had originally been intended for use in one three-dimensional model, but both the high cost of retrieval and transport, and the disturbed state upon arrival precluded such a test. The 953 mm diameter sample was instead divided by four parallel chords, and ear-marked for four plane strain models: CSC1, CSC2, CSC3 and CSC4. Each section provided a soil specimen just slightly wider than the minimum required width of 152 mm, and quite adequate in length and height to fill the maximum model dimensions of 737 mm and 210 mm respectively.

The concrete shell around the first sample was cut with a circular saw, as each segment was required, and sealed between model making events, in order to preserve the moisture content. An elongated "U" shaped cradle of 1.5 mm thick steel plate was pressed into the soil, figure 4.1, and then lifted out carrying the "intact" soil specimen. The soil, trimmed to the precise required length using a cheesewire, was pushed into the centrifuge strong box liner (see section 2.2) and all further preparation was executed in the liner which provided a rigid support for the remaining operations.

Again using the cheesewire, a rough soil profile was cut, the



proportions delineated by two templates placed one on either side of the soil and line r. The resulting soil profile was uneven in the clay nodules which were cut by the cheesewire, the two sides immediately adhered again, due to the negative pore pressures set up by the cutting, and the whole nodule pulled out along the fissure, rather than along the fine wire cut surface. The final smooth profile was gradually carved to the dimensions of the template to achieve a smooth surface. Any areas of the model surface which were left rough or uneven were smeared with remoulded clay. This roughness was particularly a problem along the sides, where it was important to have an even surface so that the soil and strongbox interface would be smooth and continuous, and so that the grid of silvered plastic indicator balls used to indicate plane strain deformation, would be held firmly in the clay, and be indicative of soil movement.

The liner and soil model were then inserted into the centrifuge strongbox. At the back of the slope, on the right of the models in Table 4.1, a 10 mm wide space was excavated, the full height and width of the model, and filled with medium 14/25 Leighton Buzzard sand. By supplying water to this "reservoir filter" and thus to the whole cross-section of the back of the model by an underlying connection to the reservoir, a pattern of saturated seepage was to be achieved similar to that observed in the prototype. This same method of application of groundwater was used independently by Mitchell and Williams\* for a field situation in 1977. By supplying a head of water greater than the height of the embankment, a second purpose was also served: the excess which overtopped the filter and thus drained across the surface of the embankment simulated surface runoff conditions which always accompany prototype failure. All excess water was drained away at the left side of the models in Table 4.1,

---

\* Williams, Queen's University, Canada, personal communication, 1978.

at a height comparable to the elevation of the prototype Ottawa River level. Problems encountered with leakage along the model boundaries eventually lead to the enclosing of this reservoir on its two previously open vertical sides.

With the reservoir in place, the grid of silvered plastic indicator balls was marked out on the cross-section of the model, pressing the balls into the soft, remoulded surface of the soil. Bearing plates for the spindle of the displacement transducers were then countersunk in order to diminish the effects of their presence. The perspex front to the centrifuge strongbox was clamped into position with the clamping ring, sealing the model cavity on three sides with the GACO rubber gasket.

The techniques of preparation did not change appreciably with the horizontally retrieved samples, the biggest difference being the method in which the soil was removed from its sampling/shipping tube. Of the remaining seven samples received, the 610 mm long cylinder which was retrieved in November 1976 was used in model CSC10, and the samples retrieved in June 1977 were used in models numbered CSC20 through CSC25.

In forming models from all horizontal samples, a rectangular section, open ended, hollow, greased extrusion box, which was the exact width and maximum height of the model, and the same length as the sampling tube was pushed into the end and down the whole length of the cylinder in a single, controlled stroke, using a 500 ton Amsler compression testing machine. The extrusion box, full of soil, was restrained while the cylinder and the excess soil were drawn up and over the top. The extrusion box was disassembled, each of its four sides removed individually, preceded by a pass of the cheesewire to release any clay which was adhering to the metal box, and moved onto the liner as the sides came off. The model was then constructed by the same procedure as the previous ones, although surface patching was minimal with these higher quality samples.

In the last four models, CSC22, CSC23, CSC24 and CSC25, a different type of hydraulic system was used, in which uplift was to be applied to the length of the underside of the model by way of an enclosed under filter, and the usual full height reservoir filter was abandoned. As the extrusion box was being disassembled, the underside at which the soil was to form the interface with the liner, was removed first. A flat bottomed trench, 15 mm in depth, was excavated into the soil the necessary length of the model, and the full width, save two 10 mm wide margins along the lengthwise edges. These clay boundaries were intended to seal in the uplift forces. This trench excavation was then filled with 14/25 Leighton Buzzard sand, through which the uplift pressures could be easily transmitted. At the right end of the model in Table 4.1, where the water entered, the uplift filter layer was increased in depth, as recommended by Dr F. Tavenas\*, in an attempt to simulate some of the effects of the sloping bedrock, overlain by highly permeable sand, which may be a factor in landslide prediction (La Rochelle et al (1970)). The surface runoff was maintained in these models using a separate water supply line feeding directly onto the model surface.

Other slight variations in model preparation were implemented during the progression of the test programme. One was the use of a strong submerged debris overflow box, the width of the model and 100 mm long, intended to provide a sink for landslide debris such as is provided in the prototype by the Ottawa River. This was used in models CSC21, CSC22, and CSC23, although without good results.

After the video tape camera came into use with the centrifuge in November 1977, a continuous visual tape record of the test was possible. In order to highlight more precisely the soil movements during recording, two sets of white stripes were imposed on the model: one sprayed diagonally on the inside backplate of the strongbox, and one applied in

---

\*F. Tavenas, Laval University, Canada, personal communication, 1977.

vertical stripes to the cross-section of the clay itself, which was visible to the camera. This latter set of stripes was applied using a variety of trial materials: kaolin powder, spray paint, and brush paint; each had their disadvantages, but each helped to immediately illuminate soil movement.

One of the later and valuable additions to the models was the introduction of miniature DRUCK pore pressure transducers. Although Hird (1974) had used them with good effect at UMIST, Padfield (1978) had experienced great difficulty with getting good results from them. After a succession of experiences, the DRUCK transducers now are used routinely to monitor pore pressure with great accuracy, under the difficult conditions of high centrifugal acceleration in a moving soil mass. The current DRUCK transducers are 6 mm in diameter and were inserted into a prebored, horizontal hole, and backfilled with remoulded clay. Only two such transducers were available at the time of the final tests of this model test series.

In the last two models, CSC24 and CSC25, the slopes were surcharged with lead shot gently pressed into the terrace of the model slope; by the spacing of the shot, the surcharge for the two models was  $0.45 \text{ kN/m}^2$  and  $0.36 \text{ kN/m}^2$  respectively, at earth's gravity.

A typical completed model of the Rockcliffe site is pictured in figure 4.16.

#### 4.2 Logic of the Test Programme

The object of these tests, as discussed earlier in section 3.5, was to observe and define the mechanisms of failure occurring in this clay, including retrogressive slip, by study of reduced scale centrifuge models. One check on the relevance of the results to natural phenomena was a comparison of small scale models to the documented full scale prototype Rockcliffe landslide. A different check on the relevance of models to full scale events was the internal consistency of the results of tests

of a variety of slopes: the factors influencing both prototype and model events could be investigated to some extent by testing a variety of model slopes unrelated to specific prototypes.

The stress path followed in the prototype was one typical of excavation, until the critical combination of stresses was reached and failure occurred (see Mitchell (1975)). Such a stress path was attempted in modelling the slope instability in intact samples of a remoulded, post glacial, marine clay at Lodalen, Norway, by Lyndon and Schofield (1978). The essence of the procedure is to prepare a sample, taken at one single point in a prototype profile, in such a way that soil at different positions within this uniform soil sample is brought into the different states of soil at other points in the prototype profile. The essential feature of the procedure is altering water content and effective stress state in a long preparative consolidation process.

In discussing that work, Tavenas (1978) explained the good correlation between that model and the Lodalen prototype, in both soil properties and failure phenomenon, as a result of the unstructured nature of the Lodalen soil. He went on to express concern regarding the establishment of prototype conditions in a structured clay, such as Champlain Sea clay. In some respects, the properties attributed by Tavenas to intact Champlain Sea clay in the St Lawrence valley differ from those attributed to fissured Champlain Sea clay in the Ottawa region by Mitchell. Tavenas considered that phenomena of ageing or secondary consolidation, and thixotropic hardening which require long and unscaled periods of time to develop at every part in the profile, have major importance in slope stability in the Champlain Sea clays with which he has experience. Although in Mitchell's triaxial tests, stress path differences are seen to alter the tendency of fissured clay to dilate or to deform plastically, his experience did not lead him to attribute significance to time effects in

the clays with which he worked. In Mitchell's (1970b) work regarding strength characteristics at the Rockcliffe site, resistance to slope failure in the low stress region is dependent upon mean normal stress and confining pressure, rather than water content and preconsolidation characteristics varying with depth.

Lack of experience in working with this sensitive, natural soil, required evolution of modelling techniques by trial and error, over the programme of testing. In order to see retrogression at as early a stage as possible in the test series, the initial approach involved loading the model under the most adverse feasible conditions: rapid undrained conditions. The closest approximation to this in centrifugal modelling is achieved by rapid acceleration of saturated specimens to high centrifugal loadings. Although the stress path approaching failure in the speed increase centrifugal models differs from the prototype excavation stress path, the difference was not felt to negate the value of the tests, and nothing short of in-flight excavation, which was not attainable, was felt to be a major improvement. The response of the models in such tests, however, did not involve retrogression. In fast draining soils, the finite time period required for the increase in centrifugal loading to be implemented, may be greater than the time required to dissipate the pore pressures, and undrained conditions may not be effectively imposed. The initial approach therefore was modified, and the second phase of testing, in which drainage occurred, was increasingly studied.

Subsequent to the initial rapid undrained loading, drained conditions at a given constant centrifugal loading were permitted to develop over a time, equivalent in the prototype to  $t_p = t_m \times N^2$ \*. During this period, the prototype seepage pattern which is often disturbed in the model during rapid increases in loading, may be re-established.

---

\* where  $t_p$  = prototype time,  $t_m$  = actual real time in the model,  
N = model scale, centrifugal loading in gravities.

The majority of centrifugal tests followed some variation on this basic test programme, including the tests which were intended to investigate the modelling of models. These latter tests were intended to examine various aspects of centrifugal modelling, rather than to model a specific prototype event.

#### 4.3 Definition of Failure

Slope stability is traditionally defined in terms of failure. In numerical analysis of slope stability, discussed in section 1.2, failure is said to occur when the safety factor, which compares the forces resisting failure to those causing failure, approaches unity. Whether failure will, in fact, occur, and what it precisely entails cannot be predicted by numerical analysis at present. It is therefore not exactly obvious how, in actual physical terms, one should define failure.

The term "failure" in soil mechanics implies inadequate performance of the soil. It therefore involves a subjective judgement and is a term dependent upon the required performance of the soil. In some cases, something as subtle in nature as excessive settlement may be deemed failure, whereas in other cases, only when soil has undergone a catastrophic shift, is it said to have failed. Failure of a riverbank of work hardening soil in which stable soil movement may occur, and be naturally self-arresting, can only be assessed subjectively. For this reason, failure will be arbitrarily deemed to have occurred when a permanent, non-elastic settlement of the crest of the slope, more than or equal to 10% of the original slope height, is observed.

The precise point at which failure is said to have occurred, in the case of a steady increase in centrifugal loading, is another point subject to interpretation. Hird (1974) suggested that the point of failure could be defined according to the rate of deflection of the slope crest. He said that failure may be judged to have occurred at the point

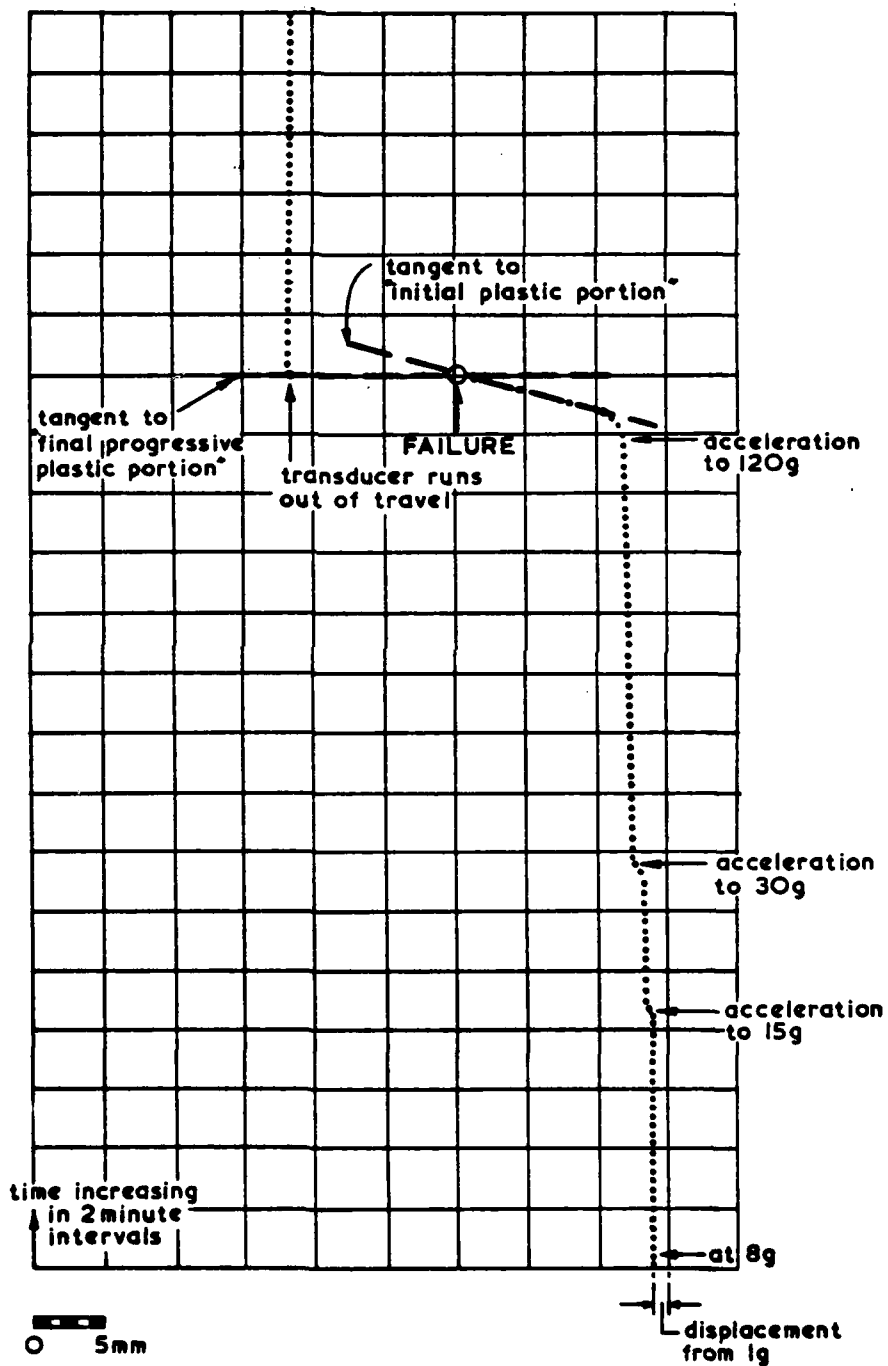


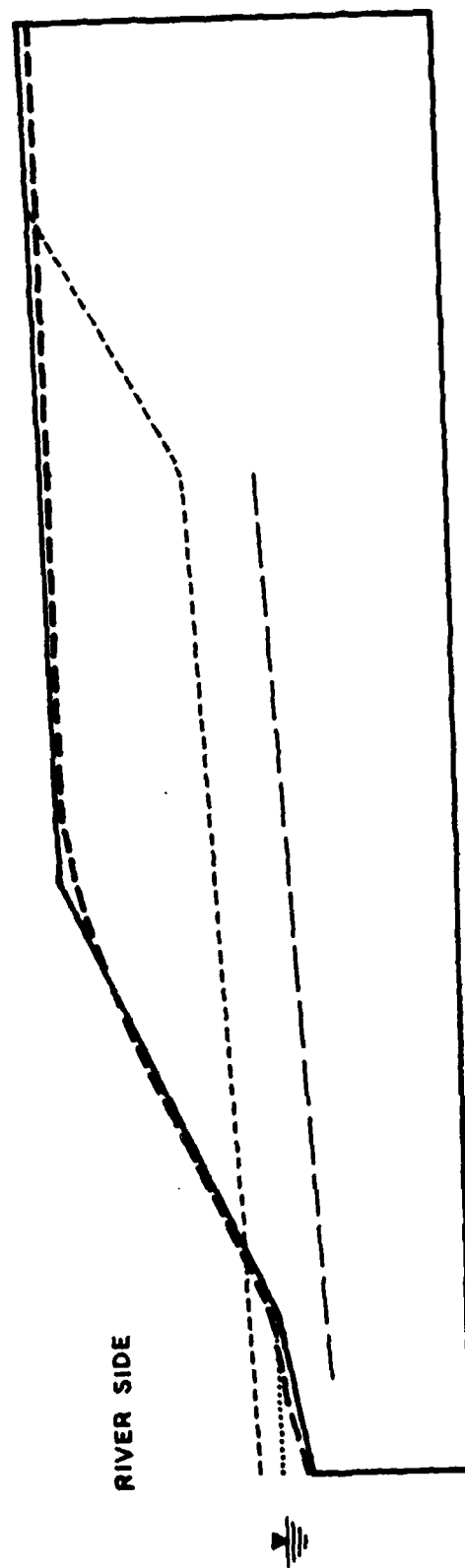
Figure 4.2 - Definition of Failure by Crest Displacement Method  
According to Displacement Transducer Output ( Fair Copy )



where the tangent to the "initial elastic portion" of the deflection curve intersected the tangent to the "final progressive plastic portion". Although Hird found difficulty in applying this method to his own results, this research has adopted that definition. It is interpreted in terms of these experiments in the manner illustrated in figure 4.2.

Beasley (1973), on the other hand, determined a different definition for model embankment failure based upon strains. He found that a natural, work softening clay, which failed in the full-scale prototype in a progressive failure mode, did not demonstrate the same obvious signs of failure in a reduced scale model. The strains measured from the model were sufficient, according to triaxial tests, to cause failure, although failure per se was not observed. This led Beasley to hypothesise that the stress-strain post-peak behaviour of soil may in fact be dependent upon non-scaled displacements, rather than on strain, for the loss of strength necessary for progressive failure to be exhibited. He attributed this to the unscaled clay particle size and the resulting unscaled thickness of failure surface. Beasley therefore defined failure in terms of the strains measured in the model. A stress-strain relationship established from triaxial tests was used to estimate a limiting strain before the onset of progressive failure. Any model was deemed to have failed if the strains anywhere in it exceeded the strains to failure of the triaxial test specimen. Bassett (1973) also developed this viewpoint.

This view may have significance as will be discussed in section 4.5.4, but in the model tests of this research, because this soil does not exhibit progressive failure in natural slopes, and exhibits small strain prior to yield, and large strain subsequent to yield, the more simple "crest displacement" definition of failure, explained above, will be used.



RIVER SIDE

model scale:

0 125mm

prototype scale:

0 12.5m

--- prototype profile of Rockcliffe  
(Mitchell 1970a)

— model profile of Rockcliffe

..... water level

- . - . prototype failure surface

----- prototype ground surface  
post-failure

Figure 4.3 - Profiles of Rockcliffe Prototype and Model Before Failure

#### 4.4 Experimental Procedure and Results

Modelling techniques evolved over the duration of this test series in response to the accumulating experience derived from each test. It is therefore logical and advantageous to discuss experimental procedure and results together, as they are intimately linked. This continual reassessment of the test results as a whole, led to a variation in the procedure of centrifugal testing. While the actual steps involved may be significant in understanding the soil response, by its exhaustive nature the details will be confined to Table 4.2, and the important generalities and their outcomes will be included in this section.

The frost damaged soil sample, received in February 1977, was used to construct four models. The first two, CSC1 and CSC2, were constructed on the chance that the Rockcliffe retrogressive landslide might be successfully modelled in a simple test with this clay. Their identical profiles, shown in figure 4.3, are in scale with the prototype with dimensions reduced 120 times. The models were subjected to similar test sequences involving rapid centrifugal loading to 120g, the full scale stress level, and in both cases there was difficulty encountered in establishing the prototype saturated pattern of seepage.

Model CSC1 had been riddled with voids before centrifugal loading as a result of the freezing and consequent soil disturbance suffered in transit. It was therefore expected that one response to centrifugal loading would be an overall compacting of the material; the change in profile and the soil deformation which did occur according to the movement of the silver indicator balls, is pictured in figure 4.4. The expected overall soil compaction was achieved, in the order of 10% vertical strain, but there were also other distinct movements below the slope, to the full depth of the model. By the "crest displacement" criterion, failure occurred at 120g, at which stage there was a differential settlement of

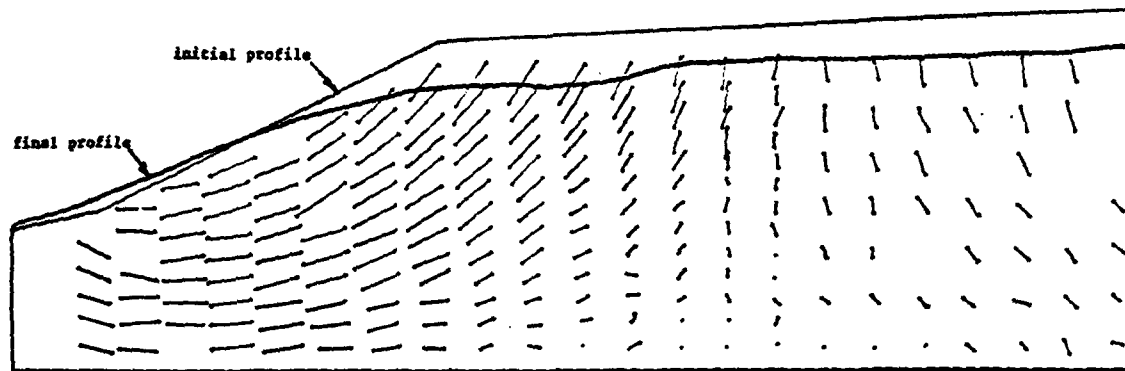


Figure 4.4 - CSC1 Model Soil Displacements

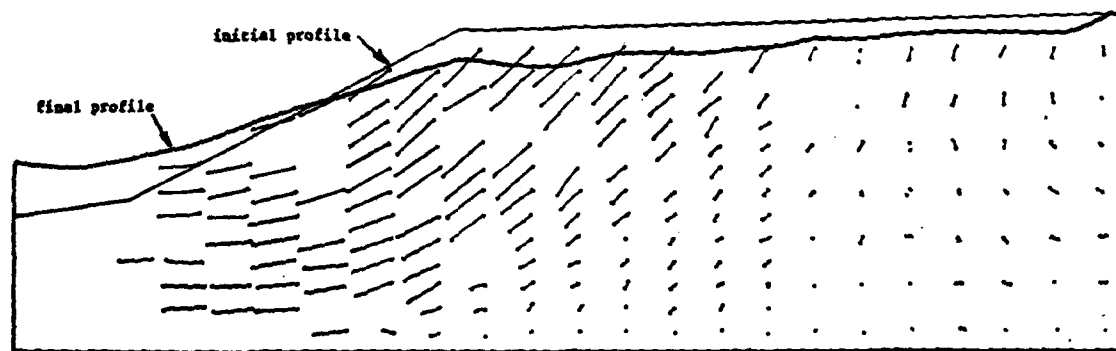


Figure 4.5 - CSC2 Model Soil Displacements

the crest, equal to approximately 28% of the original slope height, and 17% of the compacted slope height. The nature of the slope movement was difficult to assess, being somewhat obscured by the general soil compaction, and will be discussed later in section 4.5.3. The overall flattening resulted in a final slope angle of  $18^{\circ}$  to the horizontal and height 80 mm.

The site investigation after the test revealed that tension cracks had opened in the terrace of the model slope, but the overall flattened appearance was not characteristic of typical rotational failures. The voids which were previously an obvious feature of the clay mass, had decreased with the depth of the model during centrifugal loading. Moisture contents were consistently in the order of 50%, and the vane strengths measured perpendicular to the direction of centrifugal loading, varied between  $30 \text{ kN/m}^2$  and  $35 \text{ kN/m}^2$ .

Model CSC2 differed in the test procedure from CSC1 by being totally submerged in water, although probably not fully saturated, prior to simultaneous drawdown and increase in loading, but the soil response was almost identical to that of CSC1 both in appearance, and in the magnitude and shape of the *failure* movement, although there was more evidence of heaving action in the toe; figure 4.5. Failure took place at a slightly lower centrifugal loading, 115g. The final slope was  $17^{\circ}$  to the horizontal and 63 mm high.

Examination after the test revealed more pronounced tension cracks than in the previous model, and the moisture contents were marginally higher, in the range of 55%. Vane strengths were measured to be lower,  $20 \text{ kN/m}^2$  to  $30 \text{ kN/m}^2$ .

These failures in the frost damaged material were encouraging: they did exhibit clear evidence of slope movement and instability, but the horizontal movement in the model went deeper than in the prototype at

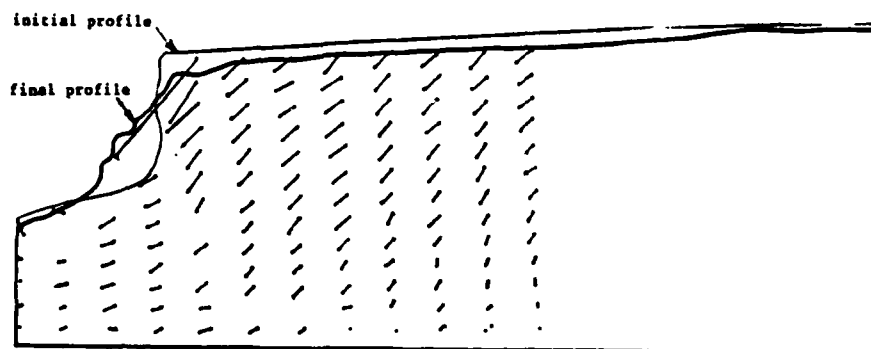


Figure 4.6 - CSC3 (  $\beta=70^\circ$  ) Model Soil Displacements

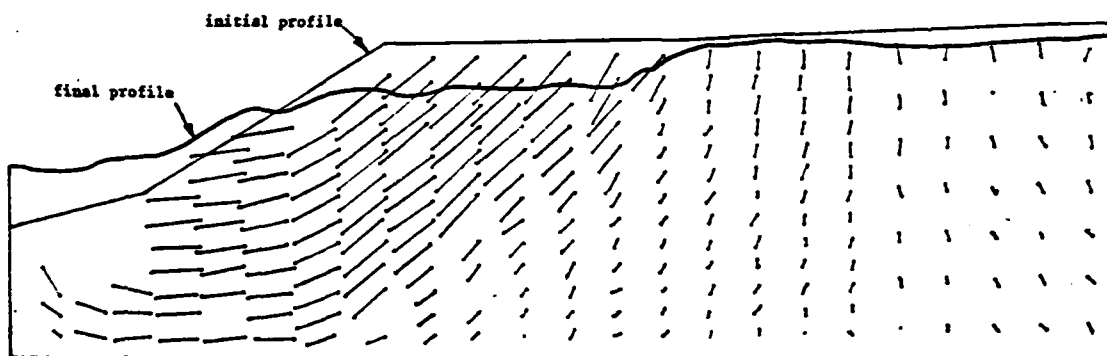


Figure 4.7 - CSC3 (  $\beta=30^\circ$  ) Model Soil Displacements

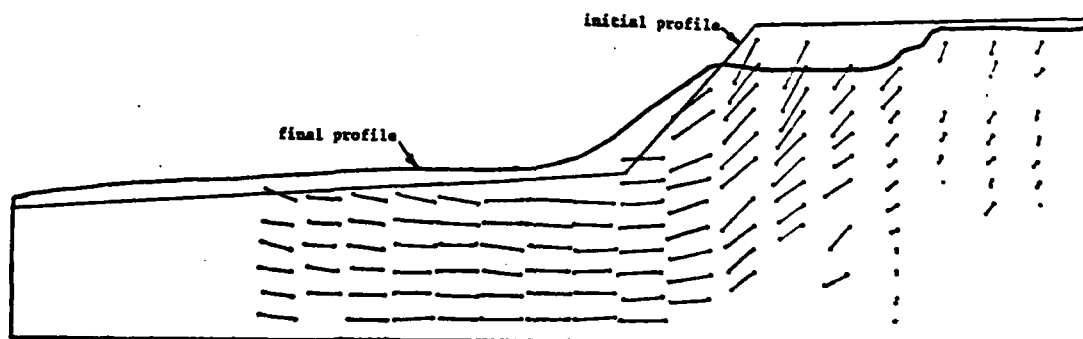


Figure 4.8 - CSC3 (  $\beta=50^\circ$  ) Model Soil Displacements

AD-A084 048

CAMBRIDGE UNIV (ENGLAND) DEPT OF CIVIL ENGINEERING  
CENTRIFUGAL MODELLING OF SOIL STRUCTURES. PART I. CENTRIFUGAL M--ETC(U)  
MAR 79 D J GOODINGS, A N SCHOFIELD

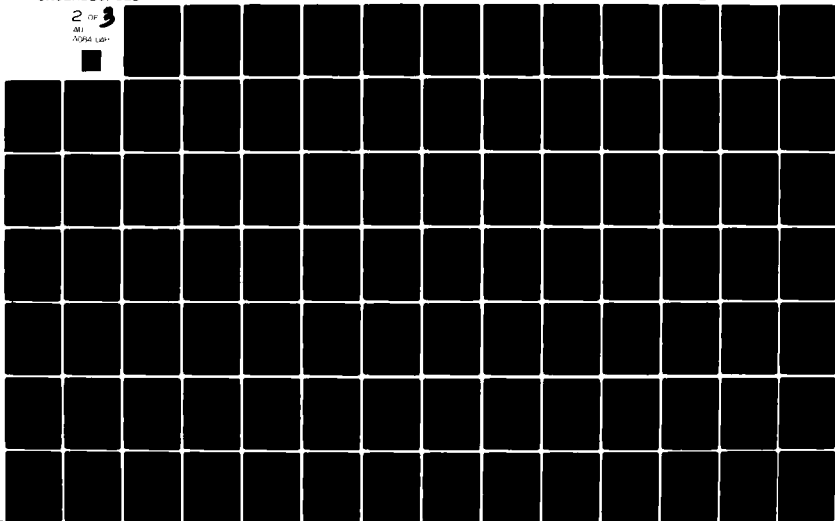
F/G 8/13

DA-ERO-76-6-040

NL

UNCLASSIFIED

2 OF 3  
DU  
FORM 100-1

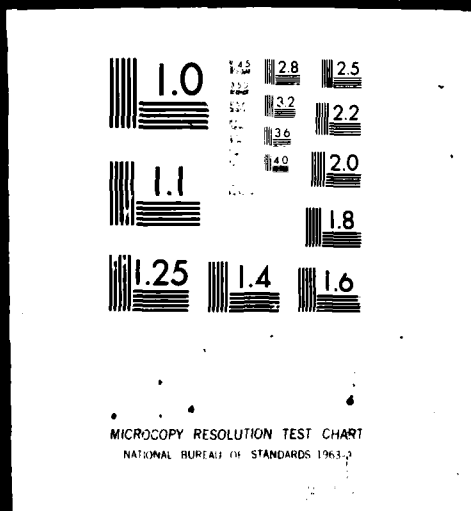


ASSIF 10

2 OF 3

AD

A084 048





Rockcliffe, and the model showed no signs of producing the one or two retrogressions which were apparent in the prototype. The next two models, CSC3 and CSC4, made from this damaged soil were therefore devoted to an exercise in the modelling of models, to examine the nature of slope failure in this material, in a set of models not related to any existing specific prototype.

Model CSC3 was designed to be tested three consecutive times, each with a different slope angle cut back successively into the same soil mass, but all with equal height, 104 mm. The slope angles selected for the modelling exercise were  $70^{\circ}$ ,  $30^{\circ}$  and  $50^{\circ}$ ; the position of each slope in the model, and the order of modelling were based upon practical reasons according to the strain which occurred in the previous test, and the relatively inflexible positions available for the mounting of the displacement transducers.

Each slope cut with model CSC3 underwent failure, as defined previously, during a rapid increase in centrifugal loading, although each failure was slightly different in nature. The  $70^{\circ}$  slope settled and strained forward, suggesting an extensive zone of influence, but the obvious changes amounted to the opening of tension cracks on the terrace of the slope and degradation of the slope, so that its final angle was  $54^{\circ}$  and height 90 mm; figure 4.6. This failure occurred at 57g, but seemed almost certainly affected by the proximity of the toe to the model boundary.

The next slope, at  $30^{\circ}$ , was cut into the failed embankment, removing a large part of the most strained area in the slope, but leaving the foot of the slope essentially at the same position. The failure, which occurred at 62g demonstrated a distinct and extensive zone of failure, accompanied by toe heave, figure 4.7, and was very similar to CSC2. The failed material had broken into a nodular rubble and sat at

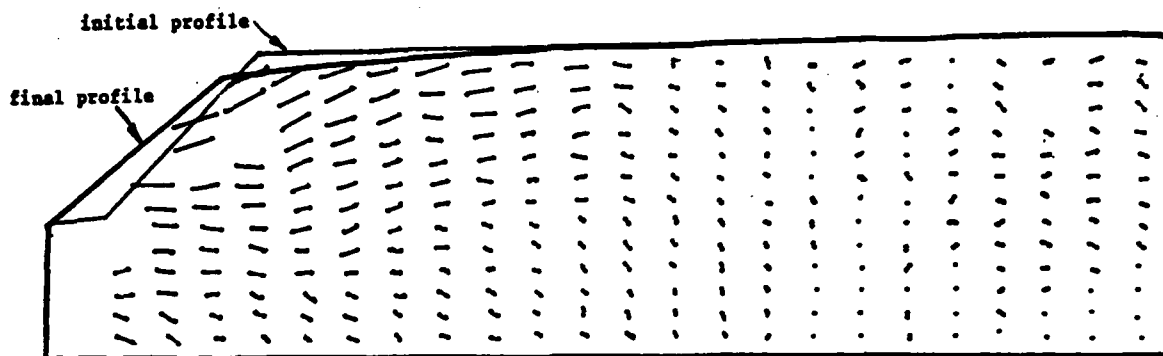


Figure 4.9 - CSC4 ( h=100mm ) Model Soil Displacements

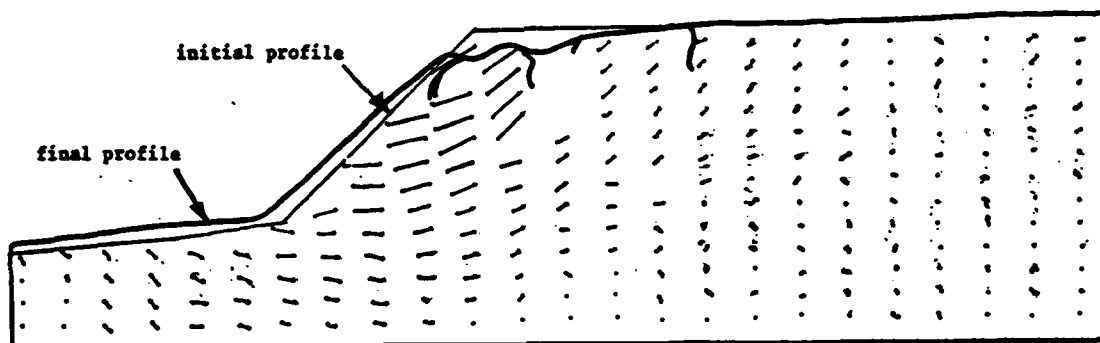


Figure 4.10 - CSC4 ( h=125mm ) Model Soil Displacements

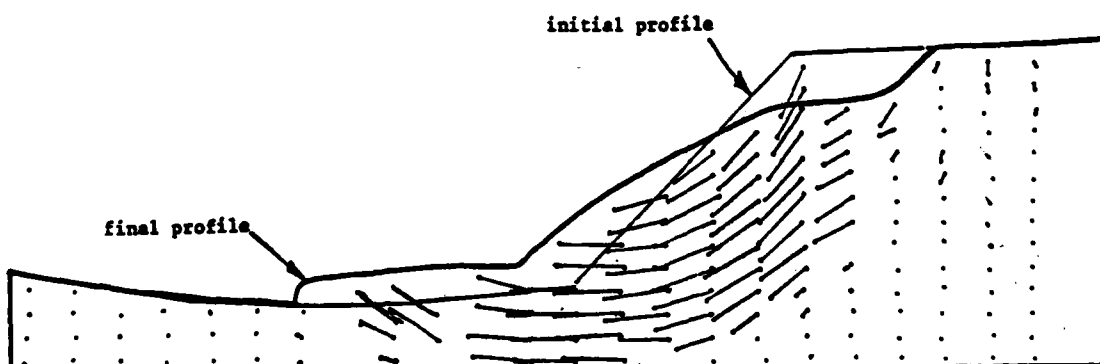


Figure 4.11 - CSC4 ( h=150mm ) Model Soil Displacements

a low contorted angle.

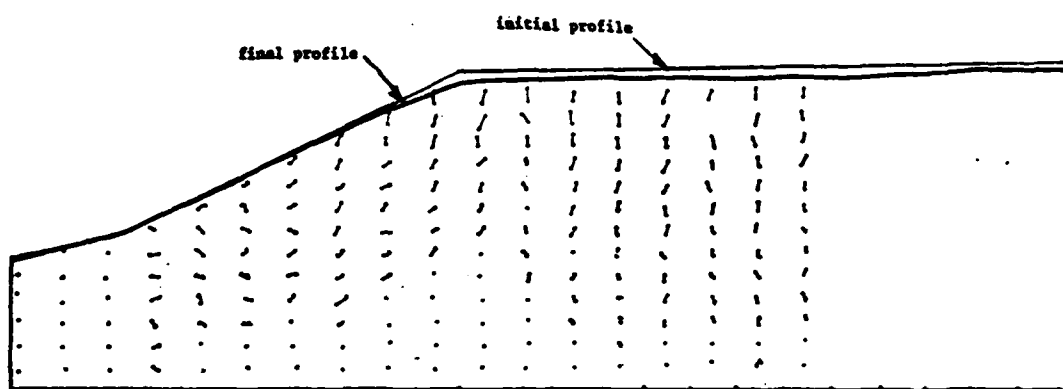
The last slope,  $50^{\circ}$  to the horizontal, was cut with the intention of eliminating the largest possible portion of the failed embankment material, although the continually strained foundation soil was necessarily still a part of the model. The resulting failure, figure 4.8, which occurred at 77g, showed marked horizontal movement through the full depth of the model foundation layer, and consequent heave in the toe. The final slope was measured to be  $37^{\circ}$  and 66 mm high.

Moisture contents taken after each test indicated no appreciable change from that at which it had arrived, 48% to 56%, despite its continued contact with free water.

Model CSC4 was used to model three heights of slopes with identical angles. The angle  $45^{\circ}$  was selected as best within the range of centrifugal modelling indicated by the results of CSC3. The first slope was cut to be quite close to the model boundary, with height equal to 100 mm. The failure which occurred at 104g indicated a combination of marked horizontal and shear movement, figure 4.9, similar in nature to the  $70^{\circ}$ , 104 mm high slope of CSC3. The similarity was felt to be the result of model boundary interference in both cases. The major movement was shallow in nature, although accompanied by an adjacent zone of strain. Tension cracks were noted in the terrace.

The next slope was cut to a height of 125 mm in such a way as to eliminate the major portion of the previously strained region. The failure, which occurred at 79g, figure 4.10, was dominated by one principal, shallow zone of failure, accompanied by other, less pronounced regions of strain. The failure profile was characterised by tension cracks in the terrace and there was some evidence of the soil breaking into nodules.

The final cut in this soil mass was a slope 150 mm in height. Its well defined failure, figure 4.11, which occurred at 70g, reached down to



0 10 mm

Figure 4.14 - CSC10 Model Soil Displacements

the soil-liner interface, although it did not appear to be adversely affected by this boundary. Little other movement was noted in the adjacent soil mass, nor was there evidence of this soil breaking into the characteristic nodular form of debris; figures 4.12 and 4.13.

The final site investigation showed moisture contents to be typically between 48% and 58%, and undrained horizontal vane strengths in the range of 24 kN/m<sup>2</sup> to 33 kN/m<sup>2</sup>.

The models constructed from the damaged soil shipment had been useful, however model CSC10 presented the first reasonable opportunity to model the prototype landslide, constructed in undisturbed soil shortly after its arrival in Cambridge. Within the limitation that this soil sample was shorter than the model container length, the profile of CSC10 was made to be identical to CSC1 and CSC2, so that all resembled the Rockcliffe geometry. Model CSC10 was subjected to a rapid increase in centrifugal loading to 120g three times, and held at that stress level for various periods of time, the sum of which in prototype time was the equivalent of more than a year. The small soil deformations which occurred did so almost entirely during the first loading; figure 4.14. These might be interpreted as the beginning of failure movement, however an attempt to initiate some sort of obvious failure by extending the slope height to be almost 50% higher, at the same inclination, was unsuccessful in producing any further model response. At least part of this resistance to failure was attributed to the proximity of the model boundaries, in spite of the shallow failure anticipated from prototype experience.

The site investigation showed the model to be visually almost unaffected by the centrifugal loading. Moisture contents in the range of the in situ values, 67% to 72%, and vane tests measured horizontally, 17 kN/m<sup>2</sup> to 30 kN/m<sup>2</sup>, offered no obvious explanation for the failure of the soil to respond in the manner of Rockcliffe.

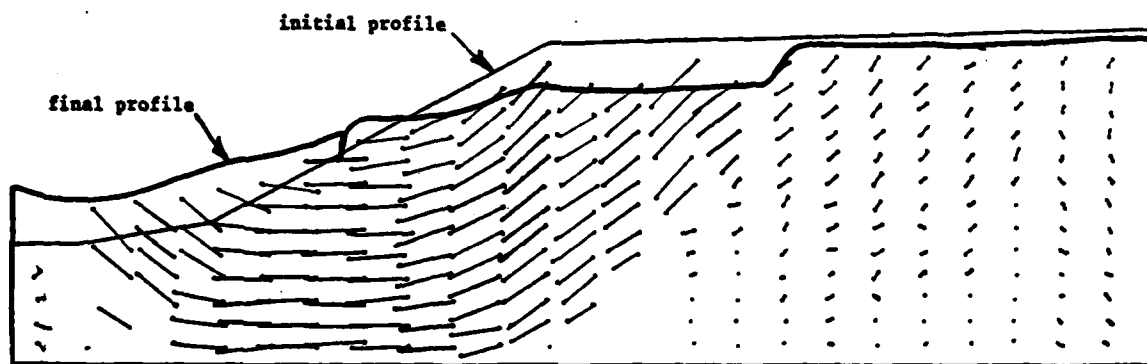


Figure 4.15 - CSC20 Model Soil Displacements

Various explanations were hypothesised and studied. The failure to establish the prototype seepage conditions, although the test had been performed in the presence of ample free water, was considered. Hindrance due to the proximity of the slope to the model boundaries was also a possibility, although the displacements which did occur were not similar in nature to those noted in the first, cramped slopes of models CSC3 and CSC4: these slopes were also near to the model boundaries, but demonstrated a failure of a sort, regardless. This study, therefore, identified two features of possible significance: the dissimilar seepage conditions and the proximity of the toe of the slope to the model boundary, both of which could be improved in future models by enclosing the model reservoir, filter and changing the model proportions to permit more room at the toe of the slope in future models. It remained unclear, however, why CSC10 had not failed.

Model CSC20 marked the beginning of the final and most recently sampled shipment of undisturbed soil specimens. While deviations might have been expected in the previous samples, these last six at the very least were expected to be self consistent. This first model was again constructed in similarity with Rockcliffe, allowing extra soil at the toe for soil movement. During an increase in centrifugal loading, the model responded at 116g with an obvious and deepseated failure; figure 4.15. Accompanying the initial slope movement was a suggestion of the beginnings of a retrogressive movement, highlighted by the relative lack of deformation in the adjacent soil. The extension of the failure beyond the toe of the slope and the apparent minimisation of interference of the model boundaries, both seemed to confirm the importance of the conditions at the toe of the slope for the development of the initial slip. It seemed possible, however, that the model boundaries may have been responsible for preventing the complete exodus of debris from the crater and

therefore possibly impairing the full development of retrogression.

The site investigation revealed that the failure block or wedge had remained essentially intact, although showing distress at the centre, resulting from both a collision with the model boundary, and the non-circular nature of the failure surface. There was also an absence of the characteristic breakdown into nodules, and only small tension cracks were noted in the remaining terrace, figures 4.16 and 4.17. Moisture contents were typically in the range of 57% to 67%, and the horizontal vane strengths between 22 kN/m<sup>2</sup> and 30 kN/m<sup>2</sup>.

The behaviour of this model seemed encouraging, exhibiting failure accompanied by indications of retrogression, at the correct modelling scale, although model movements were deeper than the prototype landslide. The object of the next model was to encourage the development of retrogressions by providing an escape for the initial slide debris, comparable to the role played by the Ottawa River.

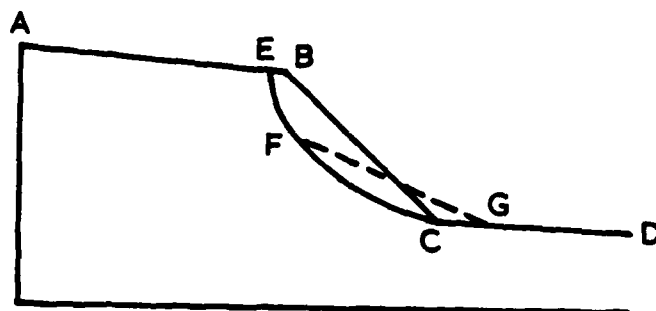
Model CSC21 was constructed to be similar to CSC20, but with two modifications: the slope angle was steepened to 35°, and a submerged overflow box was positioned at the toe, in anticipation that the failing soil might develop sufficient momentum to spill into it. Two rapid loadings were imposed, one to 130g and one to 150g: neither were successful in producing any significant strains. This lack of strain was reminiscent of the experience with CSC10, and the site investigation revealed little illuminating evidence. Vane strengths and moisture contents were typical of those found in CSC20, which had failed at a shallower angle.

Tavenas\* suggested, based upon La Rochelle et al (1970), that the missing essential factor in these models was the application of artesian conditions at the toe of the slope. The overdeep nature of the slip circles

---

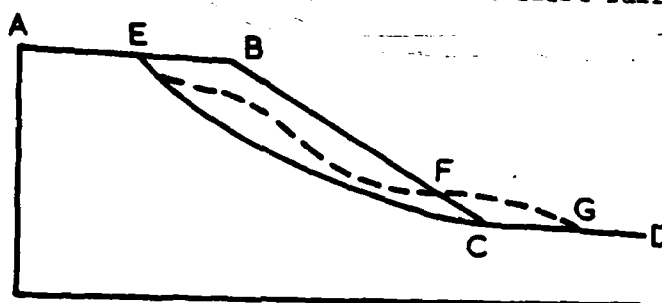
\*F. Tavenas, Laval University, Canada, personal communication, 1977.





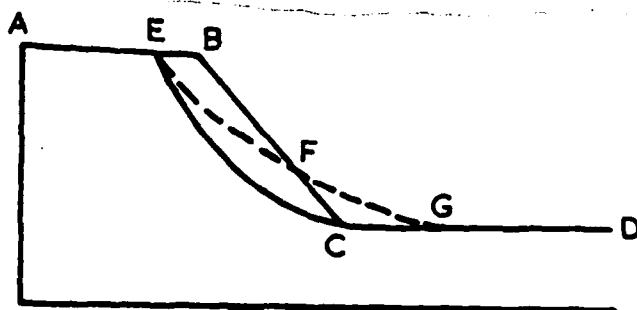
5cm (a) 38g original profile ( $\beta_0 = 40^\circ$ )  
initial failure surface  
profile after first failure

ABCD  
EFC  
AEFGD



(b) 95g profile at 95g before uplift  
flowslide failure surface  
profile after failure

ABCD  
EC  
AEFGD



(c) 148g initial profile ( $\beta_0 = 40^\circ$ ) at 20g  
initial failure surface  
profile after failure (148g)

ABCD  
EC  
AEFGD

Figure 4.18 - CSC22 Progression of Failure

observed thus far, as compared to that established at the Rockcliffe prototype landslide, and the apparent inconsistency of the soil response were both possibly attributable to the absence of uplift pressures.

Model CSC22 was constructed in the same proportions as CSC20 to resemble Rockcliffe, but with the submerged debris overflow box introduced in CSC21, and with the facility for uplift to be applied to the underside of the model. One change in the visual monitoring system was also made: the introduction of continuous viewing and recording on videotape which required the forfeit of the precision, still photographs. Observed and recorded in this test, however, was an interesting phenomenon which would otherwise have gone unnoticed.

The model was subjected to four successive rapid centrifugal loadings, twice with uplift applied, and little strain was noted. The model slope was subsequently steepened to  $32^{\circ}$ , but still indicated none of the strains associated with failure, even when loaded to 135g. When the slope was further steepened to  $40^{\circ}$  to the horizontal, still 104 mm high, the response observed was very different from any previous tests. At 38g, during an acceleration to 95g, the model slope underwent a shallow slip as defined in figure 4.18a, crumbling into the nodular form of debris, typical of the prototype. At 95g, the model responded immediately to the application of uplift with two successive soil movements, both distinctly flowsliding in nature, and each lasting three seconds and recorded on closed circuit television. Both involved shallow layers of soil, leaving the non-transported soil apparently undisturbed. The final profile is shown in figure 4.18b and the overall appearance in figures 4.19 and 4.20.

The model was cut again to  $40^{\circ}$  and retested in a similar fashion, however, only the initial shallow slope failure was observed, occurring at 20g immediately after drawdown. The final profile is pictured in figure 4.18c.

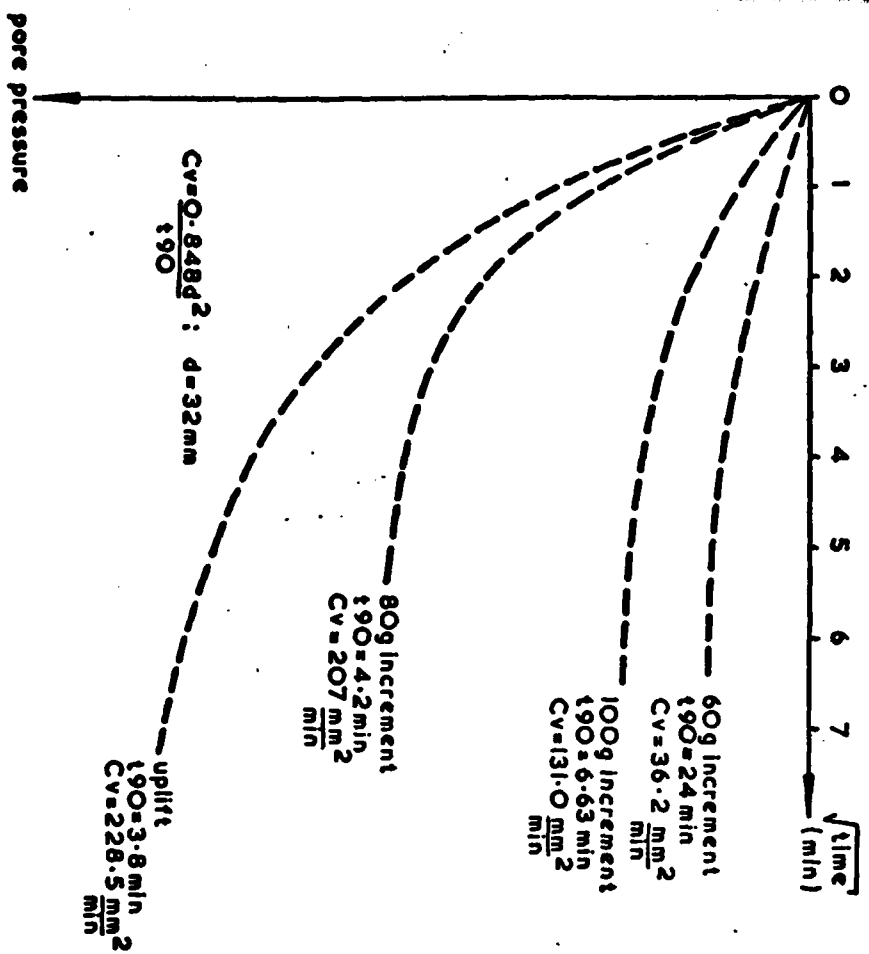


Figure 4.21 - CSC23 Pore Pressure Dissipation During Centrifuge Test

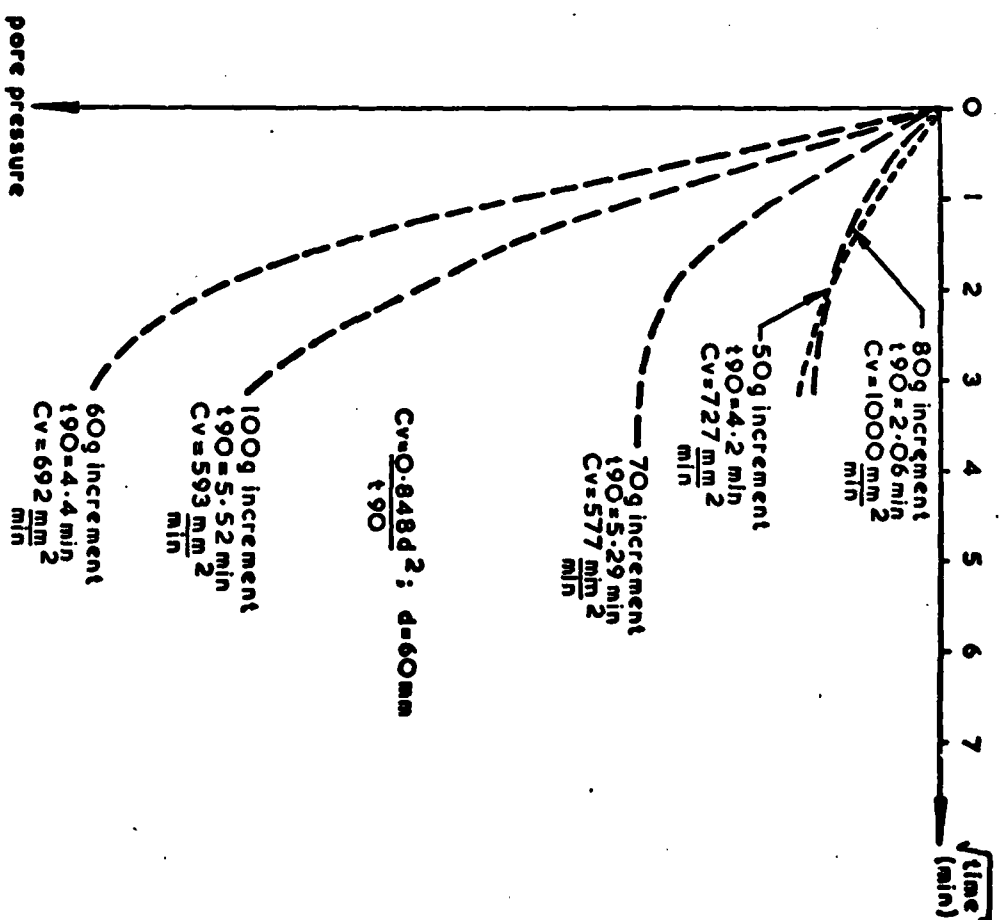


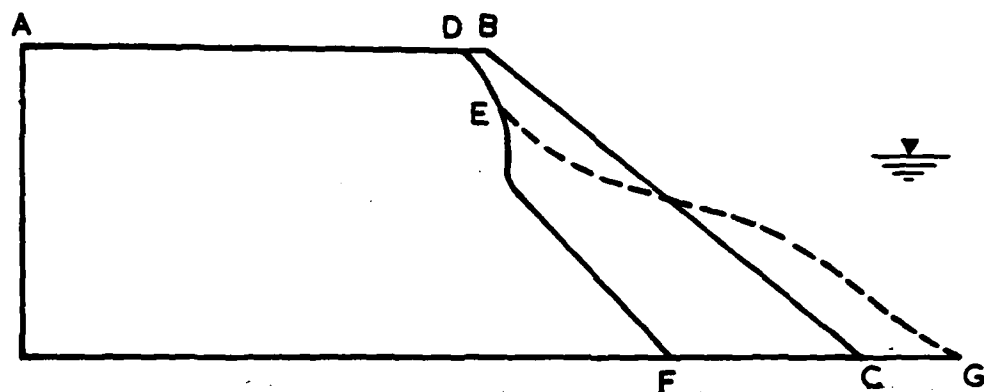
Figure 4.25 - CSC24 Pore Pressure Dissipation During Centrifuge Test

The site investigation revealed in both failures, breakdown of the soil into nodules characteristic of the prototype failure, which decreased in size according to the distance travelled. Moisture contents were slightly higher than previous models, between 65% and 83%, however horizontal vane strengths were typically between  $18 \text{ kN/m}^2$  and  $29 \text{ kN/m}^2$ .

Model CSC22 had been subjected to repeated high stress levels, and its unusual behaviour, in comparison to previous models, was suspected to be in some way a result of this stress path. Model CSC23 was constructed to investigate this hypothesis by cutting a slope of height equal to 104 mm, at a similar angle of  $39^\circ$ . To highlight any deformations below the model surface a series of strongly defined white stripes were imposed on the model surface.

The response of the model, CSC23, subjected also to repeated high centrifugal loadings, with a variety of slope profiles, was different from CSC22, only severely steepened slopes responded with failure in the nature of slope degradation and uplift was not successful in initiating any flowsliding events.

This model was the first to be monitored with pore pressure transducers, embedded within the embankment as shown in table 4.1. The transducer located in the toe was constantly submerged. It showed immediate and predictable increments of response to the changing weight of the head of water, but strangely did not register any response to the application of uplift. The transducer within the slope, directly beneath the crest, but not constantly submerged, fluctuated erratically as surface runoff water filled and drained from the fissures after drawdown. Two disproportionate increases in pore pressure in this transducer were noted, possibly indicating some sort of stable soil movement, however these quickly decayed away, as did one short duration decrease in pore pressure, when uplift was applied at 120g.



0 5cm

(a) 40g

original profile ( $\beta_0 = 45^\circ$ )

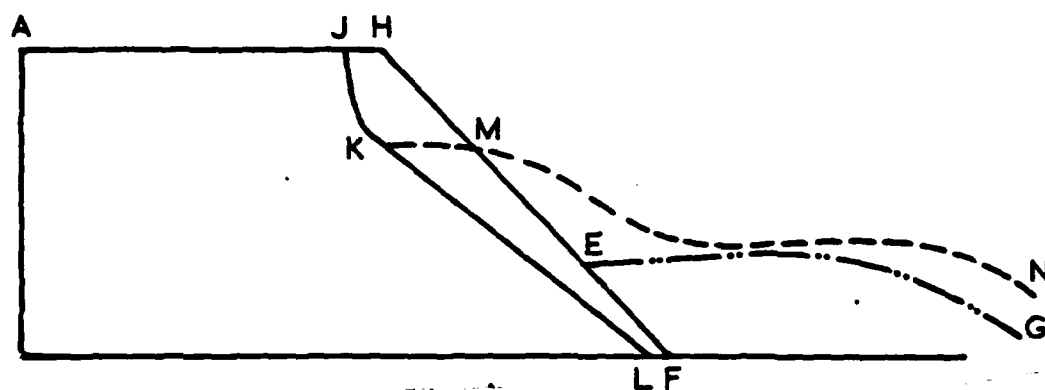
initial failure surface

profile after first failure

ABC

DEF

ADEG



(b) 120g

profile at 40g immediately  
after uplift

final failure surface

final profile

AHF ( intact material )

EG ( debris )

JKL

AJKMN

Figure 4.22 - CSC24 Progression of Failure

Long periods at different centrifugal loadings permitted the measurement of the rates of pore pressure dissipation, figure 4.21, and the calculation of  $c_v$  from the observed values of time to 90% pore pressure equilibrium. The resulting values of  $c_v$  varied somewhat but averaged at about  $151 \text{ mm}^2/\text{min}$ , much higher than that derived from the oedometer tests.

Moisture contents and vane strengths measured after the test indicated values typical of CSC20 and CSC21.

The response of soil models CSC20 through CSC23, all constructed from samples retrieved at the same time and place, was inconsistent. Uplift affected failure mode, but had not provided the essential condition for uniform model response, and it seemed that the behaviour of the models was dependent upon a factor unknown to, and perhaps beyond the control of the researcher. It was thus logical that the last two undisturbed soil specimens again be devoted to a further investigation of the modelling of models.

Two models were constructed with slopes of  $45^\circ$  to the horizontal, founded directly upon the liner without a soil foundation layer, and surcharged with an overburden layer of lead shot. These models had been designed to demonstrate failure, since only by observing actual failure could comments on slope stability be made. The two models differed from each other only in that the first one was, in each dimension, 25% larger than the second.

Model CSC24 responded to an increase in centrifugal loading to 40g by the observed propagation of an inclined plane failure surface first noticed at 38g at the elevation of the free water level, and propagating into the adjacent soil, first downward to the soil-liner interface, then upward, finally reaching the top surface through a tension crack; figure 4.22a. The application of uplift caused the slide debris to move along



the liner and a retrogression developed. The boundaries of the movements are shown in figure 4.22b. Subsequent loading to 120g caused no further response. The overall final appearance is pictured in figures 4.23 and 4.24.

Two pore pressure transducers were embedded in the model in positions shown in table 4.1, and were submerged at all times. The response of the transducer in the underlying filter was consistent with the changing weight of overhead water; the pore pressure change indicated an uplift at the toe only equal to  $r_u = 0.34$ , rather than the higher value,  $r_u = 0.62$ , which had been applied at the source of uplift. No pore pressure response to failure was recorded in this transducer, however the transducer buried in the clay did show a sudden, short duration reduction in pore pressure equal to  $13 \text{ kN/m}^2$  during failure. This same transducer responded to uplift with an immediate  $6 \text{ kN/m}^2$  reduction in pressure, which was partially recovered. Long periods of consolidation in subsequent increases in loading indicated a coefficient of consolidation,  $c_v$ , much higher than measured before:  $575 \text{ mm}^2/\text{min}$  to  $1000 \text{ mm}^2/\text{min}$ , and the dissipation of pore pressures was correspondingly rapid, giving a permeability equal to  $3 \times 10^{-3} \text{ mm/min}$ , figure 4.25.

Model CSC25 was expected to demonstrate similar behaviour to model CSC24 which failed at 40g, but being only 4/5 of that model in height, was expected to fail at centrifugal loadings 25% higher, i.e. 50g, for modelling of models to be achieved. At 40g however, the smaller slope of CSC25 unexpectedly failed, with an inclined plane of slip propagating through the soil in a manner similar to CSC24. The model response to uplift and speed increase also was similar, although the final profile was shallower and had demonstrated two, rather than one retrogression; figures 4.26 and 4.27.

Pore pressure response, recorded by transducer output showed that



the uplift applied to the embankment was the equivalent of  $r_u = 0.30$ , rather than the intended full height of  $r_u = 0.62$  imposed at the source of the uplift, and even this level of uplift at the toe quickly decayed away to  $r_u = 0.24$ ; the proportion of uplift lost through the filter material was in similar proportion to CSC24. The transducer embedded in the clay, responded to failure with a sudden decrease in pore pressure of  $6 \text{ kN/m}^2$  indicating clearly the onset of dilation in the soil, and responded to uplift with an immediate and fully recovered reduction of  $4 \text{ kN/m}^2$  at 50g. No other irregularities were recorded, and  $C_v$  was much lower than in CSC24, at  $115 \text{ mm}^2/\text{min}$ , more in the range of CSC23.

Moisture contents and horizontal undrained vane strengths measured were typical of this test series.

In summary, the sequence of actions recorded in Table 4.2 can be described as explorations of the behaviour of eleven samples formed into nineteen different slope configurations, of which fourteen displayed some sort of slope instability, but at the time of completion of the test series, the factors causing instability were only partially understood.

#### 4.5 Discussion

##### 4.5.1 Measurement of in-test soil response

One of the advantages provided by centrifugal model testing is the opportunity to monitor soil behaviour during the test and to measure soil properties after the test, something which is rarely achieved in the instance of prototype failures. The techniques employed in these tests included the output of pore pressure and displacement transducers during the test, displacements, and hence deformations determined after the test by comparing successive still photographs taken of the model during the test, and vane strengths and moisture contents taken after the test. It

is appropriate to consider the limitations in each of these, however, in order to understand their validity and significance in assessing model behaviour.

The justifiable concern that the insertion of any measuring device into soil may alter subsequent behaviour, is of particular importance in reduced scale modelling. The 6 mm diameter pore pressure transducers which were used in the last three models of this series, CSC23, CSC24, and CSC25, were inserted into the clay models by the shortest possible path, in the horizontal rather than the vertical direction, in order to diminish the effect of their presence. As mentioned earlier in section 3.9, however, the fact that there exists simultaneously a two-level system of permeability, and thus two pore pressure regimes, may also present difficulty as to which pore pressure is significant in problems of slope stability, and which pore pressure is being measured.

The two systems of permeability which co-exist are the permeability of the cemented clay nodules, and the permeability of the network of fissures which define the nodules. At low stress levels relevant to slope stability problems, the mode of failure involves dilation along the fissures and the corresponding increased pressure on nodules involves a little local shearing of the nodules at their contact point, but it is the reduction in pore pressure in the network of fissures which signifies the onset of failure. The pore pressure transducers would ideally measure the pore pressure in the fissures, and both the density of the fissures, and the disturbance inherent in embedding the transducers, make it more than likely that this would be the case. The accurate and quick response of the transducers to externally imposed changes in pressure indicated that this was so. At moments of unpredicted shear and stress changes in the soil, transducers close to the zone of failure, recorded negative pore pressure changes. This was a valuable indication of model response, although

there were not enough transducers available for this research to give definitive data.

Displacement transducers were also used for immediate in-test monitoring of model response. They were used throughout the test series to record vertical displacement at the crest, and in particular to determine the moment of failure (see section 4.3). Their response was considered accurate and instantaneous, within their range.

The determination of soil deformation at various stages of the test was achieved by comparing successive photographs in which soil movement was noted by the change in position of the original grid of silvered indicator balls. Inherent in this is the assumption that the displacements of the balls are representative of continuous and smoothly varying plane strain soil movements in the model. Discontinuous movements of discrete nodules of clay and all effects of side friction, local movement of the balls, and three dimensional, rather than purely plane strain soil response, are disregarded.

It must also be assumed that the margin of error in establishing the position of the balls is tolerable. In this present thesis, the film measuring machine was not used, but it is appropriate to comment that Bassett (1973) noted the accuracy of strain measurement on the Cambridge apparatus is typically between  $\pm\frac{1}{2}\%$  and  $\pm\frac{1}{4}\%$  strain. In a material such as Champlain Sea clay where yield has often occurred at a strain less than 1%, the film measuring technique may not have been accurate enough, even if it had been attempted. La Rochelle et al (1973) independently encountered a similar problem when trying to evaluate strain prior to failure in vane testing in Champlain Sea clay. It is on this basis that strain measurement was not carried out in these tests, although very useful qualitative images of soil deformation were produced. Bassett and Horner (1977) noted that pictures of soil response are still useful to practising

engineers and finite element users, to visualise the overall pattern of shear strains and developing failure mechanisms, and these were produced whenever possible.

Vane strengths and moisture contents are both typical measurements taken in field and laboratory instances of failure to quantify those aspects of failure. Their value in defining at-failure conditions will be diminished by any time dependent changes, and the significance of such changes subsequent to failure becomes magnified in reduced scale centrifugal models.

The time between any model event observed to occur during a centrifuge test and the moment of vane and moisture content measurement, will, for practical reasons, range from one hour to several days. The dissipation of failure pore pressures during that period will have occurred much faster in the model than in the prototype, in fact  $N^2$  times faster, and thus the moisture will also be correspondingly redistributed. In many soils the removal of centrifugal loading will cause swelling and cavitation until a new equilibrium is achieved at earth's gravity, further complicating the significance of moisture contents and vane strengths. In cemented, fissured clays, which are characterised by little swelling, and a highly permeable system of fissures, the return to an equilibrium of stress and moisture redistribution at earth's gravity is almost immediate. Thus vane and moisture conditions measured after a centrifuge test may be reminiscent but probably not truly representative of the conditions existing in the soil models at the moment of failure.

In addition to these considerations, the laboratory vane which was used in these tests was 29 mm long and 19 mm in diameter, which would have the equivalent in a prototype 120 times larger of 3.5 m long and 2.3 m in diameter, clearly out of proportion to any full scale field vane testing. Therefore, with all these limitations in mind, the significance of vane

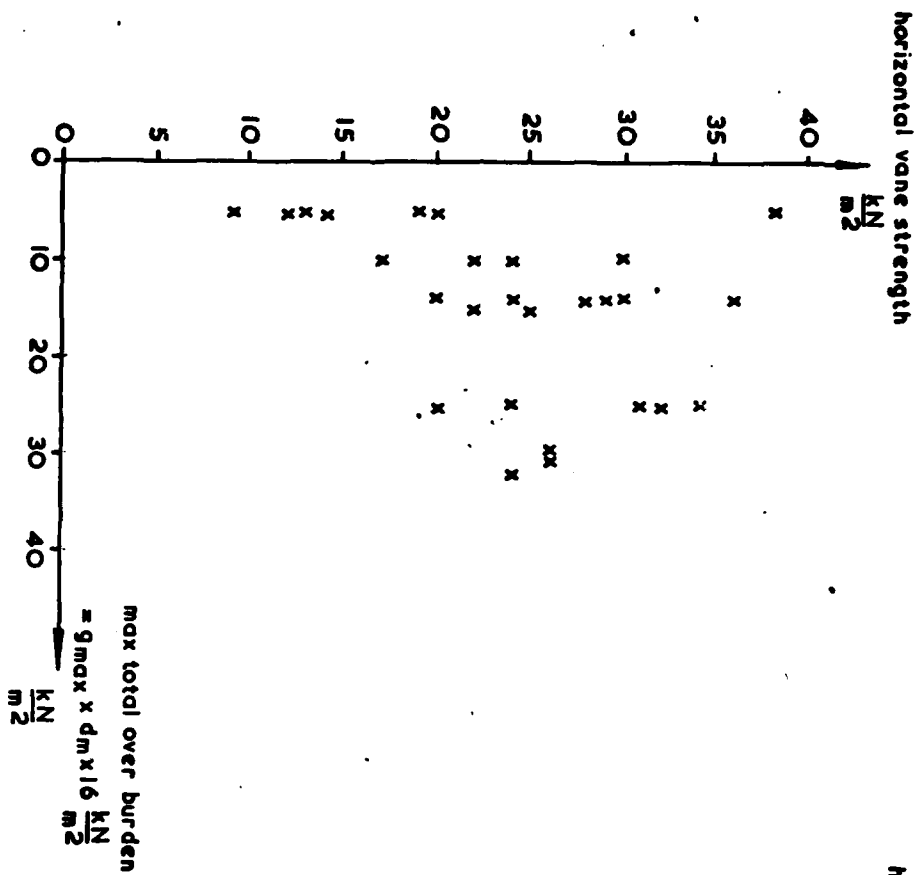


Figure 4.28 - Vane Strength vs Maximum Overburden After Centrifugal Loading

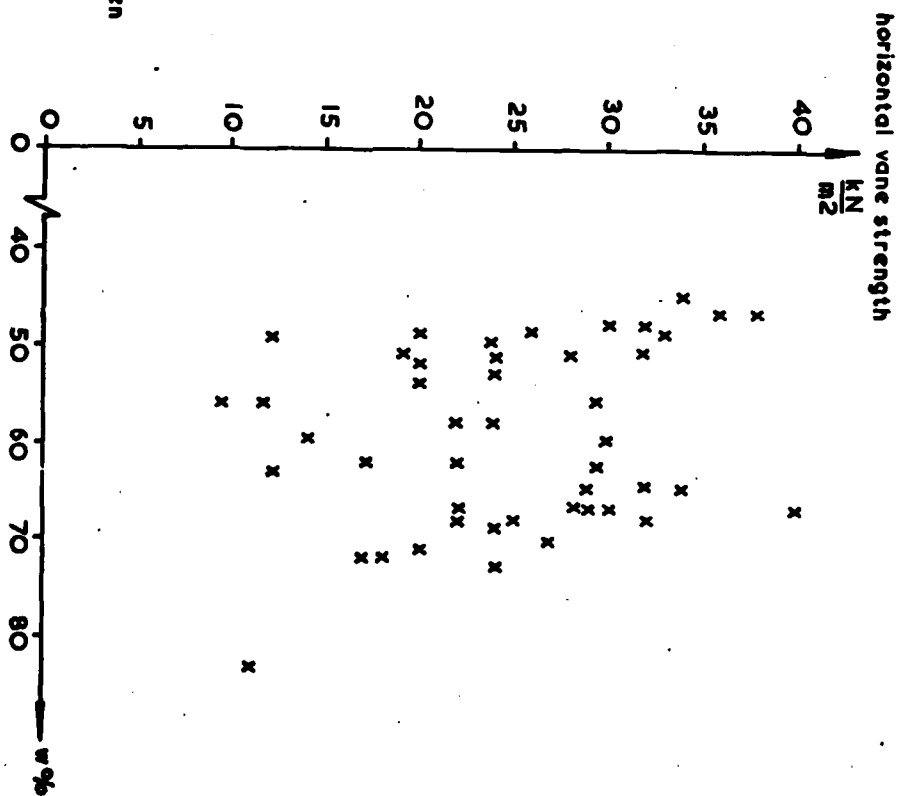


Figure 4.29 - Vane Strength vs Moisture Content After Centrifugal Loading

tests and moisture contents was restricted to comparison between models and was not intended to be extended to comparison with the prototype.

The vane strengths which were measured involved insertion of the vane perpendicular to the vertical plane section of the model, introducing the further complicating problem of anisotropy. These strengths varied in value between  $9 \text{ kN/m}^2$  and  $40 \text{ kN/m}^2$ , the majority being less than  $35 \text{ kN/m}^2$ . There was a general trend toward an increase in vane strength with model depth, although no direct correlation could be drawn between vane strength and the maximum overburden pressure imposed (figure 4.28); neither could any relationship between vane strength and moisture content be formulated (figure 4.29). Such an absence of correlation, however, may be expected in a cemented soil which has been subjected for a geologically insignificant time to effective stress levels which are less than the preconsolidation pressure.

It is of interest that vane strengths measured at the Rockcliffe site in soil above the assumed depth of failure were consistently less than  $35 \text{ kN/m}^2$ , and suddenly increased to  $100 \text{ kN/m}^2$  below the assumed depth of failure. It is conceivable that failure occurred at this depth because of deterioration of undisturbed undrained shear strength from  $100 \text{ kN/m}^2$  to  $35 \text{ kN/m}^2$  above that depth. In this research, the models were built from soil retrieved above that depth in the backscarp of a slope which had failed up to that point, and then a year later failed again; they may have possessed characteristics which placed them on the verge of failure. The response to the horizontal stress release, which would have effects only slightly deeper than the toe, may have been such a factor which caused a reduction in strength. Some samples, the high quality and virtually undisturbed horizontal tube samples, may have been sampled in regions which had not yet experienced this stress relief. The conditions which would later be important for the development of failure in the pro-

prototype behind the backscarp, might not then be duplicated or speeded up in a model on a centrifuge. Other models, the ones constructed from the frost damaged soil, in contrast, may have been accelerated in time to this critical state by the freezing and thawing process. Further consideration will be given to this in section 4.5.4.

#### 4.5.2 Drainage conditions at failure

It is appropriate here to define what is meant by drained and undrained soil conditions, in order to assess the conditions which prevailed during slope failure. Drained conditions are defined by Terzaghi and Peck (1948) to be those under which changes in stress are applied slowly enough, with respect to the ability of the soil to drain, that no excess pore pressure develops, whereas undrained conditions are those where the change of stress relative to this ability to drain occurs so rapidly that no dissipation of pore pressure takes place.

The exact occurrence of these conditions is a laboratory phenomenon where the boundary conditions of a finite soil specimen are controlled. Whenever any free or infinite boundary is introduced, these conditions no longer strictly apply, but to a reasonable approximation one or the other (drained or undrained condition), is usually assumed.

In a centrifuge test where the boundaries of a given prototype are made finite and the dimensions are reduced  $N$  times, the dissipation of pore pressures occurs  $N^2$  times as fast in the model as in the prototype. Thus while drained conditions may be easily modelled, the maintenance of undrained conditions is less easy. This is particularly a problem when using natural soil, if the soil is neither very permeable, as a gravel or sand, or very impermeable, as a homogeneous, unfissured clay, especially when changes in pore pressure becomes an important factor in the mass movements of soil observed; inertial effects scale with respect to

prototype time,  $N$  times faster in model than in prototype, rather than  $N^2$  times, which is the scaling rule for dissipation of excess pore pressures.

It has been mentioned earlier in sections 3.9 and 4.5.1, that the Ottawa area Champlain Sea clay has two relevant permeabilities: that of the network of the fissures, and that of the nodules. While the rate of consolidation may be governed by the permeability of the clay nodules, in a dilatant failure which occurs by failure along the fissures, it is the permeability of the fissures which is relevant. It is also known that as dilatancy occurs, the permeability increases accordingly.

Williams\* measured the initial permeability before failure, by field piezometer tests, to be in the order of  $1.5 \times 10^{-5}$  mm/s, which is almost as free draining as a very fine sand. Therefore before failure in the prototype, it is the general rule that drained conditions prevail; this is the premise upon which Eden and Mitchell (1970) Sangrey and Paul (1971) and Mitchell (1975) based their slope stability analyses. It is even more likely to be the case that drained conditions will prevail in the model where pore pressure dissipation will occur  $N^2$  times faster than in the prototype.

The prevalence of drained conditions was confirmed in the later models where pore pressure transducers embedded in the soil responded almost instantly to various boundary pore pressure stimuli and in the case of increases in loading, equilibrium was established very quickly. The corresponding coefficient of consolidation,  $c_v$ , was large, varying from 100 mm<sup>2</sup>/min to 1000 mm<sup>2</sup>/min.

In the case where a model slope has failed during an increase in centrifugal loading, some excess pore pressures may be present, however the very time which is taken to execute changes in loading is usually sufficient for dissipation of a significant proportion of the excess pore

---

\*D. Williams, Queen's University, Canada, personal communication, 1978.



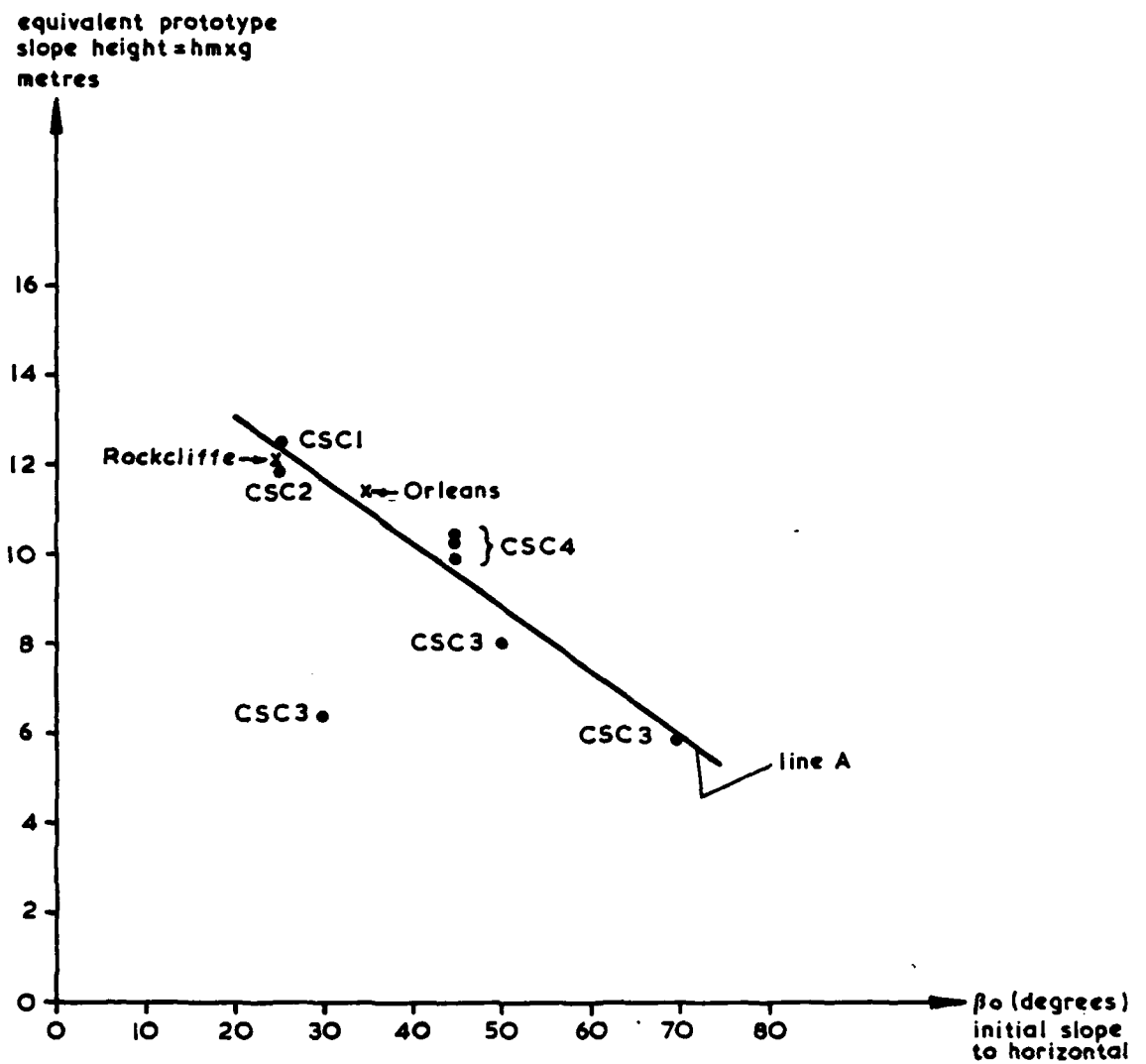


Figure 4.30 - Equivalent Slope Height at Failure vs Slope Angle  
( CSC1 through CSC4 )

pressures generated in this way. Therefore, although saturated conditions may be the case in this clay, model tests will almost certainly display drained behaviour in the undisturbed soil, even during periods of increase in centrifugal loading. It is more than likely, although unsubstantiated, that this will also be the case in the disturbed, frost damaged clay, due to its more open structure. It is therefore probable that rapid undrained loading was never strictly achieved in these tests, and it is also likely that it is not achieved in either initial prototype slope failure or the first retrogressions in the prototype.

#### 4.5.3 Discussion of the individual tests

This section will discuss some implications of the individual tests, grouping the models into two basic categories, and noting their relevance to prototype behaviour where applicable. The two groups are defined by the model soil condition upon arrival: the vertical sample altered by frost in transit was used to construct the first group of four models, CSC1 through CSC4; the horizontal tube samples which were essentially undisturbed were used to construct the second group of models, CSC10, and CSC20 through CSC25. These two groups also demonstrated different and unexpected soil behaviour.

The first models made of the frost damaged soil, CSC1 and CSC2, corresponding in geometry to a plane strain slice of Rockcliffe 18 m in width, failed respectively at 12.5 m and 12.0 m equivalent prototype heights. Their failure resembled slope flattening, more than the abrupt rotational failure expected from the prototype experience.

Models CSC3 and CSC4 were devoted to modelling of models. The three slopes in CSC3 failed with the following equivalent prototype slope dimensions: the  $70^{\circ}$  slope failed at 5.9 m, the  $50^{\circ}$  slope at 8 m, and the  $30^{\circ}$  slope at 6.4 m. The three  $45^{\circ}$  slopes cut at different scales in model CSC4, all failed at equivalent prototype heights within 6% of

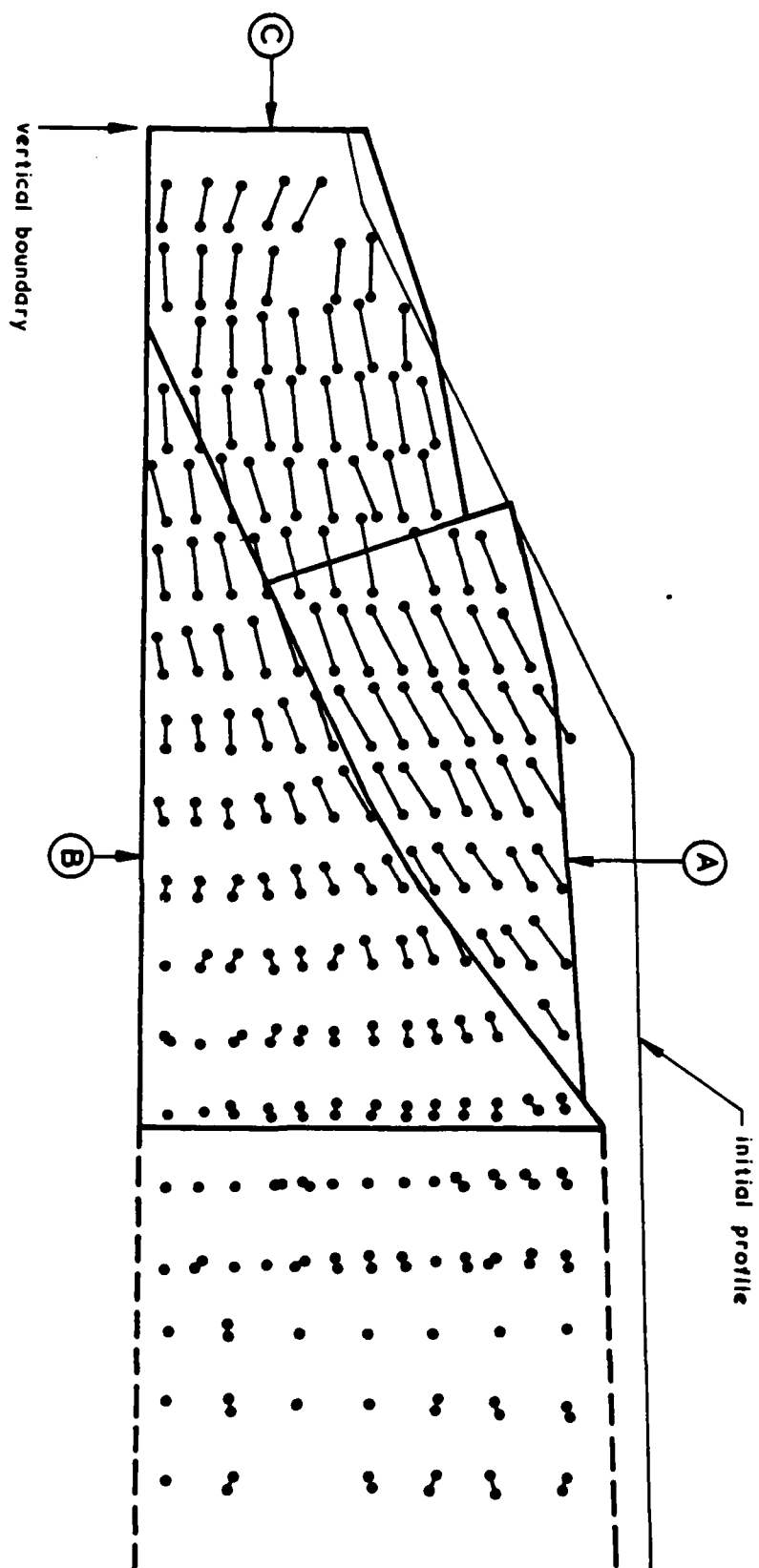


Figure 4.31 - Three Part Failure Mechanism ( Displacements of Model CSCI  
With Component of Vertical Compaction Removed )

each other, varying between 9.9 m and 10.5.

Data of failure of these four models, CSC1 through CSC4, as shown in figure 4.30 fit a single line, line A. It is of interest to note that data of both the Rockcliffe prototype landslide, and another Ottawa area landslide occurring at Orleans (see Mitchell and Markell, 1974) also plot on this line. The tests show self consistent behaviour within the range of model scales used, but raise the question of similarity between this "damaged" material and the in situ soil at failure in the prototypes.

The shape of the failures observed in these models consistently assumed a three part failure. By removing the component of compaction, which occurred during the initial centrifugal loading of each of these four, frost damaged models, and re-examining the model soil displacements, as shown in figure 4.31, an interesting pattern of failure emerges. The failures observed involved not so much rotational movement, as a combination of translation, shear and compression. Referring to figure 4.31, it appears that one block, A, has undergone uniform translation: the displacement vectors are parallel and uniform in length. The wedge below block A, designated as B, has been sheared and slightly elongated in response to the movement of A, sliding at some points along the interface between the soil and the rigid model base. At the toe of the slope, block C has been compressed: the displacement vectors become progressively shorter as the vertical boundary is approached, and the block consequently increases in depth due to the compression.

The second group of models, which were constructed from the essentially undisturbed horizontal tube samples, showed more variable results. Data of critical equivalent prototype height and slope angle, figure 4.32, did not all lie on the same line that fitted data of the first group of models. Three of the second group of models showed essentially no failure; one showed quite erratic behaviour (CSC22); three models adhered

equivalent prototype  
slope height =  $h_m \times g$   
metres

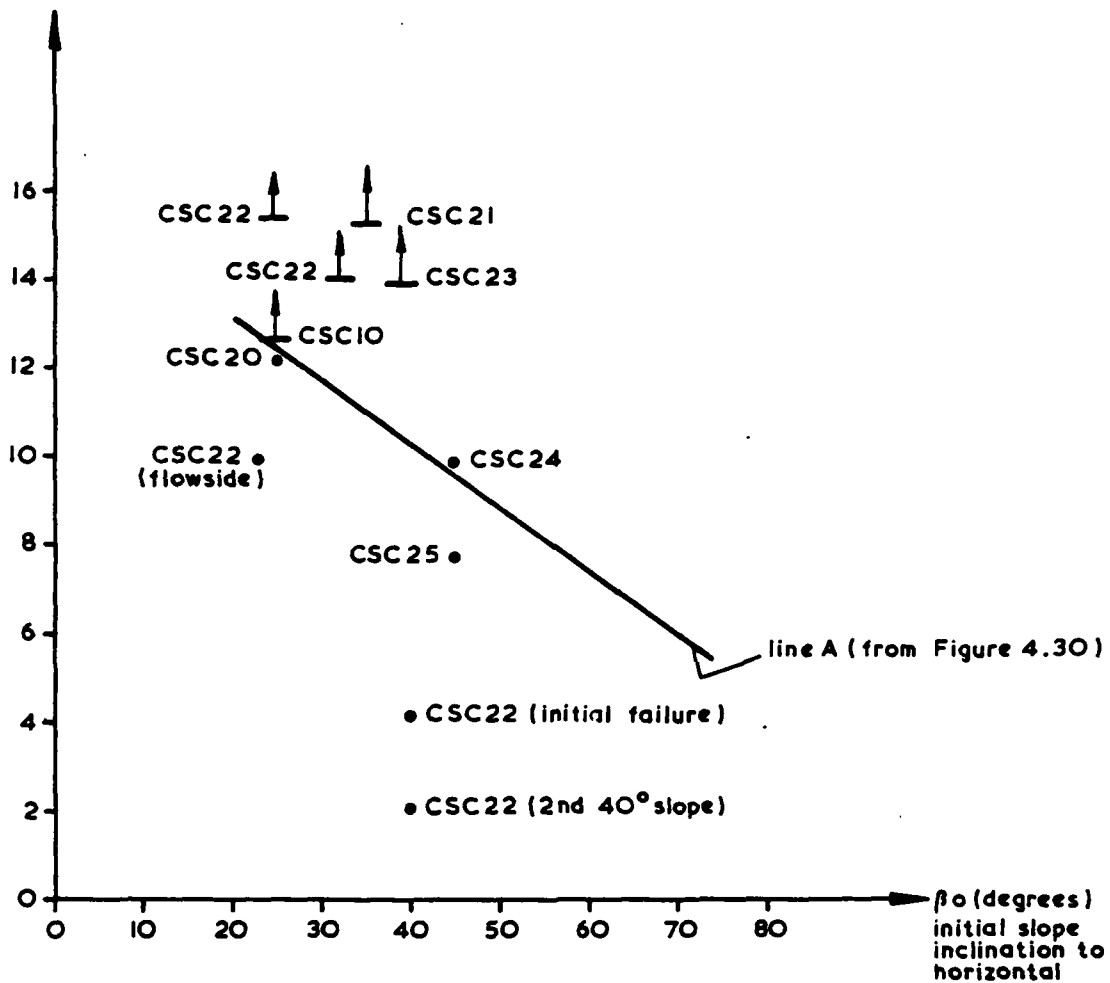


Figure 4.32 - Equivalent Slope Height at Failure vs Slope Angle  
( CSC10, CSC20 through CSC20 )

reasonably to the original line of correlation. Of this last group of three, CSC20, which was in the geometry of the Rockcliffe prototype landslide, showed a pattern of failure very similar to the three part phenomenon discussed above. This seemed to indicate both that those movements observed in the frost damaged soil models were not unlike those in the supposedly intact soil, and also that those movements may not be dissimilar to prototype failures, although the depth of failure seemed to disagree with that established at the prototype landslide. The introduction of opportunity for strain, not existing in the prototype, in the form of material disturbance in the first group of models, and possibly an imperfect fit between soil and model boundaries in all models, may have permitted a deeper and more complex mechanism to develop in the models than in the prototype, but the basis of the failures observed may be correctly representative of the prototype\*. The lack of correlation of several of the tests of the second group suggested a possible inherent variation in the soil condition: there may be various degrees of disturbance pre-existing at different points on the site sampled, or introduced during the handling of the soil; this aspect will be further discussed in section 4.5.4.

The effect of uplift was also investigated in this second group of models, and it seemed that the highly permeable fissured soil used in these experiments may respond to uplift in a manner differing from unfissured clay. Uplift did not appear responsible for the initiation of slope failure in any of the models, but did influence the subsequent mode of failure. In model CSC22, the soil underwent several cycles of preliminary stressing. When a shallow toe failure finally occurred, the debris broke down into the characteristic nodular form, and the subsequent application of uplift transformed this debris into a flowslide. The preliminary stressing and initial failure seemed to be sufficient to

---

\*The depth of failure was not expected to extend to the full model depth, and consequently the angle of friction between the clay and the liner was not measured.

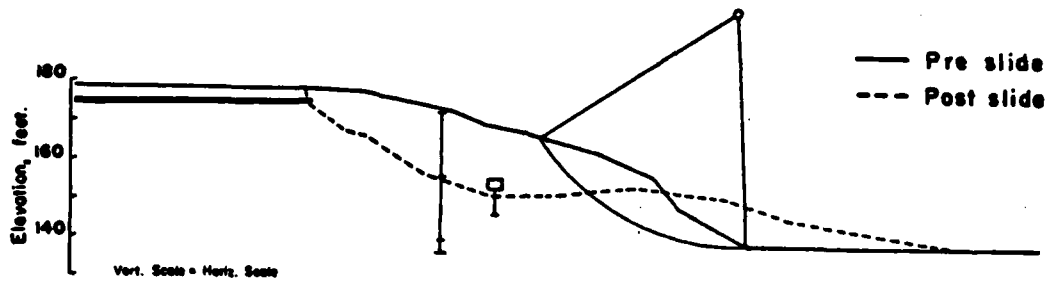


Figure 4.33 - Preslide and Postslide Centreline Contours at the  
Rockcliffe Parkway Slide ( 1969 )  
( Sangrey and Paul, 1971 )

destroy the structure and reduce the permeability of the once highly permeable, fissured clay, to a point at which high pore pressures could be retained, and the soil was borne away in a flowslide manner.

It would be unusual but not impossible for such a transformation of soil structure to occur in nature. If such a transformation did occur, only the initiation of the flowslide, caused by uplift, would be correctly modelled; the distance travelled and the time over which the movement was sustained in the model might not be modelled correctly at the same  $\frac{1}{N}$  scale, as the lifespan of flowsliding depends on the rate of pore pressure dissipation which is scaled  $\frac{1}{N^2}$  times. It is interesting to compare the development and final profile of model CSC22 (figure 4.18b) to that of a landslide which occurred 2.5 km upstream of the site of sampling, figure 4.33. The similarity suggests that the phenomenon modelled may also occur in nature.

In the second group of models where modelling of models was studied in CSC24 and CSC25, the result did not confirm the repeatability of tests and the correctness of scaling laws in this intact material. Both slopes were in the same geometry, at  $45^\circ$  to the horizontal, but at different scales. Their modes of failure were strikingly similar: an inclined plane of failure rapidly propagated through the slope to form the first failure, and subsequent retrogression involved a combination of nodular degradation and intact sliding. The respective equivalent prototype heights at failure, however, were not in agreement, despite the similarity of failure mechanisms.

These model tests suggest possible, but unconfirmed answers to the problem of prototype failure in fissured Ottawa area Champlain Sea clay. Much may depend on the state of the soil just prior to failure as to the propagation and shape of failure, the effects of uplift, and the significance of the fissures; speculation on the absence of the desired



retrogressions in the reduced scale model is also possible and these aspects will be discussed in the following section 4.5.4.

#### 4.5.4 General trends in model behaviour

Slope stability in Ottawa area Champlain Sea clay has been studied by others by field survey subsequent to full scale failure, with numerical analysis based upon soil properties derived from laboratory tests. This present research, founded upon such a background, has identified new features of prototype slope failure in reduced scale centrifugal model study. Certain features of failure have been confirmed, and new insight into failure mechanisms, some previously speculated, and some not, have been observed. New information on reduced scale centrifugal models has also been achieved.

Ottawa area Champlain Sea clay is an unusual material characterised by a cemented, fissured structure which develops yield at strains often less than 1%. At stresses greater than yield strain is large. This characteristic was observed to occur in the models, and permitted easy delineation of zones of failure.

Previous successful slope stability analyses which were carried out using the Bishop method of slices assumed a circular, rotational failure. Critical failure circles in those analyses were consistently through the toe, and the approximate correctness of this depth of failure was confirmed in the field by vane testing in the crater of landslides. Such a failure surface was not, in general, observed in these model tests.

Following Taylor's (1948) notation, if we designate the slope height by  $H$ , and the depth to any surface below the crest by  $DH$ , then for the Rockcliffe slope failure surface, the value of  $D$  was approximately 1.1. The model dimensions chosen should have been fully sufficient to contain any such failure, since the rigid base was at a depth  $D = 1.92$ . The

introduction of model boundaries such as the vertical boundary in front of the toe, and the horizontal model boundary at the base did mean that there were rigid boundaries much closer to the model slope than in the prototype and it is possible that these soil and model boundaries were an imprecise fit. In some cases slip occurred along the model base, and in other cases failure occurred close to the toe of the slope. This variation indicated that the failure may have been either impeded or altered by the model boundaries, but it is unlikely that failure was caused by them.

The slope failures observed in this present series of tests have been consistently non-circular, contrary to Bishop's assumption and have fallen into three categories: intact slope failure, slope degradation, and flowsliding.

Intact slope failure occurred in several models, built of both disturbed and undisturbed soil. In models where Taylor's parameter  $D$  was larger than unity and slope failure was characterised by movement of an intact wedge or block of soil, failure was consistently deeper than the toe of the slope, and was without resulting degradation to the nodular soil state. Soil displacement, discussed previously in section 4.5.3, did not appear to be either circular or rotational, but rather occurred in a three part interaction of shear and translation. It is correct in material displaying dilative failure that a regular, circular surface should not occur, although the non-circular surface which would be correct would be a logarithmic spiral curve: such a curve leads to constant dilation at all points along the failure surface. This observed occurrence of translation, rather than rotation, does not appear to have been suggested previously in discussion of Champlain Sea clay slope instability displacements.

Two model slopes, CSC24 and CSC25, were constructed directly on the hard base of the centrifuge strong box liner, so that Taylor's parameter  $D = 1$ ; this was equivalent to a bedrock outcrop at the toe of a prototype slope. These model slopes also showed initial intact soil movement; failure was observed to occur as an inclined plane of failure which propagated rapidly through the soil at  $47^{\circ}$  and  $40^{\circ}$  to the horizontal in the two models. The soil material both above and below the line of failure remained virtually unstrained. The time required for this behaviour may well reflect the time needed for development of stress and strain discontinuities.

Failure by slope degradation generally occurred in the steeper slopes, and in the models made from undisturbed soil, this was not accompanied by other strain in the remaining soil slope. Material crumbled into nodules and fell from the face of the slope above the toe, rolling and slipping into a talus which lay across the original location of the toe of the slope. This was indicative of dilative failure at the individual nodular level, rather than along a single failure surface, as in the intact soil movement described above. Such behaviour on the nodular level was sometimes observed to occur in a backscarp subsequent to initial intact soil movement.

Failure by flowsliding was an unusual mode of failure which occurred in direct response to uplift, although uplift alone was insufficient to trigger its occurrence. The fissured soil typically was too permeable to retain the high pore pressures necessary for flowsliding, which may be provided by uplift. If the soil, however, were continually stressed and degraded, as occurred in model CSC22, so that the structure of the soil was broken down, and the permeability was correspondingly reduced, then the effect of uplift sometimes proved to be sufficient to initiate flow-

sliding. Mitchell\* noted that earthflows are not observed in fissured clays as a rule. In those clays, then, uplift may alter the mode of subsequent behaviour, but probably not the occurrence of initial failure.

A feature of the prototype slides which was not observed in the majority of the reduced scale models, was retrogression. One model, CSC20, may be interpreted as showing the initiation of retrogressive movement, however the failure of the model to duplicate the prototype evacuation of the landslide crater which would then leave an unsupported backscarp susceptible to retrogression, may explain this behaviour. Both Beasley (1973), and Bassett (1973) emphasised that certain soil behaviour, such as the loss of strength with deformation, may be dependent upon unscaled displacement rather than strain. This may also well apply to the loss of strength which is characteristic of sensitive soils and which may be responsible for the evacuation of the prototype landslide crater. If the movement of material away from the site down shallow slopes depends not upon strain, but rather on unscaled displacement, then such prototype behaviour may not be expected to be modelled. Only in two models, CSC24 and CSC25, was obvious retrogression observed: by the application of uplift, the necessary reduction in friction was achieved which permitted the initial wedge of failure material to move away from the remaining steep backscarp, which subsequently failed again.

A dominant feature of this model test series is that models made of frost damaged soil behaved in a self-consistent manner and correlated well with two known prototype landslides, whereas the essentially undisturbed material neither demonstrated self consistent behaviour, nor did it correlate well with the prototype failure which occurred at the Rockcliffe sampling site. This behaviour may be indicating two features about failure, one with respect to the role of the fissures, and one with

---

\*R.J. Mitchell, 1977, Queen's University, Canada, personal communication.

respect to stress release.

The densely fissured structure of the Ottawa area Champlain Sea clay distinguishes it from other cemented, sensitive clays and imparts to it a unique mode of slope instability (see sections 3.3 and 3.4). Sangrey and Paul (1971) investigated landsliding in the Ottawa area, an area known to have two different deposits of sensitive fissured clay. They concluded that landslides occurred almost exclusively in the densely fissured fresh water clay, rather than in the underlying less fissured, marine clay, in spite of the lower undrained shear strength and greater sensitivity of the marine clay. In the low stress regions relevant to slope stability, the failure mechanism is a function of the strength of the cementation bonds and the frequency of the fissures. The dilative mode of failure, in which the fissures open between nodules, occurs more easily in the densely fissured clay than a shearing mode of failure in which there is displacement through the cemented nodules. The fissure spacing is therefore critical in dilatant failure. In the freshwater clay, this spacing varies from 1 mm to 10 mm; in the marine clay the spacing is much larger, varying from 150 mm to 200 mm. This, they asserted, is the basis for the critical difference in behaviour, and the unscaled frequency of fissures in the reduced scale models, may have significant influence on model behaviour.

It is an inherent feature of centrifugal modelling that provided soil and boundary conditions in a given model correspond to those in a given prototype, every soil element in that reduced scale model is subjected to precisely the correct stress path for that equivalent prototype. In a series of triaxial tests, this could be investigated by a vast number of subtly changing assumed prototype stress paths. Eden and Mitchell (1970) executed a large number of triaxial tests on block samples taken from the Rockcliffe site, over a range of the possible prototype stress conditions. In each 36 mm by 72 mm long cylindrical sample, they tested the

soil to failure under a given single stress condition. They also varied their specimen size from 36 mm diameter, to 72 mm diameter, and based upon the similarity of the results, they rejected the existence of any size effects on their results from the regular 36 mm diameter specimen size.

In this series of centrifuge tests, the minimum model soil thickness was 80 mm at the toe of the slope, more than the diameter of the largest specimen tested by Eden and Mitchell. This section of soil, however, was not subjected to a single overall stressing condition as in a triaxial test, but rather to continuously varying stress conditions. Each element in the soil was made to feel the stress path of an element which is, perhaps, 120 times larger, as in the case of Rockcliffe; changes in stress direction and magnitude occurred 120 times faster, and components involved in the failure mode were playing a correspondingly larger role.

In the case of homogeneous clays, the principle structural component is the clay particle, which is considered to be far too small to produce any significant size effects, except, perhaps when considering the unscaled thickness of a failure surface (see Beasley (1973) and section 4.3). Cemented, fissured clays in which the fissures dominate the mode of failure may be a different case. The fissure spacing no longer appears to the model slope to be between 1 mm and 10 mm, but N times larger, which, in the case of Rockcliffe, becomes effectively 120 mm to 1200 mm. The failure mode observed, which is very dependent upon the role of the fissures in dilation, as explained by Sangrey and Paul (1971), may now be determined by a new function of cementation strength and frequency of fissure spacing. Dilatant behaviour may then depend on the chance positioning of the fissures in the reduced scale models, and in the case where the fissure arrangement is not conducive to failure, the cementation bonds will characterise the failure model.

The soil from which models CSC1 through CSC4 were made, was damaged, and yet at the same time retained some semblance of the original fissured, cemented, sensitive nature. This damaged material also compared favourably with the undisturbed soil when tested in triaxial tests. If the frost had damaged the soil by breaking apart the original arrangement of fissure blocks sufficiently to make them less perfectly interlocking, and possibly slightly smaller in size, for instance, all to the minimum natural dimension of 1 mm, then the energy required to achieve dilation would be much less. The behaviour of such models may then be expected to be more similar to the prototype than those models made of undisturbed soil, and at the same time the triaxial test results could still appear similar to the undisturbed triaxial results in the same way that Eden and Mitchell's (1970) two sizes of triaxial specimens did not reveal any size effects.

Suklje (1967) also made relevant comments on the importance of the role of fissures. He said that in the gently inclined portions of a potential slip surface crossing the main direction of fissuring, the greater resistance to shear failure encountered may stabilise the slope. If the frequency of fissures is effectively reduced as in a reduced scale model, then this reinforcing effect may be increased, markedly decreasing the number of feasible potential failure surfaces.

On figures 4.30 and 4.32, which relate equivalent prototype slope height, to slope angle, tests CSC1 through CSC4, with the exception of one slope in test CSC3, are self-consistent. The results of models CSC10, and CSC20 through CSC25, on the other hand, lie more often off than on that line of correlation. Three model slopes did not even fail within the speed limitation of the centrifuge, and of the ones which did fail, three lie reasonably close to the line, and model CSC22 behaved in a seemingly erratic, changing fashion. These undisturbed soils did not act

in a self-consistent manner.

The erratic behaviour observed in the reduced scale models constructed of undisturbed soil, which is composed of an exact fitting network of fissures, may be governed by the chance positioning of the fissures. In contrast, the disturbance of the soil which occurred when the large vertical sample was frozen seemed to be sufficient that at reduced scale modelling within the range between  $\frac{1}{70}$  scale and  $\frac{1}{120}$  scale, behaviour in this first group of models was self consistent. When carrying out reduced scale modelling of soils with large particles, such as sand or gravels, particles of large size are usually removed. In the case of cemented, fissured, sensitive clay, it would be ideal to retain those structural characteristics of the clay, and at the same time increase the frequency of fissuring to be more in scale with the reduction of model dimensions. Remoulding is not a realistic alternative, as the dominant features of the soil structure which are important at low stresses, would be lost. Freezing and thawing seemed to break down the fissure blocks somewhat, and pry them apart so that in this less tightly interlocked state, less energy was required to initiate dilation. The precise nature of these effects is, however, unknown and this cannot yet be depended upon.

The unscaled role of fissures in centrifugal models of this soil is clearly a problem for all reduced scale modelling. Considering the importance of fissures in the failure mode, it was anticipated that this might pose a complication in these models. However, since some prototype failure characteristics were observed, and good correlation with prototype events was achieved by some soil models, another important and unanticipated feature of soil conditions at prototype failure may be duplicated in some soil models and not in others.

The models constructed of the frost damaged soil were self consistent, with the exception of one slope, and also correlated well with two proto-



type landslides in the Ottawa area; the undisturbed samples, on the other hand, were much more erratic in behaviour. This suggests that some feature of the frost damaged soil may be more similar to the prototype landslide soil at the moment of failure than the undisturbed samples. Such a difference may be a change in soil structure prior to failure at the prototype slope, which is not modelled in the centrifuge. The opening of tension cracks in the prototype prior to failure suggests that this phenomenon may be some form of horizontal stress release.

The erratic pattern of failure observed in the models constructed from undisturbed soil may have been the result of varying degrees of disturbance, either pre-existing at the sampling site, or introduced during model preparation. Such disturbance which may cause a change in soil structure, and consequent loss of strength, similar to horizontal stress release, may conceivably have been introduced into the large vertical soil sample by freezing and subsequent thawing. The frozen material experienced this effect, however, throughout the model depth, rather than the effect being restricted to soil above the toe, as in the prototype. This may explain why the weakened material displayed soil movement much deeper than noted in prototype landslides. The fact that vane strengths measured in the model soil agree with the range of undrained shear strengths measured in the prototype landslide debris adds weight to this hypothesis.

These model tests have introduced new information to the understanding of failure mechanisms occurring in the Ottawa area Champlain Sea clay. The shape of failure, the effect of uplift, and the possible importance of horizontal stress release have been discussed. The limitations on reduced scale centrifugal modelling with regard to unscaled time effects, structural characteristics in the form of fissures, and the relationship of displacement to loss of strength have also been considered.

#### 4.6 Conclusion

This series of reduced scale centrifugal modelling of slope stability in Ottawa area Champlain Sea clay involved the initial task of successful retrieval and transport of intact samples to Cambridge University from the site of a previous landslide at Rockcliffe, Canada. This was achieved in the case of seven horizontal tube samples, and presumably would also have been the case in the one large vertical sample, had the soil not undergone winter frost damage in transit.

Regardless of the condition of receipt, all samples were used, to form eleven models into nineteen different slope configurations, and at the conclusion, benefit was derived from each of these models. Fourteen slopes showed some sort of slope instability, varying from deep intact soil movement, to slope degradation, to flowsliding. Speculation has been possible with regard to the mechanisms of slope failure, the possible importance of horizontal stress release prior to slope failure, and the influence of uplift on the mode of slope failure occurring subsequent to initial instability of prototype slopes in Champlain Sea clay. Centrifugal modelling has been seen to be limited by unscaled effects, such as structural characteristics in the form of fissures, and time effects in the form of stress release response.

The research set out to broadly investigate failure mechanisms in a clay which may sometimes develop disastrous slope instability. The conclusion is broadly as follows. In the frost damaged state, slopes of this material can stand to heights indicated by the line A in figure 4.30. The strength of relatively undamaged material is less predictable. Its initial failure may be much affected by release of horizontal stress, and can involve inclined planes of rupture behind a slope with displacements which resemble behaviour of soft brittle rock more than of plastic soil. Subsequent to failure with pore water uplift pressures at the toe, the

debris may remould as it flows away and become less permeable than it was in the original fissured, undilated state; this material, which can now retain high pore pressure within itself can flowslide away.

## CHAPTER 5

### COAL MINE WASTE - INTRODUCTION

#### 5.1 Mine Waste

Significant problems and expense are posed to the mining industry in the disposal of mine waste each year. The current rate of production of mine waste in Britain is 163 million tonnes per annum (Taylor (1978)), and in the United States disposal of mine waste is expected to approach  $3 \times 10^9$  tonnes per year by 1980 (Blight (1977)). The typical disposal method in waste heaps and waste embankment dams has produced the largest man-made structures on earth, the only individually discernible works visible from a satellite in orbit 900 km high (Blight (1977)). This aesthetically undesirable method of disposal may give rise to additional problems in the form of leachates which pollute adjacent streams and groundwater, embankment fires and slope instability (Holubec (1976)); when water is ponded behind waste embankments, the problems are often worsened, and in the case of slope instability, more complicated, and the consequences of failure worse.

These embankments, which are continually under construction, growing in height and area, have not hitherto been designed on a geotechnically sound basis (Blight (1977)). Common disposal practice includes hydraulic filling and endtipping, which provide for no compaction control. Such techniques were largely abandoned in the construction of conventional dams with the introduction of good earth moving and compaction equipment, and subsequent to failure of the world's largest hydraulic fill dam, the Fort Peck dam in Montana, U.S.A., in 1938 (Wilson and Squier (1969)).

In the coal mining industry the disposal of waste is a particular problem, composing 9% to 33% of the total material removed from the ground (Cowherd (1977)). The rate of production of such waste in the United Kingdom is at present

58 million tonnes per year, and areas of disposal account for 30% of all derelict land in the country. In the United States, colliery waste disposal is expected to increase to  $1 \times 10^9$  tonnes per year by 1980\*.

Slope instability is a serious problem in coal waste. Two recent disasters, the Aberfan, Wales disaster in 1966 responsible for 144 deaths (Davis et al (1967)), and the Buffalo Creek, West Virginia disaster in 1972, causing 118 deaths (Corp et al (1975)), are sufficient evidence of the difficulty and dangers in coal mine waste embankment instability. The problem is clearly deserving of research attention. In recognition of this general problem, Malushitsky (1975) investigated slope instability of open cast sulphur and manganese mine waste embankments in the Ukraine, over six years, using the centrifugal modelling technique. His work established the usefulness of this approach to these largely unexplored problems in coal mine waste, undertaken in this research.

## 5.2 Coal Mine Waste Disposal Practice

The waste which is produced in coal mining may take as many as three different forms, depending upon the type of mining and the processing stage. In the case of open cast or strip mining, the initial waste is the overburden; this waste may or may not be suitable for disposal in homogeneous embankments, and typical precautions, such as providing for dissipation of excess pore pressures during construction in less permeable soil, must be taken. In both open cast and underground mining operations, two further types of waste are produced according to the processes of extraction treatment, one coarse waste and one fine waste. These wastes present their own special difficulties, and disposal methods are usually adapted so that both types may be deposited at the same site. The coarse type of waste is the subject of this research, in the normal combined disposal configuration.

---

\* F.C. Townsend, Waterways Experiment Station, U.S. Corps of Engineers, U.S.A., personal communication, 1977.

The natural geological development of coal seams occurs in sedimentary rock, surrounded by layers of sandstone, siltstone, limestone, clay or mudstone, and shale. The coal seam is not usually thick enough to allow the extraction of coal without any of the adjacent material, and as the seam is approached and mined, both coal and adjacent material are removed. The coal is prepared for use, in one or two stages, and two correspondingly different types of waste are produced. Crushing and cleaning of the coal to a coarse state, for heat and steam generation, produces a coarse discard of usual maximum size 125 mm, composed of the surrounding sedimentary rocks. This waste is transported by conveyor belts, trucks and aerial tramways to the disposal site, where it is usually dumped uncompacted, either down the face of an embankment, or in horizontal lifts. Further processing of the coal to a finer grained quality for the metallurgy industry, produces a light weight waste, or tailings, which is pumped in a slurry form to be deposited and dammed behind the coarse embankment (Holubec (1976)).

Tipping and disposal configurations of the coarse discard and tailings may adopt a number of geometries depending upon the nature of the available disposal area. Dry tipping of the coarse discard alone, generally forms the simplest and safest tips, provided the foundation material is competent and dry. At Aberfan, coarse discard tipped over top of an intermittent spring resulted in catastrophic failure.

The problem of disposal of both fine and coarse waste usually results in a combined method of disposal, where the coarse embankment is used to retain a slurry pond often within hill slopes on two or three sides, if such topographic features are available. This dam often causes enclosure of a watershed, and failure to accommodate in design the volume of rain runoff emptying into the dammed area has caused failure as a result of unexpectedly high seasonal runoff.

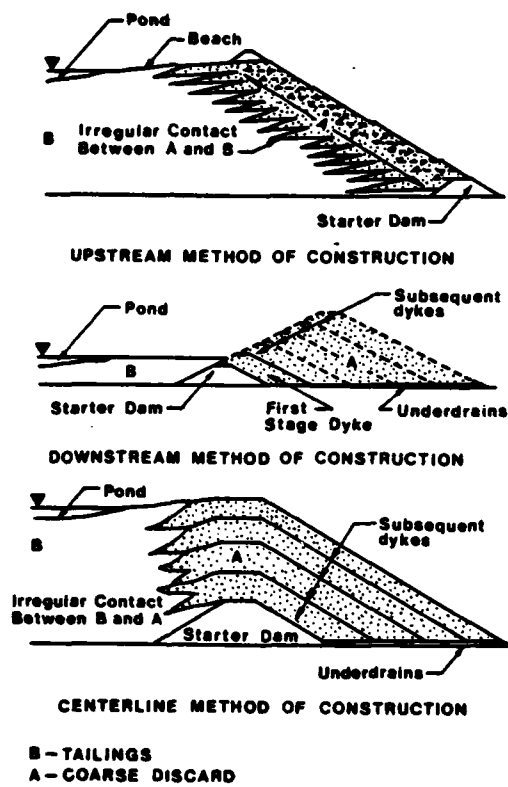


Figure 5.1 - Typical Design Sections of Tailings Dams  
 ( Mittal and Morgenstern, 1975 )

Although other, safer methods have been proposed (Mittal and Morgenstern (1975)), traditionally one of three methods of disposal construction is used. Figure 5.1 illustrates these three waste disposal construction practices, all of which involve a combination of an embankment of generally uncompacted, tipped coarse discard, retaining a pool of water and a beach of hydraulically filled tailings. The upstream construction method in which successive lifts of coarse discard are founded upon previous beaches of hydraulically filled tailings, is at once the oldest and most unsafe type of design. This method has two attractive features, the maximum downstream limit of the dam is immediately defined, and construction itself is cheaper. The two safer methods, downstream and centreline construction, in contrast, continually advance their boundaries downstream as extra dam height is required, and may require extra, coarse borrow material.

Any of these methods which rely for embankment stability upon the hydraulically filled tailings beach, constitutes poor design: the low shear strength, low density, and low effective stress of the tailings when submerged, make it a poor embankment material. In addition, the fact that it is continually submerged, makes direct observation of any initial instability impossible, until the consequences have advanced to a dangerous stage. Coarse discard, however, is also a poor quality and changing material for embankment dams. The engineering properties of these two materials, are discussed in the next section (Holubec (1976), Blight (1977)).

### 5.3 Engineering Properties of Coal Mine Waste

The most significant geotechnical features of coal mine waste is that it is continually changing, being weathered both physically with handling, and chemically by weathering. In addition, it is light in weight, and when submerged it loses most of its frictional strength due to buoyancy.



The specific engineering properties of coarse discard and tailings are outlined below.

Coal discard from the initial stages of mining, is composed principally of shale and mudstone (30% to 70%), coal and carbonaceous shales (15% to 50%), and sandstone and siltstone (up to 10%). The properties of shale and mudstone dominate the engineering properties of the coarse discard, and they are especially susceptible to mechanical and chemical weathering, changing with time and handling methods. In contrast the low quality coal and carbonaceous shales are reasonably resistant to weathering, but their low weight and combustible nature make them also undesirable from the standpoint of slope stability. Sandstone and siltstone are the most stable components, but by their low proportion, they are the least important in influencing engineering properties.

The coarse discard as a whole, has an average specific gravity generally less than that of normal soil, ranging from 1.7 to 2.4, and its unit weight is often correspondingly low, varying in the range of  $19 \text{ kN/m}^3$  when fresh, to as low as  $7 \text{ kN/m}^3$  for the most weathered refuse. The implications of such low unit weight are particularly apparent when the waste is submerged, its frictional shear strength substantially reduced by the reduction in effective stress.

The shear strength parameters of coarse discard are also particularly sensitive to the stress conditions, and weathering which has occurred. As the proportion of fine material increases in the coarse discard with the breakdown of the weak particles, due to either chemical or physical weathering, the effective angle of friction may be reduced. Holubec (1976) mentioned a change in angle of friction as dramatic as  $14^\circ$ , changing from  $\phi' = 40^\circ$  for fresh coal waste, to  $\phi' = 26^\circ$  for weathered material at high confining pressures. Wahler and Schlick (1976) are noted by Blight (1977) to define a smaller but still variable range between  $40^\circ$  and  $34^\circ$ , and

such changes in frictional properties are also substantiated by Taylor (1978).

Permeability of coarse discard also changes over time according to weathering. It may typically vary from  $10^{-3}$  mm/s to  $10^{-5}$  mm/s in material in which some weathering has occurred but compaction is still low, although extreme values, from 1 mm/s for freshly deposited coal waste, to  $10^{-7}$  mm/s for densely compacted, coarse, but weathered material, have been measured, the lowest value being even less than the typical permeability of tailings. Migration of tailings fines into the coarse waste may also cause a reduction of permeability, and deposition in lifts may permit segregation of particle sizes giving rise to anisotropic permeability, and even anisotropic shear strength.

The fine tailings waste ponded behind the coarse discard, is composed predominantly of the light and highly erodible coal and carbonaceous shale washings which are reasonably stable over time with respect to weathering. The specific gravity is low, ranging from 1.4 to 2.0, and the hydraulic fill method of deposition, which permits the material to exist at very high moisture contents, varying often between 20% and 65%, results in a low unit weight, between  $16 \text{ kN/m}^3$  and  $7 \text{ kN/m}^3$ . Segregation of particle sizes, which is a consequence of the hydraulic filling procedure, causes other variations in properties, in particular shear strength and permeability: shear strength may typically vary from  $c' = 14 \text{ kN/m}^2$ ,  $\phi' = 32^\circ$ , to  $c' = 0$ ,  $\phi' = 40^\circ$ ; permeability is typically between  $10^{-2}$  mm/s and  $10^{-6}$  mm/s, while the compression index is usually between 0.2 and 0.3. Such properties of low unit weight, high moisture content and low permeability may create special problems in tailings stability with respect to liquefaction (Holubec (1976), Blight (1977)).

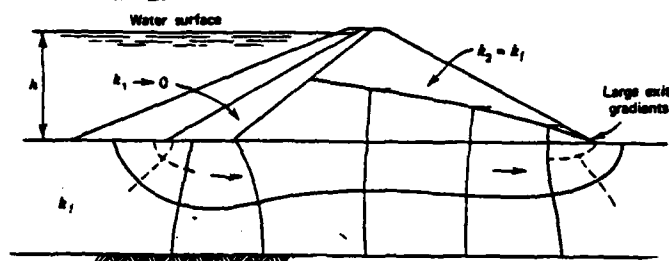


Figure 5.2 - Seepage Pattern of Embankment Dam with Upstream Impermeable Blanket and Permeable Foundation  
( Cedergren, 1973 )

#### 5.4 Slope Stability in Embankment Dams

The general lack of experience in sound geotechnical design and the consequent scarcity of documentation of mine waste embankment performance, offers little aid to the conscientious designer of waste heaps, and attention is generally turned to conventional embankment dams for precedents of safe design. By envisaging a coal mine waste embankment dam as having two simple parts, the main body of the embankment composed of the coarse discard, and an upstream blanket of sedimented fine tailings with low permeability, usually not covering the full height of the upstream face of the main embankment, in the manner typical of downstream disposal (see section 5.2), a coal mine waste embankment dam may be directly compared to conventional embankment dams.

A dry, essentially frictional material will remain stable to great height in an embankment built at an inclination equal to or less than its natural angle of repose, provided the foundation material is competent and contains no springs. The introduction of water and seepage forces will alter the stability, and although a stable embankment can be designed under most conditions, full consideration must be given to the most adverse likely circumstances so that proper design precautions may be made. One quarter of dam and reservoir failures are precipitated by seepage problems, (Cedergren (1973)), and provided excess pore pressures are permitted to dissipate in the coarse discard embankments during construction, this may be expected to be a significant design consideration in mine waste embankment dams also.

In considering seepage effects, the permeability of both the embankment and underlying foundation soils is important to determine the throughflow volume and the shape of the phreatic surface. The shape of the embankment, especially at the throughflow exit point, is equally important to stability. In the case where the foundation layer is permeable, a situation as illustrated in figure 5.2 may occur. Piping and

ratholes may develop, leading to backsapping and eventual dam failure, if precautionary measures are not taken, such as the implementation of internal drainage to control large exit gradients. If, on the other hand, the foundation layer is effectively impermeable, then different problems, no less severe, still exist for the designer.

Regardless of the height and permeability of the upstream beach of tailings, it is inevitable that some quantity of throughflow will occur in the coarse discard of the embankment dam. Throughflow has been investigated in conventional embankment dams, usually with reference to rock-fill dams. Rockfill is defined by Leps (1973), in terms of ground water flow, as non-cohesive particles which are essentially larger than one half inch in diameter, which include no more than 30%, and preferably no more than 10% by weight, less than U.S. No. 4 sieve, or about 5 mm diameter; material which is finer than this is classified as earthfill. In the case of borderline materials which possess between 10% and 30% smaller than U.S. No. 4 sieve, the water flowing through the material may cause segregation and blocking of the voids in the fill, thereby dominating flow characteristics\*. Johnson (1971) maintained that even though turbulent throughflow may occur in rockfill, an approximation to laminar flow still gives acceptable results, and therefore all throughflow may be approximated by Darcy's law.

The throughflow configurations which may arise in conventional embankment dams or impermeable foundations have been defined by previous researchers, although the bulk of their conclusions regarding stability under the different seepage patterns have been drawn from field observation rather than from laboratory tests. Many are of direct relevance to mine waste embankment dams.

---

\* Coal mine waste may fall into this border line category, although it may also be classified as earthfill, especially as it weathers (Holubec (1976)).

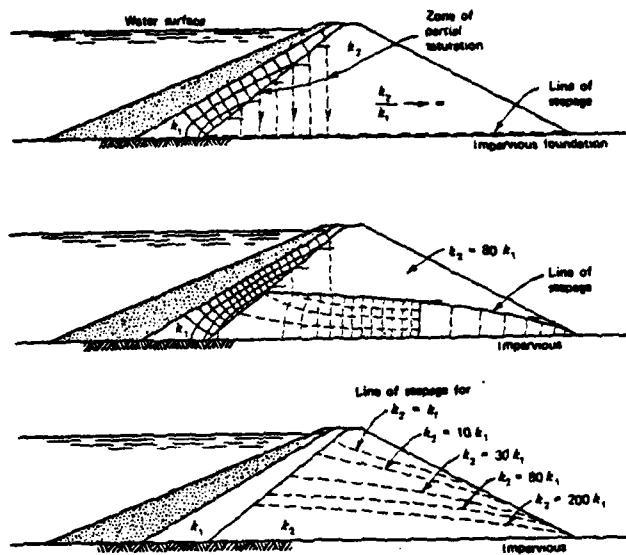


Figure 5.3 - Seepage Pattern of Embankment Dam with Upstream Blanket of Low Permeability and Impermeable Foundation ( Cedergren, 1973 )

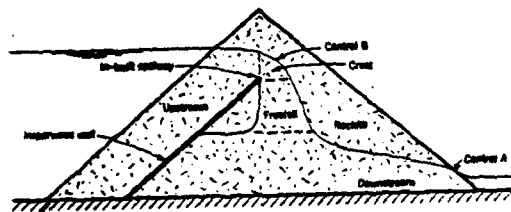


Figure 5.4 - Freefall Throughflow Conditions ( Parkin et al, 1966 )

The first such throughflow condition which may develop is the normal mine waste disposal working configuration where the reservoir level is below the top of the upstream blanket of low permeability tailings. Figure 5.3 illustrates the significance of the relative permeability of the material composing the body of the embankment compared to the permeability of the upstream blanket. Low permeability in the latter will limit the volume of throughflow, and decrease the detrimental effects of seepage by reducing the head in a stable upstream region.

As the level of the impounded water increases in height, usually so also does the upstream blanket of tailings. In the instance where this is not the case, so that the reservoir level exceeds the height of the tailings beach, possibly because of rainfall, but is still below the crest of the coarse discard embankment, the resulting condition may be compared to that of an inbuilt spillway dam. Such a seepage configuration, known as the "freefall" condition, is shown in figure 5.4 (Parkin et al (1966)).

Further increase in the reservoir level over the height of the upstream tailings beach but still below the embankment crest, may eventually exceed the combination of heights which define the freefall condition, and the phreatic surface will assume a shape which slopes continuously from upstream to the exit point, as if no upstream tailings blanket existed.

The rise in reservoir level may finally reach the most extreme stability condition which involves overtopping. In this case, both internal seepage, and surface erosion may simultaneously undermine embankment stability. Overtopping is the single largest cause of embankment dam failures, but even under this extreme condition it is possible to design for stability. Weiss (1951) gained field experience in this extreme condition; Wilkins (1963) recommended reinforcing measures to stabilise embankments in cases of through and overflow; Olivier (1967) outlined

design measures associated with the selection of safe downstream embankment profiles, and erosion resistant cover rock. Each author emphasised the prevention of local erosion, as local erosion may lead to flow concentration at the trouble area, further aggravating the problem and subsequently developing into retrogressive sliding, erosion, and eventual breaching of the embankment dam.

The shape of the phreatic surface for the simple conditions of throughflow described above may be distorted by anisotropic permeability in either the upstream tailings beach or the coarse discard embankment. Segregation of particle size in the hydraulically filled tailings beach results in permeability decreasing as the distance from the discharge point increases, and, in addition, although to a less significant degree, is complicated by some horizontal anisotropy from the horizontal deposition of material. Since most of the impounded water will be in contact with the finest, and least permeable tailings under normal working conditions, however, throughflow is effectively reduced to a low level. The method of coarse discard placement may also result in anisotropic permeability. Leps (1973) explained that in the placement of graded material through either air or water, segregation of particle sizes may occur, resulting in a higher concentration of fines at the top of the lift. He noted that the consequent anisotropic permeability may be greater in the horizontal direction than in the vertical direction by a factor as large as five. Migration of the fines either from the tailings beach or from within the coarse discard embankment may also be responsible for unexpected distortions in the shape of the phreatic surface.

Typical deepseated slope stability analyses of embankment dams can include limit equilibrium approaches, such as the effective stress method of slices of Bishop and Morgenstern (1960); in a following section of this thesis, the slope stability calculation of Bishop and Morgenstern



(1960) will be applied in calculation of observed deepseated failures, related to high pore pressure within the embankment, in order to examine such a line of analysis. Wedge analyses have also been recommended by Fyodorov (1965), and Blight (1977), as have finite element methods (Corp et al (1975)). Each involves assumptions with regard to failure mechanisms and pore pressure distribution, which usually have not been verified in the field, and which introduce soil properties estimated from laboratory conducted tests.

Mine waste embankment dams are different from conventional embankment dams by being constantly under construction, changing daily in shape and height. Sluices and embankment dam freeboard are therefore difficult and costly to maintain. Such factors make the installation of toe drains, careful embankment profile design and downstream slope surfacing an effective defence against disaster. The capability of the main waste embankment dam itself, to safely pass the necessary quantities of through and overflow based upon experience, derived from conventional dam construction may be an important design technique in preserving stability.

While it is unfair to criticise these design methods because disasters have occurred in both mine waste and conventional embankment dams, it is clear that any other line of repeatable model testing, such as reduced scale centrifugal modelling, can provide some new insight into seepage flow, pore pressure distribution and failure mechanisms.

### 5.5 Object of the Model Tests

Two sets of tests were undertaken by Cambridge University for the centrifugal model study of the stability of coal mine waste embankments. They were both carried out for the U.S. Corps of Engineers Waterways Experiment Station.

The intention of the first set of models in fulfillment of the first proposal, later designated as models MW1 through MW13, was to investigate

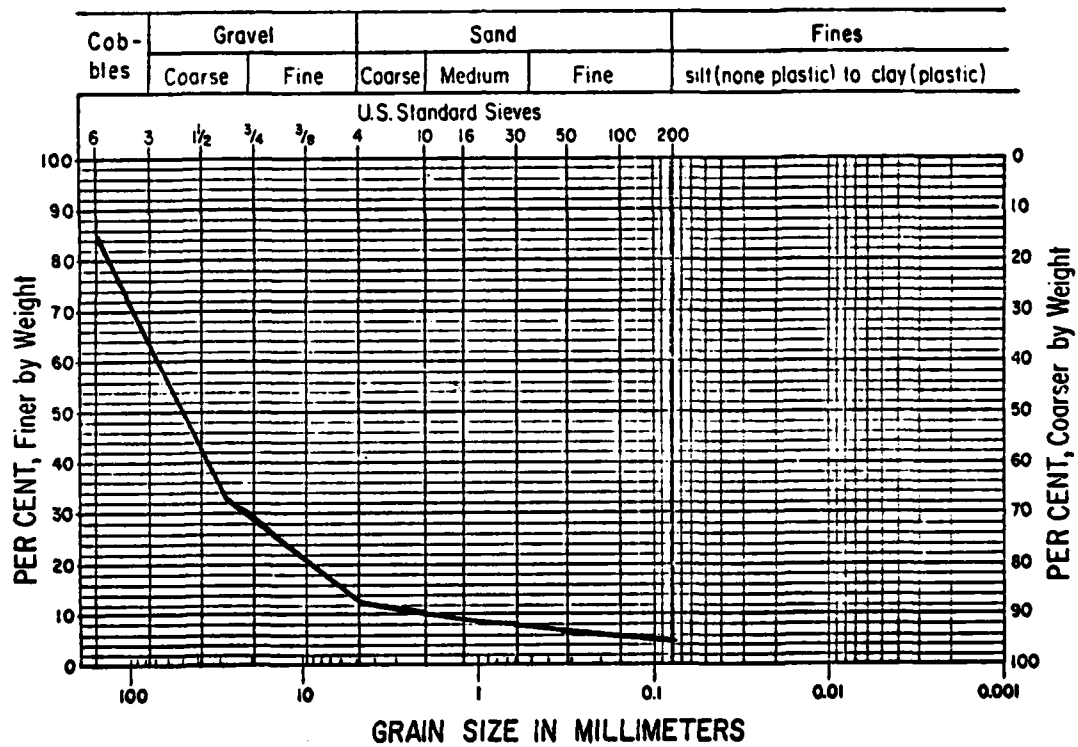


Figure 5.5 - Particle Size Distribution of Key Material  
( U.S. Army Corps of Engineers )

the importance of both the slope angle and the rate of embankment construction, and where applicable, the detrimental effects of seepage on the stability of coal mine waste embankments. The second contract set out as a parametric study, termed the "modelling of models", to study the role of model scale and particle size gradation in embankment stability behaviour, and in addition, two secondary factors: the method of model preparation and the effect of the embankment-strongbox interface. Six models were tested, models MW20 through MW25.

As must often be the case in new research, the line of study deviated from the original intentions, when unexpected significant factors became evident. The previously established background of centrifugal modelling of mine waste embankments, founded mostly upon Malushitsky's (1975) work, on relatively impermeable overburden soils, was quickly found to be of little assistance: the coal waste coarse discard proved to be a radically different material. The research pursued here, moved quickly into areas largely uninvestigated in the field, but particularly unexplored in laboratory and centrifugal modelling.

#### 5.6 The Coal Mine Waste Test Material

The coal mine waste material used in these centrifuge tests was retrieved from an active coal mine waste embankment dam in New Mexico, U.S.A. Eight sealed barrels of disturbed material were sent to Cambridge, at the in situ moisture content. These barrels included one barrel of material used in the central, undrained key section which ran down the centre of the base of the embankment, one barrel of the natural, underlying, clayey foundation soil, and six barrels of material from the mid-height of the coarse discard embankment, which had been sieved in New Mexico, prior to shipping to remove all particles larger than 13 mm.

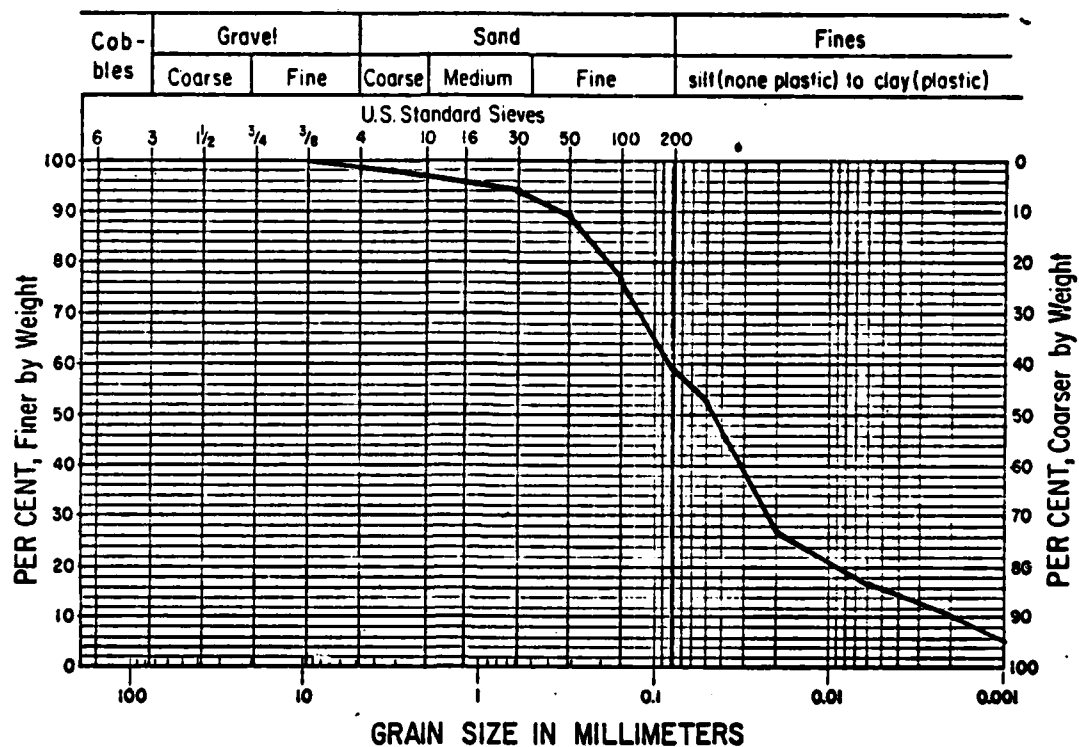


Figure 5.6 - Particle Size Distribution of Foundation Soil  
( U.S. Army Corps of Engineers )

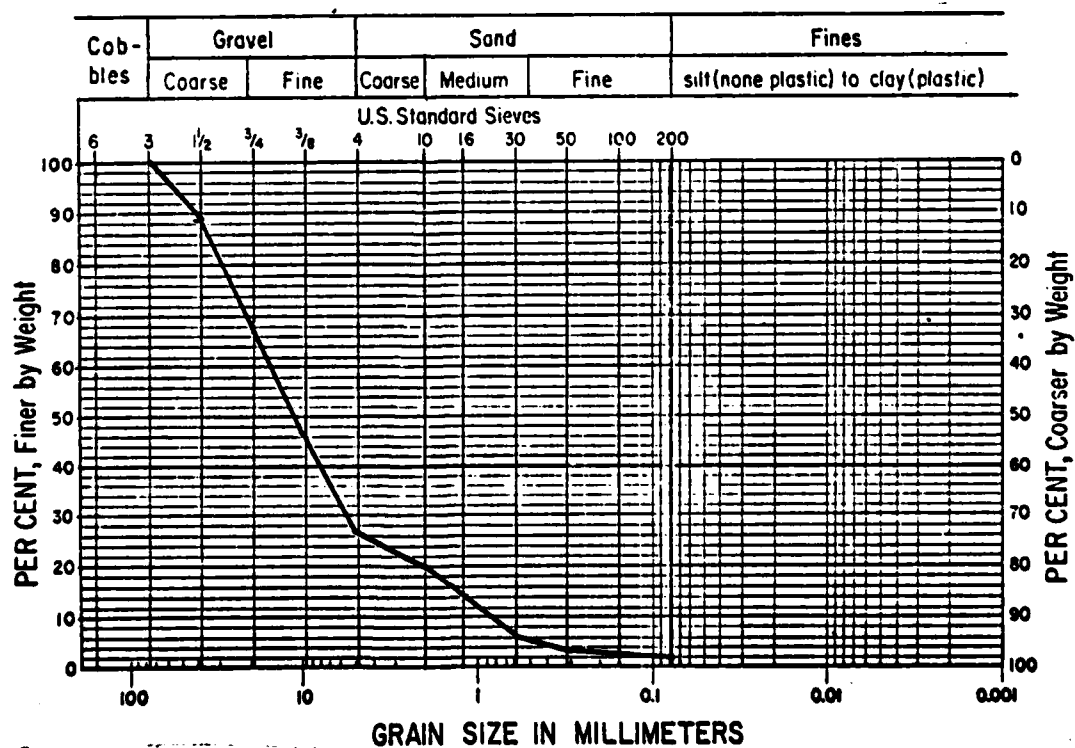


Figure 5.7 - Particle Size Distribution of Whole Coarse Discard Coal Waste  
( U.S. Army Corps of Engineers )

The particle distribution curves for these three soil materials are shown in figures 5.5 through 5.7 as prepared by the U.S. Army Corps of Engineers for the whole soils. For the coarse discard, the important features are:

maximum size	76 mm
D <sub>85</sub>	30 mm
D <sub>50</sub>	10.1 mm
D <sub>30</sub>	5.5 mm
D <sub>10</sub>	0.9 mm
% < 0.075 mm	2%

Al-Hussaini and Townsend\* measured the geotechnical properties of this coarse discard, and found them to be as follows:

bulk unit weight	15.4 kN/m <sup>3</sup>
natural water content	8.6%
dry unit weight	14.2 kN/m <sup>3</sup>
c'	11 kN/m <sup>2</sup>
φ'	30.5°

The sieved, coarse discard received was damp, and uniform in colour and texture, and removal of the portion larger than one half inch in diameter had reduced the dry unit weight at in situ stress levels typically to 11.8 kN/m<sup>3</sup>. This material, however, was further altered for the model test programme, as is discussed in section 6.4.

---

\* M. Al-Hussaini and F.C. Townsend, 1977, U.S. Army Corps of Engineers, U.S.A., personal communication.

## CHAPTER 6

### COAL MINE WASTE EXPERIMENTS

#### 6.1 Logic of the Test Programme

When the first research proposal was drafted for centrifugal modelling of slope stability in coal mine waste embankments, the major existing work in this area of research was the extensive experimental background accumulated by Malushitsky (1975) on centrifugal modelling of relatively impermeable mine waste material heaps. Malushitsky had paid considerable attention to rate of construction failures, and it was expected that this would be a feature of interest in the coal mine waste embankments.

When the material arrived from New Mexico, it was at once clear that what had been sent was relatively permeable. The particle size distribution was immediately altered by removing all particles greater than 2.36 mm (see section 6.4), and failure due to rate of construction was attempted, simulated in the centrifuge by steadily increasing centrifugal loading, increasing all soil stresses. In the first models MW1 to MW3 embankments as steep as  $45^{\circ}$  to the horizontal, subjected to rapidly increasing speed, did not undergo failure even with the introduction of an inflow of water. The material was too permeable for this type of failure.

In models MW4 through MW8, rate of construction failure was again attempted using a fraction of the material which passed through a smaller mesh size, 1.18 mm. Failure was observed, but factors such as the simulated rate of construction, and slope angle, proved less significant than the initial moisture content, largely uncontrollable in the method of model preparation. This model material was already less permeable than the "correct" scale reduction of permeability for the New Mexico prototype soil, and so rate of construction was not judged to be a concern in this relatively free draining material.

Attention was turned instead to the detrimental effects of seepage on slope stability, in models MW9 through MW13. By bringing the model embankment to full scale without failure, and then increasing throughflow from a rear reservoir, deep seated retrogressive failures were observed. Different embankment configurations were modelled to investigate their effects on slope stability under throughflow conditions, including the introduction of a toe drain, an enclosed undrained key, and uplift forces. The final report, Goodings et al (1977), concluded this contract.

The second contract was intended to investigate the influence on model behaviour of various parameters; following Malushitsky's (1975) usage, this was termed the "modelling of models". Two principal aspects of initial interest were model scale and particle size distribution, with special attention to their effects on stability, permeability, and rate of retrogression; two secondary factors, the method of model preparation and the influence of the interface between the model soil and the centrifuge strongbox, were also to be considered. A new method of materials mixing was also introduced (see section 6.4.).

The new study was begun, and immediately an unanticipated complication was encountered: the particle size distribution was expected to be important, but because of change of particle size distribution induced by different mixing and handling techniques, it became the dominant feature of model behaviour, and in some respects seemed to change progressively. The resulting models in this series, MW20 through MW25, were used principally to investigate seepage effects and failure by erosion, using varying particle size distributions. By changing the method of model construction in one model MW21, and altering the model soil interface with the centrifuge strongbox by introducing an underlayer of preconsolidated kaolin in two models, MW21 and MW22, the six tests completed the second experimental programme, outlined in Goodings and Schofield (1978).

The conclusions of the two model series were unexpected. The new factors which became apparent in the tests made it not possible to fulfill the expectations of complete "modelling of models", and in both cases, the emphasis of the test programme changed as test data was accumulated. Nonetheless, important information relevant to prototype coal mine waste embankments was derived, and additional aspects of centrifugal modelling also became apparent. Details of these model tests and their implications are discussed in the following sections.

#### 6.2 Mine Waste Model Preparation

Nineteen separate coal mine waste embankment models were made for the purpose of this research: sixteen of them were constructed in a similar manner, and the other three models, MW1, MW20 and MW21, were made in quite different fashions, either to accommodate their material properties, or to investigate the effect of a change in model construction technique. The methods of model construction are outlined below.

Unlike the Champlain Sea clay models, the coal mine waste model embankments were not built within the liner (see sections 2.2 and 4.1), but rather directly on the painted steel interior of the centrifuge strongbox. This was the consequence of two considerations: the essentially cohesionless nature of the model embankment material did not lend itself to building the model in the liner separately and then shifting it into the strongbox, and the hydraulic system adopted was more easily implemented without the liner as the system required cutting a hole through and into the bottom box section of the centrifuge strongbox to provide an exit for landslide debris. The result was a new approach to model construction characteristic of cohesionless, two dimensional models, and quite different from intact clay model preparation.

In the sixteen similarly built models, the centrifuge strongbox



was laid on its back so that during construction the normal vertical plane was temporarily horizontal. The back of the box was sprayed with silicone grease to diminish side friction, and then a template which defined the embankment profile, was secured in the strongbox, while the sodden soil was gently rodded into place behind the template.

In some models, additional features such as a rear reservoir, a toe drain, or an interior key, were included. Extra templates, made to the shape of these features, were secured in position, and as the template defining the body of the embankment was filled with soil, so also were these templates (see figure 6.1). These additional features were all composed of more permeable material which had been removed from the initially received coal mine waste. Such material was between 12.7 mm and 2.36 mm in diameter, with a  $D_{10}$  size 44 times larger than the most permeable embankment soil.

Before the templates were withdrawn, the model surface was smoothed and the excess material removed. The surface was then sprayed white, and a grid of silvered plastic indicator balls was emplaced in order to later highlight soil displacements.

The templates were carefully but quickly withdrawn, and a gasket eliminator sealant was applied to the face of the box which would be in contact with the perspex front. The perspex cover was positioned, and clamped to the box, sealing the model cavity. The centrifuge strongbox was then swung to the upright position ready for mounting and testing.

As it later became apparent, certain aspects of soil retrieval and placement had special effects on the resulting model embankment soil. The particle size distribution of the soil which was to compose the body of the model embankment, had been altered from that of the material received, by wet-sieving to remove the coarser portion (see sections 6.3 and 6.4). In the first thirteen models, however, the actual retrieval of

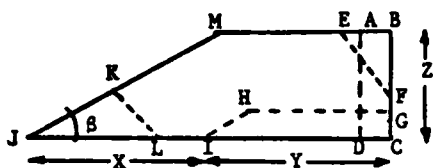
the soil from the storage barrel was also of importance. This involved bringing the soil up in scoopfuls, about one litre in volume, through some 75 mm of standing water, the majority of which immediately drained from the soil. It was not appreciated until later, however, that this washed back into the barrel, an approximately constant portion of the fine silt and clay fraction initially within each scoopful of soil, which was kept in suspension in the water in the barrel. This fine fraction only settled to the bottom of the barrel if the water was left undisturbed for many days. In the second set of six models, this continually agitated water in the barrel was removed so that although the soil was almost saturated, the rinsing effect was practically eliminated.

It was necessary that the soil be placed in a wet state so that after a short period of drainage during model preparation, approximately thirty minutes, sufficient negative pore pressures had developed in the soil that the template defining the model profile, could be removed and the model embankment would temporarily maintain its shape while the remainder of the model preparation was completed. There was concern, however, that in constructing the model perpendicular to the normal direction of prototype embankment construction, the direction of construction and drainage would permit segregation of fines and consequent abnormal strength and permeability characteristics. In the test programme there was no evidence to suggest that significant segregation had occurred, and compaction and strength characteristics of the model embankments were felt to be dominated much more by the subsequent "vertical" centrifugal loading.

The angle of friction between the coal mine waste and the painted steel interior of the centrifuge strongbox, was  $26.5^{\circ}$ . Two models, MW21 and MW22, were founded instead upon a preconsolidated 10 mm thick layer of kaolin, to investigate the importance of this interface. The moisture content of the clay was 49%, and the permeability typically  $10^{-6}$  mm/s

Table 6.1

## Model Dimensions



## Additional Features (9):

1. Type TD, toe drain, shown by shape JKL, where KL is a 45° line, 92 mm long.
2. Type K, key, shown by shape IHGC, where IH is parallel to JM, and point I is directly below M; distance GC is 60 mm.

## Reservoirs (6,7,8):

1. Type V denotes a full height vertical reservoir, ABCD, and the measurement AB is given below.
2. Type D denotes a diagonal reservoir, EBF, and the measurements EB, and EF are given below.

Material types (10) as designated in section 6.4.

1 Model No.	2 cot $\beta$	3 X (mm)	4 Y (mm)	5 Z (mm)	6 Reservoir type	Res. dimensions		9 Additional features	10 Material type	11 Top g
						7 AB/EB	8 BF			
MW 1	1	280	390	280	none	-	-	-	A	150
MW 2	1	240	425	240	none	-	-	-	A	135
MW 3	1	240	425	240	D	115	155	-	A	135
MW 4	1	240	425	240	D	115	155	-	B	132
MW 5	1	240	425	240	D	115	155	-	B	29
MW 6	1.5	360	300	240	D	115	155	-	B	19
MW 7	2	480	185	240	D	70	240	-	B	40
MW 8	2	480	185	240	V	70	-	-	B	19
MW 9	1.5	360	300	240	V	70	-	-	B	100
MW10	1.5	360	295	260	V	50	-	-	B	120
MW11	2	520	185	260	D	80	140	-	B	120
MW12	2	520	185	260	D	80	140	K	B	120
MW13	2	520	185	260	D	80	140	K, TD	B	120
MW20	2	390	315	195	D	80	130	-	MW20	120
MW21	2	390	315	195	D	80	130	-	MW21	120
MW22	2	390	315	195	D	80	130	-	MW22	120
MW23	2	390	315	195	V	70	-	-	MW23	100
MW24	2	390	315	195	V	70	-	-	MW24	50
MW25	2	390	315	195	V	190	-	-	MW25	100

(Orr, 1976). This layer was measured using the Swedish drop cone, to have an undrained cohesive strength of  $130 \text{ kN/m}^2$ , although this method typically yields a high value of undrained strength\*.

Three of the nineteen models were prepared in quite different fashions: the embankments of models MW1 and MW20 were both cut into centrifugally preconsolidated blocks of mine waste, and the embankment profile for model MW21 was cut into a laboratory compacted block of material. This latter material, MW21, was intended to investigate the effect on model behaviour of construction by static compaction. To this end, a block of material was prepared by vertically compacting five successive layers of mine waste under  $58 \text{ kN/m}^2$ , to approximately 40 mm in thickness.

The dimensions of model configurations are given in Table 6.1.

### 6.3 The Rationale Behind Changes in Particle Size Distribution

Pokrovsky's first scaling principle for centrifugal modelling was restated in section 1.4 in this form:

If two soils with identical friction, cohesion and density are formed into geometrically similar bodies, one at full scale, and one a model of  $1/N$  scale, and then if the  $1/N$  scale model is accelerated so that self-weight increases  $N$  times, the stresses at corresponding points are then similar if they are similar on the boundaries.

Therefore, if prototype soil is used to build a model, and care is taken to follow correct stress paths in initial consolidation, then all the requirements are satisfied for stress similarity. In models composed of homogeneous fine silt or clay, sampled intact from the prototype site, this is the ideal case. If, however, the prototype material contains structural components of a size such that the ratio of component size to prototype dimension is significantly smaller than the ratio of component size to model dimensions, as in the case of rockfills, or clays with organic fibres, then the material for the model should be modified to adhere more closely to the original ratio of the component size to the prototype

---

\* B.G. Clarke, 1978, Cambridge University, personal communication.

dimensions. In the case of material less fine than coarse silts, this may be achieved by a uniform reduction in particle size by the removal of the coarse fraction of the prototype material. This does not necessarily alter friction, cohesion or density, but it may alter the permeability considerably.

Comparison of the rate at which ground water moves through essentially rigid, free draining soil in a prototype, to the rate at which it moves through the same soil in a reduced scale model under centrifugal loading, illuminates two consequences of modelling. As will be discussed in section 6.7, an effect of centrifugal loading on seepage flow through a fixed flow net, is to increase the velocity of throughflow in a model in direct proportion to the increase of self weight,  $N$ , such that:

$$V_{Ng} = N V_{lg} \quad (6.20)$$

In addition, by reducing all prototype dimensions by a factor of  $\frac{1}{N}$ , the time taken for water to move between two points in the model which correspond geometrically to two points in the prototype, will be further reduced by a factor of  $\frac{1}{N}$ . This means that in a model of scale  $\frac{1}{N}$ , made of prototype soil and subjected to centrifugal loading causing an increase in self weight of  $N$  times, the time for water to seep through the model is altered:

$$t_{mNg} = \frac{t_p}{N^2} \quad (6.1)$$

In models where the velocities of seepage and of mass soil movements are both significant in the observed behaviour, it becomes important to preserve similarity in time scales, so that the events observed are qualitatively correct, and also so that they may be related to a uniform prototype time scale. By reducing all prototype dimensions by a factor of  $N$ , then mass soil movements such as landslides which occur at the same absolute velocity in model and prototype (see Goodings et al (1977)), will occur in  $N$  times less time in the model than in the prototype:

$$t_m = \frac{t_p}{N} \quad (6.2)$$

Similarity of seepage and mass movement time scales may therefore be achieved by either increasing the absolute velocity of mass soil movements by a factor of N, or by reducing the permeability by a factor of N. This latter alternative is the best choice, and may be achieved as follows.

Taylor (1948) outlined the effect on permeability of a change in particle size distribution. The engineering parameter for permeability, k, is defined in the following manner:

$$k = \frac{K \gamma_p}{\mu} \quad (6.3)$$

where k = engineering parameter for permeability expressed in units of velocity,

K = empirical constant characterising porosity of the soil structure,

$\gamma_p$  = unit weight of the pore fluid,

$\mu$  = static viscosity of the pore fluid.

From this, the parameter K, which interprets the porosity of the soil structure, can be further defined as:

$$K = D_s^2 \frac{e^3}{1+e} c \quad (6.4)$$

where  $D_s$  is taken as  $D_{10}$

e = voids ratio

c = numerical constant.

Of these parameters, e and c are relatively constant for a given particle shape and type under a particular stress regime, but  $D_s$ , usually taken as  $D_{10}$ , is capable of radically influencing the permeability:

$$k \propto K \propto D_{10}^2 \quad (6.5)$$

Therefore, in order to reduce permeability by a factor of N,

$$D_{10_m} = \frac{D_{10_p}}{\sqrt{N}} \quad (6.6)$$

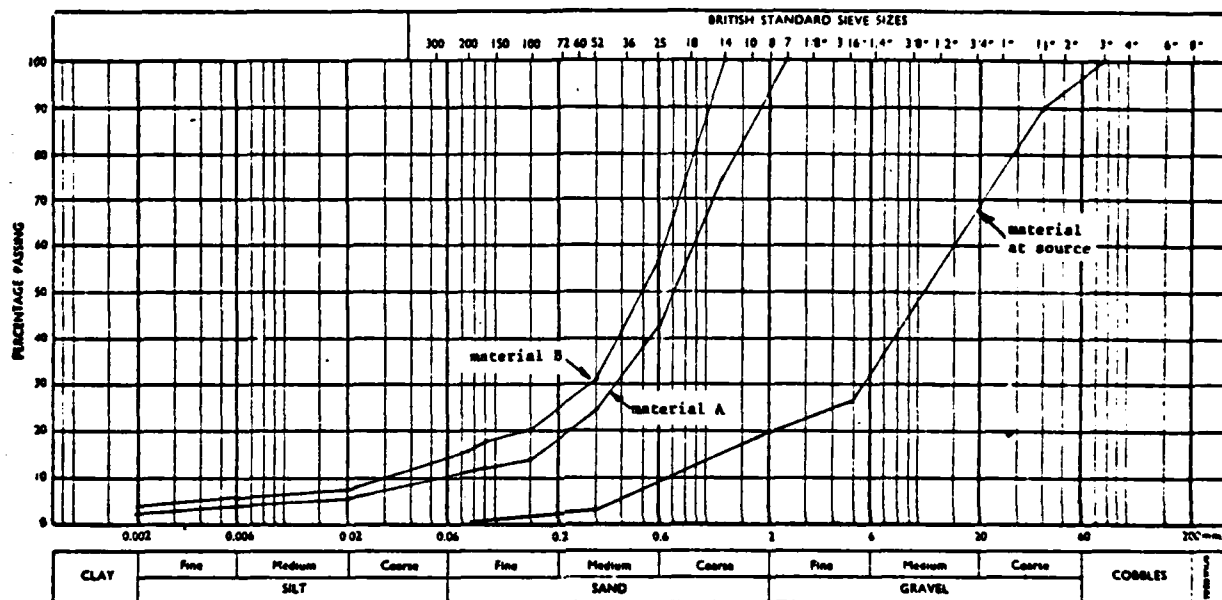


Figure 6.2 - Particle Size Distribution of Model Soil  
Materials A and B

Under conditions where a model of scale  $\frac{1}{N}$ , is constructed with soil where  $D_{10m} = \frac{D_{10p}}{\sqrt{N}}$  so that  $k_m = \frac{k_p}{N}$ , and this model is subjected to an increase in self weight of  $N$  times, then the reduction in time scale for water movement will be linearly proportional to the reduction in model dimensions:

$$t_{mNg} = \frac{t_p}{N} \quad (6.7)$$

This has now become the same ratio as the scaling of time for mass soil movements, and similarity of time scales is achieved. Further implications of changes in particle size distribution and permeability will be discussed in section 6.8.

#### 6.4 Changes in Particle Size Distribution

As explained above in section 6.3, an alteration in particle size distribution was necessary for the modelling exercise. According to that section, for models where the scale was to be  $N = 120$ , as for the first models of this series, the initial reduction in particle size was ideally by a uniform factor of  $\sqrt{120}$ , or approximately 11. To achieve this, the mine waste which arrived from New Mexico and had already been sieved to remove all particles less than one half inch (12.7 mm), was sieved again in Cambridge through a submerged mesh of 2.36 mm. The material less than 2.36 mm was retained and permitted to settle in water, and the material greater than 2.36 mm (and less than 12.7 mm) was stored separately. Most of the excess but still murky water was siphoned away twelve hours later, and on the surface of the remaining water, there floated a layer of very fine particles and a greasy slick. The remaining saturated mine waste, designated as material A when retrieved through standing water as explained in section 6.2, was similar to medium sand. According to the particle size distribution in figure 6.2, a reasonably constant reduction of particle size had been achieved, especially at the critical  $D_{10}$  size where



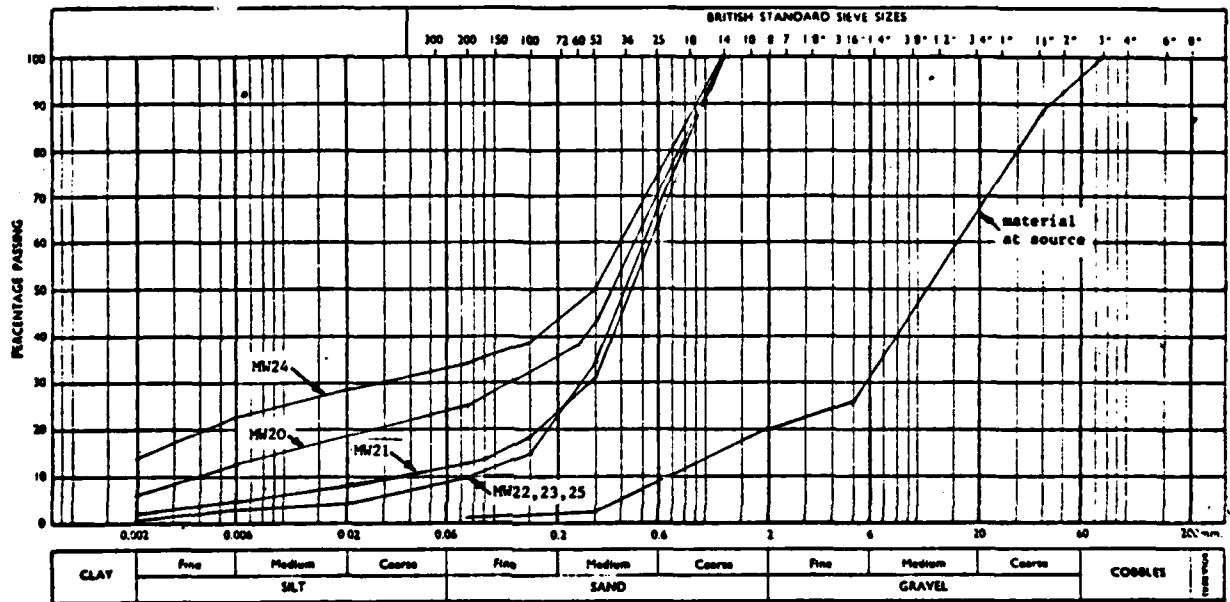


Figure 6.3 - Particle Size Distribution of Model Soil  
Materials MW20 through MW25

$$\frac{D_{10P}}{D_{10A}} = 11.$$

As explained in section 6.1, material A proved to be too permeable for the testing first envisaged, and a further reduction in permeability was undertaken by repeating the wet sieving process with material A, this time retaining material less than 1.18 mm in size. This material, B, when retrieved through standing water in the same fashion as material A, had a particle size distribution as shown in figure 6.2: the  $D_{10}$  ratio of New Mexico prototype soil to model soil was now a factor of 20. Such soil was used in models MW4 through MW13.

Between the testing of model MW13 and the next model, MW20, three and a half months elapsed. During that time material B was left submerged under some 400 mm of standing water. When the time came to prepare model MW20, the 400 mm of water was siphoned away down to the level of the top and now thick (about 10 mm) layer of fines which had sedimented out of the murky water, onto the coarser underlying soil. The remaining material, both coarse and fine, was thoroughly mixed in a Hobart 25 litre cake mixer, in order to uniformly distribute the segregated particles.

The resulting material, which was expected to be identical to the previous material B, exhibited a spongy, poorly draining consistency, clearly different from that used in the previous models, and consequently impossible to handle in the same modelling procedure. A particle size distribution analysis showed this material, designated as MW20, had a much higher proportion of fines than material B (see figure 6.3), and further, that by retrieving this material through standing water, as explained in section 6.2, a material similar to material B was obtained. Two aspects of material handling at once became evident: the fine portion of soil was significantly diminished by retrieval through standing water, and the material was progressively and spontaneously degrading within times in the order of months, substantiated by Taylor (1978). The

effect of the proportion of fines on material properties was discussed in section 5.3, but the most immediately obvious effect in this research was the reduction in permeability.

The material was used in model MW20, but the low permeability prevented the examination of the effects of throughflow on embankment stability, as was observed in models MW9 through MW13. The material was therefore altered for the next test, and this was achieved by removing by sedimentation, a controlled amount of the finest portion. The new, more permeable material achieved was used in model MW21, and designated as such in figure 6.3. A second reduction in the proportion of fines was undertaken, and this material was used in models MW22 and MW23 (see figure 6.3).

The portion of fine material removed during the second sedimentation, that is the fines which differentiated the soil used in model MW21 from that used in models MW22 and MW23, was saved and dried, to be used at a later date. Half the volume of these fines was returned to the soil after test MW23, expecting to achieve material with a value of permeability between that of models MW21 and MW23. The resulting soil designated as MW24 in figure 6.3, was very different from that expected. The proportion of fines was much in excess of any previous soil model. The drying and handling process had significantly degraded the fine portion, reinforcing the suspicion of degradation in material B. The soil used in the final soil model, MW25, was prepared in such a way as to remove a large portion of the fines which had been added to MW24. The resulting soil was almost identical to that soil used in MW22 and MW23.

The changes in permeability in models MW20 through MW25 were unexpected to a large extent, and while this altered the emphasis of the mine waste experiments, it highlighted the importance of handling procedures in both model and prototype. The consequence of such changes was

different types of failure, thus demonstrating the significance of assessing precisely, the particle size distribution of a coal mine waste embankment at the time of deposition, and its change over time, in order that correct precautions may be taken against failure. The testing of these models, described in the following sections, make apparent the effects of material properties.

#### 6.5 Definition of Failure

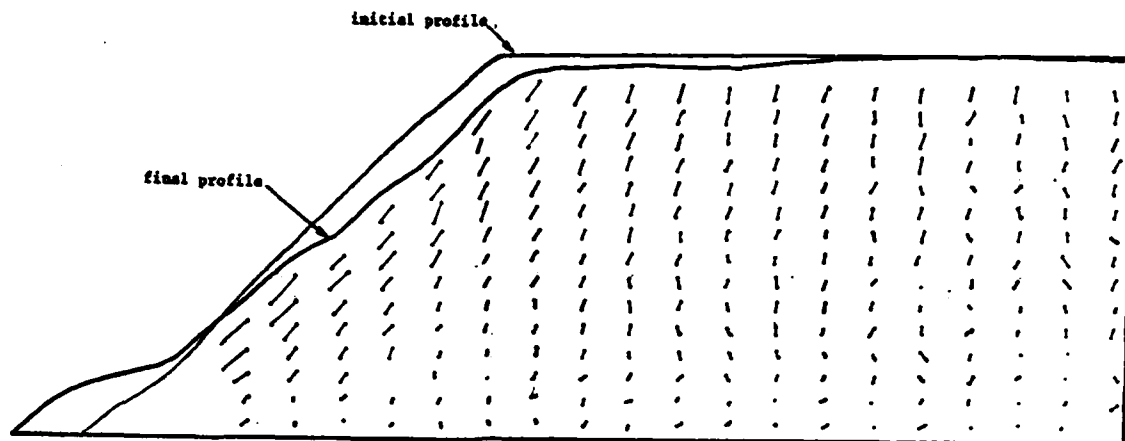
As explained earlier in section 4.3 with reference to clay slopes, the condition of failure in slope stability is a subjective judgement, heavily dependent upon the consequences of the unexpected soil behaviour. Wilson and Squier (1969), in discussing performance of dams, noted that the condition of failure in embankment dams may be constituted by many different circumstances. They named five such categories of failure, of which only two involved destruction and loss of the dam, and of life and property.

For the purposes of this thesis, any radical change in soil profile which leads to or is judged capable of leading to breaching of the embankment dam, will constitute failure, whether it is the result of deep seated mass soil movements, or of erosive damage which may lead at first to localised retrogressive sliding and eventually to danger of instability of the whole dam. In both cases, the movement of a substantial amount of embankment material downstream may also be sufficient to qualify as failure, even if breaching does not occur.

The designation of failure in mine waste model embankment dams therefore remains unquantified and subjective, however the failures which were observed in these tests were qualitatively quite obvious.

#### 6.6 Experimental Procedure and Results

Even more than in the case of the Champlain Sea clay centrifuge tests, the techniques and emphasis of modelling coal mine waste embankment dams



Note: Displacement diagrams from successive inflight photographs show embankment on right of picture.

Figure 6.4 - MW1 Model Soil Displacements

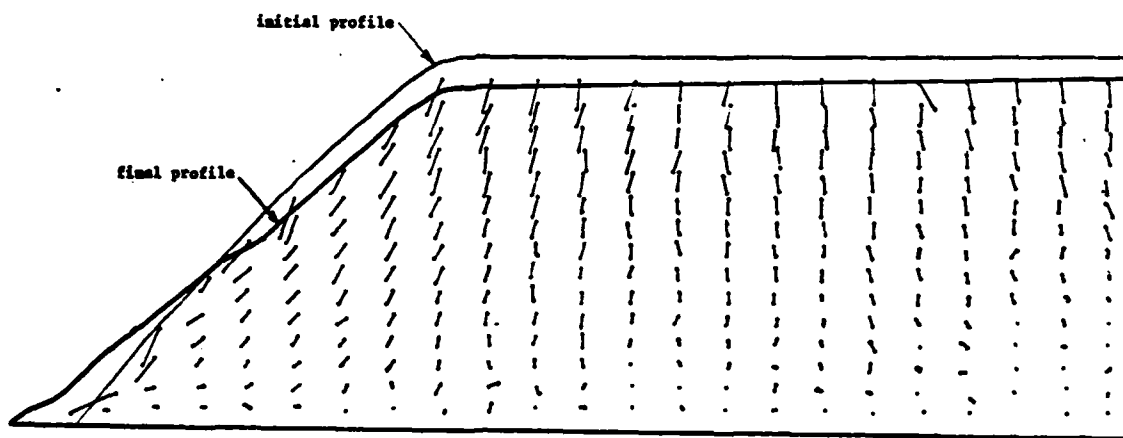


Figure 6.5 - MW2 Model Soil Displacements

changed in response to the accumulating data of the test sequence. It is therefore logical and advantageous to present the experimental procedure and results of these tests together. The details of the procedure of centrifuge testing are provided in table 6.2, and only the most important aspects are mentioned in this section. Determination of the permeability of various models is also included in table 6.3, calculated according to the throughflow characteristics.

The preparation of model MW1 took place in two stages. A block of material A was consolidated on the centrifuge, at 100g for 20 minutes, after which the embankment profile was excavated in the resulting soil mass, and testing of the embankment stability, under simulated rapid rate of construction conditions, followed.

The model was subjected to a rapid increase in centrifugal loading to 150g and the response involved an overall 6% vertical compaction, accompanied by a forward shearing action in the front section of the embankment, most pronounced forward of the crest, figure 6.4. The embankment, however, remained stable, adjusting to the high stress levels by settling on a new profile at  $39^{\circ}$  to the horizontal, and failure was not judged to have occurred. The phase of preconsolidation, which caused a reduction in moisture content to 12.5% and consolidation to a dry density of  $1260 \text{ kg/m}^3$ , was thought to be responsible for this stable behaviour.

Model MW2 was therefore constructed without a preconsolidation phase, to test the stability of a loosely tipped embankment under conditions of simulated rapid rate of construction. Rapid centrifugal loading to 135g caused an overall 6% vertical compaction, as in model MW1, and a similar forward shearing movement, although this shearing response affected a greater portion of the embankment, figure 6.5. The final, resulting slope angle was again  $39^{\circ}$  to the horizontal, and the moisture content marginally higher, at 14%, but failure was not judged to have occurred.

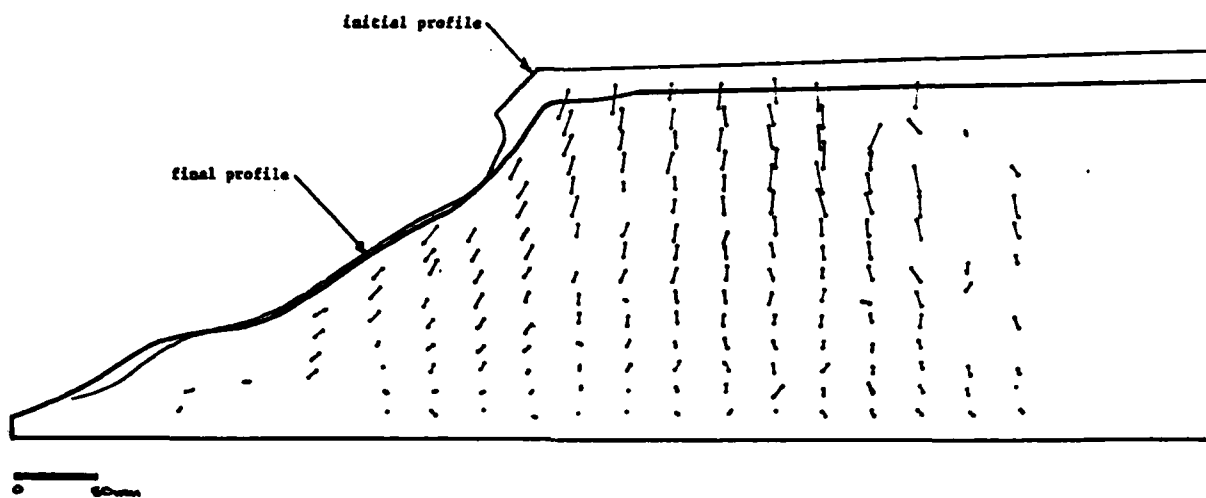


Figure 6.6 - MW3 Model Soil Displacements ( 10g to 135g )

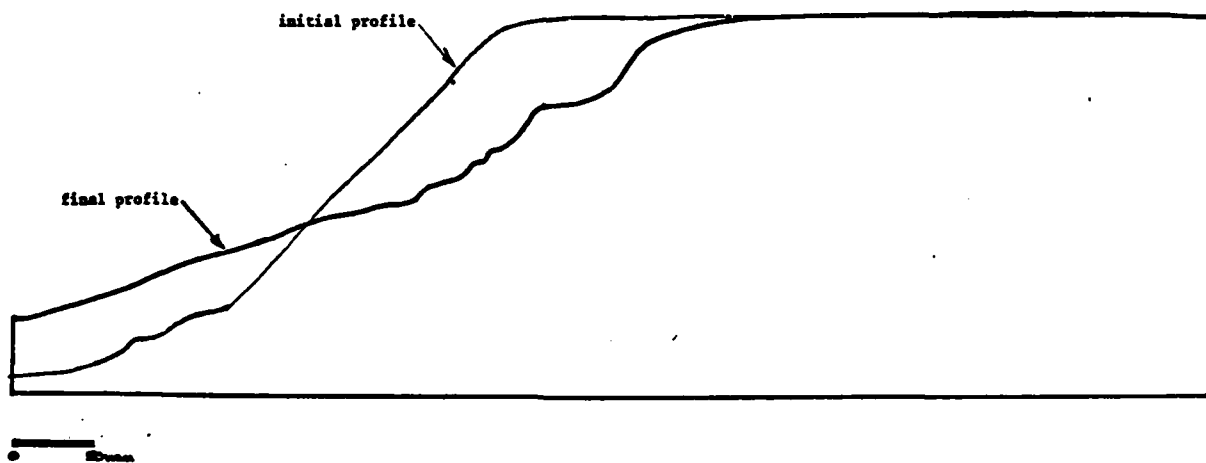


Figure 6.7 - MW4 Change in Model Profile

Model MW3 was built, still using material A, but with a stone-filled rear reservoir which could be flooded with water, to simulate embankment construction in the presence of an upstream reservoir. The model was subjected to a rapid increase of centrifugal loading to 135g, in the presence of steady throughflow from the reservoir. The resulting changes in profile had been principally achieved by 10g, however, subsequent shear and compaction occurred. The model responded with 8% vertical compaction and an average reduction in slope angle from  $45^{\circ}$  to  $28^{\circ}$ , figure 6.6. Moisture content measured before and after the test indicated a reduction from 26% at the time of model construction, to 16% after centrifugal testing.

This material had shown itself to be too free draining to demonstrate rate of construction failure due to the generation of excess pore pressures, under the most adverse conditions which could be imposed. The decision was therefore made to alter permeability by removing the coarse portion of material A, to form a new material B (see section 6.4).

Model MW4, constructed in dimensions identical to model MW3, but with the new material B, was subjected to a rapid increase in centrifugal loading to 132g, in the presence of a continuous inflow of water to the reservoir, of approximately  $37 \text{ mm}^3/\text{mm-s}$ . During the increase in centrifugal loading, the crest displacement transducer indicated a sudden vertical movement, and the change in profile which was occurring, is shown in figure 6.7. Observation of the model after the test indicated that some retrogressive sliding had occurred, accompanied by some forward shearing, but the character of the model surface was dominated by erosion, figures 6.8 and 6.9.

Moisture contents taken before and after the test indicated only a slight reduction from 26% to 23%, in response to centrifugal loading, the final level notably greater than that found in previous models made of



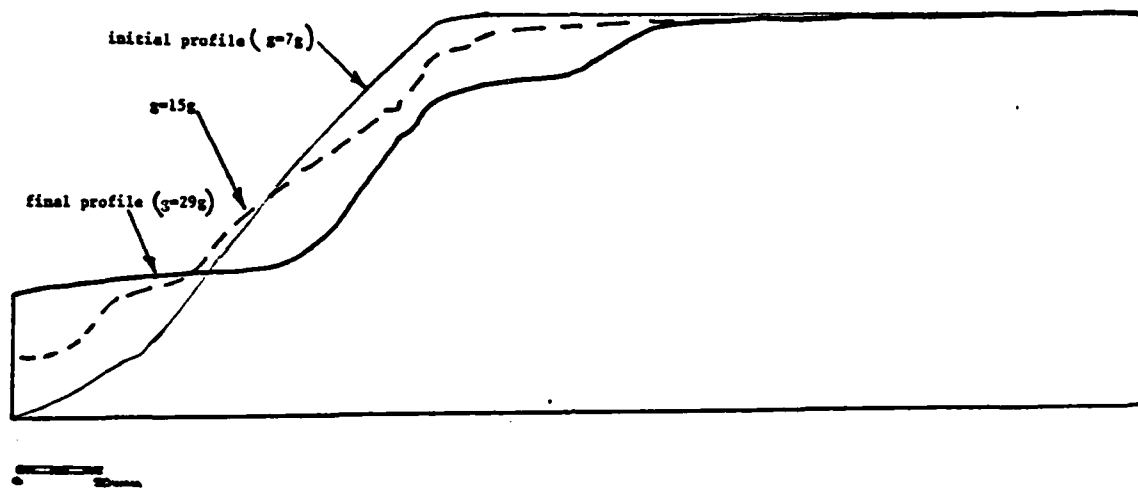


Figure 6.10 - MW5 Change in Model Profile

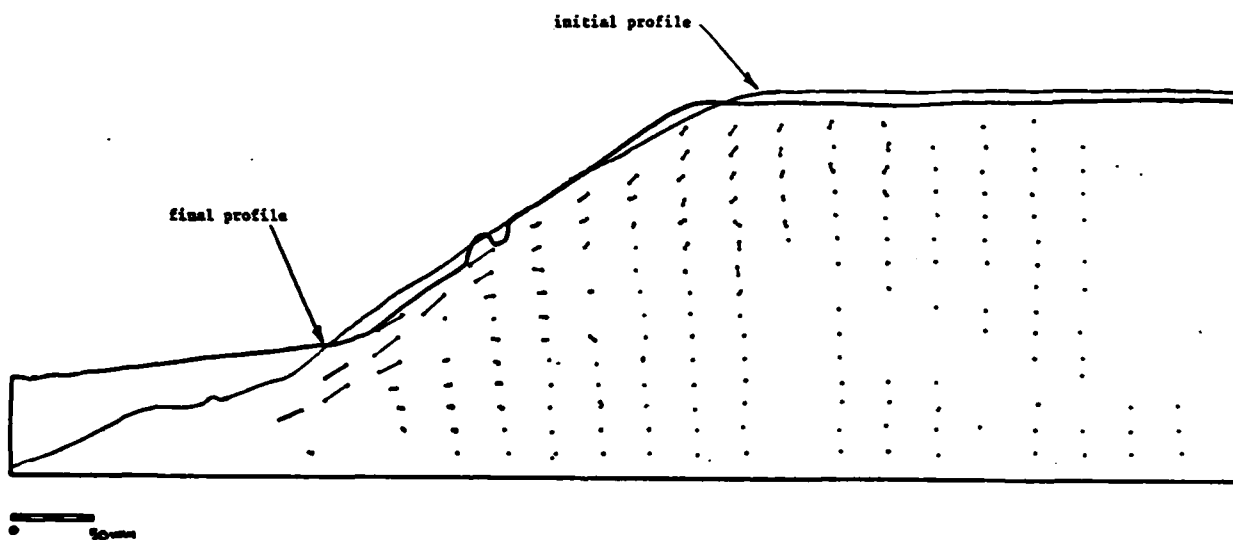


Figure 6.11 - MW6 Model Soil Displacements

material A.

Model MW5 was built to confirm the unclear point of failure in model MW4. The model, when subjected to an increase in centrifugal loading, with a constant throughflow of  $37 \text{ mm}^3/\text{mm-s}$ , showed a sudden crest displacement occurring at 26g. The changes in profile, shown in figure 6.10, are very similar to those which occurred in model MW4, as was the final moisture content at 24%.

All previous models had been constructed at slope angle  $45^\circ$ . Model MW6 was built with a shallower embankment inclination, at IV : 1.5H or  $33.7^\circ$  to the horizontal. This model failed during an increase in centrifugal loading, at 19g, according to the output of the displacement transducer at the crest. Figure 6.11 shows the change in profile, and the displacements which occurred on the front soil surface of the model. It was evident on examining the model that the dominant feature of failure was erosion down the back surface of the model, rather than regular, internal, plane strain slope instability.

Another feature of failure also became evident with this model test. The moisture expelled from the soil by centrifugal loading, was the dominant feature of failure, much more so than subtle changes in slope angle, and this parameter was largely uncontrolled by this method of model preparation.

Model MW7 was tested to investigate the effect of throughflow under conditions of changing centrifugal loading, with special attention to the changing position of the phreatic line. The model embankment was built of material B, with a slope inclination of IV : 2H ( $26.5^\circ$ ). It was slowly loaded to 40g without an external supply of water, and then unloaded to 20g. At 20g a throughflow of  $37 \text{ mm}^3/\text{mm-s}$  was introduced, and with further reduction in centrifugal loading eventually to 1g, the phreatic surface rose, and an erosion beach was formed. This test emphasised the inter-

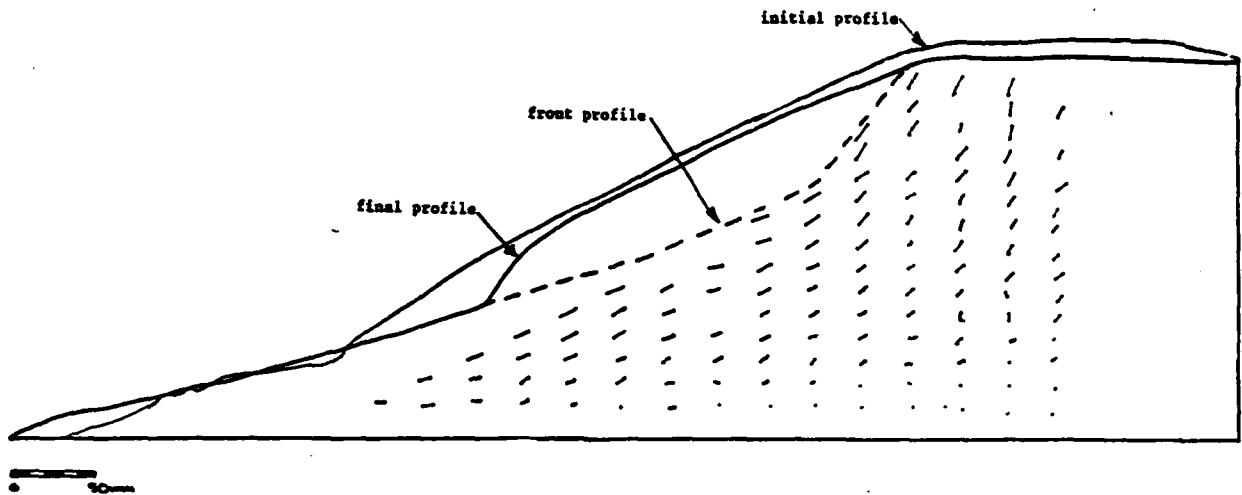
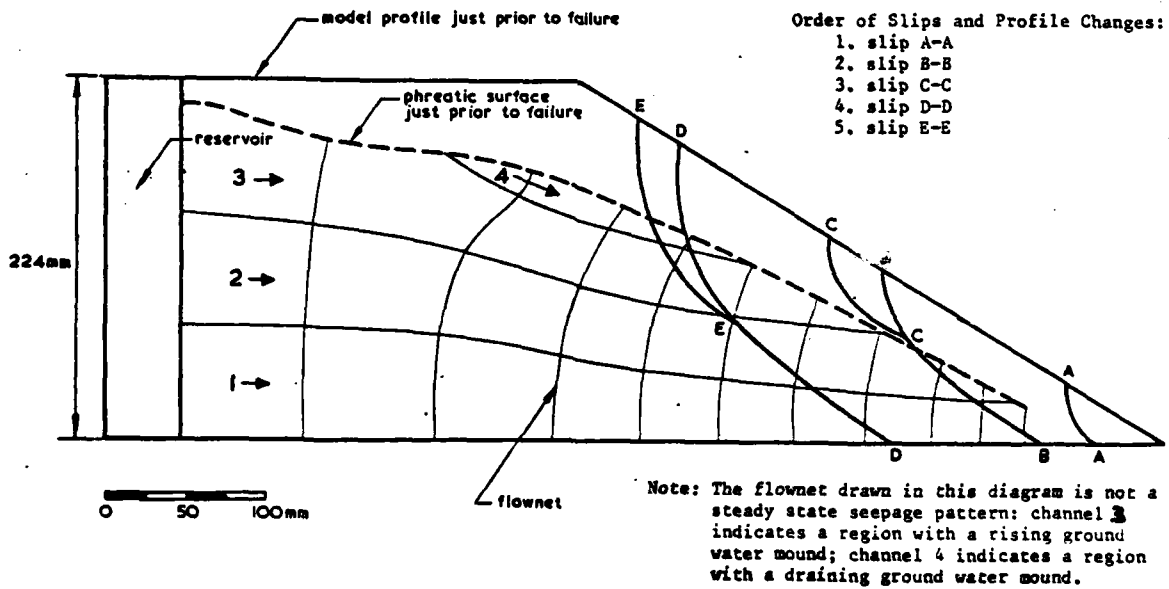


Figure 6.12 - MW8 Model Soil Displacements



Note: Diagrams from successive inflight video record show embankment on left of picture

Figure 6.13 - MW9 Progression of Deep-seated Failures

dependence of the phreatic line, the throughflow quantity, and the centrifugal loading, but before further investigation was made into this aspect of stability, one further rate of construction test was executed.

Model MW8, built of material B in an embankment profile of IV : 2H ( $26.5^{\circ}$ ) was subjected to a rapid increase in loading, exhibiting failure at 3lg. Compaction, forward shearing and erosion were significant features of model response, as for previous tests, figure 6.12.

Model MW9 marked the beginning of two new aspects of testing: the testing method was altered, and continuous observation during the test was now possible by video camera, although this eliminated in-test still photography. The maximum available influx of water was also greatly increased with new, larger water supply lines.

Model MW9 was an embankment, at slope angle of IV : 1.5H ( $33.7^{\circ}$ ), made of material B. It was accelerated slowly to 100g, taking particular care at the lower centrifugal loading that the excess moisture expelled from the model did not damage the embankment profile significantly. Only after the model seemed stable at 100g, was an influx of water, equal to  $147 \text{ mm}^3/\text{mm-s}$ , introduced into the rear reservoir. As the phreatic line established itself, a deep seated retrogressive failure was observed to occur, the progression of which is drawn in figure 6.13. After the last retrogression had occurred, the continued throughflow of water eroded the embankment until breaching was achieved, reshaping the surface of failure into a beach of debris, figure 6.14.

Model MW9 had established a class of failure which was of interest. It was not a rate of construction failure that Malushitsky had studied, but rather a new phenomenon characteristic of this particular class of mine waste embankment under throughflow conditions. The next four tests, MW10 through MW13 studied variations on this mode of failure. The beach of erosion debris also proved to be a recurring feature of model failures

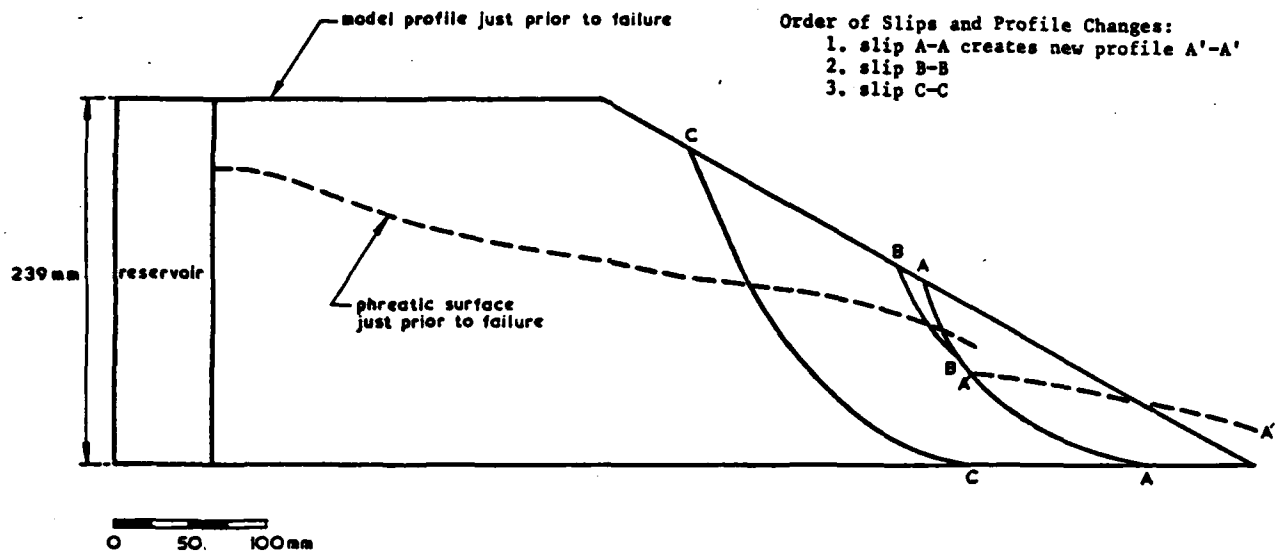


Figure 6.15 - MW10 Progression of Deep-seated Failures

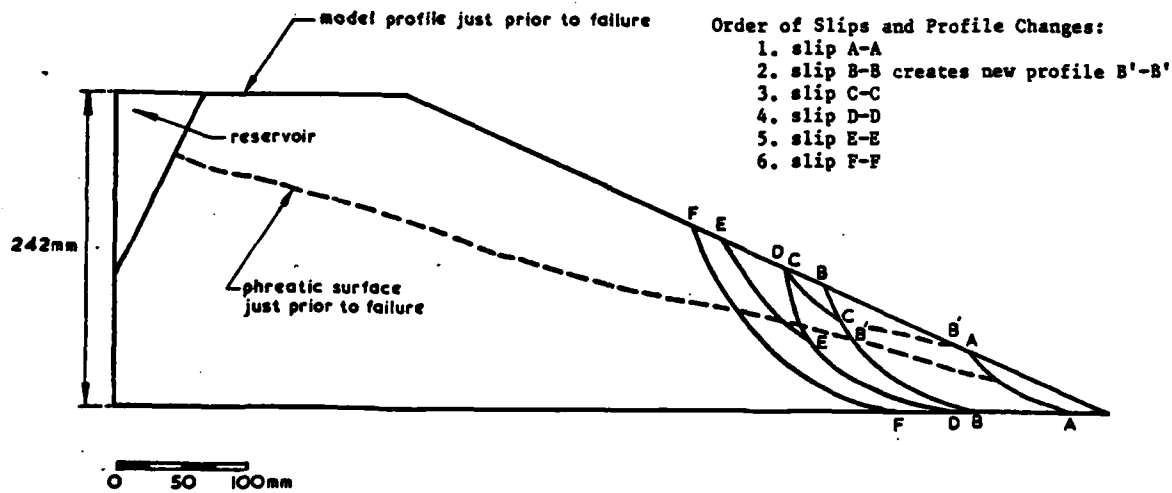


Figure 6.17 - MW11 Progression of Deep-seated Failures

and the data of erosion beach slopes and their angles, will be discussed in section 6.8.3.

Model MW10 was a slightly larger scale version of model MW9, built to slightly larger dimensions and subjected to slightly higher centrifugal loading, 120g. Greater control of throughflow was exercised by increasing the influx in stages, although fine regulation of flow was still impossible. When the throughflow was increased to full capacity,  $147 \text{ mm}^3/\text{mm-s}$ , a pattern of retrogressive slips was observed, markedly similar to those observed in model MW9 (see figure 6.15). By shutting off the water supply after such movement had occurred, the model surface was not reshaped by subsequent erosion, and the final profile is shown in figure 6.16.

Model MW11 was built at a shallower slope, IV : 2H ( $26.5^\circ$ ), and subjected to a centrifugal loading of 120g. Three increments of throughflow preceded failure, which occurred in a retrogressive mode similar to that observed in models MW9 and MW10, although the retrogressions were typically smaller, but more numerous, figure 6.17. The sharpness of the retrogressive slip escarpments was lost and the final profile features were smoothed when the overflow of reservoir water occurred as the embankment dam was breached.

The dry density of the embankment after the test was  $1400 \text{ kg/m}^3$ , and of the erosion beach,  $1260 \text{ kg/m}^3$ ; the moisture content of the embankment was 11%.

Model MW12 was built to the same dimensions as MW11 with the inclusion of one additional feature: a permeable, undrained key. In prototype embankment construction, it is a practice sometimes adopted that a longitudinal section called the key, be included at the centre of the embankment. To form this key in practice, a strip of top soil is removed and a mound of coarse waste is placed along the proposed longitudinal centre line of the waste embankment. This mound of key material is subsequently

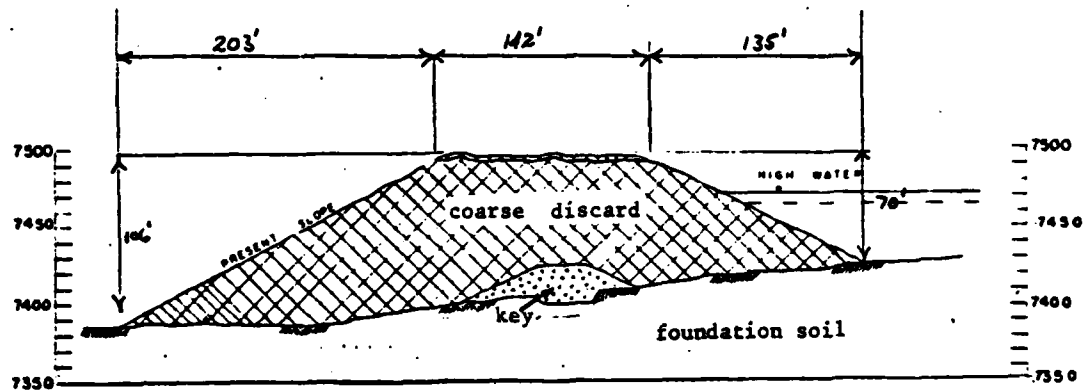


Figure 6.18 - Field Embankment Cross-Section with Key  
( U.S. Army Corps of Engineers )

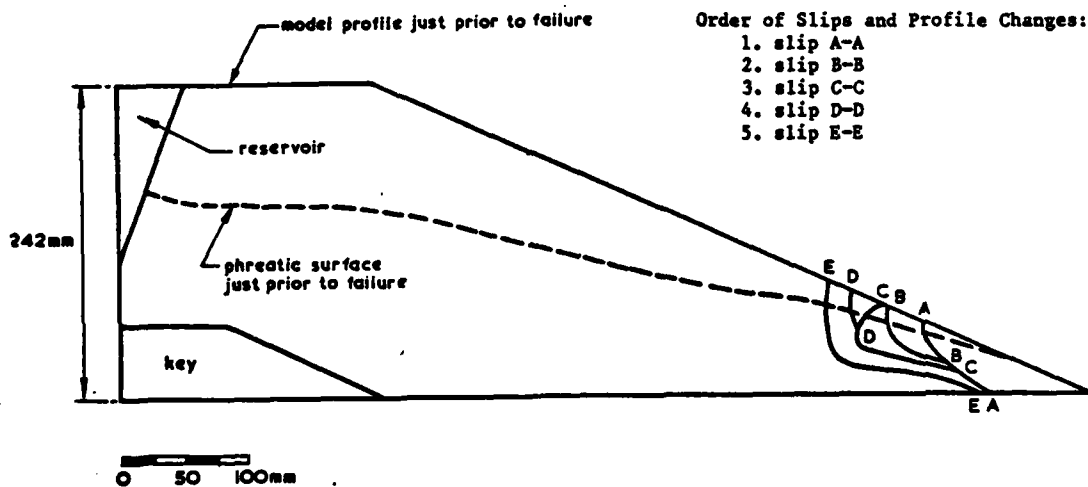


Figure 6.19 - MW12 Progression of Deep-seated Failures

buried below the rising waste heap embankment, but is supposed to provide an effective, frictional key between the central, highly loaded part of the embankment and its foundation (see figure 6.18). Since the key material which is used is more permeable than the material composing the body of the embankment, it is intended to provide drainage for the embankment under throughflow conditions. This will serve to increase embankment stability by increasing effective stresses. This drainage of the key is a feature sometimes neglected, and model MW12 investigated the effect of absence of drainage in the key.

The model was subjected to an increase in self-weight of 120 times, and at the second increment of throughflow,  $53 \text{ mm}^3/\text{mm-s}$ , failure was initiated: small rapid retrogressions were observed (see figure 6.19). A final increase of throughflow to  $177 \text{ mm}^3/\text{mm-s}$  caused extensive retrogressive erosion, (see figures 6.20 and 6.21).

This model failed in a retrogressive fashion at a much lower rate than the otherwise identical model MW11. The inclusion of an enclosed, permeable section sufficiently altered seepage characteristics that slope stability was radically reduced. The next model, MW13, however demonstrated the dominant beneficial effects of the inclusion of a toe drain in an embankment which is otherwise unstable in the presence of large throughflows.

Model MW13 was made of material B, to the same dimensions as model MW11, but with the inclusion of both a key, as in model MW12, and a toe drain. The model was loaded to 120g, and the maximum throughflow which could be supplied for that test was initiated. This resulted in an almost full reservoir level with a throughflow of  $159 \text{ mm}^3/\text{mm-s}$ . The slope remained stable under these conditions for 139 minutes, figure 6.22.

The centrifuge was momentarily stopped, while a slurry of kaolin and water was emptied into the model reservoir, to simulate the hydraulically



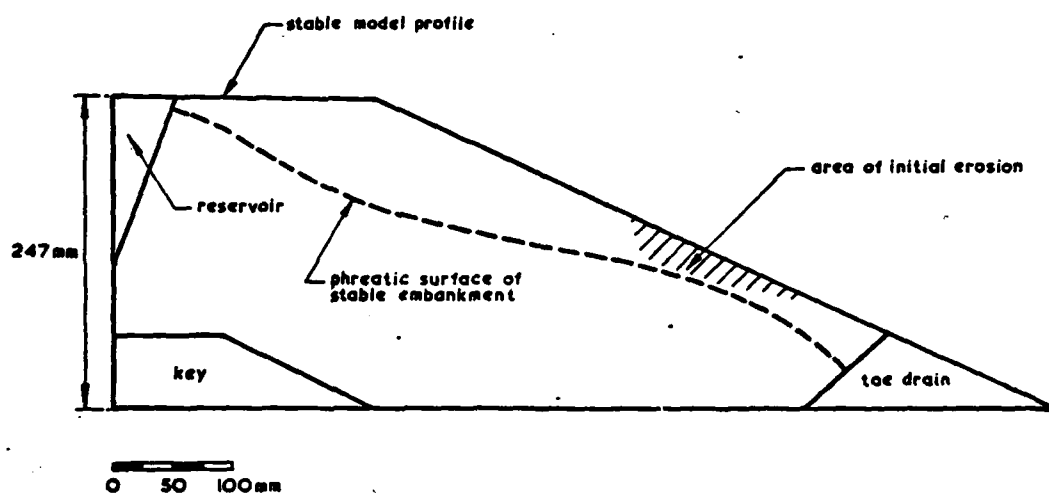


Figure 6.22 - MW13 Stable Throughflow Conditions

deposited upstream blanket of tailings in a prototype coal mine waste embankment dam. This caused effective sealing of the upstream face of the dam, virtually eliminating throughflow, although infiltration of the slurry into the body of the embankment was noted. At this point, uplift was applied with a large flow of water radiating from the key and equal in head to just greater than the height of the embankment crest, so that  $r_u = 0.77$ . Rather than deep seated failure which might have been expected, the limits of the water applied in the uplift expanded until it reached the surface of the embankment slope, just above the toe drain. As the water drained off the surface, erosion occurred, and as more water drained from more of the embankment surface area, widespread erosion constituted failure.

This first set of models had demonstrated that in lightweight, free-draining material, such as usually characterises the coarse discard of coal mine waste, rate of construction is not the major concern, but rather the effects of excessive throughflow or overflow once the embankment dam has gone into operation. The limit of safe flow was governed by the height of the phreatic line, the throughflow volume, and the inclusion of permeable zones such as an undrained key, which reduced stability, or a toe drain which increased stability. The next set of tests endeavoured to identify the influence of various soil parameters, on the character of slope stability studied in the first thirteen models.

The soil for model MW20, which was expected to be identical to material B, proved in fact to be quite different, and required a correspondingly different method of preparation (see sections 6.2 and 6.4). This involved a preparative period of preconsolidation on the centrifuge, for 125 minutes at 90g, after which an embankment with slope angle IV : 2H ( $26.5^\circ$ ) was excavated in the soil block, now at 21% moisture content, and dry density  $1326 \text{ kg/m}^3$ .

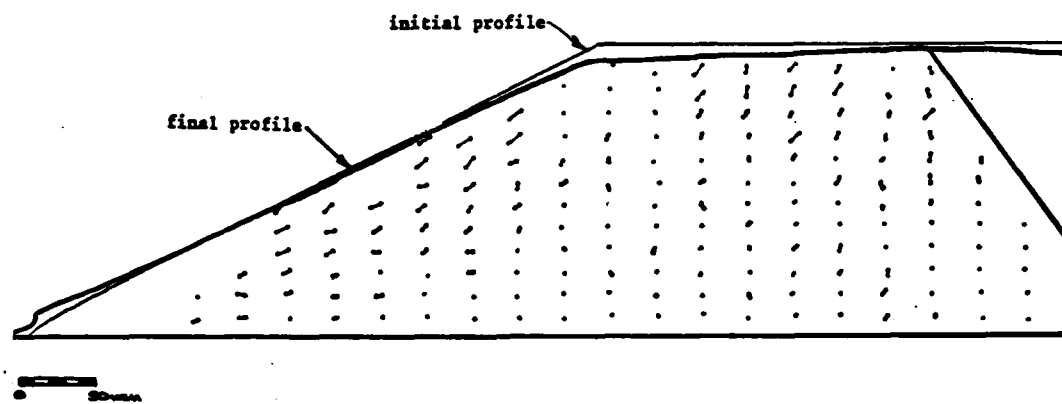


Figure 6.23 - MW20 Model Soil Displacements

The model embankment was reloaded to 120g, and although some movement in the toe occurred during the increase in loading, in addition to some forward shear in the zone in front of the crest, figure 6.23, the model appeared to be stable at 120g. The introduction of the inflow of water to the reservoir, at a rate equal to  $127 \text{ mm}^3/\text{mm-s}$ , caused almost immediate overtopping and severe erosion. It is unlikely, judging from the laboratory derived value of permeability for this soil,  $k = 1.2 \times 10^{-6} \text{ mm/s}$ , that appreciable throughflow occurred.

The type of failure in which throughflow was the critical feature of slope instability, as in models MW9 through MW13, could not be expected to occur in a model embankment of material as impermeable as that in model MW20. A change in particle size distribution was therefore undertaken for the soil used in model MW21 (see section 6.4); the new permeability, measured in the laboratory consolidometer, was  $2.2 \times 10^{-5} \text{ mm/s}$ .

A different method of model preparation was also followed, which involved vertical static compaction of five layers of soil of equal thickness (40 mm), under  $58 \text{ kN/m}^2$ . The moisture content of the resulting soil block varied from 17% at the bottom, to 23% at the top, and the average dry density was  $1480 \text{ kN/m}^3$ . The block thus formed had been founded on a 10 mm thick preconsolidated kaolin base (see section 6.2). The model embankment excavated in this block of soil material was identical in dimensions to model MW20. The vertical compaction method of preparation had one immediately obvious consequence: the water draining to the upper surface, in response to compaction, brought with it a portion of the fines, which were then deposited on the layer interface.

The model was loaded to 120g, at which stress level it was stable. Subsequent introduction of throughflow, to a maximum quantity of  $75 \text{ mm}^3/\text{mm-s}$ , caused a pattern of erosion which constituted failure, and although a typical erosion beach was observed, the character of erosion was different from

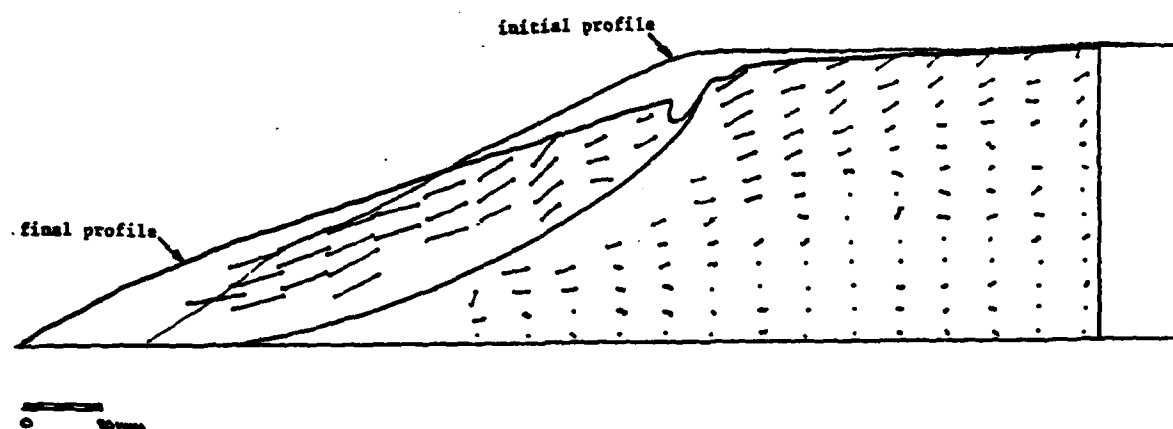


Figure 6.26 - MW24 Model Soil Displacements After First Slip

that observed in previous models: erosion was observed to occur in the form of a narrow gully, the top of which coincided with the exit level of the phreatic line. This was coincident with the top of the third layer, 114 mm high (figure 6.24). Of interest also, was the value of permeability measured according to the flownet pattern observed,  $k = 0.006 \text{ mm/s}$ , which was much higher than that measured by laboratory consolidometer,  $2.2 \times 10^{-5} \text{ mm/s}$ .

Measurements taken after the test showed that further compaction had occurred, to a dry density of  $1540 \text{ kg/m}^3$  and that the average moisture content was 18%.

The soil for the next model, MW22, was altered to again achieve a more permeable material. This embankment, also built on a layer of kaolin, was built to the dimensions of model MW20, in the usual manner of loose construction. The model was subjected to an increase in self-weight of 120 times and was stable. Water was then introduced to the rear reservoir at the rate of  $109 \text{ mm}^3/\text{mm-s}$  and it was observed that such a through-flow quantity in a material this permeable, was barely sufficient to be noticed. By reducing in steps the centrifugal loading, however, two changes occurred: the phreatic line rose, and erosion was eventually initiated. Erosion was first observed at 40g, and by 20g, was very obvious, in the form of a debris beach. The permeability calculated from the resulting flownet patterns observed during the test, averaged  $0.04 \text{ mm/s}$ . Dry density and moisture content measured subsequent to testing were  $1400 \text{ kg/m}^3$ , and 20%, respectively.

Model MW23 was constructed in manner and to dimensions, identical with model MW22, although with a differently shaped rear reservoir, and with a larger water supply system. The model was centrifugally loaded to 100g, and then by altering throughflow and loading, the consequent changes in phreatic line and erosion characteristics were noted. Under the first

quantity of throughflow introduced,  $52 \text{ mm}^3/\text{mm-s}$ , the slope was observed to be stable from 100g to 50g, but the next increment of throughflow,  $112 \text{ mm}^3/\text{mm-s}$ , although stable at 100g, was sufficient to cause observable erosion and sediment transport, when the centrifugal loading was reduced to 75g. Further combinations of throughflow and centrifugal loading were tried before the completion of the test, figure 6.25. Dry density of the remaining embankment after the test was  $1365 \text{ kg/m}^3$  and the moisture content was 16%.

A less permeable material was the object of the alteration in particle size distribution undertaken for model MW24 (see section 6.4). The result was a soil of unexpectedly low permeability,  $4.2 \times 10^{-7} \text{ mm/s}$ . After it was shaped into an embankment in the usual manner of model preparation, the model was subjected to an increase in self-weight, gradually increasing to 15g. At 15g, the model embankment slumped in a plane strain rotational movement, to  $16^\circ$  to the horizontal (figures 6.26 and 6.27). Further increases in self-weight caused corresponding reductions in the angle of inclination of the embankment slope, and the last movement was characterised by retrogressive slipping to  $7^\circ$  at 50g, figure 6.28. The dry density measured after the test was  $1308 \text{ kg/m}^3$ , and the moisture content, 20%.

The final model, MW25, was made of soil similar to that used in models MW22 and MW23. By introducing various throughflows at various centrifugal loadings, erosion was observed to occur at a throughflow of  $121 \text{ mm}^3/\text{mm-s}$  as the centrifugal loading was reduced from 100g to 30g. Erosion was then permitted to continue for some minutes at 20g. The dry density measured after the test was  $1385 \text{ kg/m}^3$ , and the water content was 22%.

This second set of models had investigated the initially proposed parameters of the second research contract, but two factors in particular had been emphasised: particle size distribution, which is sensitive to handling procedures and weathering, may govern the type of failure most

liable to occur, and the interplay of throughflow characteristics, centrifugal loading and erosion had also been demonstrated.

#### 6.7 Effects of Water Flow in Centrifugal Models

The dominant feature of the majority of failures observed in these models of coal mine waste embankments was the effect of water through and overflow. It is noted in section 5.4 that this is typical of prototype embankment dam failures, and it is therefore appropriate to examine the correctness of model events, in which water plays a dominant role, as related to prototype response.

In soils of low permeability and high compressibility, the stress state may significantly alter the moisture content of the soil, and this process may require some period of time to occur. When this is the case, the movement of pore water which permits consolidation as the excess pore pressure, generated by the change in stress state, dissipates, is governed by Terzaghi's equation of primary consolidation:

$$T_v = \frac{c_v t}{H^2} \quad (6.8)$$

In a model made of prototype soil to a scale of  $\frac{1}{N}$ , such that the maximum distance to free drainage,  $H$ , is also reduced by  $N$  times in the model, then the time for dissipation of pore pressures to occur in a homogeneous saturated soil will be correspondingly decreased  $N^2$  times, such that:

$$t_m = \frac{t_p}{N^2} \quad (6.9)$$

In zones in which this same soil is broken into separate blocks with air voids between them, so that drainage is characterised by consolidation of isolated blocks from which water moves into adjacent air voids, Terzaghi's equation 6.8 must introduce the block size rather than the zone size. If the soil in the model is broken into these same size blocks

---

\* where  $T_v$  = dimensionless time factor,  $c_v$  = coefficient of consolidation  
 $t$  = time,  $H$  = length of longest drainage path.  
 † where  $t_m$  = time for model consolidation,  $t_p$  = time for prototype consolidation,  $N$  = scale reduction of model.



AD-A084 048

CAMBRIDGE UNIV (ENGLAND) DEPT OF CIVIL ENGINEERING F/G 8/13  
CENTRIFUGAL MODELLING OF SOIL STRUCTURES, PART I. CENTRIFUGAL M--ETC(U)  
MAR 79 D J GOODINGS, A N SCHOFIELD DA-ERO-76-6-040

NL

UNCLASSIFIED

3 1/4  
AD  
A084 048

END

DATE

FILED

6-80

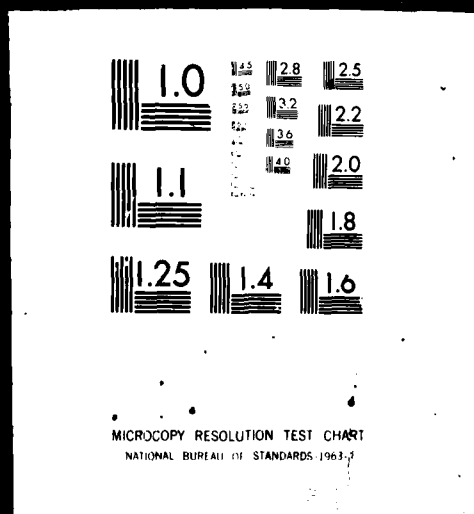
DTIC

AD551F10

3 OF 3

AD

A084 048



as in the prototype, then the rate of such movement of water remains unchanged in reduced scale centrifugal modelling, and  $t_m = t_p$ . Experimental work by Malushitsky (1975) on waste heaps of mine overburden, indicated that in models where a lower zone of saturated soil and an upper zone of unsaturated soil are of equal significance, the correct proportion of scaling for the model is:

$$t_m = \frac{t_p}{(N)^a}, \text{ where } a = 1 \quad (6.10)$$

Movement of water through soils which have an essentially rigid soil skeleton, independent of stress state, and are highly permeable in nature, is governed by a more simple law, Darcy's law:

$$v = ki^* \quad (6.11)$$

provided that the flow remains laminar. In such soils, large quantities of water may pass through, and emerge from the face of the embankment. The consequent erosion may cause significant damage.

Once water has emerged from the embankment, in the usual case that the surface water movement is turbulent, flow is governed by the Manning equation for steady uniform open channel flow:

$$v = \frac{1}{n} R^{2/3} S^{1/2} \quad \text{Henderson (1971)} \quad (6.12)$$

These latter two types of flow, the internal seepage governed by Darcy's law and the turbulent surface flow governed by the Manning equation, dominated the failures observed in this test series. They will be further discussed in the following sections.

#### 6.7.1 Darcy's law

Darcy's law fits experimentally the apparent velocity of water moving in a straight line from point A to point B. It is valid for laminar flow,

---

\* where  $v$  = discharge velocity,  $k$  = coefficient of permeability,  $i$  = hydraulic gradient.

† where  $v$  = fluid velocity,  $n$  = Manning's roughness coefficient,  $R$  = hydraulic mean radius,  $S$  = sin(longitudinal slope).

which is numerically defined by Reynolds number for pipe flow:

$$Re = \frac{v D \rho}{\mu} < 2000^* \quad (6.13)$$

Scott (1963) noted for most soil ranging up to coarse sand in permeability, that the rate of flow is well below this conservative upper limit:

$$3 < Re < 10.$$

In the range of velocity where Darcy's law is applicable, velocity of throughflow is determined by the product of two parameters, the permeability,  $k$ , and the hydraulic gradient,  $i$ . In soil mechanics, permeability is defined in units of velocity, to describe the speed at which water may travel through soil at earth's gravity under a given driving force, and it is assumed to be a material property. The driving force which causes the water to move through the soil, is described in soil mechanics by the geometric ratio, hydraulic gradient, defined at earth's gravity as:

$$i = \frac{h}{l} \quad (6.14)$$

where  $i$  = hydraulic gradient

$h$  = difference in height of two open ended columns of water when the two columns are inserted into the soil, one at point A and one at point B

$l$  = straight line distance between points A and B.

The actual force causing the movement of water is the pressure gradient,  $i'$ :

$$i' = i \times \gamma_w \quad (6.15)$$

where  $i'$  = pressure gradient

$i$  = hydraulic gradient

$\gamma_w$  = unit weight of water.

---

\* where  $Re$  = Reynolds number,  $v$  = velocity,  $D$  = diameter of pipe or soil pores =  $D_{10}$ ,  $\rho$  = density of fluid,  $\mu$  = static viscosity of fluid.

In a model at earth's gravity, made of prototype soil at scale  $\frac{1}{N}$  of that prototype, so that all dimensions are reduced N times, the hydraulic gradients of both model and prototype are equal:

$$i_m = \frac{h_m}{l_m} = \frac{h_p}{N} \times \frac{N}{l_p} = \frac{h_p}{l_p} = i_p^* \quad (6.16)$$

as are the pressure gradients:

$$i'_m = i_m \times \gamma_w = i_p \times \gamma_w = i'_p \quad (6.17)$$

When this model is subjected to centrifugal loading, such that the self-weight of all elements is increased by N times, certain changes occur. If the shape of the flownet is maintained, then the hydraulic gradient according to the definition in equation 6.16 remains constant, while the pressure gradient increases by a factor of N, such that:

$$i'_{mNg} = i_m \times N\gamma_w = Ni'_{m1g} = Ni'_p^+ \quad (6.18)$$

On the other hand, the pressure gradient could only be kept constant if the hydraulic gradient were reduced N times according to equation 6.14. This would require a reduction in the parameter  $h_m$ .

The consequence of these changes in centrifuge models is that the hydraulic gradient, as originally defined in equation 6.14, no longer adequately describes the force driving the water through the soil. A new <sup>of Darcy's law</sup> definition/is appropriate, in terms of pressure gradient:

$$V = \frac{ki'}{\gamma_w} \quad (6.19)$$

where  $\gamma_w$  = unit weight of water at earth's gravity in order to relate it to normal prototype conditions.

\* where  $i_m$  = hydraulic gradient of the model,  $h_m$  = loss of head of water in model between A and B,  $l_m$  = distance in model between A and B,  $h_p$  = loss of head of water in prototype between geometrically corresponding A and B,  $l_p$  = distance in prototype between geometrically corresponding A and B, N = factor of dimension reduction in model,  $i_p$  = hydraulic gradient of the prototype.

+ where  $i'_m$  = pressure gradient in the model,  $i'_p$  = pressure gradient in the prototype,  $i'_{mNg}$  = pressure gradient in the model at Ng,  $i'_{m1g}$  = pressure gradient in the model at 1g.

A consequence of this effect of centrifugal modelling is as follows: in a model with a given flownet established at earth's gravity, which is then subjected to an increase in self-weight of  $N$  times, but with the original flownet maintained, the seepage velocity of the water through the soil will increase by  $N$  times:

$$v_{Ng} = v_{lg} \times N^* \quad (6.20)$$

It then becomes relevant to check that the flow of water is still laminar, and therefore still governed by Darcy's law. If a coarse sand with a Reynolds number of 10 (Scott, 1963) in a model at earth's gravity, is increased in self-weight by a factor of  $N = 150$ , then the velocity, and consequently the Reynolds number, are both increased by 150 times. The Reynolds number becomes 1500, still less than 2000, the conservative upper limit of laminar pipe flow.

#### 6.7.2 Scaling of flownets and adjacent regions of moisture

The geometric pattern in a soil of the paths along which water will flow when subjected to hydraulic gradients, and of the orthogonal lines of equipotential head, is known as the flownet. The equipotentials are in general governed by the Laplace equation (Taylor (1948)):

$$\frac{\partial^2 h}{\partial x^2} + \frac{\partial^2 h}{\partial z^2} = 0 \quad (6.21)$$

where  $x$  and  $z$  are the axes of space. At any point in a prototype embankment under atmospheric pressure,  $h$  is the height above a given datum to which water would rise in an open stand pipe from that point.

When we consider a reduced scale model, at scale  $\frac{1}{N}$ , we find that it can be subjected to seepage flow such that the flownet and the top seepage line retain a fixed pattern under conditions of an increase in self-weight. Relative to the prototype, the model height of water,  $h$ , is reduced  $N$  times with the reduction in all model dimensions and we consider that the

---

\* where  $v_{Ng}$  = water velocity in a model at  $Ng$ ,  $v_{lg}$  = water velocity in a model at  $lg$ .

Laplace equation remains unchanged. All dimensions of the flownet are reduced in the same proportion: the shape and proportions of the flownet in the model are identical to the shape and proportions of the flownet in the prototype.

In the case of anisotropic flow, where  $k_z \neq k_x$  for instance, the Laplace equation is altered to:

$$\frac{\partial^2 h}{\partial x_t^2} + \frac{\partial^2 h}{\partial z^2} = 0 \quad (6.22)$$

$$\text{where } x_t = \sqrt{\frac{k_z}{k_x}} x \quad (6.23)$$

The relative value of  $k_z$  and  $k_x$  is not altered by centrifugal loading, and the distorted shape of the prototype anisotropic flownet, is correctly reproduced in the model.

Above the top flowline of groundwater there exists a zone of continuous capillary rise. The height of this zone is governed by the equation:

$$h_c = \frac{2 T_s}{\gamma_w R} \quad (\text{Taylor (1948)}) \quad (6.24)$$

In reduced scale models built with prototype soil and tested at earth's gravity, the height of continuous capillary rise is unscaled and may obscure certain flow effects. If this same model, however, is subjected to an increase in self weight of  $N$  times, then the height of capillary rise is reduced in proportion to the increase in self weight of the water and the whole model. The zone of capillary rise in the model is therefore reduced in the same proportion as the reduction of model dimensions:

$$h_{cmNg} = \frac{h_{cp}}{N} \quad (6.25)$$

In the case where a soil of reduced permeability is used in the model, for example,  $k_p = a k_m$  is achieved by reducing prototype particle size

\* where  $h_c$  = height of continuous capillary rise,  $T_s$  = surface tension,  $\gamma_w$  = unit weight of water,  $R$  = radius of pores.

+ where  $h_{cmNg}$  = height of capillary rise in the model at  $Ng$ ,  $h_{cp}$  = height of capillary rise in the prototype.

in the proportion:  $D_{10_p} = \sqrt{a} D_{10_m}$  (see section 6.3), then the height of capillary rise in the centrifugal model at  $N_g$  is disproportionately large, by a factor of  $\sqrt{a}$ :

$$h_{cmNg} = h_{cp} \times \frac{\sqrt{a}}{N} \quad (6.26)$$

In either case, however, whether the prototype soil, or a soil with reduced permeability is used, the effect of centrifugal loading will be to reduce continuous capillary rise much closer to scale than would be the case in a reduced scale model at earth's gravity.

Above the zone of continuous capillary rise, there is a zone of partially saturated soil which is not governed by equation 6.24. The movement of water through this zone is discussed above in section 6.7. Pokrovsky and Fyodorov (1965) discussed this interstitial water trapped at the grain contacts. For soil in a centrifugal model to act as it does in the prototype, they placed a limit on the largest pore size, at various levels of centrifugal loading, for which errors are negligible: if the product of the largest grain diameter, in millimetres, times the centrifugal loading expressed as the multiple of increase in self-weight, is less than 470, then the distortion occurring in the water menisci leading to loss of water from the grain contacts is considered tolerable. For the Cambridge geotechnical centrifuge, in which the top speed ~~corresponds~~ to 150g, the largest particle diameter in soil models at that level of centrifugal loading, should not exceed  $470/150 = 3.13$  mm. If this is true, then the total soil height affected by discontinuous capillary tension will be unscaled and unaffected.

### 6.7.3 Seepage forces

The pressure gradient which causes water to move in soil is lost along the path of movement in the form of viscous friction, dissipated by drag against the soil particles. The seepage force per unit volume is defined



to be:

$$j = \gamma_w i_{\max}^* \quad (6.27)$$

When a reduced scale model is subjected to a centrifugal loading equal to  $Ng$ , the seepage force is also increased by  $N$  times, so that:

$$j_{Ng} = N j_{lg}^{**} \quad (6.28)$$

The success of seepage forces initiating internal erosion within a soil structure, is primarily dependent upon the mean effective stresses holding the soil in place. The increase in self-weight caused by centrifugal loading will cause an increase in effective stress in the same proportion as the increase of seepage forces. Internal erosion should therefore be modelled correctly.

Steady seepage forces which reduce overall slope stability are also found to increase in proportion to the forces which stabilise slopes. Goodings et al (1977) investigated this with regard to seepage in a long slope of essentially frictional soil for two cases: seepage parallel to the slope, and horizontal seepage near the toe of the embankment. They determined that the limiting slope in both cases is affected neither by centrifugal loading nor by permeability. The limiting slope angle for steady seepage parallel to the slope is:

$$\phi' = \tan^{-1} \left( \frac{\gamma \tan \beta}{\gamma'} \right)^{\dagger} \quad (6.29)$$

and for horizontal seepage near the toe:

$$\phi' = \tan^{-1} \left( \frac{\cos \beta \sin \beta}{\cos^2 \beta - \frac{\gamma_w}{\gamma}} \right) \quad (6.30)$$

\* where  $j$  = seepage force per unit volume,  $\gamma_w$  = unit weight of water,  $i_{\max}$  = maximum hydraulic gradient.

\*\* where  $j_{Ng}$  = seepage force in a model at  $Ng$ ,  $j_{lg}$  = seepage force in a model at earth's gravity.

† where  $\phi'$  = angle of internal friction,  $\gamma$  = bulk unit weight of the soil,  $\gamma'$  = buoyant unit weight of the soil,  $\gamma_w$  = unit weight of water,  $\beta$  = angle of inclination of the slope.

As the slope angle,  $\beta$ , becomes small, the two cases define almost the same minimum angle of friction,  $\phi'$ , for stability with seepage.

At the point when water moving through an embankment emerges and flows down the face, a new class of water flow and failure arises, characterised by erosion and sediment transport. The effects of this phenomenon can be even more extreme in an embankment of material as light-weight as coal mine waste, than in conventional embankment dams. The capability of the centrifuge to model such events will be discussed in the following sections.

#### 6.7.4 The Chezy and Manning formulae

As water overtops or emerges from the face of an embankment, the resulting turbulent overflow is governed by the Chezy equation for uniform steady flow:

$$V = \sqrt{\frac{2g}{\lambda}} R^{\frac{1}{2}} S^{\frac{1}{2}} * \quad (\text{Streeter (1951)}) \quad (6.31)$$

and in wide, open channel flow, where the depth of flow is much less than the width of the flow, this is modified to the Manning equation:

$$V = \frac{1}{n} d^{\frac{2}{3}} S^{\frac{1}{2}} + \quad (\text{Henderson (1971)}) \quad (6.32)$$

In a reduced scale model subjected to an increase in self-weight by a factor of  $N$ , a variety of otherwise unnatural conditions occur depending upon the degrees of similarity imposed.

In the simplest case where a model with turbulent surface flow of depth  $d$ , is subjected to an increase in self-weight of  $N$  times, but  $d$  remains constant, the corresponding change in velocity, according to

---

\* where  $V$  = velocity of flow,  $g$  = earth's gravitational acceleration,  
 $\lambda$  = dimensionless coefficient,  $R$  = hydraulic radius = area of flow/  
wetted perimeter,  $S$  = sin (angle of inclination).  
+ where  $n$  = Manning roughness coefficient,  $d$  = depth of flow in m

equations 6.31 and 6.32, is:

$$V_{ng} = \sqrt{\frac{2gN}{\lambda}} R^{\frac{1}{2}} S^{\frac{1}{2}} = \frac{1}{n} d^{\frac{2}{3}} S^{\frac{1}{2}} N^{\frac{1}{2}} = N^{\frac{1}{2}} V_{lg}^* \quad (6.33)$$

All other cases will be based upon this relationship.

If we next take the instance of a centrifugal model at  $N_g$ , and a prototype, through which ground water in both instances, is moving at the same velocity, because the permeability of the model has been reduced to be  $N$  times less than the prototype, such that:

$$v_p = v_{mNg} = v_{m1g} N^{**} \quad (6.34)$$

(see section 6.7.1), then the volume of throughflow per same unit width of model and prototype is governed only by the ratio of their reservoir heights:

$$\frac{h_m}{h_p} = \frac{1}{N} = \frac{q_m}{q_p}^{**} \quad (6.35)$$

At earth's gravity, the emerging overflow down the face of the prototype embankment is governed by the simple Manning equation for wide open channel flow. From equation 6.32:

$$V_p = \frac{1}{n_p} d_p^{\frac{2}{3}} S^{\frac{1}{2}} ** \quad (6.36)$$

and for a unit width:

$$q_p = V_p d_p = \frac{1}{n_p} d_p^{\frac{2}{3}} S^{\frac{1}{2}} d_p \quad (6.37)$$

In a reduced scale model at  $N_g$ , from equation 6.33:

$$V_m = \frac{1}{n_m} d_m^{\frac{2}{3}} S^{\frac{1}{2}} N^{\frac{1}{2}} \dagger \quad (6.38)$$

\* where  $V_{Ng}$  = velocity of flow at  $N$  gravities,  $V_{lg}$  = velocity of flow at earth's gravity.

\*\*where  $v_p$  = prototype velocity of flow,  $v_{m1g}$  = model velocity of flow at earth's gravity,  $v_{mNg}$  = model velocity of flow at  $N_g$ ,  $h_m, h_p$  = reservoir heights in model and prototype,  $q_m, q_p$  = throughflow in model and prototype,  $n_p$  = Manning's roughness coefficient for the prototype,  $d_p$  = depth of prototype flow in m.

† where  $d_m$  = depth of flow in a model at  $N_g$  in m.

and for the same unit width as in the prototype,

$$q_m = v_m d_m = \frac{1}{n_m} d_m^{2/3} S^{1/2} N^{1/2} d_m \quad (6.39)$$

Since  $q_p = q_m \times N$ , from equation 6.35, then

$$\frac{1}{n_p} d_p^{2/3} S^{1/2} d_p = N^{3/2} \frac{1}{n_m} d_m^{2/3} S^{1/2} d_m \quad (6.40)$$

$$\left( \frac{d_p}{d_m} \right)^{5/3} = \frac{n_p}{n_m} N^{3/2} \quad (6.41)$$

$$\frac{d_p}{d_m} = \left( \frac{n_p}{n_m} \right)^{3/5} N^{9/10} \quad (6.42)$$

If we take for the next case, the instance of comparing the overflow in a model at  $N_g$ , to the overflow in the same model at earth's gravity, where the phreatic level is maintained constant, at both  $N_g$  and earth's gravity, then since:

$$v_{Ng} = N v_{lg} \quad (6.20)$$

$$q_{Ng} = q_{lg} \times N \quad (\text{from 6.35})$$

At earth's gravity:

$$q_{lg} = v_{lg} d_{lg} = \frac{1}{n} d_{lg}^{2/3} S^{1/2} d_{lg} \quad (6.43)$$

and at  $N_g$ :

$$q_{Ng} = v_{Ng} d_{Ng} = \frac{1}{n} d_{Ng}^{2/3} S^{1/2} N^{1/2} d_{Ng} \quad (6.44)$$

Since:

$$q_{Ng} = q_{lg} \times N \quad (\text{from 6.35})$$

then:

$$\frac{1}{n} d_{Ng}^{5/3} S^{1/2} N^{1/2} = \frac{1}{n} d_{lg}^{5/3} S^{1/2} N \quad (6.45)$$

and:

$$\left( \frac{d_{Ng}}{d_{lg}} \right)^{5/3} = N^{1/2} \quad (6.46)$$

$$\frac{d_{Ng}}{d_{lg}} = N^{3/10} \quad (6.47)$$

For a final case, if we take a model at earth's gravity with flow  $q_{1g}$ , and subject the model to a centrifugal loading of  $N_g$ , but maintain constant through flow, such that:

$$q_{Ng} = q_{1g} \quad (6.48)$$

then:

$$q_{1g} = \frac{1}{n} d_{1g}^{5/3} S^{1/2} \quad (\text{from 6.43})$$

and

$$q_{Ng} = \frac{1}{n} d_{Ng}^{5/3} S^{1/2} N^{1/2} \quad (\text{from 6.44})$$

Therefore

$$\frac{1}{n} d_{1g}^{5/3} S^{1/2} = \frac{1}{n} d_{Ng}^{5/3} S^{1/2} N^{1/2} \quad (6.49)$$

$$\left( \frac{d_{Ng}}{d_{1g}} \right)^{5/3} = N^{-1/2} \quad (6.50)$$

$$\frac{d_{Ng}}{d_{1g}} = N^{-3/10} \quad (6.51)$$

#### 6.7.5 Erosion and sediment transport

When water seeping through an embankment emerges either at the toe, or on the face of the slope as a spring, or in the most extreme case when an embankment is overtopped, the damaging effect of the water on embankment stability is in the form of erosion and sediment transport. The initial spread of an unacceptable blanket of debris downstream may, in itself, be adequate to define failure, but the local steepening of the slope, and subsequent retrogressive sliding and eventual breaching of the embankment, which may follow, makes the initiation of erosion an event to be avoided under any circumstances. Such events were observed in the coal mine waste embankment models in this research; the correctness of the events observed in terms of prototype events is discussed below in light of the existing theoretical and experimental background.

In the study of erosion and sediment transport in cases of riverbed flow (see, for example, Henderson (1966), Graf (1971), Yalin (1972)), it is known that particles will begin to move when the boundary shear stress exerted on particles by the overflowing water exceeds a critical shear stress. The exerted shear stress is defined by Henderson (1966) to be:

$$\tau = \gamma_w d S^* \quad (6.52)$$

and the critical shear stress which must be exerted on the particles for erosion to occur, is defined by Shields-Straub to be (Henderson (1966)):

$$\tau_c = \psi(\gamma_s - \gamma_w) D_{50}^+ \quad (6.53)$$

Erosion will occur when  $\tau \geq \tau_c$ :

$$\gamma_w d S \geq \psi(\gamma_s - \gamma_w) D_{50} \quad (6.54)$$

and therefore:

$$d \geq \psi \left( \frac{\gamma_s - \gamma_w}{\gamma_w} \right) \frac{D_{50}}{S} \quad (6.55)$$

By substituting this into the Manning equation for open channel flow:

$$q = \frac{1}{n} d^{5/3} S^{1/2} \quad (6.37)$$

the threshold flow, that overflow which will cause the initiation of erosion, becomes:

$$q_t = \frac{(\psi)^{5/3}}{n} D_{50}^{5/3} \left( \frac{\gamma_s - \gamma_w}{\gamma_w} \right)^{5/3} S^{-7/6} \quad (6.56)$$

Several experimentalists have concerned themselves with determining values for the constants  $\psi$  and  $n$ . Manning's roughness coefficient,  $n$ , was found to be proportional to  $D_{50}^{1/6}$ , although the constant of proportionality varied according to the researcher. Chang (1939), defined

---

\* where  $\tau$  = shear stress,  $\gamma_w$  = unit weight of water,  $d$  = depth of flow  
 $S$  = sin (downstream slope).

† where  $\tau_c$  = critical shear stress,  $\psi$  = constant empirically derived, usually between 0.03 and 0.06, called the Shields number,  
 $\gamma_s$  = unit weight of solids,  $D_{50}$  median grain size.

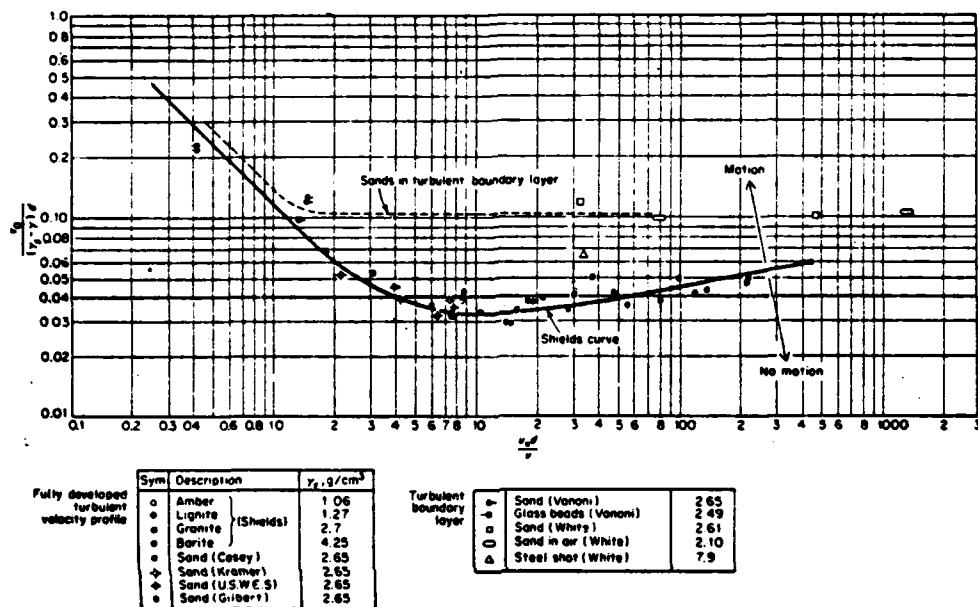


Figure 6.29 - Shields Diagram; Shields Number vs Reynolds Number  
( Graf, 1971 )

n as:

$$n = 0.0166 D_{50}^{1/6} \quad (D_{50} \text{ in mm}) \quad (6.57)$$

$$= 0.0525 D_{50}^{1/6} \quad (D_{50} \text{ in m}) \quad (6.58)$$

which altered equation 6.56 to:

$$q_t = 19.05 \psi^{5/3} D_{50}^{3/2} \left( \frac{\gamma_s - \gamma_w}{\gamma_w} \right)^{5/3} S^{-7/6} \quad (6.59)$$

Other extensive experimental work to determine values for  $\psi$  in terms of a dimensionless parameter called the shear Reynolds number, led to a curve to relate the two values, shown in figure 6.29. The shear Reynolds number is defined as:

$$Re_* = \frac{u_* D_{50}}{\nu} \quad \text{Yalin (1972)} \quad (6.60)$$

where  $Re_*$  = shear Reynolds number

$u_*$  = shear velocity

$$= \left( \frac{\tau_o}{\rho} \right)^{1/2} \quad \text{Graf (1971)} \quad (6.61)$$

$$= (g d S)^{1/2} \text{ for constant two dimensional flow} \quad (6.62)$$

$\tau_o$  = shear velocity at the boundary

$\rho$  = density of water

$g$  = gravitational acceleration

$d$  = depth of flow

$S$  = sin (slope angle)

$D_{50}$  = median grain size

$\nu$  = kinematic viscosity

$$= 1.2 \times 10^{-6} \text{ m}^2/\text{s at } 55^\circ\text{F}$$

The Shields number,  $\psi$ , is defined from equation 6.53 as:

$$\psi = \frac{\tau_o}{(\gamma_s - \gamma_w) D_{50}} \quad (6.63)$$

and in the case of a sloping riverbed, there is typically a slope multiplying factor applied to the Shields number:

$$\cos \beta \left( 1 - \frac{\tan^2 \beta}{\tan^2 \phi} \right)^{1/2} \quad (6.64)$$



where  $\beta$  = angle of slope

$\phi$  = angle of internal friction.

In the case of canals and riverbeds, effects of seepage into the bed may also be important in increasing the erodibility of the soil.

Oldenzien and Brink (1974) used the work of Martin and Aral (1971), and pointed out that for the same value of  $\psi$ , erosion will occur under a lower value of  $\tau$ , in the presence of seepage:

$$\frac{\tau}{((\gamma_s - \gamma_w) - F_s) D_{50}} = \psi_s^* \quad (6.65)$$

where  $F_s$  = seepage force  $\perp$  bed per unit area

$$= c \gamma_w \frac{dh}{dy} \quad (\text{Martin and Aral (1971)}) \quad (6.66)$$

$c$  = constant between 0.35 and 0.4

$\frac{dh}{dy}$  = hydraulic gradient  $\perp$  bed

$\psi_s$  = value of  $\psi$  under seepage conditions

Olivier (1967) investigated the problem of safe over and throughflow for engineering application to rockfill embankment dams. Based on this background of riverbed erosion, he examined the problem first for cases of overflow, and he was able to experimentally confirm equation 6.59 for erosion of sloping faces of dams in these terms:

$$q_t = k' D_{50}^{3/2} \left( \frac{\gamma_s - \gamma_w}{\gamma_w} \right)^{5/3} S^{-7/6} \quad (6.67)$$

Threshold flow,  $q_t$ , he defined as that overflow during which the movement of one particle would cause the movement of many others; he further stated that collapse flow,  $q_c$ , at which point total erosional collapse would result, would be approximately 20% greater than threshold flow.

Olivier's area of concern was with flow for which values of  $\psi$  had become asymptotic to some value, approximately equal to 0.06 (see figure 6.29).

\* Oldenzien and Brink (1974) define equation 6.65 as:  $\psi_s = \frac{\tau}{(\gamma_s - \gamma_w) D_{50} - F_s}$ , but where  $F_s$  is the seepage force per unit area; equation 6.65, however, is relevant to the erodibility of a single particle, so that  $F_s$  must also be multiplied by  $D_{50}$ , as shown above.

Such flow he found to have little sensitivity to slope angle in determining his constant  $k'$ ; his values of  $k'$  reflected the more dominant qualities of particle shape, interlocking effects and packing. Although he applied his results to design in the case of combined through and overflow, he had not results that separately considered seepage effects. He relied upon results of experiments with combined flow to justify his statement that in throughflow conditions, equation 6.67 made an acceptable, although conservative estimate of threshold flow.

In the case of centrifugal modelling of erosion and sediment transport events in embankment dams, certain unnatural changes occur in these equations, and in the flow of water as first discussed in section 6.7.4. In the instance of a model with overflow  $q$ , flowing down the face of an embankment at depth  $d_{lg}$ , which is subjected to an increase in self-weight of  $N$  times, but with the same overflow  $q$ , the following changes occur.

$$\frac{dN_g}{d_{lg}} = N^{-0.3} \quad (6.51)$$

and

$$\gamma_{wN_g} = N \gamma_{wlg} \quad (6.68)$$

Therefore from equation 6.52

$$\tau_{N_g} = \gamma_{wlg} d_{lg} S N^{0.7} \quad (6.69)$$

and from equation 6.53,

$$\tau_{cN_g} = \psi(\gamma_{s1g} - \gamma_{wlg}) D_{50} N \quad (6.70)$$

In the case where seepage forces,  $F_s$ , are important, it is worth noting that these also increase  $N$  times, so that:

$$\tau_{cN_g} = \psi\{(\gamma_{s1g} - \gamma_{wlg}) - F_s\} D_{50} N \quad (6.71)$$

Erosion in response to overflow occurs when  $\tau_{N_g} = \tau_{cN_g}$ , and the critical depth of overflow measured at  $lg$ , which will cause erosion at  $Ng$ , will be:

$$d_{lg} = \psi \left( \frac{\gamma_s - \gamma_w}{\gamma_w} \right) \frac{D_{50}}{S} N^{0.3} \quad (6.72)$$

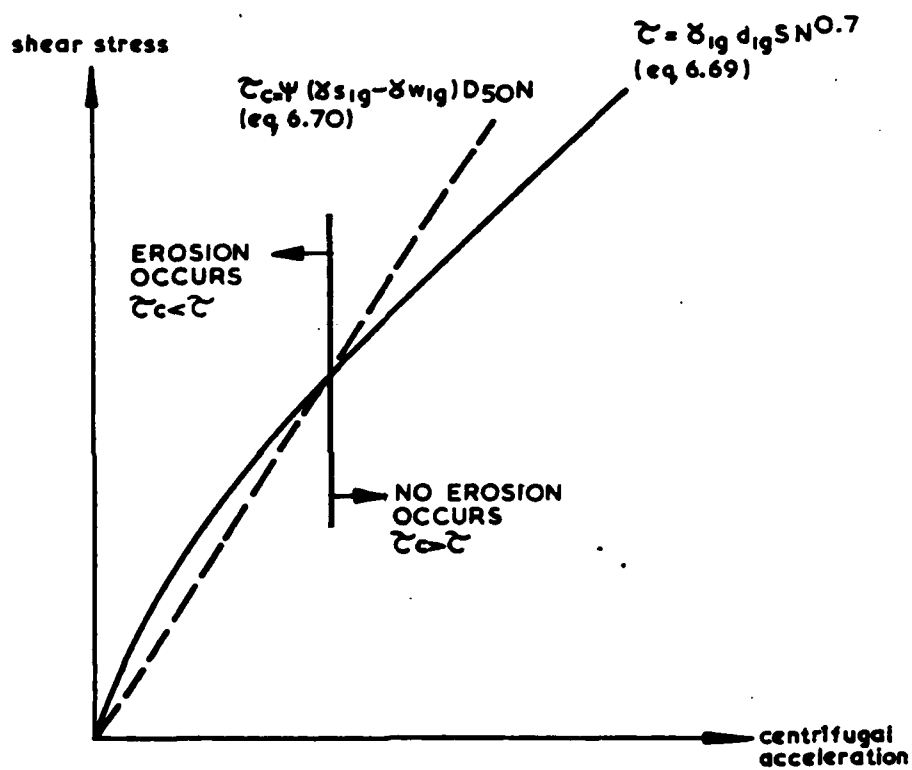


Figure 6.30 - Effect on Erosion Characteristics with Change in Centrifugal Loading and Constant q

Substituting equation 6.72 into equation 6.37, the effect on Olivier's threshold flow, equation 6.67, is simply found to be a factor  $(N^{0.3})^{5/3} = N^{1/2}$ , giving:

$$q_t = k' D_{50}^{3/2} \left( \frac{\gamma_s - \gamma_w}{\gamma_w} \right)^{5/3} S^{-7/6} N^{1/2} \quad (6.73)$$

An interesting aspect of erosion peculiar to centrifugal modelling is that where the two variable parameters in a model are the overflow,  $q$ , and the centrifugal loading,  $N$ , initiation of erosion may be achieved either by increasing the overflow at a given  $N$  value, or by reducing  $N$  at a constant  $q$ . Figure 6.30 illustrates the latter of these effects.

The ultimate value of reduced scale models is their capability to predict full scale events, and so it is important to determine the relationship between centrifuge model and prototype. If we take for example, a model which is geometrically similar to, but  $N$  times smaller in every dimension, than a given prototype, and subject that model to an increase in self weight of  $N$  times, and if that model is constructed of soil with permeability such that for throughflow:

$$v_p = v_m Ng \quad (6.20)$$

then:

$$q_m = \frac{q_p}{N} \quad (6.35)$$

If the same constant of proportionality is imposed on overflow, then the events in that model are related to that prototype in the following manner. At the initiation of erosion,  $\tau = \tau_c$ , for both model and prototype. Therefore:

$$\frac{\tau_m Ng}{\tau_{cm} Ng} = \frac{\tau_p}{\tau_{cp}} \quad (6.74)$$

and:

$$\frac{N \psi_m (\gamma_{s1g} - \gamma_{w1g}) D_{50m}}{N \gamma_{1g} d_{mNg} S} = \frac{\psi_p (\gamma_s - \gamma_w) D_{50p}}{\gamma_w d_p S} \quad (6.75)$$

so that:

$$\frac{D_{50m}}{D_{50p}} = \frac{d_{mNg}}{d_p} \frac{\psi_p}{\psi_m} \quad (6.76)$$

When  $q_m = \frac{q_p}{N}$ , according to equation 6.42:

$$\frac{d_{mNg}}{d_p} = \left( \frac{n_m}{n_p} \right)^{3/5} N^{-0.9}$$

and according to Chang's (1939) definition for  $n$ , (equation 6.58):

$$\frac{d_{mNg}}{d_p} = \left( \frac{D_{50m}}{D_{50p}} \right)^{0.1} N^{-0.9} \quad (6.77)$$

then

$$\frac{D_{50m}}{D_{50p}} = \left( \frac{D_{50m}}{D_{50p}} \right)^{0.1} N^{-0.9} \frac{\psi_p}{\psi_m} \quad (6.78)$$

$$= \left( \frac{\psi_p}{\psi_m} \right)^{10/9} N^{-1} \quad (6.79)$$

(6.80) ~~deleted~~

This relationship is likely to be in contradiction to that required for correct modelling of permeability which requires that  $\frac{D_{10m}}{D_{10p}} = N^{-1/2}$ , in order that  $k_p = k_m \times N$  (see section 6.3). For this reason, two conflicting notional prototype grain size distributions may be said to be modelled at once: one defined in terms of  $D_{10}$ , which governs permeability, and the other defined in terms of  $D_{50}$ , which governs the initiation of erosion.

Once erosion has begun, the Shields number,  $\psi$ , may be used to relate the time scales of model and prototype with respect to sediment transport, by using a non-dimensional sediment transport rate equation, such as Einstein's bedload equation:

$$\frac{q_s \rho^{1/2}}{(\gamma_s D_{50})^{3/2}} = f \left( \frac{1}{\psi} \right)^* \quad (\text{Graf (1971)}) \quad (6.81)$$

\*where  $q_s$  = bedload rate in  $m^3/\text{unit time/unit width}$ ,  $\rho$  = density of water.

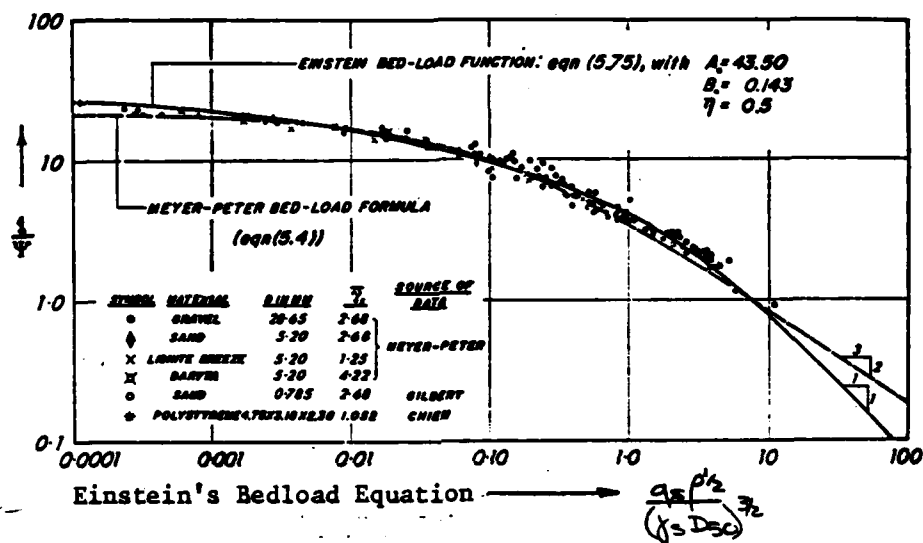


Figure 6.31 - Sediment Transport Relation ( Yalin, 1972 )

If the Shields numbers of the model and the prototype are equal, according to the conditions above, then:

$$\frac{q_{s_m}}{q_{s_p}} = \left( \frac{\psi_p}{\psi_m} \right)^{3/2} = 1 \quad (6.82)$$

In the event that the Shield numbers are not equal, a curve such as that shown in figure 6.31, may be used to relate them.

## 6.8 Discussion

Model tests in this series were undertaken to investigate slope instability in one type of coal mine waste embankment dam. In the process of the research, three classes of failure were investigated and observed in response to different simulated prototype situations. These included rate of construction failure, deep seated mass instability in response to throughflow conditions, and failure by erosion and downstream sediment transport. Although the primary parameters of interest which became evident were particle size distribution and throughflow characteristics, other factors such as the effects of compaction, uplift, a clay underlayer and the inclusion of permeable sections in the embankment, were also studied. The tests provided insight, not only into prototype behaviour, and regular stability analysis, but also into certain new aspects of centrifugal modelling. These will be discussed in the following sections.

### 6.8.1 Individual tests and prototype relevance

The reduced scale centrifuge models tested in this series investigated a variety of instability problems: this section will discuss the implications of the various tests and their relevance to full scale situations.

The basic embankment dam configuration modelled in these tests was the downstream construction type (see section 5.2). This is characterised by a main coarse discard embankment, of which the lower part of the

upstream face is overlain by a blanket of low permeability tailings, and the upper part of the upstream face may be in contact with a lagoon of impounded water. The standard model geometry represented a plane strain embankment section built in a loose, wet tipped fashion, with a downstream slope of between IV : 1H ( $45^{\circ}$ ) and IV : 2H ( $26.5^{\circ}$ ) and a flat crest of varying width. The model upstream geometry usually included some reservoir arrangement which simulated one of two conditions: either a diagonal reservoir not extending to the full depth of the embankment, which approximated the presence of an upstream blanket of tailings, equal in height to the bottom of the diagonal reservoir, or a full height reservoir, which, by permitting the application of water to the full embankment height, may be thought to simulate the case where the crest was sufficiently wide that any effects of the upstream configuration were eliminated. In all but two models, the embankment foundation was presumed impermeable, and the angle of friction between the embankment and foundation, was  $26.5^{\circ}$ .

Within this one standard configuration, three classes of embankment dam instability were studied. These included rate of construction failure in models MW1 through MW6, MW8, and MW24, deep seated mass slope instability in the presence of throughflow, in models MW9 through MW13, and failure by excessive erosion and downstream sediment transport in models MW7, MW20 through MW23 and MW25. The models will be discussed in these groups.

It was expected, as discussed in section 6.1, that investigation of rate of construction failure, would dominate the test series. In all, eight tests were performed which were related to rate of construction, with varying parameters, the most dominant of which were particle size distribution, initial moisture content and volume of throughflow.

Three  $45^{\circ}$  embankment models, MW1, MW2 and MW3 were built of material



A, a relatively free draining\* material, taken from the whole coarse coal mine discard, and subjected to rapid rate of construction. Models MW1 and MW2, prepared in two different fashions, but responding almost identically, with 6% vertical compaction, and forward shear, stabilising at  $39^\circ$ , indicated that in such permeable material, the method of waste disposal, by loose tipping or compaction, was not important to slope stability. In the presence of constant throughflow in the case of MW3, the change in profile in response to rapid rate of construction was more marked, but still not disastrous. Rate of construction at the fastest equivalent prototype rate of 32 m in 12 hours (as in MW3) in a coarse material of similar mechanical properties, but where permeability is controlled by a  $D_{10}$  size of  $0.5 \text{ mm}^\dagger$ , was found not to be critical.

The next four models, in which rate of construction was studied, were built of a less permeable material, B,  $k_m \approx 0.02 \text{ mm/s}$ . Models MW4, MW5, MW6 and MW8 were constructed at three different slope angles, and subjected to simulated rapid rate of construction conditions in the presence of throughflow. The dominant factor in failure was the rate at which the largely uncontrolled volume of capillary water was expelled from the soil in the period of increase of centrifugal loading. With the quickly changing centrifugal loading it was not possible to relate the observed model erosion events to prototype events. Further testing of rate of construction failure was therefore abandoned, except for one model, MW24, later in the series.

\*By comparing the  $D_{10}$  size of material A, to the  $D_{10}$  size of material B for which the permeability is known to be  $0.02 \text{ mm/s}$ , it can be extrapolated that the permeability of material A, is  $k \approx 0.08 \text{ mm/s}$ . In a model of scale  $1/N$ , made of this soil, the equivalent prototype permeability would be  $N \times 0.08 \text{ mm/s}$ .

$^\dagger D_{10}$  of material A =  $0.06 \text{ mm}$   
 Maximum g for model MW3 =  $135g$   
 Average g =  $135/2 = 67.5$   
 $k_p \propto N \propto D_{10}^2$  (see equation 6.5)  
 Equivalent prototype  $D_{10} = \sqrt{67.5} \times 0.06 = 0.5 \text{ mm}$ .

Model MW24 was built in the midst of a series of tests concerned with the effects of particle size distribution. The soil had an unexpectedly high percentage of silt and clay particles, 33%, and was measured to have a correspondingly low permeability of  $4.2 \times 10^{-7}$  mm/s. It failed in response to a too rapid rate of construction, equivalent in the prototype to building an embankment <sup>of the same permeability</sup> 1.7 m high over a thirty minute period, and then leaving it to consolidate for 18 hours, before attempting to increase the height to 2.8 m, over an hour, at which point it immediately failed. Further simulated increases in height aggravated failure, and finally retrogressive slipping occurred. It is not surprising that failure occurred in response to excess pore pressures in a material with such low permeability. Certain handling processes such as transport of coarse waste on a long conveyor belt, with continuous vibration and damage to the large but weak fragments of waste, can result in much finer particle size distribution in the waste after transport. This model test MW24, serves as an example of the way such breakdown of waste may lead to rate of construction failure.

The next set of models, MW9 through MW13, investigated the destabilising effects of throughflow and a high phreatic surface, on embankments in which  $c' = 0$ , and  $\phi' = 34.7^\circ$ , described the triaxial soil strength properties (see section 6.8.2). The soil (material B) of bulk unit weight  $16.4 \text{ kN/m}^3$ , was modelled to have an equivalent prototype permeability of approximately 2 mm/s. Two embankments were built with slope angle IV : 1.5H ( $33.7^\circ$ ) three were built with inclination IV : 2H ( $26.5^\circ$ ), and two realistic modifications were made to the embankment configuration.

Models MW9 and MW10 were both built at inclination  $33.7^\circ$ , although they simulated embankments of different heights. Retrogressive failure occurred in both embankments in an almost identical pattern of events.

\* these times are based upon an N value of 12g, i.e. the mean of 9g and 15g (see table 6.2), an acceleration rise time of 30 seconds, and  $N^2$  scaling for time.

The reservoir level at failure in MW10 was 82% of full embankment height, at a throughflow of  $147 \text{ mm}^3/\text{mm-s}$ , and although useful comment cannot be made on the relative critical throughflows and phreatic lines, as that of model MW9 was not closely monitored, the striking similarity of failure pattern suggested that the shape of failure was related to the slope angle.

Models MW11 through MW13, investigated the effects on stability of variations in embankment geometry, as might be imposed in prototype embankments. Model MW11, built with a slope angle of  $26.5^\circ$  and a diagonal rear reservoir, failed in a retrogressive manner. The reservoir height at failure was 80% of the full embankment height, and the throughflow volume,  $147 \text{ mm}^3/\text{mm-s}$ , was the prototype equivalent of  $1.1 \text{ m}^3/\text{min}$  through an embankment  $31\text{m}$  high; the  $r_u$  value in the toe region, where failure began, was 0.4. Its pattern of retrogressive failure was not unlike that observed in model MW10, but the individual slips were in general smaller and more numerous. This further suggested the influence of slope angle on the characteristics of failure.

Model MW12 was built in the same geometry as model MW11, but with the inclusion of a central, undrained, highly permeable key\* similar to one which may be included in a prototype embankment. This embankment failed in a retrogressive manner, but with smaller, less uniformly shaped slices than in model MW11. The throughflow at failure was much lower,  $53 \text{ mm}^3/\text{mm-s}$  ( $\approx 0.4 \text{ m}^3/\text{min}$  in a prototype 120 times larger), the reservoir was at 63% of full embankment height, but the local  $r_u$  value in the toe was higher than in MW11, at 0.5. It was evident that the inclusion of the highly permeable, undrained key had altered the seepage pattern sufficiently that instability was induced at a much lower level of throughflow. Hodge and Freeze (1977) confirm theoretically, the correctness of this observation.

---

\*  $D_{10}$  of material B =  $0.03 \text{ mm}$ ,  $D_{10}$  of key material  $\approx 3.5 \text{ mm}$ ,  $\frac{D_{10}}{D_{10B}} = 117$   
 $k = D_{10}^2 \cdot \frac{k_{\text{key}}}{k_B} = 13611.$

Model MW13, the last in this group, was made in the geometry of model MW11, but with the inclusion of both a highly permeable, undrained key, and an equally permeable toe drain. This model was used to demonstrate three effects. The embankment withstood a maximum throughflow of  $159 \text{ mm}^3/\text{mm-s}$  ( $\approx 1.1 \text{ m}^2/\text{min}$  in a prototype 120 times larger) from an almost full reservoir, without sign of instability. This demonstrated that the beneficial effects of the toe drain were sufficient to offset the deleterious effects of the undrained key, and in general increased overall embankment stability. Introduction of a kaolin slurry, such as might simulate an upstream beach of tailings extending to the full embankment height, almost completely sealed the embankment to throughflow, although the migration of fine material some 15 mm into the coarse discard embankment was noticed. The final introduction of uplift pressure ( $r_u = 0.77$ ) from the key, as if the embankment had been built over a natural, intermittent spring, was sufficient to cause failure. This failure, however, was characterised by erosion down the embankment face, rather than by deep seated soil movement.

This set of five model embankments investigated a problem of prototype slope instability, caused by high phreatic surfaces under conditions of throughflow. Throughflow, it was observed, may be tolerated in an embankment dam, provided the phreatic line has less than a certain critical slope, especially in the region of the toe. Inclusion of an undrained, highly permeable key, however, may cause distortion of the flownet in such a way that at a smaller volume of throughflow, instability may occur. Conversely, inclusion of a highly permeable toe drain significantly improves stability, even in the presence of a key. In addition, for any proposed embankment geometry, attention must be paid to the foundation conditions, not only with regard to competency and relative permeability, but also to the existence of intermittent springs, which may be responsible for uplift

pressures and subsequent failure.

Failure in models MW20 through MW23, MW25, MW7 and MW13 was constituted by erosion damage and excessive downstream sediment transport; there was a notable absence of deep seated failure. Within these seven model embankments, all built at  $26.5^\circ$  to the horizontal, four different particle size distributions of the same soil, were used, and three different methods of model preparation. Failure by erosion was initiated either by an increase in throughflow, at a constant centrifugal loading, or by a reduction in centrifugal loading at a constant throughflow, this latter technique being an interesting feature peculiar to centrifugal modelling. In each case, erosion was initiated at the toe, where the full accumulation of throughflow was available. Further attention is devoted to erosion characteristics in section 6.8.3, but an overview will be discussed here.

Models MW7, MW23, and MW25 were similar <sup>in</sup> two respects: the method of model preparation in each simulated loose tipped construction, and the way in which erosion was initiated was by reducing centrifugal loading, while maintaining a constant throughflow. It appeared, based upon these tests, that loose tipping tended to give rise to a fairly even distribution of the throughflow across the model width, permitting in general, the highest stable throughflow, by avoiding flow concentrations.

Model MW22 also fell into this category, but is worthy of special note for two reasons. The restricted water supply available during this test, when compared to the combination of the soil permeability, and high centrifugal loading gave rise to the stable freefall condition, as defined by Parkin et al (1966), a condition not easily realisable in normal reduced scale modelling. Model MW22 was also different in that the embankment was founded upon a layer of preconsolidated kaolin, rather than on the painted steel surface of the centrifuge strongbox as in other models. Its similarity of response, in particular to model MW25, suggested that in erosion failures, the foundation-embankment interface was not significant, provided

that the foundation layer was less permeable than the coarse discard.

Models MW20, MW21 and MW13 were constructed using different methods, and different particle size distributions of the same soil, however erosion was initiated in each case at constant full scale stress level, in response to an increased through<sup>flow</sup>/ or overflow. Model MW20 represented an embankment of low permeability material,  $1.2 \times 10^{-6}$  mm/s, successfully raised without rate of construction failure, to the prototype equivalent height of 23.4 m. The embankment was incapable, however, of passing significant throughflow, and a high reservoir level quickly overtopped the embankment, eroding a gully which eventually caused breaching. In cases of overtopping, gullying and consequent flow concentrations may be more of a risk than in uniform throughflow conditions.

Model MW21 was constructed to represent the same prototype dimensions as model MW20, but was composed of five vertically compacted layers of more permeable soil. The compaction process caused segregation of the particle sizes, so that a concentration of the finest portion was observed to be deposited on the top of each layer, as predicted by Leps (1973) for deposition in lifts. This led to some anisotropy in the permeability and in the consequent throughflow pattern, but Hodge and Freeze (1977) noted that horizontal anisotropic permeability can be beneficial to slope stability. Olivier (1967) noted that as the density of particle packing increases, so also does the stable overflow. The results of this test however, seemed to contradict Olivier's finding and erosion occurred before it was predicted, in the form of a narrow gully. Compaction may sometimes lead to particle segregation and consequent flow concentrations which undo the beneficial effects of closer particle packing.

In model MW13, no erosion was observed under normal throughflow conditions due to the presence of a coarse toe drain, and even under uplift conditions, which caused a large volume of water to drain down the face of

the embankment, the toe stayed intact and offered the slope stability, while the finer embankment material suffered severe erosion damage.

These three tests emphasised the importance of protecting against the initiation of erosion and the role that particle segregation may have in contributing to flow concentration. The extreme consequences of overtopping, which led to the worst erosion effects were also demonstrated, while the beneficial effects of toe drains, and of coarse erosion resistant surfacing were emphasised.

The models of this test series were successful in modelling three classes of prototype failure. The two dominant failure modes, deep seated failure and failure by erosion and sediment transport, will be discussed further in the following sections, and the most important single soil parameter (particle size distribution) will be given special attention in section 6.8.4.

#### 6.8.2 Regular slope stability analysis

It is usual in assessing slope stability, to base a theoretical prediction, which considers the most adverse slope configuration and the worst likely ground water conditions, upon numerical representation of laboratory or in situ tested soil parameters and behaviour characteristics. Reduced scale models may also be the subject of regular slope stability analysis, and although fewer assumptions are necessary about the stress and boundary conditions in the stability analysis than in a full scale slope, certain soil strength properties remain to be quantified in regular laboratory tests.

In ten of the nineteen coal mine waste models, a relatively stable phreatic line was visible from the video record of the tests, and in four of these same models, deep seated failure was observed to occur. This presented a good opportunity to investigate the value of simple

numerical analysis in predicting the observed failures. This section will be concerned with the comparison of regular slope stability analysis against observed model slope instability. The numerical analysis will use Bishop's (1955) effective stress, limit equilibrium method of slices, simplified by the Bishop and Morgenstern (1960) stability coefficients, which were later augmented by O'Connor and Mitchell (1977).

Under the conditions of the research contract, all laboratory soil strength properties were to be measured by the U.S. Waterways Experiment Station (W.E.S.). From drained, unsaturated triaxial tests, they defined the properties of the coarse discard coal waste which was less than 76 mm, as:

$$\gamma_{\text{dry}} = 15.4 \text{ kN/m}^3$$

$$c' = 11 \text{ kN/m}^2$$

$$\phi' = 30.5^\circ*$$

Later similar tests, also by W.E.S., on the actual model soil materials, gave the following strength parameters:

material B	$c' = 0$	$\phi' = 34.7^\circ$
MW22, MW23	$c' = 23 \text{ kN/m}^2$	$\phi' = 30.5^\circ$
MW24	$c' = 24 \text{ kN/m}^2$	$\phi' = 26.9^\circ$
	$c_u = 28 \text{ kN/m}^2$	$\phi_u = 15.1^\circ$
MW25	$c' = 18 \text{ kN/m}^2$	$\phi' = 30^\circ+$

all with dry unit weight of approximately  $13.7 \text{ kN/m}^3$ .

As the largest particles were removed from the coarse discard received, in preparation for modelling at Cambridge, two subtle changes in the soil properties were noticed. The unit weight was reduced, indicating a slight change in the mineral content which left behind a higher proportion of the light weight component of the waste: coal and carbonaceous shale. As the proportion of silt and clay increased, the cohesion component

\*M. Al-Hussaini, F.C. Townsend, 1977, W.E.S., U.S.A., personal communication.

†F.C. Townsend, 1978, W.E.S., U.S.A., personal communication.

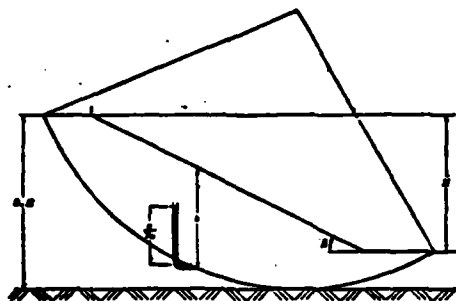


Table 6.4

Slope Stability Analysis

Safety factor =  $m - n r_u$ ;  $m, n$  from Bishop and Morgenstern (1960) and O'Connor and Mitchell (1977)

Soil Parameters:



$$\gamma_b = 16.4 \text{ kN/m}^2$$

$$*r_u = \frac{u}{\gamma_w} \frac{1}{HY_b}$$

(taken from video pictures)

$$D = 1$$

(Bishop and Morgenstern (1960))

Table 6.4(a)

Test No	$c'$ ( $\frac{\text{kN}}{\text{m}^2}$ )	$\phi'$ (degrees)	$\cot\phi$	H (mm)	N	$\frac{c'}{\gamma H N}$	$r_u^*$	m	n	SF
MW 9	0	39	1.5	240	100	0	0.40	1.25	1.80	0.53
MW10	0	39	1.5	260	120	0	0.30	1.25	1.80	0.71
MW11	0	39	2.0	260	120	0	0.40	1.65	2.05	0.83
MW12	0	39	2.0	260	120	0	0.50	1.65	2.05	0.63
MW13	0	39	2.0	260	120	0	0.28	1.65	2.05	1.08

Table 6.4(b)

Test No	$c'$ ( $\frac{\text{kN}}{\text{m}^2}$ )	$\phi'$ (degrees)	$\cot\phi$	H (mm)	N	$\frac{c'}{\gamma H N}$	$r_u^*$	m	n	SF
MW20	23.5	33	2	195	120	0.061	0	2.23	1.85	2.23
MW21	23.0	35	2	195	120	0.060	0.50	2.30	2.00	1.30
MW22	23.0	35	2	195	120	0.060	0.02	2.30	2.00	2.26
MW23	23.0	35	2	195	100	0.072	0.35	2.45	2.05	1.76
MW25	18.0	35	2	195	100	0.056	0.19	2.30	2.00	1.92

tended also to increase, and the angle of friction decreased. Holubec (1976) commented on this trend of decreasing angle of friction with an increasing proportion of fines.

Models MW9 through MW13 were all made of material B, and in four of those five models, deep seated failure was observed to occur in response to throughflow conditions. In normal situations of slope stability, three dimensional effects are at work, although two dimensional analysis is usually considered satisfactory, erring slightly on the conservative side; soil strength data from the triaxial test is considered directly applicable. In the centrifuge model tests of this research however, plane strain conditions were a more correct approximation in the slope failures observed, and a correction should therefore be made to the triaxial data listed above, to account for this. Such a modification may be achieved using two equations from Schofield and Wroth (1968):

$$M = \frac{q}{p} = \frac{6 \sin \rho}{3 - \sin \rho} \quad \text{where } \rho = \phi' \text{ (triaxial)}$$

(C.S.S.M. equation 8.13)

$$\frac{M}{\sqrt{3}} = \tan \phi' \quad \text{where } \phi' = \phi' \text{ (plane strain)}$$

(C.S.S.M. equation C.12)

In the case of material B, measured by W.E.S. to have  $c' = 0$ ,  $\phi' = 34.7^\circ$  (triaxial),

$$M = \frac{q}{p} = \frac{6 \sin (34.7^\circ)}{3 - \sin (34.7^\circ)}$$

$$= 1.41,$$

$$\frac{M}{\sqrt{3}} = \tan \phi' = 0.811,$$

from which  $\phi' = 39^\circ$  in plane strain.

In table 6.4(a) the predictions based upon the soil strength properties  $c' = 0$  and  $\phi' = 39^\circ$  are given for models MW9 through MW13. Failure was predicted, as observed, in models MW9 through MW12, and stability was correctly predicted in model MW13. The analysis may be criticised as

overly conservative but the following comments may be made on embankment behaviour, nonetheless. The undrained, highly permeable key section in model MW12 caused distortion to the pattern of throughflow which resulted in a higher phreatic line in the critical region of the toe than would be expected for this throughflow rate, when compared to MW11; Hodge and Freeze (1977) predicted that undrained, highly permeable sections reduce slope stability, as was observed. The inclusion of a toe drain, however, was sufficient to eliminate the deleterious effects on slope stability of the undrained key, and permitted a high reservoir level and accompanying high phreatic surface, to exist without slope instability by reducing the free water level in the critical toe region to a safe level of  $r_u$ .

In models MW20 through MW23, and MW25, the phreatic line also was visible but deep seated failure was not observed. For three of these models, the soil parameters were measured by W.E.S., and for the remaining two, engineering judgement may be exercised in selecting appropriate values. Looking at the particle size distributions, the soil strength parameters for model MW21, not directly tested by W.E.S., may be assumed to be similar to those obtained for MW22; for model MW20, an average of the parameters for MW24 and MW22 may be used. Again applying the same process to transform  $\phi'$  triaxial to  $\phi'$  plane strain, the following parameters are useful in regular stability analysis:

MW20	$c' = 23.5 \text{ kN/m}^2$	$\phi' = 33^\circ$
MW21	$c' = 23 \text{ kN/m}^2$	$\phi' = 35^\circ$
MW22	$c' = 23 \text{ kN/m}^2$	$\phi' = 35^\circ$
MW23	$c' = 23 \text{ kN/m}^2$	$\phi' = 35^\circ$
MW25	$c' = 18 \text{ kN/m}^2$	$\phi' = 35^\circ$

In table 6.4(b) the stability calculations are shown for these slopes. In the absence of failure, little comment can be made on the value of the analysis with these parameters, except that where stability was predicted

in these back calculations, it was consistently observed, before the numerical analysis. The effect on slope stability of the kaolin underlayer in models MW21 and MW22 was not tested, neither was the effect of compaction in layers, in MW21, although Hodge and Freeze (1977) commented in this respect, that horizontal anisotropic permeability will improve slope stability, in cases of seepage.

Regular slope stability analysis of these models is fully consistent with the observed soil behaviour, although it may be suspected that an overly conservative estimate was made in the case of the four models in which deep seated failure did occur, but by confirming each other, the two methods of stability analysis have supported each other's predictions.

#### 6.8.3 Surface erosion and sediment transport

The effects of water throughflow and overflow in these tests of model coal mine waste embankments, consistently dominated model behaviour in every case but model MW24. The rushing of water either out of soil pores, or through the model from an external source, visibly affected model profile characteristics, even when secondary in importance to the primary failure mechanisms.

In models MW1 through MW8, with the exception of MW7, changes in model profile were caused by a combination of expelled capillary water, and externally supplied throughflow, rushing through the model during simulated rate of construction conditions. The results of this action are difficult to assess or predict: the quantity of water from these two sources was responsible for erosion but was unmeasured and changing. The worst condition for erosion in a centrifuge model, large throughflow and low centrifugal loading, dominated model behaviour, but was unknown. Therefore, in cases where erosion dominated model behaviour, simulated rate of construction conditions did not provide useful information on prototype response.

In eleven of these models, however, erosion played an important role in embankment behaviour, and occurred under known conditions of throughflow, and gradually changing centrifugal loading. Previous experimentalists' work done with application to riverbed flow considered conditions of constant overflow, and also gave some attention to combined throughflow and overflow (see section 6.7.5), and while this work may be directly applied in cases of overtopping, additional examination is appropriate for application to throughflow in embankment dams.

In throughflow conditions, where the water springs from the embankment face, there are two extremes of erosion conditions. At the highest point on the embankment where water begins to spring from the face and drain away, the overflow is very small, and seepage forces perpendicular to the face, which will here be called uplift forces, have negligible effect. At the toe, conversely, the worst conditions prevail: the direction of flow out of the embankment is nearly parallel to the foundation, applying maximum uplift seepage force on the surface particles <sup>in this case.</sup> In addition to this maximum uplift all throughflow above the toe which has drained down the embankment face, has accumulated at the toe level. Under these conditions, equation 6.65 applies:

$$\frac{\tau}{((\gamma_s - \gamma_w) - F_s) D_{50}} = \psi_s \quad (6.65)$$

According to equation 6.66:

$$F_s = c \gamma_w \frac{dh}{dy} \quad (6.66)$$

Under throughflow conditions, the seepage component perpendicular to the slope  $\frac{dh}{dy}$ , is calculated as:

$$\frac{dh}{dy} = \sin \beta \frac{dh}{dy_H} \quad (6.83)$$

where,  $\frac{dh}{dy}$  = component of hydraulic gradient perpendicular to the bed

$\beta$  = angle between the bed and the direction of water flow

Table 6.5

## Effect of Seepage Force on Bearing Pressure

$$F_{slg} = c \gamma_w \frac{dh}{dy} = c \gamma_w \sin \beta i_{lg} \quad (\text{from equations 6.66 and 6.85})$$

$$\text{where } i_{lg} = \frac{q}{h_{Ng} k N}, \quad c = 0.35, \quad \gamma_w = 2.36 \times 9.81 \text{ kN/m}^3$$

Test No	cot $\beta$	$\frac{q}{h_{Ng}^2}$ ( $\frac{\text{mm}^2}{\text{s}}$ )	$h_{Ng}$ (mm)	$k$ ( $\frac{\text{mm}}{\text{s}}$ )	N	$D_{50}$ (mm)	$i_{lg}$	$F_{slg} \times D_{50}$ (kN/m <sup>2</sup> )	$(\gamma_s - \gamma_w) i_{lg} D_{50}$ (kN/m <sup>2</sup> )	$\Delta^*$ (kN/m <sup>2</sup> )
MW 9	1.5	147	8	0.03	100	0.5	6.13	$5.83 \times 10^{-3}$	$6.67 \times 10^{-3}$	$0.84 \times 10^{-3}$
MW10	1.5	147	43	0.03	120	0.5	0.95	$9.04 \times 10^{-4}$	$6.67 \times 10^{-3}$	$5.77 \times 10^{-3}$
MW11	2	147	18	0.03	120	0.5	2.27	$1.74 \times 10^{-3}$	$6.67 \times 10^{-3}$	$4.93 \times 10^{-3}$
MW12	2	53	33	0.03	120	0.5	0.45	$3.42 \times 10^{-4}$	$6.67 \times 10^{-3}$	$6.33 \times 10^{-3}$
MW21	2	75	113	0.007	120	0.43	0.79	$5.21 \times 10^{-4}$	$5.74 \times 10^{-3}$	$5.22 \times 10^{-3}$
MW22	2	109	6	0.03	40	0.40	15.14	$9.28 \times 10^{-3}$	$5.34 \times 10^{-3}$	< 0
MW23	2	112	7	0.07	75	0.40	3.05	$1.87 \times 10^{-3}$	$5.34 \times 10^{-3}$	$3.47 \times 10^{-3}$
MW25	2	121	9	0.08	30	0.40	5.60	$3.43 \times 10^{-3}$	$5.34 \times 10^{-3}$	$1.91 \times 10^{-3}$

$$^* \text{Bearing pressure} = \Delta = [(\gamma_s - \gamma_w) - F_{slg}] D_{50} \text{ at } i_{lg}$$

$$\begin{aligned} \frac{dh}{dy_H} &= \text{true hydraulic gradient} \\ &= i \end{aligned}$$

Since

$$v = k i \quad (6.11)$$

$$= \frac{q}{h}$$

where  $h$  = exit height

then:

$$i_{lg} = \frac{q}{h_{Ng} k N} \quad (6.84)$$

and for cases of horizontal outflow at the toe:

$$F_s = c N(\gamma_w) \sin \beta \frac{q}{h_{Ng} k N} \quad (6.85)$$

The denominator of equation 6.65 represents the effective bearing pressure below a single layer of particles, each of diameter  $D_{50}$ . In many of the models, the uplift force,  $F_s$ , represents a significant reduction, as shown in table 6.5. Under these conditions, the susceptibility to erosion in the toe increases markedly.

Taking model MW23 as an example, and determining the critical through-flow at 75g, when erosion was actually noticed, using the curve in figure 6.29 as a guide for  $\psi_s$ , we get:

$$\frac{\gamma_w S}{((\gamma_s - \gamma_w) - F_s) D_{50}} d_{Ng} = \psi_s \quad \text{from (6.65)}$$

From Manning's equation:

$$d_{Ng} = \left( q \frac{D_{50}^{1/6} 5.25 \times 10^{-2}}{S^{1/2} N^{1/2}} \right)^{0.6} \quad \text{from (6.39)}$$

From table 6.5, at 75g:

$$((\gamma_s - \gamma_w) - F_s) D_{50} = 0.26$$

From equation 6.60:

$$Re_* = \frac{(g d S)^{1/2} D_{50}}{v}$$

It is observed that when  $\psi = 0.035$ , and  $Re_* = 31$ , which corresponds to a point on the curve in figure 6.29, the value for  $d_{Ng}$  is  $2.7 \times 10^{-5}$  m and

for  $q = 9.7 \text{ mm}^2/\text{s}$ . At 75g, higher flows than this were observed to exist in model MW23 without unacceptable erosion damage, and it is appropriate to reconsider the actual sequence of erosion events which will occur in embankment dam throughflow in engineering terms of failure.

Erosion may be initiated at the toe, as predicted by the above calculations, in the presence of the combined effects of full overflow and the worst seepage conditions. This erosion may cause a local change in profile, with a shallow debris beach at the toe, and behind that a steep, small scarp which will be left connecting the beach to the remaining embankment which remains at its original slope angle, provided the water continues to exit only through the beach and not through the steep scarp, and if cohesion or negative pore pressures in the soil are adequate to maintain this small, steep scarp, then a stable condition may be achieved, which will not constitute engineering failure and which may not be observed in the centrifuge model, although erosion will have been initiated.

If the exit level,  $h$ , of the phreatic line rises so that it exits in the scarp, due to either an increase in throughflow, or a reduction in centrifugal loading, then retrogressive erosion will occur. The combined uplift seepage forces and slightly reduced overflow will act on the steep scarp face, and the local profile will change continually as back sapping occurs. While the angle of the final shallow beach of debris may be predicted assuming regular overflow conditions, as throughflow will be almost parallel to the beach surface so that uplift forces are negligible, an engineering assessment of the initiation of erosion failure may be less simple.

This is exemplified in particular in models MW22 and MW25: in both cases the bearing pressure was reduced to a very low level, according to the values in table 6.5, but the exit level of the phreatic line was also very low, so that the erosion effects were safely confined to a small



portion of the model. Only when the exit level of the phreatic line rose in response to a reduction in centrifugal loading, was erosion observed, retrogressing into the slope.

This evidence suggests that a more realistic estimate of erosion, which is significant to embankment dam engineering may require an approximation of a new value for  $\psi$ , for different flow conditions in the slope. Half way between the point of minimum erosion, at the point of height  $h$ , and the point of maximum erosion at the toe, the seepage effects and the overflow volume may both be assumed to be half that at the toe.

Using model MW23 for calibration, a model in which erosion was observed in its earliest stages, the new calibration of  $\psi$  would be as follows:

$$\frac{\gamma_w d_s}{((\gamma_s - \gamma_w) - \frac{F_s}{2}) D_{50}} = \frac{d_{Ng} \times \sin 26.5}{(1.36) 0.4 \times 10^{-3} - 9.52 \times 10^{-5}}$$

$$\psi = 0.076$$

and

$$k' = 0.26$$

when

$$d_{Ng} = 7.65 \times 10^{-5} \text{ m}$$

Alternatively, using Olivier's simple method, where seepage forces are ignored, and all throughflow is assumed to be overflow, to calibrate  $\psi$ , and assuming that erosion was noticed only when the collapse throughflow was achieved, then for MW23:

$$d_{Ng} = 1.04 \times 10^{-4} \text{ m}$$

$$\psi = \frac{\gamma_w d_s}{(\gamma_s - \gamma_w) D_{50}} = 0.0853$$

$$k' = 0.315.$$

Note that Olivier achieved typical values for  $k'$  in cases of overflow, between 0.23 and 0.19, indicating that estimates of critical throughflow using equation 6.67 and calibration for overflow may be conservative by as much as 40%.

Table 6.6

## Data of Erosion and Sediment Transport

1 Test No	2 $D_{50}$ (mm)	3 $\cot \theta_0$	4 $q_{app}$ ( $\frac{m^3}{mm-s}$ )	5 $N_{t,pred}$ (g)	6 $N_{c,pred}$ (g)	7 $N_{c,obs}$ (g)	8 $q_{t,pred}$ at $N_{c,obs}$ ( $\frac{mm^3}{mm-s}$ )	9 $q_{c,pred}$ at $N_{c,obs}$ ( $\frac{mm^3}{mm-s}$ )	10 $q_{f,app}$ ( $\frac{mm^3}{mm-s}$ )	11 $N_f$ (g)	12 $i_{instable}$ (degrees)	13 $i_{meas}$ (degrees)	14 $q_{app, proto}$ ( $\frac{m^2}{min}$ ) at $N_{c,obs}$	15 $D_{50, proto}$ (mm) at $N_{c,obs}$
M20	0.35	2	127	207	144	120	97	116	127	120	21	3	0.9	42
M21	0.43	2	75	39	27	120	132	158	75	120	46	18	0.5	52
M22	0.40	2	109	102	71	30	59	71	109	20	13	15	0.2	12
M23	0.40	2	112	108	75	75	93	112	329	66	8	19	0.5	30
M25	0.40	2	121	126	86	30	59	71	121	20	12	13	0.2	12
M7	0.5	2	37	6	4	1	15	18	37	1	12	-	0.002	0.5
M9	0.5	1.5	147	158	110	100	117	140	147	1	4	5	0.9	50
M10	0.5	1.5	147	158	110	120	128	154	147	1	4	-	1.1	60
M11	0.5	2	147	95	66	120	165	198	147	1	4	8	1.1	60
M12	0.5	2	53	12	9	120	165	198	177	1	3	-	0.4	60
M13	0.5	2	159	111	77	120	165	198	900	120	6	8	1.1	60
5.5*		2	159	<1	<1	120	6024	7229	900	120	>90	45	1.1	660

$$\tau_{Toe \text{ drain}} \quad k' = 0.315 \quad N_t = \left[ \frac{q_c}{0.315} (D_{50})^{-3/2} (1.36)^{-1/3} (\sin \theta)^{7/6} \right]^2 \quad q = 0.315 D_{50}^{3/2} (1.36)^{5/3} (\sin \theta)^{-7/6} N_t^{1/2}$$

$$\tau_{y_0} = 2.36 \times \tau_w$$

$$\frac{\tau_y - \tau_w}{\tau_w} = 1.36$$

$$i_{instable} = \arcsin \left( \frac{0.315 D_{50}^{3/2} (1.36)^{5/3} N_t^{1/2}}{q} \right)$$

## Explanation of column headings

- |                    |  |                      |  |
|--------------------|--|----------------------|--|
| 1. Test No         | Test number  | 9. $q_{c,pred}$      | Throughflow predicted for collapse conditions at $N_{c,obs}$ |
| 2. $D_{50}$        | Median grain size of model soil  | 10. $q_{f,app}$      | Final throughflow applied                                    |
| 3. $\cot \theta_0$ | Cotan of initial model slope angle   | 11. $N_f$            | Final centrifugal loading at $q_{f,app}$                     |
| 4. $q_{app}$       | Throughflow applied  | 12. $i_{instable}$   | Predicted stable angle at $q_{c,pred}$ and $N_f$             |
| 5. $N_{t,pred}$    | Centrifugal loading predicted for threshold characteristics with $q_{app}$ | 13. $i_{meas}$       | Measured final angle   |
| 6. $N_{c,pred}$    | Centrifugal loading predicted for collapse characteristics with $q_{app}$  | 14. $q_{app, proto}$ | Equivalent throughflow in prototype of scale $N_{c,obs}$     |
| 7. $N_{c,obs}$     | Centrifugal loading when erosion observed with $q_{app}$                   | 15. $D_{50, proto}$  | Equivalent prototype median grain size of scale $N_{c,obs}$  |
| 8. $q_{t,pred}$    | Throughflow predicted for threshold conditions at $N_{c,obs}$              |                      |  |

A test of these two calibration and prediction methods may be made by choosing one case of overflow, MW20, and one case of throughflow, MW22. According to experimental data, model MW20 was subject to erosion at 120g when  $127 \text{ mm}^2/\text{s}$  was applied. From  $\psi = 0.076$ , the critical flow is predicted to be  $80 \text{ mm}^2/\text{s}$ , and the collapse flow  $96 \text{ mm}^2/\text{s}$ . In comparison, when  $\psi = 0.0853$ , the critical flow is predicted to be  $97 \text{ mm}^2/\text{s}$ , and the collapse flow  $116 \text{ mm}^2/\text{s}$ . For the second case, the experimental data for MW22 indicates that a throughflow of  $109 \text{ mm}^2/\text{s}$  caused erosion at 30g. If  $\psi = 0.076$ , and half the maximum seepage force and half the full throughflow are considered to be the representative conditions, then the minimum centrifugal loading for stable flow is in excess of 30000g, clearly an unrealistic prediction in light of the experimental data. If seepage forces are ignored, and  $\psi$  taken to be 0.0853, then threshold conditions are predicted to occur at 98g, and collapse flow conditions at 68g. In these two extreme cases, then, Olivier's design rule, which disregards seepage forces, gives more realistic predictions from the point of view of embankment dam engineering, when calibrated from the engineering data.

In Table 6.6, the data concerning erosion are detailed, using the calibration value:  $k' = 0.315$  ( $\psi = 0.0853$ ) in Olivier's design rule. Prediction of erosion is in general quite good, and permits a variety of comments to be made on embankment characteristics.

Model MW23, for which the calibration of  $k'$  was performed, has values of observed and predicted critical throughflow which are as expected. Under the worst throughflow conditions,  $q = 329 \text{ mm}^3/\text{mm-s}$  at 66g, erosion continued for 5.5 minutes. The predicted angle of stability for this throughflow at that centrifugal loading is  $8^\circ$  to the horizontal. The final angle measured in the model, however, is  $19^\circ$ . This may indicate that the process of erosion was not complete when the water supply was shut off, or that the calibration value has a margin of safety in combined

through and overflow.

In models MW20 and MW21, throughflow was increased while centrifugal loading was maintained at the full scale stress level. The predicted collapse flow for model MW20,  $116 \text{ mm}^3/\text{mm-s}$  was less than that applied,  $127 \text{ mm}^3/\text{mm-s}$ , and so erosion was predicted as observed. Gullying, leading to flow concentration, was observed in the final model profile. This non-uniform distribution of flow explains the observation that the predicted stable angle,  $22^\circ$  to the horizontal, is much greater than the measured final angle,  $3^\circ$ .

Model MW21 was also thought to be subject to flow concentrations, which may have arisen from the particle segregation caused in embankment preparation by compaction: erosion occurred at a level of throughflow less than half of that predicted, and appeared in the form of a gully. This extended as high as the phreatic exit point, coinciding with a layer boundary. The final measured beach angle was also much more shallow than that predicted and is consistent with a flow concentration. Although Olivier found that close particle packing led to a higher threshold flow, the seemingly contradictory results of this test would caution against the construction of embankments by methods which may give rise to particle segregation and consequent danger of flow concentration.

Models MW7, MW22 and MW25 failed by erosion, initiated by reducing centrifugal modelling with a constant throughflow. In each case, erosion was observed to occur after it was predicted to begin, the estimate therefore being conservative, although considering the indirect view of the embankment perhaps not as conservative as it would at first appear. The final angle predicted in models MW22 and MW25 corresponded very well to the measured final erosion beach angle and from these tests four comments may be made. The  $k' = 0.315$  value, calibrated under throughflow conditions in a IV : 2H slope successfully predicted erosion in this material. Under

conditions of uniformly distributed throughflow, as seemed to be the case in models prepared by loose tipping, judging from the evenly distributed erosion beach, the maximum throughflow was achieved. In model MW7, observation of erosion after the centrifuge was stopped, revealed the development and collapse of erosion channels or pipes with time; this phenomenon would explain the gradual increase in embankment permeability over the period of a test, as shown in table 6.3. Model MW22, which was founded on a layer of kaolin, responded similarly to model MW25, suggesting that in this class of failure, the underlayer, provided it is less permeable than the embankment material, is not important to the observed behaviour.

In models MW9 through MW13, deep seated failure in the presence of throughflow was the primary feature of failure. The role of the throughflow was to raise the phreatic surface until mass instability was observed, but the effects of throughflow after failure, and in some cases, prior to failure, may be of interest in slope stability considerations.

Models MW9 and MW10 were both built at slope angle IV : 1.5H (33.7°). In the case of MW9, the throughflow quantity was in excess of that required to initiate erosion. The quick deep seated failure response of the model embankment to the rising phreatic line may have hidden initial toe distress caused by erosion, and the final erosion beach measured, compared well with that predicted indicating good correlation. Model MW10 behaved in a fashion similar to MW9, and although the applied throughflow exceeded the predicted threshold throughflow, it did not exceed the predicted collapse condition. In both cases the primary deep seated failure may have been preceded by erosion distress at the toe. In models MW11 and MW12, built at a shallower inclination, the throughflow applied was less than that predicted to cause failure, seeming to confirm that toe erosion was not essential to this class of failure.

Model MW13, built in the same geometry, but with a toe drain of particle size eleven times larger than the embankment soil, resisted erosion without difficulty under normal throughflow conditions. As will be discussed in section 6.8.4, an increase in  $D_{50}$  by a factor of  $n$ , will permit an increase in safe throughflow of  $n^{1.5}$  times. Even under the most severe conditions applied, uplift pressure which flooded the embankment with approximately  $900 \text{ mm}^3/\text{mm-s}$  for sixty seconds, the toe drain stayed intact, although the material in the body of the embankment suffered severe erosion as the flooding water drained from the embankment face.

For each of these models, the equivalent prototype throughflow and median particle size for the initial erosion events observed, is also included in table 6.6. The range of  $D_{50}$  particle sizes, for the body of the embankment, is from 0.5 mm to 60 mm. In comparison, the New Mexico coarse discard coal mine waste has a typical  $D_{50}$  of 11 mm, which was simulated by the initial erosion events of models MW22 and MW25, both of which were loose tipped embankments. The class of embankment protection observed in model MW13, if desired in the New Mexico waste heap, would require cobbles in the range of 132 mm median diameter.

These models demonstrated the importance and rough predictability of erosion in both model and prototype using Olivier's equation and a calibration factor appropriate to the specific flow conditions. They emphasised the significance of surface material, slope angle, toe drains, and measures to prevent flow concentration, which, with proper design, may eliminate the need for extra freeboard, sluices and bypasses in mine waste embankment dams.

Two classes of model failure were observed in these tests, and in both the flow of water was significant, but the two classes of water flow, one internal flow, and one open flow, are not governed by mutually compatible scaling laws. Further consideration will be given to this important aspect in the following section.

#### 6.8.4 Comments on particle size distribution

Three classes of failure were studied and observed in this model test series; these included rate of construction failure, deep seated failure, and failure by erosion and sediment transport. In each case, the model response was governed by a combination of conditions, but the dominant feature throughout the nineteen tests, was the particle size distribution.

In the case of material with the lowest proportion of fines in it, resembling freshly deposited coarse discard waste, the component of cohesion was low, and the friction angle typically high. Such material is not, in general, susceptible to failure by too rapid rate of construction, as indicated in tests MW1 through MW8. It is more susceptible to deep seated failure after the embankment dam has come into operation in the presence of throughflow, demonstrated in models MW9 through MW12. Localised distress at the toe due to erosion may precede deep seated failure, but is not necessary for the initiation of mass soil movement, although erosion after the initial failure, may aggravate conditions downstream by spreading a beach of debris, if throughflow continues. The dominant class of failure, however, may be predicted by simple analysis using Bishop and Morgenstern (1960) slope stability coefficients, provided that the soil strength parameters are known.

Inclusion of very permeable sections in the embankment can alter significantly, the seepage pattern of throughflow, and predictions must take into careful consideration their presence, whether it is the stabilising effects of a toe drain, or the deleterious effects of an undrained, central key. The designer must be aware of particle size distribution of both the main embankment body, and significant variations within the embankment.

As the material suffers weathering, both physically and chemically, the proportion of fines increases, and there is a corresponding increase

in the component of cohesion, and a decrease in the angle of friction. The material may become more competent to withstand regular slope instability, but another and quite different problem may arise, in the form of erosion and sediment transport.

An embankment which, when freshly deposited, passed a stable throughflow of  $q$ , will pass a smaller throughflow as the particle sizes are reduced by weathering. Provided the upstream reservoir level stays constant, and if the particle size is uniformly reduced by a factor of  $n$ , so that  $D_{50w}$  in its weathered state is related to  $D_{50f}$  in its fresh state, by  $D_{50w} = \frac{D_{50f}}{n}$ , and similarly  $D_{10w} = \frac{D_{10f}}{n}$ , then both the permeability of the embankment and the throughflow volume are reduced by  $n^2$ . With this uniform reduction in particle size, the resistance to erosion is also reduced, but the tolerated safe throughflow is reduced proportional to  $n^{3/2}$ . Provided erosion was not initially a problem it will become even less so, under these circumstances.

In the case where sluices do not control the upstream reservoir level, so that the rate of throughflow regulates this height, this ideal case will not apply. As weathering causes a reduction in particle size, and consequent reduction in permeability, the reservoir level may rise, as the throughflow per unit height decreases. If the water level rises by more than  $n^{1/2}$ , so that throughflow is reduced by less than  $n^{3/2}$ , erosion may become a problem, as the throughflow exceeds that which can be safely tolerated. The rising phreatic line will also result in a rising throughflow exit height, so that soil previously not required to resist erosion due to overflow, will be required to do so. If the influx of water to the reservoir exceeds the throughflow for long enough, the reservoir level will exceed the height of the embankment. Under such circumstances, the worst erosion is realised, and in particular gullying may develop, intensifying the erosion damage.



Although such developments would suggest that throughflow should not be used over long periods of time to regulate reservoir level, with certain measures, in which some sluices may play a part, throughflow can be tolerated and used to advantage, to control short term high water levels. These measures would include careful design of the downstream slope angle, surfacing and effective toe drains, in full recognition of the particle size distribution which may change over time.

In soil with the greatest proportion of fines, the volume of throughflow is low. A high phreatic line in the embankment due to low permeability, may cause mass instability, although short term fluctuations in the upstream reservoir level may not last long enough to dangerously increase downstream phreatic lines. Overtopping, in the absence of sluice control of the reservoir level, may also be of greater risk than in more permeable embankments, which are capable of safely passing some of the excess water, and the consequent erosion is worse with the finer particle size. It is only in this most weathered material, however, that attention must be paid to the maximum permissible rate of construction. Material in such a degraded state, at the time of embankment construction may be produced by certain handling methods, such as long conveyor belts, which cause marked degradation during transport to the waste site, but it should be pointed out that even though such a material state is not the normal case, embankments of this material may still be raised in waste of low permeability, provided time is permitted for dissipation of excess pore pressures generated during construction.

This research has brought attention to the importance of particle size distribution in coal mine waste. Each mining operation will produce a waste with different properties according to the mining and handling techniques and their effect on the material mined, and each waste will have correspondingly different stability problems. The nature of coal mine waste is such that these properties will also change over time. The proto-

type design consequence of this is that each material must be analysed separately, and in addition, its likely future properties must be considered.

Certain aspects of centrifugal modelling, pertinent to particle size distribution are also worth noting. It has been explained in section 6.7.5, that the modelling laws governing the scale of particle size distribution curves in reduced scale centrifugal models, are incompatible for erosion and permeability. Erosion events observed to occur in a model with  $D_{50m}$ , are related to events in a prototype,  $N$  times larger in every dimension, as  $D_{50p} = N D_{50m}$ , whereas in a model with permeability,  $k_m$ , related to a prototype with permeability,  $k_p = N k_m$ , requires that  $D_{10p} = D_{10m} \sqrt{N}$ . It is not likely that model soil will conform simultaneously to both requirements. This means that centrifugal modelling of events in which both permeability and erosion effects are important is not simple to achieve. With direct attention to these models, however, the following comments can be made.

If a model, in which erosion is observed to occur, is proved to be stable with respect to deep seated failure at the observed level of phreatic surface in the model, then it can be assumed that in a prototype, in which all particle sizes are assumed to be  $N$  times larger, so that  $k_p = N^2 k_m$ , the relative geometry of phreatic surfaces in the model and prototype will be  $1/\sqrt{N}$  as high in the prototype as in the model, and deep seated failure will be even less likely in the prototype than in the model. Conversely, in a model in which a given throughflow causes deep seated failure but not erosion, the same phenomenon of deep seated failure but no erosion cannot necessarily be expected in a prototype. Therefore, for a given throughflow and consequent erosion, predictions of deep seated failure in a reduced scale centrifuge model, are conservative, and conversely, for a model in which a given phreatic surface gives rise to deep seated failure, erosion characteristics are modelled unconservatively.

## 6.9 Conclusions

This research investigated slope stability problems in coarse discard coal mine waste embankment dams. The material used in the models was coarse discard, sampled from an active coal mine waste heap in New Mexico, U.S.A., and altered throughout the test series by removing various quantities of the fine and coarse portions. Nineteen models were made with this material, using a basic technique of preparation resembling wet, loose tipping downstream construction, but also including two alterations in method, all of which simulated possible prototype configurations.

Centrifugal modelling with these specimens demonstrated three classes of failure, including rate of construction failure, deep seated mass slope instability under throughflow conditions, and failure by excessive erosion and sediment transport. The single most significant factor in the test series was the particle size distribution of the soil, but the effects of throughflow, variations in geometry, which included the influence of a toe drain and an undrained permeable key, layered compaction of the embankment, uplift, embankment slope angle and a kaolin foundation layer, were also studied. Theoretical analysis of water movement, both through and over soil in reduced scale centrifugal models, was investigated, and two mutually incompatible scaling criteria were established.

The experiments showed that the effects of particle distribution, affected not only by handling, but also changing with time in response to weathering, was important in determining the class of failure at risk. Coarse discard coal mine waste embankment dams should generally be free from the problems of a too rapid rate of construction, studied by Malushitsky. The two major classes of failure generated by throughflow or overflow of water are deep seated instability, and failure by erosion and sediment transport. Both of these failure types could be predicted by conventional analysis, but have conflicting particle scaling criteria which prevent

• correct centrifugal modelling of events in which both factors are simultaneously important.

## CHAPTER 7

### GENERAL CONCLUSIONS

#### 7.1 Slope Failures

The experimental programme of this research investigated slope failures in two prototype materials using the technique of reduced scale centrifugal modelling.

In models of Champlain Sea clay, a fissured, cemented sensitive Canadian soil, three classes of failure were observed: intact slope instability involving dilatant behaviour along a single failure plane, slope degradation into a talus of soil nodules, and flowsliding in degraded soil, in response to the application of uplift pressures. The behaviour of the model slope was affected by a three tiered hierarchy of soil components. In its intact condition the plane failure surface resembled more that of a soft brittle rock than of a plastic soil. At the intermediate stage of breakdown, the soil dilated along the microfissures which defined the individual soil nodules, and fell as a talus. In the final state of degradation, the fine rubble and remoulded nodules comprised a soil of much lower permeability, capable of retaining excess pore pressures, in particular those induced by uplift, and responded by flowsliding. The state of the soil was felt to be affected by its stress history and horizontal stress release: in the prototype, seasonal cycling of stress conditions would be very significant.

In the coal mine waste embankment models, three classes of failure were also observed: intact deep seated slope failure in response to the high phreatic line due to throughflow conditions, mass erosion of individual soil particles with drainage of throughflow down the embankment face, and retrogressive failure in response to excess pore pressures generated by rate of construction conditions. The dominant feature which determined which

class of failure would occur in different samples of this material was particle size distribution, as discussed in section 6.8.4, changing in prototype conditions with handling and weathering.

The causes of the failures observed in these two prototype soils were very different, but a significant common feature was the role of the changing component size. With a given soil, the effects of stress changes over time, through seasonal variation, with handling and weathering, may change soil response, and these changes may be subtle and unexpected.

Liquefaction flowsliding, an initial interest of the research, was observed to occur in both model prototype materials to a limited degree in their final level of degradation. In this state the permeability of the once relatively free draining soil was reduced to a level which was capable of retaining high pore pressures, and therefore was susceptible to liquefaction flowsliding. This is a simple, but important conclusion of the research.

## 7.2 Centrifugal Modelling

Reduced scale centrifuge modelling permitted the safe observation of many types of prototype slope failure under controlled boundary conditions using two prototype soil materials, but in relating the observed model behaviour to prototypes, certain scaling difficulties arise.

In experiments with Champlain Sea clay, two features in particular were felt to be important in governing the type of soil response observed: horizontal stress release and the network of microfissures. Both of these features were impossible to scale in similarity with the model scale and this difficulty was assumed to explain certain inconsistencies in model behaviour.

In the coal mine waste, several realistic modifications in particle size distribution were achieved. Their effects on the class of failure,

by erosion due to throughflow drainage or by deep seated failure in response to a high phreatic line, could be predicted with conventional equations, and related to prototype behaviour with the derived scaling laws. These laws, however, were not mutually compatible, preventing the modelling of prototype events in which both phenomena were simultaneously significant.

In both materials, flowsliding was also observed to begin. The continuation of such behaviour is dependent upon the retention of excess pore pressures, and in reduced scale models, where dissipation of pore pressures occurs  $N^2$  times as fast in model as in prototype, difficulty will be encountered in modelling similarly scaled continued flowsliding.

In spite of these difficulties in assembling a complete picture of prototype behaviour, the centrifuge provided an experimental technique, permitting controlled monitored testing of new failure mechanisms and phenomena with unfamiliar soil materials.

REFERENCES

- Avgherinos, P.J. (1969) Centrifugal testing of models made of soil, Ph.D. Thesis, Cambridge University.
- Avgherinos, P.J., A.N. Schofield (1969) Drawdown failures of centrifuged models, Proc. 7th Int. Conf. on S.M. and F.E., vol. 2, p. 497-505.
- Bassett, R.H. (1973) Centrifugal model tests of embankments on soft alluvial foundations, Proc. 8th Int. Conf. on S.M. and F.E., vol. 2.2, p. 23-30.
- Bassett, R.H., J.N. Horner (1977) Centrifugal model testing of the approach embankment to the M180 Trent Crossing, Internal Report, King's College, Univ. of London.
- Beasley, D.H. (1973) Centrifugal modelling of soft clay strata subject to embankment loading, Ph.D. Thesis, Cambridge University.
- Bishop, A.W. (1955) The use of the slip circle in the stability analysis of slopes, Geotechnique (5), p. 7-17.
- Bishop, A.W. (1967) Progressive failure - with special reference to the mechanism causing it, Proc. Geotech. Conf., Oslo 1967, vol. 2, p. 142-150.
- Bishop, A.W., N. Morgenstern (1960) Stability coefficients for earth slopes, Geotechnique (10), p. 129-150.
- Bjerrum, L. (1973) Problems of soil mechanics and construction on soft clays and structurally unstable soils, Proc. 8th Int. Conf. on S.M. and F.E., vol. 3, p. 111-159.
- Blight, G. (1977) Slopes in mining and industrial waste, Proc. 9th Int. Conf. on S.M. and F.E., vol. 2, p. 600-604.
- Bolton, M.D. (1972) Reinforced earth - a centrifuge study, D.O.E. Research Contract Report, U.M.I.S.T.
- Bolton, M.D., R. English, C.C. Hird, A.N. Schofield (1973) Ground displacements in centrifugal models, Proc. 8th Int. Conf. on S.M. and F.E., vol. 1.1, p. 65-70.
- Bozozuk, M., A. Labrecque (1969) Downdrag measurements on 270 foot composite piles, A.S.T.M. Special Technical Publication 444, p. 15-40.
- Britto, A.M. (1979) Thesis in preparation, Cambridge University.
- Burn, K.N., J.J. Hamilton (1968) Settlements of a high embankment on Leda clay, Canadian Geotechnical Journal (5), p. 299-312.
- Cabrera, J.G., I.J. Smalley (1973) Quick clays as products of glacial action: a new approach to their nature, geology, distribution and geotechnical properties, Engineering Geology, p. 115-133.



- Cedergren, H.R. (1973) Seepage control in earth dams, Embankment Dam Engineering, p. 21-46, ed. R.C. Hirschfeld, S.J. Poulos; John Wiley and Sons Ltd, U.S.A.
- Chang, Y.L. (1939) Laboratory investigation of flume traction and transportation, Transactions, A.S.C.E., p. 1246-1284.
- Corp, E.L., R.L. Schuster, M.M. McDonald (1975) Elastic-plastic stability analysis of mine waste embankments, Report of Investigations 8069, Spokane Mining Research Center, Spokane, Washington, United States Department of the Interior, U.S.A.
- Cowherd, D.C. (1977) Geotechnical characteristics of coal mine waste, Proc. A.S.C.E. Speciality Conf. on Geotech. Practice for Disposal of Solid Waste Materials, Ann Arbor, Michigan, June 13-15, U.S.A.
- Craig, W.H. (1973) Discussion: up to date method of investigating the strength and deformability of soils, Proc. 8th Int. Conf. on S.M. and F.E., vol. 4.2, p. 15-16.
- Crawford, C.B. (1953) Settlement studies on the National Museum building, Ottawa, Canada, Proc. 3rd Int. Conf. on S.M. and F.E., vol. 1, p. 338-345.
- Crawford, C.B. (1963) Cohesion in an undisturbed sensitive clay, Geotechnique (13), p. 132-146.
- Crawford, C.B. (1968) Quick clays of eastern Canada, Engineering Geology, vol. 2, No. 4, p. 239-265.
- Davis, H.E., M. Harding, V. Lawrence (1967) Report of the tribunal appointed to inquire into the disaster at Aberfan on October 21st, 1966, Her Majesty's Stationery Office, London.
- Dawson, G.M. (1899) Remarkable landslide in Portneuf County, Quebec, Geological Society of America Bulletin (10), p. 484-490.
- Eden, W.J., E.B. Fletcher, R.J. Mitchell (1971) South Nation River landslide, May 16, 1971, Canadian Geotechnical Journal (8), p. 446-451.
- Eden, W.J., R.J. Mitchell (1970) The mechanics of landslides in Leda clays, Canadian Geotechnical Journal (7), p. 285-296.
- Eden, W.J., R.J. Mitchell (1973) Landslides in sensitive marine clays in eastern Canada, Highway Research Record, no. 463, p. 18-27.
- Endicott, L.J. (1970) Centrifugal model testing of soil models, Ph.D. Thesis, Cambridge University.
- English, R.J. (1973) Centrifugal model testing of buried flexible structures, Ph.D. Thesis, U.M.I.S.T.
- Fredlund, D.G., J. Krahn (1977) Comparison of slope stability methods of analysis, Canadian Geotechnical Journal (14), p. 429-439.
- Fyodorov, I.V. (1965) Slope stability in hydraulic fill structures, Proc. 6th Int. Conf. on S.M. and F.E., vol. 11, p. 472-476.

- Gadd, N.R. (1963) Surficial geology of Ontario map-area, Ontario, Quebec 62-16, Geological Survey of Canada.
- Garneau, R., J.P. Le Bihan (1977) Estimation of some properties of Champlain clays with the Swedish fall cone, Canadian Geotechnical Journal (14), p. 571-581.
- Graf, W.H. (1971) Hydraulics of sediment transport, McGraw-Hill, U.S.A.
- Goodings, D.J., R.G. James, A.N. Schofield, R.N. Taylor, F.C. Townsend (1977) Centrifugal model tests of coal waste embankments, Report to the European Research Office of the U.S. Army Corps of Engineers, Cambridge University.
- Goodings, D.J., A.N. Schofield (1978) Further centrifugal model tests of coal waste embankments, Report to the European Research Office of the U.S. Army Corps of Engineers, Cambridge University.
- Henderson, I.M. (1977) Open channel flow, Macmillan Co., U.S.A.
- Hird, C.C. (1974) Centrifuge model tests of flood embankments, Ph.D. Thesis, U.M.I.S.T.
- Hodge, R.A.L., R.A. Freeze (1977) Groundwater flow systems and slope stability, Canadian Geotechnical Journal (14), p. 466-476.
- Hoek, E. (1965) The design of a centrifuge for the simulation of gravitational force fields in mine models, Journal of South African Inst. Mining and Metallurgy, p. 455-487.
- Holubec, I. (1976) Geotechnical aspects of coal waste embankments, Canadian Geotechnical Journal (13), p. 27-39.
- Howsam, P. (1974) Some groundwater flow studies using centrifuge modelling technique, Ph.D. Thesis, U.M.I.S.T.
- Janbu, N. (1977) Slopes and excavations in normally and lightly over-consolidated clays, Proc. 9th Int. Conf. on S.M. and F.E., vol. 2, p. 549-561.
- Johnson, H.A. (1971) Flow through rockfill dams, A.S.C.E. Journal of the S.M. and F. Div., vol. 97, no. SM2, p. 329-340.
- Karrow, P.F. (1961) The Champlain Sea and its sediments, from Soils in Canada, ed. R.F. Leggett, Royal Society of Canada Special Publications, p. 97-108.
- La Rochelle, P., J.-Y. Chagnon, G. Lefebvre (1970) Regional geology and landslides in the marine clay deposits of eastern Canada, Canadian Geotechnical Journal (7), p. 145-156.
- La Rochelle, P., M. Roy, F. Tavenas (1973) Field measurements of cohesion in Champlain clay, Proc. 8th Int. Conf. on S.M. and F.E., vol. 1.1, p. 229-236.
- Laps, T.M. (1973) Flow through rockfill, from Embankment Dam Engineering, ed. R.C. Hirschfeld, S.J. Poulos, J. Wiley and Sons, U.S.A., p. 87-108.

- Lo, K.Y. (1970) The operational strength of fissured clays, Geotechnique (20), p. 57-74.
- Lo, K.Y. (1972) An approach to the problem of progressive failure, Canadian Geotechnical Journal (9), p. 407-429.
- Lo, K.Y., C.F. Lee (1974) An evaluation of the stability of natural slopes in plastic Champlain clays, Canadian Geotechnical Journal (11), p. 165-181.
- Lo, K.Y., J.P. Morin (1972) Strength anisotropy and time effects of two sensitive clays, Canadian Geotechnical Journal (9), p. 261-277.
- Lyndon, A. (1972) Centrifugal model test of a natural clayslope failure, Ph.D. Thesis, U.M.I.S.T.
- Lyndon, A., A.N. Schofield (1978) Centrifugal model tests of the Lodalen landslide, Canadian Geotechnical Journal (15), p. 1-13.
- Mair, R.J. (1979) Thesis in preparation, Cambridge University.
- Malushitsky, J.I. (1975) The centrifugal testing of waste heap embankments, Budivelnik Publishing House, U.S.S.R., (in translation B.R.E. 1978).
- Martin, C.S., M.M. Aral (1971) Seepage force on interfacial bed particles, Proc. A.S.C.E. Journal of the Hydraulics Division, vol. 97, HY7, p. 1081-1100.
- Mikasa, M., N. Takada, K. Yamada (1969) Centrifugal model test of a rockfill dam, Proc. 7th Int. Conf. on S.M. and F.E., vol. 2, p. 325-333.
- Mitchell, R.J. (1970a) Landslides at Breckenridge, Pineview Golf Club, and Rockcliffe, Division Building Research, N.R.C.C., Canada, Technical Paper no. 322.
- Mitchell, R.J. (1970b) On the yielding and mechanical strength of Leda clays, Canadian Geotechnical Journal (7), p. 297-312.
- Mitchell, R.J. (1975) Strength parameters for permanent slopes in Champlain Sea clays, Canadian Geotechnical Journal (12), p. 447-455.
- Mitchell, R.J., W.J. Eden (1972) Measured movements of clay slopes in the Ottawa area, Canadian Journal of Earth Sciences (9), p. 1001-1013.
- Mitchell, R.J., A.R. Markell (1974) Flowsliding in sensitive soils, Canadian Geotechnical Journal (11), p. 11-31.
- Mitchell, R.J., R.D. King (1977) Cyclic loading of an Ottawa area Champlain Sea clay, Canadian Geotechnical Journal (14), p. 52-63.
- Mitchell, R.J., K.K. Wong (1973) The generalized failure of an Ottawa valley Champlain Sea clay, Canadian Geotechnical Journal (10), p. 607-616.
- Mittal, H.K., N.R. Morgenstern (1975) Parameters for the design of tailings dams, Canadian Geotechnical Journal (12), p. 235-261.

- Morris, D.V. (1979) Thesis in preparation, Cambridge University.
- O'Connor, M.J., R.J. Mitchell (1977) An extension of the Bishop and Morgenstern slope stability charts, Canadian Geotechnical Journal (14), p. 144-151.
- Oldenzien, D.M., W.E. Brink (1974) Influence of suction and blowing on entrainment of sand particles, Proc. A.S.C.E. Journal of the Hydraulics Division, vol. 100, HY7, P. 935-949.
- Olivier, H. (1967) Through and overflow rockfill dams - new design techniques, Proc. I.C.E., vol. 36, p. 433-471.
- Orr, T.L.L. (1976) The behaviour of lined and unlined model tunnels in stiff clay, Ph.D Thesis, Cambridge University.
- Padfield, C.J. (1978) The stability of riverbanks and flood embankments, Ph.D. Thesis, Cambridge University.
- Parkin, A.K., D.H. Trollope, J.D. Lawson (1966) Rockfill structures subject to overflow, A.S.C.E. Journal of the S.M. and F. Div., vol. 92, SM6, p. 135-152.
- Penner, E. (1965) A study of sensitivity in Leda clay, Canadian Journal of Earth Sciences (2), p. 425-441.
- Penner, E., K.N. Burn (1978) Review of engineering behaviour of marine clays in eastern Canada, Canadian Geotechnical Journal (15), p. 269-282.
- Pokrovsky, G.I., I.S. Fyodorov (1935) An investigation by means of models of stress distribution in the ground and the settling of foundations, Technical Physics of U.S.S.R., vol. 5, no. 4, p. 299-311.
- Pokrovsky, G.I., I.S. Fyodorov (1936) Studies of soil pressures and soil deformation by means of a centrifuge, Proc. 1st Int. Conf. on S.M. and F.E., vol. 1, p. 70.
- Pokrovsky, G.I., I.S. Fyodorov (1968), Centrifugal modelling in the construction industry (in translation B.R.E. 1975).
- Pokrovsky, G.I., I.S. Fyodorov (1969) Centrifugal modelling of mining works (in translation B.R.E. 1975).
- Polshin, D.E., N.Y. Rudnitski, P.G. Chizhikov, T.G. Yakoleva (1973) Centrifugal model testing of foundation soils of building structures, Proc. 8th Int. Conf. on S.M. and F.E., vol. 1.3, p. 203-208.
- Raymond, G.P., D.L. Townsend, M.J. Lojkasek (1971) The effect of sampling on the undrained soil properties of a Leda soil, Canadian Geotechnical Journal (8), p. 546-557.
- Roscoe, K.H., J.B. Burland (1968) On the generalised stress-strain behaviour of 'wet' clay, Symposium on Engineering Plasticity, Cambridge p. 535-610.
- Roscoe, K.H., A.N. Schofield, C.P. Wroth (1958) On the yielding of soils, Geotechnique (8), p. 22-52.

- Rowe, P.W. (1975) Displacements and failure modes of model offshore gravity platforms founded in clay, Offshore Europe '75, Aberdeen, 218.1-218.6.
- Rydweski, J. (1958) Experimental and analytical determination of the stresses in buttress dams, Ph.D. thesis, Cambridge University.
- Sangrey, D.A. (1970) Discussion on causes of clay sensitivity, A.S.C.E. Journal of the S.M. and F. Div., vol. 96, SM3, p. 1067-1070.
- Sangrey, D.A. (1972) Naturally cemented sensitive soils, Geotechnique (22), p. 139-152.
- Sangrey, D.A., M.J. Paul (1971) A regional study of landsliding near Ottawa, Canadian Geotechnical Journal (8) p. 315-335.
- Schofield, A.N., C.P. Wroth (1968) Critical state soil mechanics, McGraw-Hill, London.
- Scott, R.F. (1963) Principles of soil mechanics, Addison-Wesley Publishing Co., U.S.A.
- Scott, R.F., N.R. Morgan (1977) Feasibility and desirability of constructing a very large centrifuge for geotechnical studies, Prepared for the National Science Foundation, Washington, D.C., U.S.A.
- Soderman, L.G., R.M. Quigley (1965) Geotechnical properties of three Ontario clays, Canadian Geotechnical Journal (2), p. 167-189.
- Streeter, V.L. (1971) Fluid mechanics, McGraw-Hill, U.S.A.
- Šuklje, L. (1967) Comments on rate effects, Proc. Geotechnical Conference Oslo (1967), vol. 2, p. 150-153.
- Tavenas, F.A. (1978) Centrifugal model tests of the Lodalen landslide: Discussion, Canadian Geotechnical Journal (15), p. 621-624.
- Tavenas, F.A., J.-Y. Chagnon, P. La Rochelle (1971) The Saint-Jean-Vianney landslide: observations and eye witness accounts, Canadian Geotechnical Journal (8), p. 463-478.
- Tavenas, F.A., S. LeRoueil, P. La Rochelle, M. Roy (1978) Creep behaviour of an overconsolidated clay, Canadian Geotechnical Journal (15), p. 402-423.
- Taylor, D.W. (1937) Stability of earth slopes, Journal Boston Society of Civil Engineers, vol. 24, July 1937, no. 3.
- Taylor, D.W. (1948) Fundamentals of Soil Mechanics, John Wiley and Sons Inc., U.S.A.
- Taylor, R.K. (1978) Properties of mining wastes with respect to foundations, from Foundation Engineering in Difficult Ground, ed. F.G. Bell, pub. Butterworth and Co. Ltd, U.K., p. 175-203.
- Terstepanian, G.I., M.N. Goldstein (1969) Multi-stored landslides and strength of soft clays, Proc. 7th Int. Conf. on S.M. and F.E., vol. 2, p. 693-700.

- Terzaghi, K., R.B. Peck (1948) Soil mechanics in engineering practice, J. Wiley and Sons Inc., U.S.A.
- Torrance, J.K. (1975a) On the role of chemistry in the development and behaviour of sensitive marine clays of Canada and Scandinavia, Canadian Geotechnical Journal, p. 326-334.
- Torrance, J.K. (1975b) Pore water extraction and the effect of sample storage on the pore water chemistry of Leda clay, from Soil Specimen Preparation for Laboratory Testing, A.S.T.M.
- Townsend, D.L., D.A. Sangrey, L.K. Walker (1969) The brittle behaviour of naturally cemented soils, Proc. 7th Int. Conf. on S.M. and F.E., vol. 1, p. 411-419.
- Turner, P.W. (1976) Mechanical design of the Cambridge geotechnical centrifuge, Cambridge University.
- Wahler, W.A., D.P. Schlick (1976) Mine refuse impoundments in the United States, Proc. 12th Int. Congress on Large Dams, vol. 1, Q44, R14, pp. 279-319.
- Weiss, A. (1951) Construction technique of passing flow over earth dams, Trans. A.S.C.E., p. 1158-1173.
- Wilkins, J.K. (1963) The stability of overtopped rockfill dams, Proc. 4th Australian Conf. on S.M. and F.E.
- Wilson, S.D., R. Squier (1968) Earth and rockfill dams, Proc. 7th Int. Conf. on S.M. and F.E., State of the art volume p. 137-223.
- Wind, H.G. (1976) Interaction of sand and L-shaped walls in centrifuge models, Ph.D. thesis, Cambridge University.
- Wong, P.K.K., R.J. Mitchell (1975) Yielding and plastic flow of sensitive cemented clay, Geotechnique (25), p. 763-782.
- Yalin, M.S. (1972) Mechanics of sediment transport, Pergamon Press, Germany.

Table 4.2 Experimental procedure

Date	Test No	Duration (min)	g	LVDT crest settlement (mm)	Comments
March 3 1977	CSC1	19	1→ 20	-	Water supply from reservoir open continuously  See figure 4.4 Displacements unknown in remainder of test (end of transducer range)
		9	20	-	
		5	20→120	21	
		4	120→ 50		
		3	50		
		2	50→120		
		5	120		
		2	120→ 50		
		13	50		
		2	50→120		
		10	120		
		9	120→ 1		
March 11 1977	CSC2	34	1→ 30	3.5	Model submerged  Simultaneous loading increase and drawdown (see figure 4.5) Displacement unknown (end of transducer range)
		14	30	0	
		3	30→120	>24	
		5	120		
		14	120→ 1		
May 17 1977	CSC3 ( $\beta=70^\circ$ )	4	1→ 8	-	Model submerged  Drawdown causes 5 mm settlement See figure 4.6 Displacement unknown (end of transducer range) Cut slope to $\beta = 30^\circ$ ; replace balls
		15	8	-	
		1	8→ 20	4.5	
		38	20	5	
		2	20→120	>14	
		9	120→ 1		
May 18 1977	( $\beta=30^\circ$ )	6	1→ 20	3	Model submerged Drawdown causes 1.5 mm settlement See figure 4.7  Cut slope to $\beta = 50^\circ$ ; replace balls
		43	20	1.5	
		4	20→120	>18	
		11	120→ 1		
			STOP		
May 19 1977	( $\beta=50^\circ$ )	8	1→ 20	3.5	Model submerged Drawdown causes 2 mm settlement See figure 4.8
		48	20	2	
		3	20→120	>34	
		13	120→ 1		
July 11 1977	CSC4 (h=100)	17	1→ 20	1	Model submerged Drawdown causes 3 mm settlement See figure 4.9  Cut slope to h = 125 mm; replace balls
		50	20	3	
		2	20→105	>32	
		15	105→ 1		
July 14 1977	(h=125)	13	1→ 20	1	Model submerged Drawdown causes 1 mm settlement See figure 4.10  Cut slope to h = 150 mm; replace balls
		24	20	1	
		2	20→ 79	>39	
		18	79→ 1		
July 15 1977	(h=150)	10	1→ 20	1.5	Model submerged Drawdown causes 2.5 mm settlement See figure 4.11
		33	20	2.5	
		3	20→ 70	>36	
		12	70→ 1		
May 20 1977	CSC10	6	1→ 20		Model submerged  Simultaneous drawdown and loading increase (see figure 4.14)  Model submerged
		81	20		
		4	20→120		
		2	120		
		7	120→ 1		
May 26 1977		31	1→120	3	Drawdown Ground water regime still not established Model resubmerged
		6	120	-	
		25	120	3	
		7	120→ 20	2	

Table 4.2 (continued)


Date	Test No	Duration (min)	$\delta$	LVDT crest settlement (mm)	Comments
May 26 1977		39	20		Simultaneous drawdown and loading increase
		3	20→120		
		15	120		
		19	120→ 1 STOP		
May 27 1977		2	1→ 20	1	Model altered:  , and submerged
		28	20	-	
		19	20→120	5	Drawdown (ground water regime established)
		17	120	0.5	
		11	120→ 1 STOP	2	
Aug 15 1977	CSC20	11	1→ 20	-	Model submerged Drawdown causes 0.5 mm settlement See figure 4.15
		46	20	0.5	
		9	20→150	>40	
		2	150		
		7	150→ 1 STOP		
Oct 7 1977	CSC21	13	1→ 20	1	Model submerged
		37	20	1	
		6	20→130	8.5	Swell back Model submerged
		3	130	0.5	
		11	130→ 1 STOP	-2	
Oct 10 1977		10	1→ 20	-	Drawdown
		22	20	-	
		5	20→120	5	
		3	150	1	
		16	150→ 1 STOP	-3	
Jan 13 1978	CSC22	9	1→ 20	0.5	Video tape; model submerged Drawdown and surface runoff begins
		33	20	0.5	
		79	20→125	3	Remove video mirror for higher loading Model submerged
		7	125→ 1 STOP	-1.5	
		5	1→ 20	0.5	Drawdown and surface runoff begins
		16	20	0.9	
		33	20→148	5	
		5	148→ 1 STOP	-1.5	Model submerged
Jan 20 1978		5	1→ 20		Videotape
		18	20		Drawdown
		16	20→120		Fault in transducer; settlement unknown
		14	120		Uplift applied
		6	120→ 1 STOP		Remove video mirror for higher loading
		3	1→ 20	-	Model submerged
		14	20	-	Drawdown
		15	20→120	1	
		4	120	0.5	Uplift applied
		11	120→148	1.5	
		7	148→ 1 STOP	-1.5	Cut slope to $\delta = 32^\circ$
Jan 23 1978	$(\delta=32^\circ)$	3	1→ 20	1	Model submerged
		15	20	1	Drawdown
		13	20→120	5	
		12	120	-	Uplift applied
		7	120→135	0.5	
		6	135	-	
		5	135→ 1 STOP	-1.5	Cut slope to $\delta = 40^\circ$



Table 4.2 (continued)

Date	Test No	Duration (min)	$\beta$	LVDT crest settlement (mm)	Comments
Jan 24 1978	$(\beta=40^\circ)$	3	1→ 20	-	Model submerged
		15	20	-	Drawdown
		15	20→ 95	2	See figure 4.18a
		7	95	20.5	Uplift applied; see figure 4.18b
		6	95→ 1	-1	
			STOP		Cut slope back, again to $\beta = 40^\circ$
		4	1→ 20		Model submerged
		16	20		Drawdown; see figure 4.18c; uplift applied
		53	20→ 148		
		4	148		
		8	148→ 1		
			STOP		
Feb 9 1978	CSC23	11	1→ 20	-	Model submerged
		23	20	0.5	Drawdown
		1	20→ 30	0.5	
		17	30	-	Uplift applied
		93	30→ 135	5	
		4	135	0.5	
		6	135→ 1	-2	
			STOP		Model altered: see table 4.1
		8	1→ 20	0.5	Model submerged
		22	20	1	Drawdown; surface runoff; uplift applied
		46	20→ 140	13	
		7	140→ 1	-1	
			STOP		Remove debris overflow box
		122	1→ 120	9	
		160	120	-	Uplift applied
		22	120→ 1	-	
			STOP		
Feb 28 1978	CSC24	10	1→ 40	3	See figure 4.22a
		32	40	>35	Uplift applied
		104	40→ 120		See figure 4.22b
		64	120		
		32	120→ 1		
			STOP		
March 9 1978	CSC25	16	1→ 40	9.5	See figure 4.26a
		16	40	-	
		45	50	9	Uplift applied; see figure 4.26b
		58	50→ 150	>18	See figure 4.26c
		75	150→ 1		
			STOP		

Table 6.2

Experimental Procedure

Date	Test No	Duration (min)	g	Crest Settlem't (mm)	Res. Ht (mm)	Flow Rate ( $\frac{\text{mm}^3}{\text{mm}^2\text{-s}}$ )	Comments
Oct 21 1977	MW 1	20	100		-	-	Consolidation
			STOP				Cut slope
		10	9	1.5	-	-	
		5	9→150	16	-	-	
		3	150→ 9	-1	-	-	
		8	9	0	-	-	
Oct 31 1977	MW 2	3	9→ 1	-1	-	-	Bulge in shape
			STOP				
		12	1→135	13.5	-	-	Settlement all achieved
		10	135	0	-	-	by 100g
			STOP				
Nov 2 1977	MW 3	11	1→135	20	-	37	Water on from 8g
			STOP				Settlement all by 100g
Nov 4 1977	MW 4	9	1→132	not known	-	37	Water on continuously
		3	132	" "	-		
			STOP				
Nov 14 1977	MW 5	2	1→ 26	-	-	37	Water on from 8g
		3.5	29	-	-		Failure
			STOP				
Nov 15 1977	MW 6	1	1→ 18	7	-	37	Water on continuously
		2.5	19	-	-		Failure
			STOP				
Nov 16 1977	MW 7	1.5	1→ 15	4.5	-	-	
		6.5	15	1	-	-	
		1	15→ 40	4	-	-	
		1	40	0	-	-	
		4	20	0	-	-	
		9	20	0	-	37	Water on
		12	20→ 1	0.5	-		
			STOP				
Nov 18 1977	MW 8	2	1→ 31	19	-	37	Failure
		3	31	>21	-		
			STOP				
Nov 30 1977	MW 9	14	1→100	not known	-	-	
		9	100	" "	-	147	Water on
			STOP				
Dec 1 1977	MW10	77	1→120	11.5			
			(60	-	121	20	
			80	-	102	20	
			80	-	179	66	
			100	-	179	66)	
		7	120	0	153	66	
			120	0	193	147	Failure
			STOP				

Table 6.2 (continued)

Date	Test No	Duration (min)	g	Crest Settlement (mm)	Res. Ht (mm)	Flow Rate ( $\frac{\text{mm}^3}{\text{mm}^2\text{-s}}$ )	Comments
Dec 6 1977	MW11	13 70	1→120 120	12.5 0 -	130 190 193	40 132 147	Failure
			STOP				
Dec 7 1977	MW12	15 61	1→120 120	10 0 -	153 170 240	21 53 177	Initial failure Overtopping
			STOP				
Dec 9 1977	MW13	15.5 31 139	1→120 120 120	10.5 0 0	- - 230	- - 159	Stable Add kaolin slurry
		11 58 30	1→120 120 120	1.5 0 0	- - -	- - 900	Initiate water Initiate uplift; erosion failure
			STOP			for 60s	
Apr 24 1978	MW20	125	90 STOP	22	-	-	Consolidation Cut slope
Apr 26 1978		31 33 11	90 9 120	0.5 4 0	- - 191+	- - 127	Failure by overtopping
			STOP				
May 4 1978	MW21	56 69	1→120 120	2.5 0 0	- 159 187	- 18 75	
			STOP				Examine model
		26 26	1→120 120	1 0	- 192	- 64	Erosion gully
			STOP				
May 10 1978	MW22	43 61	1→120 120	14 0 0	- - -	41) 105) 109	Reservoir levels not visible Add dye to water; erosion gully develops
		27	120→ 1	0	(Table 6.3)		
			STOP				
May 23 1978	MW23	16 18 5 10 18 18	1→100 100 75 50 100 75	9 1 0 0 0 0	- 53 57 82 115 121	- 52 52 52 112 112	
			STOP				Examine model
		7 18 27 8 13 11	1→100 100 66 50 100 66	1.5 0 0 0 0 0	- 115 134 134 139 183	- 105 105 105 329 329	Erosion
			STOP				

Table 6.2 (continued)

Date	Test No	Duration (min)	g	Crest Settle'm't (mm)	Res. Ht (mm)	Flow Rate ( $\frac{\text{mm}^3}{\text{mm}^2\text{-s}}$ )	Comments
May 25 1978	MW24	13.5	9	10	-	-	Undrained rotational slip Further slump to 10° Further slump to 7°
		22	15	-	-	-	
		46	25	-	-	-	
		2.5	50	-	-	-	
			STOP				
May 29 1978	MW25	22	1→100	9	-	-	Toe erosion
		27	100	0	57	55	
		14	76	0	57	55	
		61	100	0	72	95	
				0	89	121	
		6	100→ 30	0	89	121	
		4	30	0	157	121	
		3.5	30→ 20	0	175	121	
			STOP				

Table 6.3

## Permeability Values

For centrifuge model throughflow,  $q = k N h \frac{N_f}{N_d}$  (Taylor (1948))  $\therefore k = \frac{q}{h N} \left( \frac{N_d}{N_f} \right)$

Test No	% < 75 $\mu$ m	D <sub>10</sub> (mm)	Test Source	$q$ ( $\frac{\text{mm}^2}{\text{s}}$ )	N (g)	h (mm)	$\frac{N_f}{N_d}$	k ( $\frac{\text{mm}}{\text{s}}$ )
MW10	16	0.03	centrifuge	20	60	121	0.25	0.01
				20	80	102	0.25	0.01
				66	80	179	0.17	0.03
				66	100	179	0.17	0.02
				66	120	153	0.17	0.02
				147	120	193	0.17	0.04
MW11	16	0.03	centrifuge	40	120	130	0.14	0.02
				132	120	190	0.20	0.03
				147	120	193	0.20	0.03
MW12	16	0.03	centrifuge	21	120	153	0.25	0.005
				53	120	170	0.25	0.01
				177	120	240	0.33	0.02
MW13	16	0.03	centrifuge	159	120	230	0.20	0.03
MW20	26	0.0034	lg laboratory consolidation press					$1.2 \times 10^{-6}$
MW21	13	0.03	lg laboratory consolidation press					$2.2 \times 10^{-5}$
			centrifuge	18	120	159	0.40	
				75	120	187	0.50	
MW22	8	0.07	centrifuge	64	120	192	0.50	0.006
				109	120	106	0.33	0.03
				109	100	120	0.50	0.02
				109	80	122	0.31	0.04
				109	60	138	0.25	0.05
				109	40	163	0.50	0.03
MW23	8	0.07	centrifuge	109	30	181	0.25	0.08
				52	100	53	0.17	0.06
				52	75	57	0.14	0.09
				52	50	82	0.20	0.06
				112	100	115	0.25	0.04
				112	75	121	0.17	0.07
				106	100	115	0.20	0.05
				106	66	134	0.20	0.06
				106	50	134	0.20	0.08
MW24	34	<0.002	lg laboratory consolidation press					$4.2 \times 10^{-7}$
MW25	9	0.07	centrifuge	329	100	139	0.18	0.13
				329	66	183	0.20	0.14
				55	100	57	0.17	0.06
				55	76	57	0.17	0.08
				94	100	72	0.17	0.08
				121	100	89	0.17	0.08
				121	30	157	0.33	0.08
				121	20	175	0.50	0.07

\*Values of  $\frac{N_f}{N_d}$  determined from flow net sketches derived from the video tape test records. See, for example, figure 6.13.

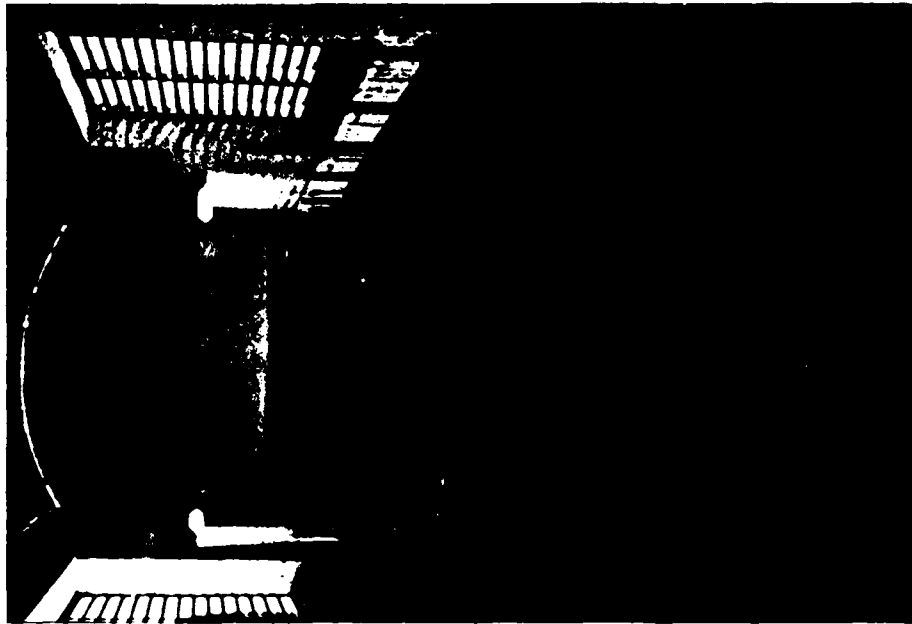


Figure 2.2 -  
2 m wide  
Corridor  
with Slip  
Ring Stack  
Foreground

Figure 2.3 -  
Rotating Arm  
of the  
Centrifuge



Figure 2.12 -  
Video Record  
Image of  
Centrifuge  
Model Test



Figure 4.1 -  
Removal of  
Model Specimen  
from Intact  
Soil Sample

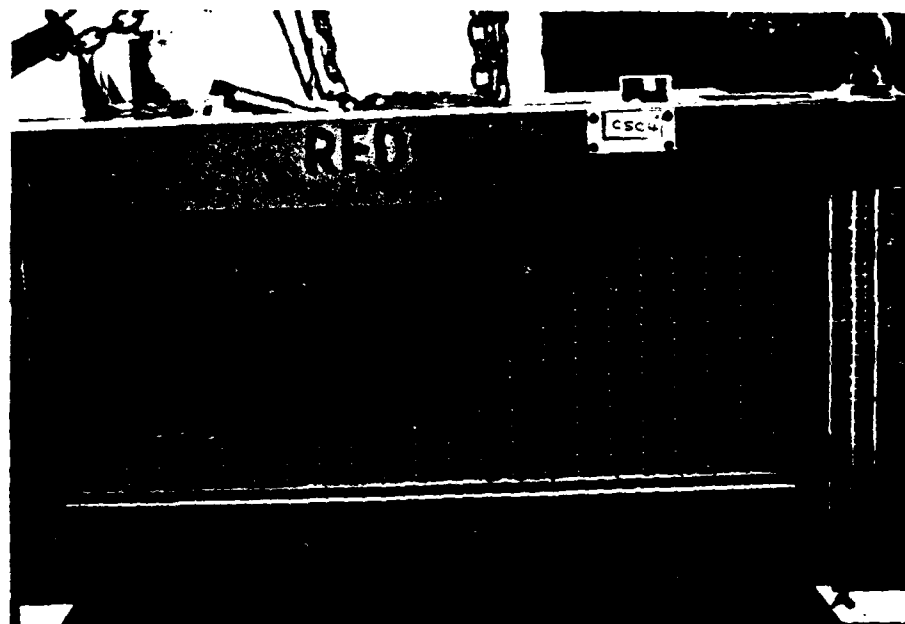


Figure 4.12 -  
CSC4 Model  
Before  
Centrifuge  
Test

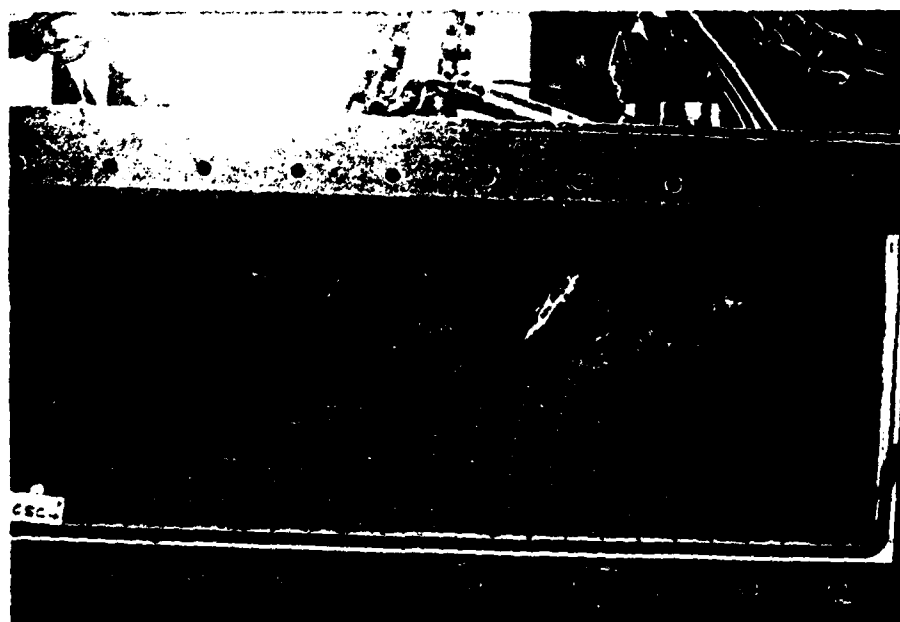


Figure 4.13 -  
CSC4 Model  
After  
Centrifuge  
Test

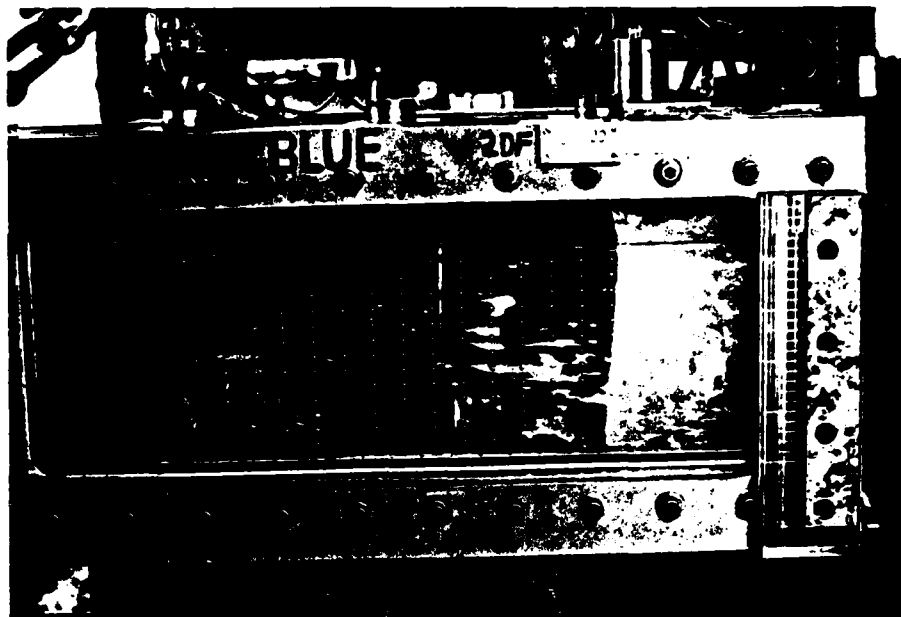


Figure 4.16 -  
CSC20 Model  
Before  
Centrifuge  
Test

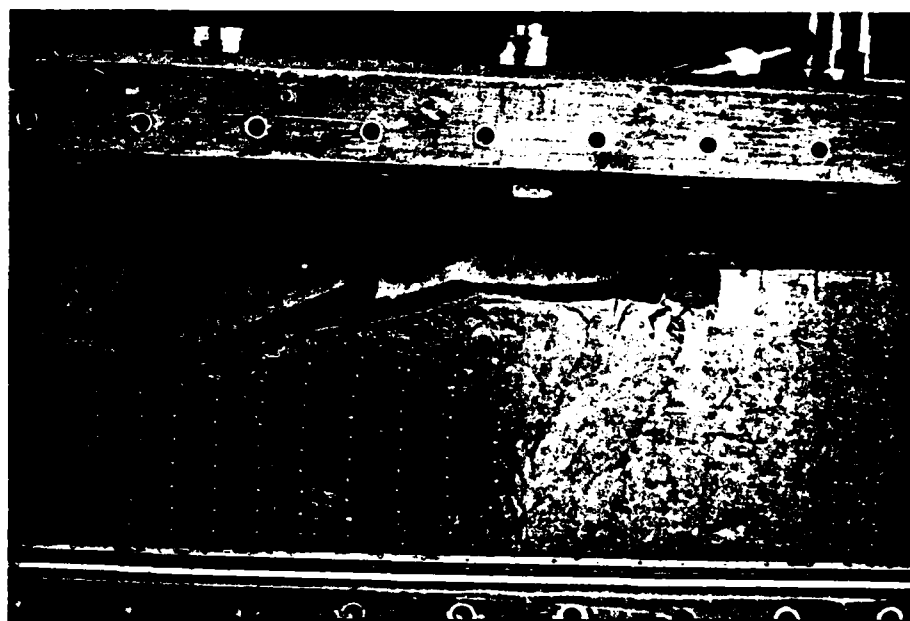


Figure 4.17 -  
CSC20 Model  
After  
Centrifuge  
Test

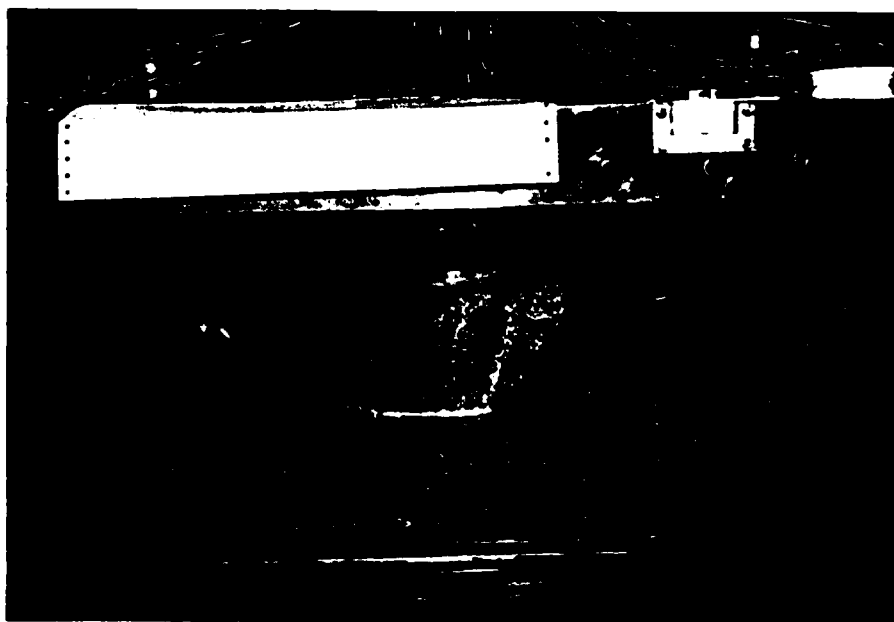


Figure 4.19 -  
CSC22 Model  
Before  
Centrifuge  
Test



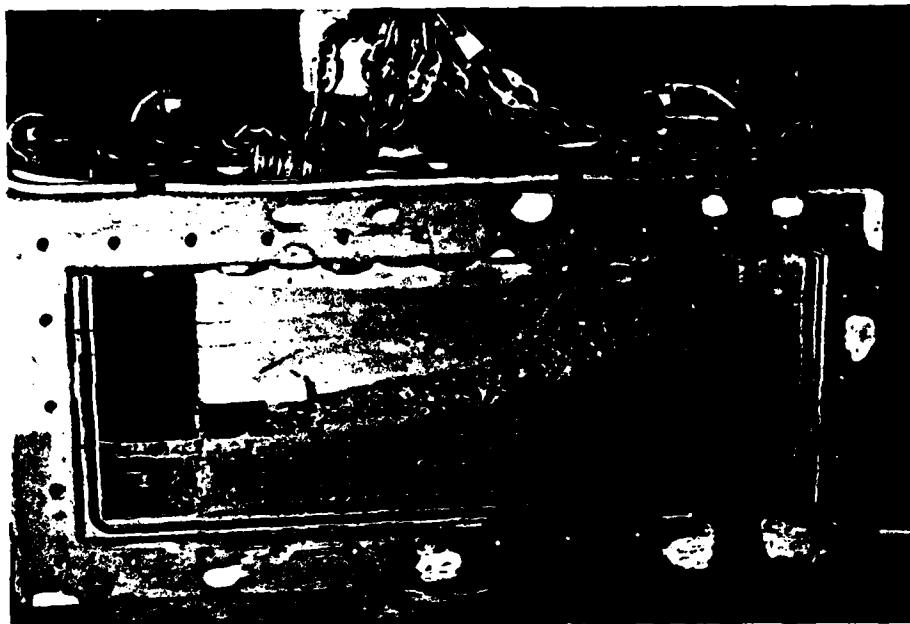


Figure 4.20 -  
CSC22 Model  
After  
Centrifuge  
Test

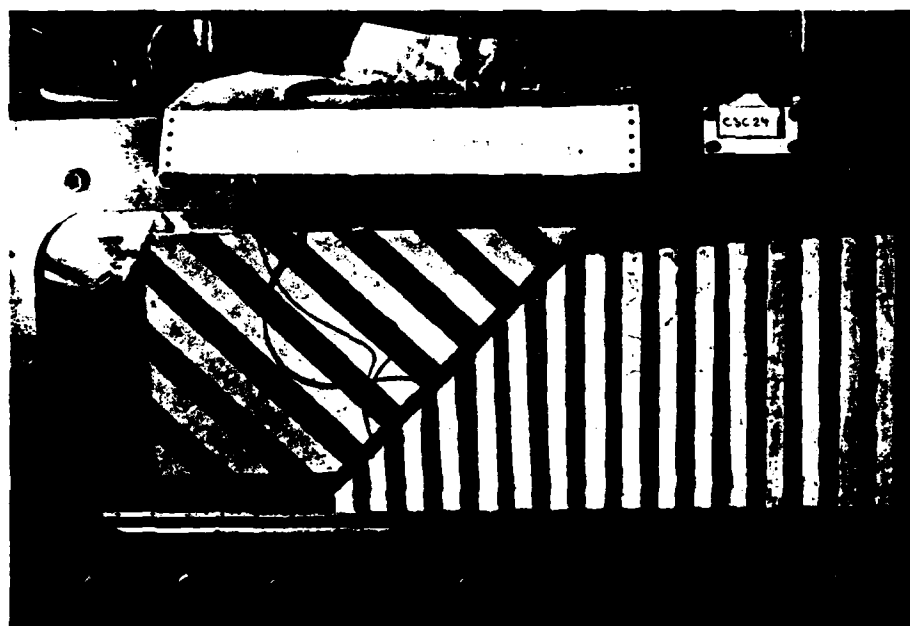


Figure 4.23 -  
CSC24 Model  
Before  
Centrifuge  
Test



Figure 4.24 -  
CSC24 Model  
After  
Centrifuge  
Test



Figure 4.27 -  
CSC25 Model  
After  
Centrifuge  
Test

Figure 6.1 -  
Model (MW13)  
During  
Preparation  
with  
Templates  
Still in  
Place

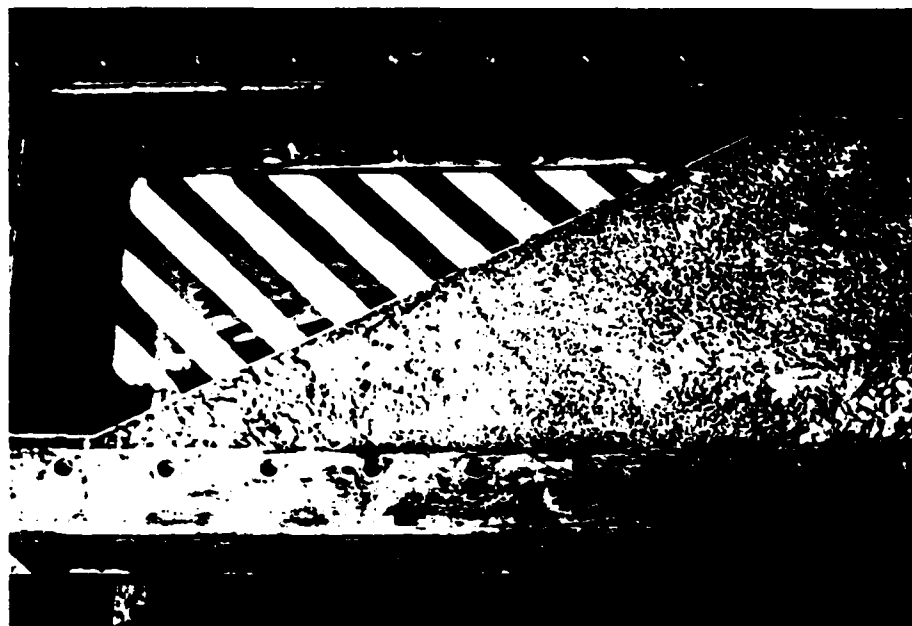


Figure 6.8 -  
MW4 Model  
Before  
Centrifuge  
Test

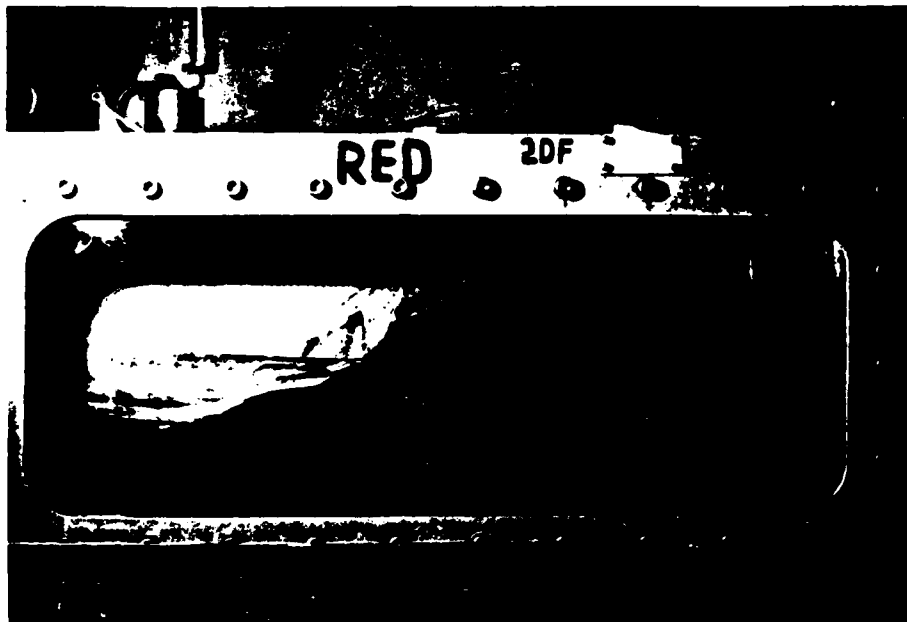


Figure 6.9 -  
MW4 Model  
After  
Centrifuge  
Test

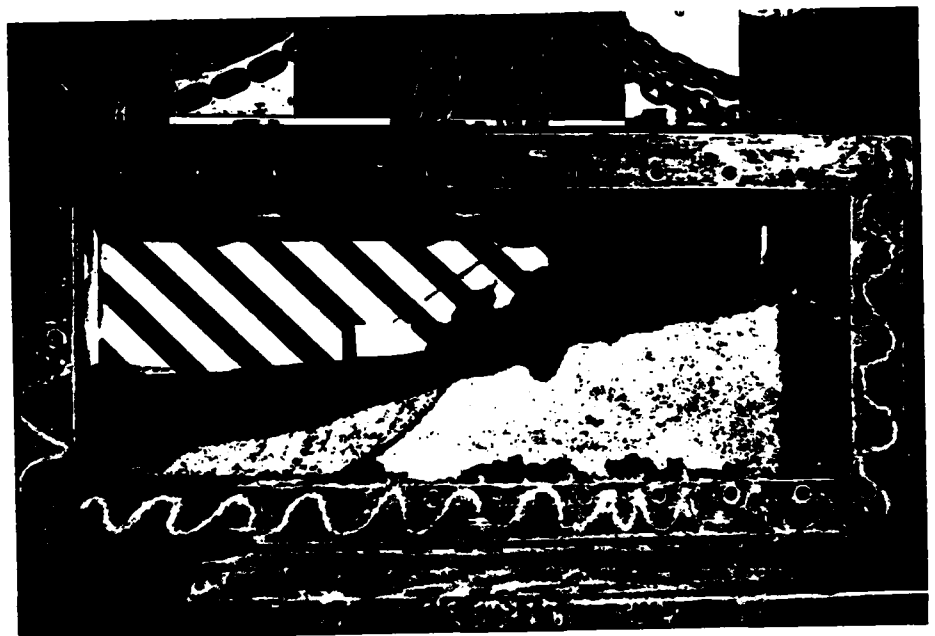


Figure 6.14 -  
MW9 Model  
After  
Centrifuge  
Test



Figure 6.16 -  
MW10 Model  
After  
Centrifuge  
Test



Figure 6.20 -  
MW12 Model  
Before  
Centrifuge  
Test

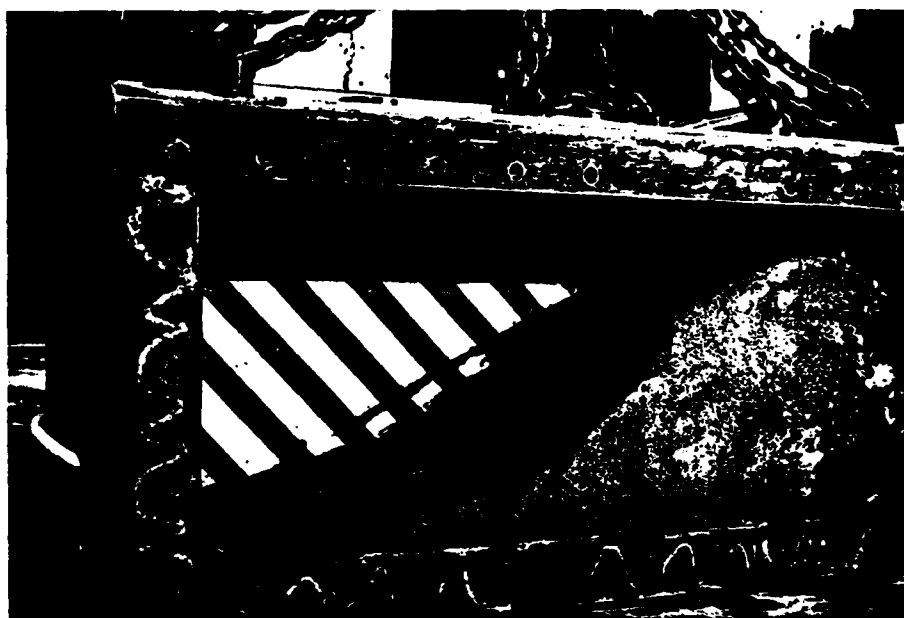


Figure 6.21 -  
MW12 Model  
After  
Centrifuge  
Test

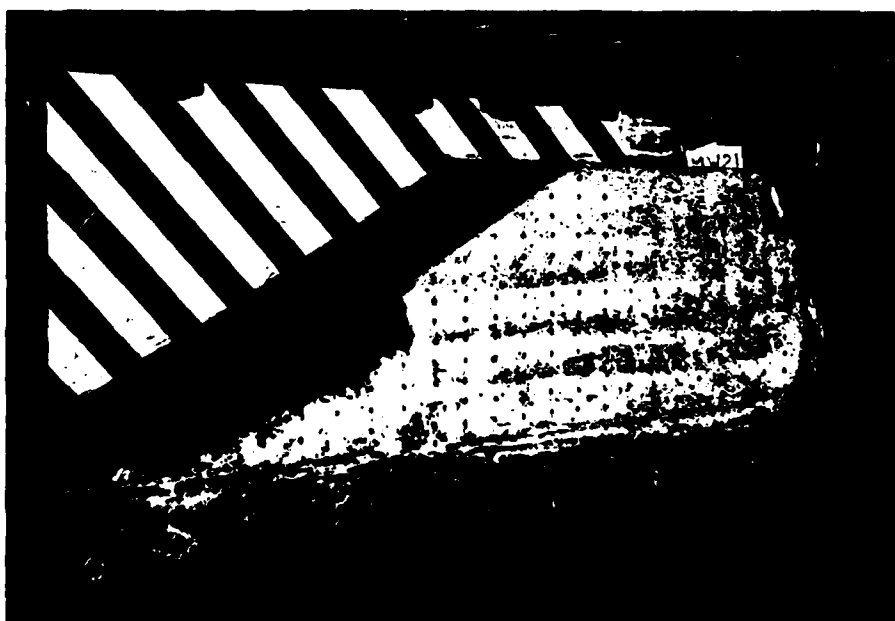


Figure 6.24 -  
MW21 Model  
After  
Centrifuge  
Test